

**University of Alberta**

**Semi-Distributed Snowmelt Modeling and Regional Snow Mapping Using Passive  
Microwave Radiometry**

by

**Purushottam Raj Singh**



A thesis submitted to the Faculty of Graduate Studies and Research in partial  
fulfillment of the degree of

**Doctor of Philosophy**

in

**Water Resources Engineering**

**Department of Civil and Environmental Engineering**

**Edmonton, Alberta**

**Fall, 2002**



National Library  
of Canada

Acquisitions and  
Bibliographic Services

395 Wellington Street  
Ottawa ON K1A 0N4  
Canada

Bibliothèque nationale  
du Canada

Acquisitions et  
services bibliographiques

395, rue Wellington  
Ottawa ON K1A 0N4  
Canada

*Your file Votre référence*

*Our file Notre référence*

The author has granted a non-exclusive licence allowing the National Library of Canada to reproduce, loan, distribute or sell copies of this thesis in microform, paper or electronic formats.

The author retains ownership of the copyright in this thesis. Neither the thesis nor substantial extracts from it may be printed or otherwise reproduced without the author's permission.

L'auteur a accordé une licence non exclusive permettant à la Bibliothèque nationale du Canada de reproduire, prêter, distribuer ou vendre des copies de cette thèse sous la forme de microfiche/film, de reproduction sur papier ou sur format électronique.

L'auteur conserve la propriété du droit d'auteur qui protège cette thèse. Ni la thèse ni des extraits substantiels de celle-ci ne doivent être imprimés ou autrement reproduits sans son autorisation.

0-612-81268-5

**Canada**

University of Alberta

Library Release Form

Name of Author: Purushottam Raj Singh

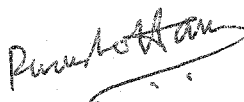
Title of Thesis: Semi-Distributed Snowmelt Modeling and Regional Snow Mapping using Passive Microwave Radiometry

Degree: Doctor of Philosophy

Year this Degree Granted: 2002

Permission is hereby granted to the University of Alberta Library to reproduce single copies of this thesis and to lend or sell such copies for private, scholarly or scientific research purposes only.

The author reserves all other publication and other rights in association with the copyright in the thesis, and except as herein before provided, neither the thesis nor any substantial portion thereof may be printed or otherwise reproduced in any material form whatever without the author's prior written permission.



Purushottam Raj Singh  
5/785, Basantpur  
Kathmandu  
Nepal

Date: August 16, 2002

University of Alberta

Faculty of Graduate Studies and Research

The undersigned certify that they have read, and recommend to the Faculty of Graduate Studies and Research for acceptance, a thesis entitled "Semi-Distributed Snowmelt Modeling and Regional Snow Mapping using Passive Microwave Radiometry" submitted by Purushottam Raj Singh in partial fulfillment of the requirements for the degree of Doctor of Philosophy in Water Resources Engineering.



Dr. Thian Yew Gan (Supervisor)



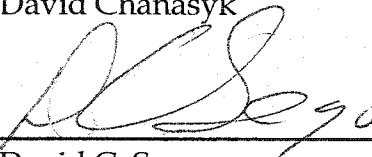
Dr. Nallamuthu Rajaratnam (Committee  
Chair and Examiner)



Dr. David G. Tarboton (External Examiner)



Dr. David Chanasyk



Dr. David C. Segó



Dr. Kevin Shook

Date: August 16, 2002

**Dedicated To My Father and Mother**

**Mr. Indra Raj Singh and Mrs. Rama Devi Singh**

## Abstract

Two semi-distributed snowmelt models (SDSM-MTI and SDSM-EBM) developed to model the basin-scale snow accumulation and ablation processes at sub-basin scale, were applied to the Paddle River Basin (PRB) of central Alberta. SDSM-MTI uses a modified temperature index approach that consists of a weighted average of near surface soil ( $T_g$ ) and air temperature ( $T_a$ ) data. SDSM-EBM, a relatively data intensive energy balance model accounts for snowmelt by considering (a) vertical energy exchange in open and forested area separately; (b) snowmelt in terms of liquid and ice phases separately, canopy interception, snow density, sublimation, refreezing, etc, and (c) the snow surface temperature. Other than the “regulatory” effects of beaver dams, both models simulated reasonably accurate snowmelt runoff, SWE and snow depth for PRB. For SDSM-MTI, the advantage of using both  $T_a$  and  $T_g$  is partly attributed to  $T_g$  showing a stronger correlation with solar and net radiation at PRB than  $T_a$ .

Existing algorithms for retrieving snow water equivalent (SWE) from the Special Sensor Microwave/Imager (SSM/I) passive microwave brightness temperature data were assessed and new algorithms were developed for the Red River basin of North Dakota and Minnesota. The frequencies of SSM/I data used are 19 and 37 GHz in both horizontal and vertical polarization. The airborne gamma-ray measurements of SWE for 1989, 1988, and 1997 provided the ground truth for algorithm

development and validation. Encouraging calibration results are obtained for the multivariate regression algorithms and dry snow cases of the 1989 and 1988 SSM/I data (from DMSP-F8). Similarly, validation results e.g., 1988 (1989 as calibration data), 1989 (1988 as calibration data), and 1997 (from DMSP-F10 and F13), are also encouraging. The non-parametric, Projection Pursuit Regression technique also gave good results in both stages. However, for the validation stage, adding a shift parameter to all retrieval algorithms was necessary because of possibly different scatter-induced darkening, which could arise even for snowpacks of the same thickness because snowpacks undergo different metamorphism in different winter years.

## ACKNOWLEDGMENTS

First and foremost, I express my sincere gratitude to my advisor Dr. Thian Yew Gan for his guidance, input, time and invaluable support from the very first day in the University of Alberta to date. It has been a very fruitful experience working with him.

I am indebted to Dr. Nallamuthu Rajaratnam for his enthusiastic and inspirational lectures, kind support at different times, invaluable advices and for serving as the chair of the thesis examining committee. I express my sincere gratitude to Dr. D. G. Tarboton, Dr. D. C. Sego, Dr. D. Chanasyk, and Dr. K. Shook for their valuable comments, suggestions, and for serving as members of the thesis examining committee.

I express my sincere thanks to Mr. Otto Mahler of Alberta Environment for his kind help in providing streamflow, snow pillow, and snow course data in time. Mr. Walter Flueck has been very helpful in keeping me informed about the beaver activities in the study area. I am also thankful to Mr. Russell Merz of Golder Associates Ltd., Abbotsford for his constant moral support.

I am very pleased to meet and share some moments with Dr. S. C. Colbeck, Dr. J. W. Pomeroy, Dr. L. S. Kutchment, Dr. G. W. Kite, Dr. R. Granger, Dr. B. E. Goodison, and others working in the field of hydrology during number of scientific conferences. Timely responses to my inquiries and requests from Dr. G. Blöschl, Dr. C. H. Luce, Dr. T. Yamazaki, Dr. G. E. Liston, Dr. J. P. Hardy, Dr. N. K. Tuteja, Dr. A. Chang, Dr. D. K. Hall, Dr. W. Abdalati, Dr. V. Lakshmi, and Dr. B. J. Choudhury are gratefully acknowledged.



I am extremely grateful to all the staffs and friends from our Blench Hydraulics Lab past and present, who have helped me with my work and goal. Perry deserves thanks for his immediate help with computer facilities and Getu for his all time helping attitude. I would like to thank Arbind Mainali, Sharad Chitrakar, Rajendra Gurung, and all the friends and families, who have provided invaluable input and pleasant company during some of the stressful moments.

Special thanks go to my friends Gandhi R. Kafle, Shiva B. Prajapati, and Ai B. Gurung for their encouragement, warm and loving friendship they provided across many thousand miles that separates us.

My parents, Jethiama, and all the family members have been with me every step of the way. I am grateful for their all time guidance, encouragement, and prayerful support. My father Indra Raj Singh, late elder father Bashudev Raj Singh, and brother Bishwa Raj Singh have always been the greatest source of inspiration in my life. To my wife Archana, thank you for all the loving support and patience. To my sons Arpan and Ayush, thank you so much for your love and understanding.

Last but not least, I would like to acknowledge the University of Alberta Ph.D. Scholarship without which I would not have even thought of coming to Canada. This research was also partly supported by an equipment and an operating grants of the NSERC of Canada.

# Table of Contents

## **Chapter 1 Introduction, Literature Review, Research Objectives, and Site Description**

1.1	Introduction.....	1
1.2	Literature Review.....	4
1.2.1	Regression Models.....	4
1.2.2	Lumped, Conceptual Models.....	5
1.2.3	Distributed Models.....	9
1.2.4	Vegetation Index.....	11
1.2.5	Surface Temperature.....	11
1.2.6	Surface Albedo.....	12
1.3	Research Objectives.....	13
1.4	Description of Study Site.....	14
1.5	Organization of Thesis.....	16
	References.....	16

## **Chapter 2 Semi-Distributed Snowmelt Model (SDSM) using Remote Sensing Data, I. Model Development**

2.1	Introduction.....	28
2.2	Model Components of SDSM.....	33
2.2.1	Transformation of Precipitation into Rain and Snow.....	33
2.2.2	Canopy and Snow Interception.....	34
2.2.3	Snow Redistribution and Air Temperature Adjustment.....	36
2.2.4	One-Dimensional Snowpack Energy and Mass Balance.....	37
2.2.4.1	Energy Fluxes at the Snowpack.....	39
2.2.4.2	Computation of Snowpack Water Balance.....	56
2.2.5	Snowmelt for each Sub-Basin.....	60
2.3	Developing SDSM within DPHM-RS.....	60

2.4	Division of a River Basin into Sub-Basins and Response Functions.....	60
2.5	Evaluation of Model Performance.....	61
2.6	Model Organization.....	62
2.7	Summary.....	63
	References.....	64

**Chapter 3    Semi-Distributed Snowmelt Model, Energy Balance Method (SDSM-EBM) using Remote Sensing Data, II. Application to the Paddle River Basin, Alberta**

3.1	Introduction.....	86
3.2	Data Description.....	88
3.2.1	Ground Based Data.....	88
3.2.1.1	Meteorological Data.....	88
3.2.1.2	Snow Course Data.....	89
3.2.1.3	Streamflow Data.....	90
3.2.1.4	Soil Data.....	90
3.2.1.5	Throughfall.....	90
3.2.2	Remote Sensing Data.....	90
3.2.2.1	Land Cover Class.....	91
3.2.2.2	Surface Albedo.....	92
3.2.2.3	Vegetation Index.....	94
3.2.2.4	Surface Temperature.....	94
3.2.2.5	Topographic Data.....	98
3.2.3	General Characteristics of Winter Data.....	98
3.3	Model Parameter Estimation.....	99
3.4	Discussion of the Results.....	101
3.4.1	Model Calibration and Validation.....	101
3.4.1.1	Basin Runoff Hydrograph.....	102
3.4.1.2	Snow Depth and Snow Water Equivalent.....	106
3.4.1.3	Surface Temperature.....	108

3.5	Summary and Conclusions.....	110
	References.....	111

**Chapter 4    A Semi-distributed, Modified Temperature Index Approach for  
Modeling Snowmelt in the Canadian Prairies using Near Surface  
Soil and Air Temperature**

4.1	Introduction.....	141
4.2	Research Objective.....	145
4.3	Paddle River Basin (PRB).....	145
4.4	Modified Temperature Index Method.....	147
4.5	Semi-Distributed Approach.....	149
4.6	Description of Data.....	150
	4.6.1 General Characteristics of Meteorological Data.....	151
4.7	Discussion of Results: Model Calibration and validation.....	154
	4.7.1 Runoff at Basin Outlet.....	155
	4.7.2 Snow Water Equivalent and Snow Depth.....	158
4.8	Summary and Conclusions.....	160
	References.....	161

**Chapter 5    Retrieval of Snow Water Equivalent using Passive Microwave  
Brightness Temperature Data**

5.1	Introduction.....	175
5.2	Research Objectives.....	178
5.3	Description of Study Site and Data.....	178
5.4	Existing Algorithms.....	179
5.5	Proposed Algorithms.....	182
5.6	Discussion of Results.....	185
5.7	Summary and Conclusions.....	190
	References.....	191

<b>Chapter 6</b>	<b>Summary, Conclusions and Recommendations for Future Works.....</b>	<b>203</b>
	References.....	207
	<b>Appendix.....</b>	<b>208</b>
A	Calibration of AVHRR Data in Channels 1 and 2 for Albedo Retrieval.....	208
B	Stability of Atmosphere.....	210
C	Geophysical Parameters derived from AVHRR Data.....	214
D	Historical Snow Course Data and Climate Trends.....	218
E	Atmospheric Attenuation Model for Microwave Remote Sensing Data....	222
F	Field Observations of Paddle River Basin.....	225

## List of Tables

Table 1.1	Summary of data collection for the study.....	25
Table 2.1	General characteristics of selected distributed and semi-distributed snowmelt models .....	77
Table 2.2	Coefficients of Eq. (2.31) (after Dery and Yau, 2001).....	79
Table 2.3	Coefficients of different versions of the force restore method.....	79
Table 2.4	Statistical criteria used in SDSM to evaluate simulated basin outflows.....	80
Table 3.1	Summary of data used in SDSM-EBM.....	116
Table 3.2a	Summary of snow course survey (SCS) data for 1998, 1999, and 2000 winters (snow depth in cm, SWE in mm) .....	117
Table 3.2b	Standard deviation of observed snow depth data for three winters.....	117
Table 3.3	Characteristics of NOAA-AVHRR satellite data.....	118
Table 3.4	Five zones (sub-basins) of Paddle River Basin (Figure 3.1a), their land use classification and corresponding area used in the SDSM.....	118
Table 3.5	Equations to retrieve albedo and spectral radiance from NOAA-AVHRR (NOAA-14 spacecraft) satellite data.....	119
Table 3.6	Surface albedo retrieved from NOAA-AVHRR for different land cover classes in each sub-basins of PRB.....	120
Table 3.7	Relationship between NDVI and Leaf Area Index (LAI) for different landuse classes.....	121
Table 3.8	AVHRR derived NDVI for different land cover classes in each sub-basins of PRB.....	122
Table 3.9	Scene surface temperature ( $T_s$ , in °K) retrieved from NOAA-AVHRR for different land classes in each sub-basins of PRB..	123

Table 3.10	Model parameters used in SDSM-EBM (1-16), and some of the important parameters used in DPHM-RS (17-19) .....	124
Table 4.1	Comparison of correlation coefficients ( $\rho$ ) between cumulative air temperature ( $\sum T_a$ ), cumulative near surface soil temperature ( $\sum T_g$ ), measured net ( $\sum R_n$ ) and solar radiation ( $\sum R_{sol}$ ) for selected winter periods in PRB such that $T_g$ was at or below freezing temperature.....	165
Table 4.2	Comparison of correlation coefficients ( $\rho$ ) between cumulative air temperature ( $\sum T_a$ ), cumulative near surface soil temperature ( $\sum T_g$ ), measured net ( $\sum R_n$ ) and solar ( $\sum R_{sol}$ ) radiation for selected winter periods in PRB used for calibrating and validating SDSM-MTI such that $T_g$ was either below, at or above freezing temperature.....	165
Table 4.3	Model parameters used in SDSM-MTI (1-12), and some of the important parameters used in DPHM-RS (13-15) .....	166
Table 5.1	Ascending and descending equatorial overpass (local) times of the SSM/I data of three DMSP satellites used in this study..	194
Table 5.2	Details of SWE estimated from airborne gamma-ray data.....	194
Table 5.3	Physiographic and atmospheric data used in this study.....	195
Table 5.4	Coefficients derived for the Proposed Algorithms [Eqs. (5.6) and (5.7)] .....	195
Table 5.5	Weekly maximum and minimum air temperature ( $^{\circ}\text{C}$ ) of Red River Basin study area covering the airborne SWE data collection periods of 1988, 1989 and 1997.....	196
Table 5.6	Mean monthly and annual precipitation (cm) of Red River Basin.....	196
Table 5.7	Summary of calibration and validation results of proposed algorithms [Eqs. (5.6) to (5.8)] .....	197
Table C.1	AVHRR derived average surface albedo for three different land cover classes used in SDSM for 1997-98, 1998-99, and 1999-00 winters.....	215
Table C.2	AVHRR derived average LAI for three different land cover classes used in SDSM for 1997-98, 1998-99, and 1999-00 winters.....	216

Table C.3	AVHRR derived average surface temperature (°K) for different land cover classes used in SDSM for 1997-98, 1998-99, and 1999-00 winters.....	217
Table D.1	Statistics of snow course data for Paddle River Headwaters snow pillow site.....	219
Table D.2	Statistics of snow course data for Mayerthorpe snow pillow site.....	220
Table D.3	Regional precipitation and temperature departure for the period 1948-2000.....	221



## List of Figures

Figure 1.1	Modeling concepts in the field of snow hydrology (a) lumped or point model, (b) fully-distributed model, and (c) semi-distributed model.....	26
Figure 1.2	Location map of the Paddle River Basin (PRB) .....	27
Figure 2.1	Energy fluxes involved during snow accumulation and snowmelt processes considered in SDSM.....	81
Figure 2.2	Snow model physics and parameterization in SDSM.....	82
Figure 2.3	Schematic diagram of snow surface temperature ( $T_s$ ) and snowpack water content ( $W$ ) profiles in Kondo and Yamazaki Method (KYM).....	82
Figure 2.4	Schematic diagram of SDSM-EBM, a snow accumulation and snowmelt model.....	83
Figure 2.5	Flow chart of DPHM-RS model.....	84
Figure 2.6	The average response function per unit rainfall or snowmelt excess for a sub-basin based on the kinematic wave theory and eight flow directions.....	85
Figure 3.1	(a) Five sub basins (1 to 5) of Paddle River Basin and its drainage network derived from DTED. H, M, and S are locations of streamflow gauge at the basin outlet, meteorological tower, and snow pillow site respectively; (b) Landuse classification of PRB derived from Landsat-TM image of August 7, 1996.....	125
Figure 3.2	Diurnal pattern of meteorological data: (a) air temperature, (b) ground temperature, (c) net radiation, (d) ground heat flux, (e) global solar radiation, and (f) wind speed measured at PRB for the 1998 winter from January 1 to April 30, 1998.	126
Figure 3.3	Diurnal pattern of meteorological data: (a) air temperature, (b) ground temperature, (c) net radiation, (d) ground heat flux, (e) global solar radiation, and (f) wind speed measured at PRB for the 1998/99 winter from October 1, 1998 to May 28, 1999.....	127
Figure 3.4	Diurnal pattern of meteorological data: (a) air temperature, (b)ground temperature, (c) net radiation, (d) ground heat	

	flux, (e) global solar radiation, and (f) wind speed measured at PRB for the 1999/00 winter from October 1, 1998 to May 28, 2000.....	128
Figure 3.5	PRB's precipitation data (water equivalent) for three winters (a) 1997/98, (b) 1998/99, and (c) 1999/2000 .....	129
Figure 3.6	PRB's hourly streamflow hydrographs at the WSC station 07BB011 near Anselmo for (a) 1998, (b) 1999, (c) 2000 winters, (d) PRB's daily average streamflow hydrograph at the WSC station 07BB011 near Anselmo for 1980-1993, (e) Unit hydro graphs for each of the five zones of PRB for different combinations of Manning's roughness: 'n1' for the forest and 'n2' for the open area.....	130
Figure 3.7	Comparison of SDSM-EBM simulated and observed runoff at the outfall of Paddle River basin (PRB): (a) for the calibration stage (Nov. 11, 1998 to May 16, 1999) using (a.1) Force Restore Method or FRM and (a.2) Snow Conductance Method SCM; (b) for the validation stage (Jan. 1, 1998 to Apr. 30, 1998) using (b.1) FRM and (b.2) SCM; and (c) for another validation stage (Jan. 1, 2000 to Apr. 30, 2000 using (c.1) FRM and (c.2) SCM .....	132
Figure 3.8	Comparison of SDSM-EBM simulated and observed SWE and snow depth (SD) for Zone 4 at the calibration stage (Nov. 11, 1998 to May 16, 1999) with maximum snow density $\rho_{\max}=250$ and $200 \text{ kg/m}^3$ using: (a) Force Restore Method or FRM for (a.1) Open Area (OA), (a.2) Deciduous Forest (DF), and (a.3) Coniferous Forest (CF); and (b) Snow Conductance Method or SCM for (b.1) OA, (b.2) DF, and (b.3) CF.....	133
Figure 3.9	Comparison of SDSM-EBM simulated and observed SWE and snow depth (SD) for Zone 4 with maximum snow density $\rho_{\max} = 200 \text{ kg/m}^3$ for the Open Area (OA), and Coniferous Forest (CF) at the validation stages: (a) Jan. 1, 1998 to Apr. 30, 1998 using (a.1) Force Restore Method or FRM, and (a.2) Snow Conductance Method or SCM; (b) Jan. 1, 2000 to Apr. 30, 2000 using (b.1) FRM, and (b.2) SCM.....	134
Figure 3.10	Comparison of SDSM-EBM simulated and observed SWE and snow depth (SD) for Zones 2 and 3 with maximum snow density $\rho_{\max} = 250 \text{ kg/m}^3$ for the Open Area (OA), and Deciduous Forest (DF) at the calibration stage (Nov. 11, 1998 to May 16, 1999) using (a) Force Restore Method or	

	FRM, and (b) Snow Conductance Method or SCM .....	135
Figure 3.11	Comparison of snow surface temperature (°K) retrieved from NOAA-AVHRR images in different land cover classes (Open Area or OA and Deciduous Forest or DF) of PRB with simulated counterparts of SDSM-EBM (FRM) for the calibration period in hours (a.1 and b.1) Early part of winter from Nov 26, 1998 to Jan 29, 1999 and (a.2 and b.2) later part of winter from Feb 13 to Apr 18, 1999 .....	136
Figure 3.12	Comparison of snow surface temperature (°K) retrieved from NOAA-AVHRR images in different land cover classes (Open Area or OA and Deciduous Forest or DF) of PRB with simulated counterparts of SDSM-EBM (Surface Conductance Method or SCM) for the calibration period in hours (a.1 and b.1) Early part of winter from Nov 26, 1998 to Jan 29, 1999 and (a.2 and b.2) later part of winter from Feb 13 to Apr 18, 1999.....	137
Figure 3.13	Comparison of snow surface temperature (°K) retrieved from NOAA-AVHRR images in different land cover classes (Open Area or OA and Deciduous Forest or DF) of PRB with simulated counterparts of SDSM-EBM (Kondo and Yamazaki Method or KYM) for the calibration period in hours: (a.1) and (b.1) Early part of winter from Nov 26, 1998 to Jan 29, 1999; and (a.2) and (b.2) later part of winter from Feb 13 to Apr 18, 1999.....	138
Figure 3.14	Comparison of snow surface temperature (°K) retrieved from NOAA-AVHRR images in different landuse classes of PRB with model simulated counterparts of SDSM-EBM using different methods: (a.1 and a.2) FRM; (b.1 and b.2) SCM; and (c.1 and c.2) KYM in the validation winter year 1998.....	139
Figure 3.15	Comparison of snow surface temperature (°K) retrieved from NOAA-AVHRR images in different landuse classes of PRB with model simulated counterparts of SDSM-EBM using different methods: (a.1 and a.2) FRM; (b1 and b2) SCM; and (c.1 and c.2) KYM in the validation winter year 2000.....	140
Figure 4.1	Location map of Paddle River basin in the Mackenzie GEWEX Study area (MAGS).....	167
Figure 4.2	PRB's meteorological data during the validation period of 1997/98 winter.....	168

Figure 4.3	PRB's meteorological data during the calibration period of 1998/99 winter.....	169
Figure 4.4	PRB's meteorological data during the validation period of 1999/00 winter.....	169
Figure 4.5	The concept of reference temperature, " $T_r = T_a + (1-\chi)T_g$ " used in the modified temperature index method of SDSM (or SDSM-MTI) .....	170
Figure 4.6	Melt Rate Factor ( $MRF = (M_{rf})^\psi$ ) for different near surface soil temperature ( $T_g$ in °C) and $M_{rf}$ exponent $\psi = 0.25, 0.5, 0.75, 1, 1.5, \& 2.0$ .....	170
Figure 4.7	Comparison of SDSM-MTI simulated and observed streamflow for PRB at the calibration ( <i>Cal</i> ) (Nov. 11, 1998 to May 16, 1999) and the validation ( <i>Val</i> ) stages (Jan. 1, 1998 to Apr. 30, 1998 and Jan. 1, 2000 to Apr. 30, 2000), such that there is no change of calibrated parameters: (a.1) for <i>Cal</i> and (b.1 and c.1) for <i>Val</i> ; with $\chi$ set to 1 but other parameters unchanged (i.e. $T_g$ is partially ignored): (a.2) for <i>Cal</i> and (b.2) for <i>Val</i> ; with $\chi$ set to 1 and $\psi$ set to 0 but other parameters unchanged (i.e. $T_g$ is completely ignored): (a.3) for <i>Cal</i> and (b.3) for <i>Val</i> ; and (d.1) is similar to (b.1) but with slightly reduced melt factors and $\psi$ set to 1 .....	171
Figure 4.8	Comparison of SDSM-MTI simulated and observed SWE and snow depth (SD) for Zone 4: at the calibration stage (Nov. 11, 1998 to May 16, 1999) with maximum snow density $\rho_{max} = 250$ and $200 \text{ kg/m}^3$ for (a.1) Open Area (OA) and (a.2) Coniferous Forest (CF); at the validation stages (Jan. 01 to Apr. 30) for OA and CF (b) 1998 with $\rho_{max} = 150 \text{ kg/m}^3$ and (c) 2000 with $\rho_{max} = 200 \text{ kg/m}^3$ ; and zone 2 and 3 at calibration stage with $\rho_{max} = 250$ for (d) OA and (e) CF.....	172
Figure 4.9	Comparison of SDSM-MTI simulated and observed SWE and snow depth (SD) in zone 4: at the calibration stage (Nov. 11, 1998 to May 16, 1999) with $\rho_{max} = 250$ and $200 \text{ kg/m}^3$ for (a.1) $\chi=1$ and $\psi=2$ , and other parameters unchanged, (a.2) $\chi=1$ and $\psi=0$ , and other parameters unchanged; similar results at the validation stages: (b) Jan. 01 to Apr. 30, 1998, and (c) Jan. 01 to Apr. 30, 2000.....	173
Figure 4.10	Comparison of PRB's simulated streamflow using SDSM-MTI and SDSM-EBM in both calibration stage of 1998/99	

	winter (Nov. 11, 1998 to May 16, 1999) and validation stages of 1998 and 2000 winters (Jan. 1 to Apr. 30) .....	174
Figure 5.1	The Red River basin study area of eastern North Dakota and northwestern Minnesota.....	198
Figure 5.2	Cumulative snowfall at the end of each month for three winter periods of Red River Basin.....	198
Figure 5.3	The calibration results for the projection pursuit regression model expressed in terms of the fraction of unexplained variance (U) versus the number of terms (Mo) using screened, ascending overpass SSM/I data of 1989.....	198
Figure 5.4	Plots of combined results (calibration and validation) of proposed algorithms without (b, e, h) and with shift parameters (c, f, i), and their comparisons with existing algorithms (a, d, g) based on screened, morning/nighttime overpass SSM/I data of 1988, 1989, and 1997. The three plots (j, k, l) of SWE derived from existing algorithms based on screened, evening overpass SSM/I data show very poor correlation with observed SWE.....	199
Figure 5.5	Scatterplots of observed SWE versus retrieved from 1997 TB data of DMSP F10, ascending (a.1 to a.4) and descending (b.1 to b.4), and DMSP-F13 descending (c.1 to c.4), based on existing (Eqs. 5.1 and 5.2) and proposed (Eqs. 5.6 and 5.7) algorithms. The fairly significant scatters found in all the plots are mainly attributed to SSM/I data only screened from wet snow cases but not cases affected by depth-hoar.....	200
Figure 5.6	Scatter induced darkening ( $\Delta TBo$ ) versus scattering albedo ( $w_o$ ) for various thicknesses (D) of dry fresh snowpack at 273 K, a case of free space microwave wavelength ( $\lambda$ ) of 10 cm (adapted from England, 1975) .....	201
Figure 5.7	A marked improvement in the retrieved SWE of existing algorithms (Eqs. 5.1, 5.2 and 5.5) results when appropriate shift parameters (SP) are added (compare a.1 to a.3 with b.1 to b.3 plotted against Eq. 5.6, and c.1 to c.3 plotted against observed SWE). The SP used for Eq. (1) are 5cm for 1989 and 9cm for 1997 (as in Eq. 5.7) and that for Eqs. (5.2) and (5.5) are -5cm for 1988 and 4cm for 1997 (as in Eq. 5.6) .....	202

## List of Plates

Plate F.1	Paddle River Basin's (a) meteorological towers, (b) snow pillow site at Paddle River H.W., and (c) snow course survey in different land cover classes.....	226
Plate F.2	Strategic locations of beaver dams observed in the Paddle River Basin (a) Highway 751 south of snow pillow site, (b) north of highway 649, (c) just upstream of WSC streamflow gauge station .....	227
Plate F.3	Details of overflow beaver dam upstream of a twin-culvert in Highway 751, south of snow pillow site, (a) a close view of an upstream and downstream end of culvert, (b) large impounding water body looking towards north-west, (c) impounding water body looking towards south.....	228

# **Chapter 1**

## **Introduction, Literature Review, Research Objectives, and Site Description**

### **1.1 Introduction**

Land masses at high latitudes are extensively covered with snow especially during late autumn, winter and early spring. Further, the snow accumulation and melt processes form an integral part of regional hydrology. Since snow produces substantial changes in the surface characteristics and the atmosphere is sensitive to physical changes of the earth surface, its presence over large areas of the earth for at least portion of the year exerts an important influence on the climate, both locally and globally. Therefore, a better knowledge of snowcover and snow water equivalent over large regions will lead to a better understanding of our climate, and will improve the estimation of spring runoff and allow better management of water resources.

On an annual basis, in the Northern Hemisphere, the percentage of land area covered by snow ranges from 7 to 40% per month (Hall, 1988). With its high

albedo, low thermal conductivity, and considerable spatial and temporal variability, the seasonal snowcover plays a key role in governing the Earth's global radiation balance, which is the primary driver of the Earth's atmospheric circulation (Liston and Sturn, 1998).

Accurate estimation of the basin-scale snow water equivalent (SWE) is still a great challenge. This is a more difficult problem in the wind swept alpine zones of Canada where blowing snow is a dominant winter phenomenon. Important physiographic and climatic factors that influence the distribution of snow are latitude, elevation, slope, aspect, orographic features, and vegetation cover. Recent studies (e.g. Goodison and Walker, 1994; Matzler, 1994; Gan, 1996; Foster et al., 1997; Tait, 1998; Singh and Gan, 2000) have shown that passive microwave data can provide useful information on the distribution of SWE but they are mainly applicable to large basins because of the coarse resolution of passive microwave footprints ( $\approx 25$  km) of Special Sensor Microwave Imager (SSM/I) currently available to the research community.

Even though only approximately one-third of the annual precipitation in the semi-arid Canadian Prairies occurs as snowfall, the spring snowmelt can generate up to 80% of its annual surface runoff (Granger and Gray, 1990). This runoff provides water for municipal water supply, irrigation, groundwater recharge, wildlife habitat etc., but it can also cause serious flooding and soil erosion problems. Therefore, the timing of spring snowmelt is an important climatic and hydrologic factor affecting the Canadian Prairies' water resources. Many operational snowmelt models, such as the Sacramento snowmelt model, use the standard degree-day approach to compute spring snowmelt. Such models generally rely on a daily air temperature, optimized melt factors, and an areal depletion curve. Some newer models incorporate satellite images to update its areal distribution instead of solely relying on an areal depletion curve (e.g., Martinec et al., 1983). The degree-day method is simple but deficient



because snowmelt also depends on factors such as topography, landuse/land cover and spatial and temporal distribution of atmospheric forcings associated with both radiation and turbulent heat fluxes.

Besides winter precipitation and air temperature, processes such as, that associated with the effects of topography (altitude, aspect, forest cover etc.) on solar radiation, densification of snow, blowing snow sublimation, local advection, etc. are responsible for the spatial and temporal variations of snow depth and SWE. Knowing these major processes will help better understand the strong interactions between the atmospheric processes and snow hydrology. The effect of snow drifting is also important because it is a primary control on the spatial distribution of SWE particularly in an open environment (Luce et al., 1998a). An adequate parameterization scheme of snow drifting and blowing snow based on the topography, vegetation cover and wind vector may achieve a good approximation of the spatial variability of snow accumulation. Recent developments in distributed hydrological modeling have recognized the general importance of redistributing snow within the basin for predicting basin snowmelt (Pomeroy et al., 1997; Luce et al., 1998a; Liston and Sturn, 1998; Hartman et al., 1999; Dery and Yau, 2001a&b). Hartman et al (1999) used a topographic similarity index to re-distribute snow. Dery and Yau (2001a) developed a non-linear regression equation to parameterize the blowing snow sublimation rate using wind speed and condensation growth parameter.

Past research has also demonstrated the importance of turbulent diffusion or local advection in the energy balance of late-lying snowfields, when bare patches appear in snow covered areas (Weisman, 1977; Olyphant, 1988; Shook, 1995; Liston, 1995). Parameterization of local advection in terms of increased melt rate based on the fraction of open area covered by snow ( $A_F$ ) in each sub-basin is possible from the Landsat-Thematic Mapper (TM), which has a spatial resolution of about 30 m.

The seasonally snow-covered area of each sub-basin can also be related to the ratio of snow depth and the threshold snow depth at which patchy snowcover just starts, which is similar to the concept of the depletion curve of Luce et al. (1998b) and Verseghy (1991).

## **1.2 Literature review**

Ideally, modeling snowmelt runoff should account for the snowmelt process occurring at the snow surface, the meltwater movements through the snowpack, and the routing of meltwater over the ice surface, bare patches of snowcover and the interconnected channel network. . At a basin scale, the overland flow process is essential (Sand, 1990). A popular research theme for snow hydrology is to explore modeling the melt rate by energy balance of the snowpack, the meltwater transport by infiltration through snow as a porous medium or unsaturated vertical flow through the snowpack ( Colbeck, 1971), and/or some form of distributed kinematic wave routing of a thin saturated layer at the base of the snowpack over the combinations of land and ice surfaces (Dunne et. all, 1976), where roughness coefficients could vary spatially and temporally at basin scale.

### **1.2.1 Regression Models**

Though non-linear relations can improve the prediction of the seasonal snowmelt runoff versus that from linear models, their use is limited by the failure of transformed data satisfy the condition of nonlinearity (Dey et al., 1992). The simplest form of snowmelt model is probably the linear regression model, where a linear empirical relationship is assumed between predictive variables and the snowmelt runoff from a catchment for at least several or more snowmelt seasons. To establish a snowmelt runoff regression model may be harder than a rainfall-runoff regression model possibly because of the greater dependence of snowmelt on atmospheric forcings than rainfall-runoff processes. For a basin of 106 km<sup>2</sup> in

Scotland, Ferguson (1984) developed two equations for two melt seasons using maximum air temperature, time from the onset of melt, and the previous day's flow. Interestingly, the coefficients were not the same from year to year and so their applications were limited.

For regression models, Zuzel and Cox (1975) found that daily air temperature gave the best result if only one meteorological variable was used, and the combination of variables that gave the best result was daily vapor pressure, wind run and net radiation, while Kussisto (1978) regressed snowmelt with air temperature and radiation. However, such models are highly site-specific and the results from one site are not transferable to other sites. Further, the assumption of linear relationships between these variables is probably not true because of the complex physical processes involved in the snowmelt.

## **1.2.2 Lumped, Conceptual Models**

The term "lumped" means that these models only deal with the mean properties of the snowpack and processes at a point, without considering spatial variability in detail (Figure 1.1a). Further, complex physical processes are simplified. However such models are widely applicable and preferred over regression models as operational snowmelt runoff models. Such models for basin-scale catchments could be implemented in a quasi-distributed manner, such as using different melt rates and input variables to different elevation bands of the catchments (Morris, 1985). Two major types of lumped conceptual models are discussed below.

### **1.2.2.1 Temperature Index (or Degree Day) Models**

Air temperature is the most commonly used index for estimating snowmelt. This is for two reasons: first, air temperatures are among the most readily available climate data. Secondly, many studies have shown that air temperature is the best single index to represent the amount of energy available for snowmelt (Anderson, 1973).

This method is often used when a simpler model is preferred, or when the available data are too limited to apply the energy balance equation.

Many operational snowmelt runoff models, such as the National Weather Service River Forecast System, NWSRFS or Sacramento snowmelt model (Anderson, 1973), HBV (Bergstorm, 1975), UBC model developed at the University of British Columbia (Quick and Pipes, 1977), CEQUEAU model developed at the Université du Québec (Charbonneau et al., 1977) and the Snowmelt Runoff Model, SRM (Martinec et al., 1983) use the temperature index (degree-day) approach. In this approach, the snowmelt rate estimated depends on the daily air temperature, some optimized melt factors, and a depletion curve that relates the mean areal snow water equivalent to the extent of snow cover empirically. These models use a different melt factor for each elevation band or basin zone, to reflect the vegetation characteristics and mean elevation of each zone. Some of these models, such as the UBC, CEQUEAU and NWSRFS, METQ98 (Ziverts and Jauja, 1999) also allow the melt factor to vary through the melt season. However, the degree-day approach may not adequately account for many climatic factors related to snowmelt. For example, Male and Granger (1981) showed that in open non-forested areas the short wave radiation exchange is the dominant melt-producing energy flux, but short wave radiation exchange was poorly correlated with air temperature. Kane et al. (1997) also tried to modify the simple temperature index snowmelt model by including wind speed. However, no improvement was found in terms of model response, which was possibly because of the mixed effects of wind in the Arctic environment where cold air blown from the north off the Arctic ocean and warm and dry air from the south.

The assumption of a uniform snow accumulation over the whole elevation range followed by a uniform snowmelt according to an assumed areal-depletion curve is not applicable to a mountainous basin (Martinec, 1980). In this case, the snow

coverage in that whole elevation range would of course remain at 100% and then drop abruptly to zero. The Snowmelt Runoff Model or SRM of Martinec (1985) uses satellite images to update its areal snowcover distribution and not solely relying on an areal depletion curve like the NWSRFS. Besides climate, the snowmelt process depends also on factors like terrain characteristics, vegetation types, and even the fraction of snow cover on ground. Using the degree-day method for a Northern Swedish catchment, Bengtsson (1982) presented the importance of nighttime refreezing on the diurnal snowmelt cycle. Gray and Landine (1988) proposed an energy budget snowmelt model (EBSM) for the Canadian Prairie, in which all the energy flux components are related empirically with the standard climatological measurements. They found that the EBSM model generally improved the snowmelt runoff simulation compared to degree-day methods. Sand (1990) applied the simple degree-day method and data-intensive surface energy models to both temperate and arctic regions and found that only the energy balance is applicable to all the test regions. Kane et al. (1997) applied three models (surface energy balance, degree-day temperature index, and the combined degree-day temperature/radiation index) to an Alaska watershed. They found that all three models perform very well, with the energy balance model being the best.

### **1.2.2.2 Energy Balance Models**

If various energy components are explicitly considered in a model, the model is an energy balance model. There is a wide range of such energy based snowmelt models, depending on which components are being measured directly, and which components are estimated empirically. The temperature index models are generally effective under normal climatic conditions if model parameters are calibrated from a representative calibration data. However, for extreme conditions (Anderson, 1976) such as very warm temperatures and little wind, low humidity and high winds or clear skies and cool temperature when the snow is ripe, the energy budget models are potentially more accurate.

Large numbers of energy balance snowmelt models with varying degree of complexity have been tested in different part of world (e.g., Anderson, 1968; Bengtsson, 1976; Obled and Rosse, 1977; Male and Granger, 1981; Braun, 1985; Kondo and Yamazaki, 1990; Jordon, 1991; Kustas et al., 1994; Kuchment and Gelfan, 1996; Tarboton and Luce, 1996; Yamazaki, 1998). One of the more widely used, one-dimensional mass and energy balance models is SNTHERM developed by Jordan (1991) for predicting snowpack properties and temperature profiles. SNTHERM calculates energy exchange at the surface and bottom of the snowpack, grain growth, densification and settlement, melting and liquid water flow, heat conduction and vapor diffusion. It accounts for changes in albedo due to grain growth, sun angle and cloud cover but it does not account for the decrease in effective albedo when the snow depth is shallow and when radiation penetrates through the snowpack to the underlying soil. This problem, which Hardy et al. (1997) observed in modeling snow ablation in a forest land of black spruce, aspen and jack pine, has been addressed by using a routine, which automatically reduces the albedo exponentially to the soil albedo when the radiation penetrates through the snowpack to the underlying soil. An estimate of litter fall on the forest floor has also been incorporated through a routine to reduce the sub-canopy snow albedo as forest litter accumulates.

Wigmosta et al. (1994) developed a distributed hydrology-vegetation model, which includes canopy interception, evapotranspiration, snow accumulation and melt, and runoff generation via the saturation excess mechanism. Landuse cover and soil properties are assigned to each digital elevation model (DEM) grid cell. Snow accumulation and melt are simulated using a single layer, energy and mass balance model. They found a significant lagging of simulated snow covers when compared with AVHRR images, partly because the varying responses of snowpack layers were not taken into consideration. Tarboton and Luce (1996) developed a spatially

distributed Utah Energy Balance Snow Accumulation and Melt Model (UEB) where the snowpack is represented by two depth-averaged state variables, snow water equivalent and energy content. The energy content is relative to a reference state of ice at 0°C and is defined as the energy content of the snowpack plus a soil layer underneath that interacts thermally with the snowpack. This procedure provides a simple approximation of the effects of frozen ground, or snow falling on warm ground. This simplified model attempts to match the time of peak of snowmelt runoff but the melt rate seems to be underestimated.

The aforementioned energy balance models do not account directly the effects of two-dimensional patchy snowcover on the local advective energy of melt processes. This limits their applications in the Prairie environment with shallow snowcover (<60 cm) or in late melting periods when turbulent fluxes are more than radiative fluxes. It has been found that the maximum snowmelt rate occurs when the land is only partially snow-covered, and often when it is slightly less than 60% of the basin area (Shook et al., 1993). Because of lower albedo, the bare ground absorbs larger amount of solar radiation than the adjacent snow patches. The energy imbalance induces an advective, turbulent transfer of latent and sensible heat from the bare ground to snow patches, enhancing the melt rate. Since advective melting is the greatest along the leading edge of a snowfield, under constant climatic conditions, the melt rate of a patchy snowcover should be related to the perimeter of the patches (Shook, 1993). A recent study on the local advection of momentum, heat and vapor during the melt of patchy snow cover by Liston (1995) showed a linear increase of melt with decreasing snow covered area for snow covered area greater than 25%, and in a strongly nonlinear fashion below that value.

### **1.2.3 Distributed Models**

Snow accumulation and ablation processes occur over a range of space-time scales in our natural environment (Blöschl and Sivapalan, 1995; Blöschl, 1999).

Distributed snow models attempt to quantify these processes by subdividing the catchment into mesh grids of high resolution. These units can be considered as hydrological response units (Leavesely, 1989) or, square grid elements, and processes with a characteristic length scale smaller than the grid size are represented implicitly (or parameterized) while processes with length scale larger than the grid size are represented explicitly by element-to-element variations (Kirnbauer et al., 1994). While most models use elevation as the primary criterion for spatial discretization, in semi-distributed models a basin is sub-divided into a small number of sub basins but in fully distributed models, a basin is often discretized into many grid cells of reasonably high resolution (Figure 1.1b).

Most distributed snow models assume uniform parameters and processes within each grid element. The processes in each element often include snow surface energy exchange and internal processes such as water and heat transport. The input data to each grid may be interpolated from surrounding observations.

In distributed modeling, the response from each individual element should theoretically be dependent on the surrounding elements but in reality they are assumed to be independent. This is one of the major concerns about applying a fully distributed snow model that ignore interactions between elements found in nature. In summary, distributed modeling involves detailed descriptions of snow processes at point scale (scale of the measurement site), and integrating the point processes to catchment scale through discretization and interpolation.

In the 80's to early 90's, it seems promising to pursue distributed modeling with grid elements of high resolution. However, the problems of excessive input data demand, and the assumptions of no interaction between adjacent grid elements, and with each element assigned the same model parameters render such models mainly for theoretical quest but with little practical value. To strike a balance between



attainable modeling resolution and data availability, it makes sense to model basin-scale snowmelt processes under a semi-distributed approach (e.g., Kite and Kouwen, 1992; Tao and Kouwen, 1989; Kite, 1995a). The semi-distributed model, where a basin is divided into several sub basins/zones/aggregated simulation area, is preferred over the fully-distributed approach because it is less computationally intensive, requires less data, and yet could achieve similar or even better results (Figure 1.1).

### **1.2.4 Vegetation Index**

The leaf area index (LAI) (Running et al., 1986), which is the area of leaves per unit area of ground surface, is one of the most important variables for partitioning energy and precipitation fluxes between plant canopies and soil surface. Therefore, the LAI estimated from satellite data has been used for estimating the interception of precipitation and evapotranspiration by canopy (Kite and Kouwen, 1992; Kite, 1995b; Kite and Spence, 1995; Kustas and Jackson, 1999; Pomeroy et al. 1998). The LAI is often retrieved from the visible and infrared bands of NOAA-AVHRR sensor at 1 km resolution or from Landsat TM at about 30 m resolution (Pietroniro et al., 1995; Emaruchi, 1998, Biftu and Gan, 2001). Kite and Pietroniro (1996) provides useful references with regards to application of remote sensing in hydrological modeling.

### **1.2.5 Surface Temperature**

The computation of upwelling longwave, latent and sensible heat fluxes requires accurate knowledge of the surface or skin temperature (Stroeve and Steffen, 1998). The surface temperature should be known to an accuracy of approximately 1°K in order to estimate the outgoing longwave flux to within 5 W/m<sup>2</sup> (Steffen et al., 1993). Remotely sensed data has been a source of information for skin temperature, based on the thermal spectral (long wave) radiation from the ground. However, the

earth surface is far from a skin or homogeneous surface with two dimensions (Vogt, 1996). Therefore, a mix of different land uses in a basin also complicates the retrieval of surface temperature.

Many studies have been devoted to developing the methodology for retrieving surface temperature from channels 4 and 5 of NOAA-AVHRR data. Qin and Karnieli (1999) extensively reviewed the most popular form of split-window algorithms including those proposed by Price (1984), Becker and Li (1990) and Oettle and Vidal-Madjar (1992). Attempts have also been made to correlate the remotely assessed composite temperature (that includes forest cover) to surface temperature with the help of forest cover fraction (Boegh et al., 1999, Kustas and Jackson, 1999).

### **1.2.6 Surface Albedo**

The importance of surface albedo in computing the earth's radiative balance has often been shown in studies related to our global climate change system (e.g., Sud and Fennessy, 1982; Laval and Picon, 1986; Vukovick et al., 1987; Laine and Heikinheimo, 1996). The surface albedo (or surface reflectivity) determines the availability of net radiation at the earth surface, which is used in different stages of hydrological processes (e.g., evapotranspiration, snowmelt etc.). Snow and ice generally have high reflectance or albedo, which means that regions having winter snowcovers, and relatively warm summer show strong seasonal variation in surface albedo. Point measurement of surface albedo is only meaningful for basins with fairly homogeneous land surface (Brest and Goward, 1987). A realistic estimate of surface albedo at adequate spatial scales over heterogeneous catchments of regional scale is only achievable via satellite measurement. Both Landsat-TM and NOAA-AVHRR data are extensively used for estimating spatially distributed surface albedo, e.g., Winther (1992) used Landsat-TM data, while Laine and Heikinheimo (1996) and Toll et al. (1997) used NOAA-AVHRR data.

### 1.3 Research Objectives

This study has four primary objectives:

- (1) To develop a semi-distributed, basin scale snowmelt model - energy balance method (SDSM-EBM) of modest data demand but maximizes the use of remotely sensed data, and that accounts for the vertical energy fluxes of snowpack (ice and liquid phases) for different land use types, redistribution of snow, canopy interception, snow sublimation and refreezing.
- (2) To develop a modified temperature index algorithm (SDSM-MTI) as an improvement over the conventional degree-day approach to model basin snowmelt processes.
- (3) To evaluate surface temperature simulated by SDSM using different methods in both open and forest covered area with respect to surface temperature derived from NOAA AVHRR data.
- (4) To estimate snow water equivalent using passive microwave brightness temperature data in a Prairie like environment.

Both SDSM-EBM and SDSM-MTI are developed as modules of the semi-distributed hydrologic model, DPHM-RS of Biftu and Gan (2001) to model year round basin hydrology.

To achieve the above objectives, the data used are: DEM, NOAA-AVHRR, hydrometeorological, snow course and streamflow data for the Paddle River Basin of Alberta for the winters of 1997/1998, 1998/1999, and 1999/2000 (Table 1.1). The model was calibrated using the winter data of 1998/99 (Nov 11, 1998 to May 16, 1999) and validated using the 1998 (Jan 1, 1998 to April 30, 1998) and 1999/2000 (Jan 1, 2000 to Apr 30, 2000) data. The calibration and validation of SDSM was done against observed streamflow at the study basin outfall, snow course data and surface temperature retrieved from satellite data. SDSM was operated within

DPHM-RS to use all the hydrologic modules of DPHM-RS (e.g., evapotranspiration, vertical water budget, surface and sub-surface runoff and channel routing, etc.) needed to simulate streamflow and other closely related variables. The performance of SDSM-MTI was compared with SDSM-EBM to assess the capability of a simple snowmelt model.

## 1.4 Description of Study Site

The study site, the Paddle River basin (PRB), which is a tributary of Athabasca River basin of central Alberta between geographical coordinates 115.72°W, 53.97°N and 115.36°W, 53.78°N is located near the town of Mayerthorpe, and is about 170 km west-north of Edmonton (Figure 1.2). PRB has a basin area of about 265 km<sup>2</sup> and elevations ranging from 749 m at the Paddle River near Anselmo (basin outlet) to about 1000 m above the mean sea level (AMSL) at the western edge of the study basin. According to Hare and Thomas (1974), PRB lies at the northwestern edge of the Prairies (Alberta Plains) and adjacent to the Northwestern Forest. PRB lies in the “short, cool summer” koeppen climatic zone (Longley, 1968), where the mean daily temperature in January is about -15.5 °C and in July is about +15.6 °C. The annual mean precipitation is approximately 508 mm (Pretula and Ko, 1982), about one-fourth of which falls between December and April. The average April 1, basin average SWE for the Paddle River is about 70 mm with a record maximum SWE of about 200 mm in 1974 (AENR, 1986). Forest, brushlands, and tree muskegs cover about 70% of the study basin and the deciduous Aspen forest is the predominant vegetation type (AENR, 1977). The rugged topography and limited access have prevented a significant agriculture development of the remaining forest areas, although the demand for grazing leases has increased substantially in recent years. The major soil group of the basin is of Hubalta series associated with Onoway and Modeste (Twardy and Lindsay, 1971), which are

characterized by strongly developed Orthic Gray Wooded features. The dominant texture is clay loam under moderately well drained conditions.

The existing deciduous and coniferous forest stands play an important role in controlling the spring flood runoff, subsurface flow and sediment production from headwater area of PRB. The catchment has a moderate hydrological response with an average land slope of 3-5 percent. The area close to the stream channels in the headwater reach of PRB is characterized as the critical zone because of the greatest potential for contributing to flood runoff (AENR, 1986). However, the recent intervention in the headwater reach of PRB both by human beings (extensive road construction and subsequent logging of forest resources) and that by beaver activities (damming of natural streams; see Woo and Waddington, 1990; Gurnell, 1998) is significant to the extent that PRB discharge at Anselmo may no longer be predominantly natural particularly during low flow years.

PRB was selected for the study, mainly because of the relatively natural stream flow of Paddle River up to the basin outflow at Anselmo (749 m AMSL), where Water Survey of Canada has been operating a permanent gauging station since October 1979. Moreover, the Paddle reservoir (located about 30 km downstream of basin outlet) does not influence flows because the probable maximum flood (PMF) level is estimated to be 711 m AMSL (Alberta Environment, 1982), which is below the basin outlet. PRB was also selected for a detailed study by Biftu and Gan (2001) using the DPHM-RS model during summer periods of 1996-1998. The National Water Research Institute (NWRI) has also selected PRB for a research work on the influence of land use changes in basin hydrology (Granger, personal communication). Data collected for this study are listed in Table 1.1.

## **1.5 Organization of Thesis**

This thesis consists of six chapters. Chapter 1 provides an overview of the general

background of past work in snowmelt modeling and remote sensing. Chapter 2 describes the processes considered in developing the SDSM-EBM model. Reviews and applications of the force restore method or FRM (Deardorff, 1978), surface conductance method or SCM (Tarboton and Luce, 1996), and Kondo and Yamazaki method or KYM (Kondo and Yamazaki, 1990) to simulate snow surface temperature is also discussed. In Chapter 3, Semi-Distributed Snowmelt Model – energy balance method or SDSM-EBM is applied to Paddle River Basin (PRB) of central Alberta, while in Chapter 4, modified temperature index method or SDSM-MTI (an improvement over the conventional degree-day method) is applied to PRB. Chapter 5 presents the development of statistical algorithms for retrieving snow water equivalent from the Special Sensor Microwave/Imager (SSM/I) passive microwave brightness temperature data for the Red River basin of North Dakota and Minnesota (Singh and Gan, 2000). Finally, summary, concluding remarks, and recommendations for future work are presented in Chapter 6.

## References

- Alberta Energy and Natural Resources (AENR) (1977), *A study of watershed management options for controlling flood runoff in the headwaters of the Paddle River*, Edmonton, ENR No. T/44, 39p.
- Alberta Energy and Natural Resources (AENR) (1986), *Watershed management in the Paddle River Headwaters*, Alberta Energy and Natural Resources, Edmonton, ENR No. T/104, 60p.
- Alberta Environment (1982), *Hydrogeology: Paddle River reservoir area near Mayerthorpe, Alberta*, Alberta Environment, Environment Protection Services, Earth Science Division, 107p.
- Anderson, E. A. (1968), Development and testing of snowpack energy balance equations. *Water Resour. Res.* 4(1):19-37.

- Anderson, E. A. (1973), *National Weather Service River Forecast System - Snow accumulation and ablation model*, NOAA Tech. Memorandum NWS Hydro-17, US Dept. of Commerce, Silver Spring, Maryland, USA.
- Anderson, E. A. (1976), *A Point Energy and Mass Balance Model for a Snowcover*, NOAA Technical Report, NWS 19, US Dept. of Commerce, Silver Spring, Md, 150p.
- Becker, F., and Li, Z. L. (1990), Towards a local split window method over land surface. *Int. J. Remote Sensing*, 11:1009-1027.
- Bengtsson, L. (1976), Snowmelt estimated from energy budget studies. *Nordic Hydrology*, 7:3-18.
- Bengtsson, L. (1982), The importance of refreezing on diurnal snowmelt cycle with application to a Northern Swedish catchment. *Nordic Hydrology*, 13:1-12.
- Bergstrom, S. (1975), The development of snow routine for the HBV-2 Model. *Nordic Hydrology*, 3:73-92.
- Biftu, G. F., and Gan, T. Y. (2001), Semi-distributed, physically based, hydrologic modeling of the Paddle River Basin, Alberta using remotely sensed data. *J. Hydrol.*, 244:137-156.
- Blöschl, G. (1999), Scaling issues in snow hydrology. *Hydrol. Proc.*, 13:2149-2175.
- Blöschl, G., and Sivapalan, M. (1995), Scale issues in hydrological modeling: a review. *Hydrol. Proc.*, 9:251-290.
- Boegh, E., Soegaard, H., Hanan, N., Kabat, P., and Lesch, L. (1999), A remote sensing study of the NDVI-Ts relationship and the transpiration from sparse vegetation in the Sahel based on high-resolution satellite data. *Remote Sens. Environ.*, 69:224-240.
- Braun, L. N. (1985), *Simulation of snowmelt-runoff in lowland and lower alpine regions of Switzerland*. *Zuricher Geographische Schriften*, Heft 21, Geographisches Institut ETH Zurich, 166p.
- Brest, C. L., and Goward, S. N. (1987), Deriving surface albedo measurements from narrow band satellite data. *Int. J. Remote Sensing*, 8:351-367.

- Charbonneau, R., Fortin, J. P., and Morin, G. (1977), The CEQUEAU model: description and examples of its use in problems related to water resources management. *Hydrol. Sci. Bull.*, 22(1):193-203.
- Deardorff, J. W. (1978), Efficient prediction of ground surface temperature and moisture, with inclusion of a layer of vegetation. *J. Geophys. Res.*, 83(C4):1889-1903.
- Dery, S. J., and Yau, M. K. (2001a), Simulation of blowing snow in the Canadian Arctic using a double-moment model. *Boundary-Layer Meteorol.*, 99:297-316.
- Dery, S. J., and Yau, M. K. (2001b), Simulation of Arctic ground blizzard using a coupled blowing snow atmosphere model. *J. Hydrometeorology* (in press).
- Dey, B., Sharma, V. K., and Rango, A. (1992), Linear or nonlinear covariance of seasonal snowmelt and snowcover in western Himalayas, *Nordic Hydrology*, 23(3):183-192.
- Dunne, T., Proce, A. G., Colebeck, C. (1976), The generation of runoff from subarctic, *Water Resour. Res.*, 12(4):677-685.
- Emaruchi, B. (1998), *A hydrologic model for forested mountain watersheds*. Ph.D. Thesis, University of Regina, Canada. 243p.
- Ferguson, R. I. (1984), Magnitude and modeling of snowmelt runoff in the Cairngorm Mountains, Scotland. *Hydrol. Sci. J.*, 29(1):49-62.
- Foster J. L., Chang, A. T. C., and Hall, D. K. (1997), Comparison of snow mass estimates from a prototype passive microwave snow algorithm, a revised algorithm and snow depth climatology. *Remote Sens. Environ.* 62:132-142.
- Gan T. Y. (1996), Passive microwave snow research in Canadian high Arctic. *Canadian J. Remote Sens.*, 22(1):36-44.
- Goodison B. E., and Walker, A. E. (1994), Canadian development and use of snow cover information from passive microwave satellite data. *ESA/NASA International Workshop*, 245-262.
- Granger, R. J., and D. M. Gray (1990), A net radiation model for calculating daily snowmelt in open environments. *Nordic Hydrology*, 21:217-234.



- Gray, D. M., and Landine, P. G. (1988), An energy-budget snowmelt model for the Canadian Prairies. *Can. J. Earth Science*, 25:1292-1303.
- Gurnell, A. M. (1998), The hydrogeomorphological effects of beaver dam-building activity. *Progress in Physical Geography*, 22(2):167-189.
- Hall D. K. (1988), Assessment of polar climate change using satellite technology. *Reviews of Geophysics*, 26(1):26-39.
- Hardy, J. P., Davis, R. E., Jordan, R., NI, W., and Woodcock, C. (1998), Snow ablation modeling in a mature aspen stand of the boreal forest. *Hydrol. Proc.*, 12(10/11):1763-1778.
- Hare, T. K., and Thomas, M. K. (1974), *Climate Canada*, Wiley Publications of Canada Ltd., Toronto.
- Hartman M. D., Baron, J. S., Lammers, R. B., Cline, D. W., Band, L. E., Liston, G. E., and Tague, C. (1999), Simulation of snow distribution and hydrology in a mountain basin. *Water Resour. Res.*, 35(5):1587-1603.
- Jordan, R. (1991), *A one-dimensional temperature model for a snow cover: Technical documentation for SNTHERM.89*. Special Report 91-16, U.S. Army Cold Regions Research and Engineering Laboratory, Hanover, N.H., 49 p.
- Kane, D. L., Gieck, R. E., and Hinzman, L. D. (1997), Snowmelt modeling at small Alaskan arctic watershed. *J. Hydrologic Engrg.*, 2(4): 204-210.
- Kirnbauer, R., Blöschl, B., and Gutknecht, D. (1994), Entering the era of distributed snow models. *Nordic Hydrology*, 25:1-24.
- Kite, G. W. (1995a), *Manual for the SLURP hydrological model*. NHRI, Saskatoon, Canada.
- Kite, G. W. (1995b), Scaling of input data for macroscale hydrologic modeling. *Water Resour. Res.*, 31(11):2769-2781.
- Kite, G. W., and Kouwen, N. (1992), Watershed modeling using land classifications. *Water Resour. Res.*, 31(12):3193-3200.
- Kite, G. W., and Pietroniro, A. (1996), Remote sensing application in hydrological modeling. *Hydrol. Sci.*, 41(4):563-591.

- Kite, G. W., and Spence, C. D. (1995), Land cover, NDVI, LAI, and evapotranspiration in hydrological modeling. In: *Application of Remote Sensing in Hydrology*, ed. G. W. Kite, A. Pietroniro, and T. D. Pultz, Proc. Symp. No. 14, NHRI, Saskatoon, Canada, 203-240.
- Kondo J., and Yamazaki, T. (1990), A Prediction Model for Snowmelt, Snow Surface Temperature and Freezing Depth Using a Heat Balance Method. *J. of Appl. Meteor.*, 29:375-384.
- Kuchment L. S., and Gelfan, A. N. (1996), The determination of the snowmelt rate and the meltwater outflow from a snowpack for modeling river runoff generation. *J. Hydrol.*, 179:23-36.
- Kussisto, E. (1978), Optimal complexity of a point snowmelt model. In: *Proceedings on modeling of snowcover runoff*, ed. S. C. Colbeck and M. Ray, US Army, CRREL, Hanover, NH, 205-209.
- Kustas W. P., Rango, A., and Uijlenhoet, R. (1994), A simple energy budget algorithm for the snowmelt runoff model. *Water Resour. Res.*, 30(5):1515-1527.
- Kustas, L. S., and Jackson, T. J. (1999), The impact on area-average heat fluxes from using remotely sensed data at different resolutions: A case study with Washita '92 data. *Water Resour. Res.*, 35(5):153-1550.
- Laine V., and Heikinheimo, M. (1996), Estimation of surface albedo from NOAA AVHRR data in high latitudes. *Tellus*, 48A(3):424-441.
- Laval, K., and Picon, L. (1986), Effect of change on the surface albedo on the Sahel climate. *J. Atmospheric Sciences.*, 43:2419-2429.
- Leavesley, G. H. (1989), Problems of snowmelt runoff modeling for a variety of physiographic and climatic conditions. *Hydrol. Sci. J.*, 34(6):617-634.
- Liston, G. E. (1995), Local advection of momentum, heat, and moisture during the melt of patchy snow covers. *J. Applied Meteor.*, 34:1705-1715.
- Liston, G. E., and Sturm, M. (1998), A snow-transport model for complex terrain. *J. Glacial.*, 44(148):498-516.
- Longley, R. W. (1968), *Climatic maps for Alberta*. University of Alberta, Canada.

- Luce, C. H., Tarboton, D. G., and Cooley, K. R. (1998a), The influence of the spatial distribution of snow on basin-averaged snowmelt. *Hydrol. Proc.*, 12 (10/11):1671-1683.
- Luce, C. H., Tarboton, D. G., and Cooley, K. R. (1998b), Sub-grid Parameterization Of Snow Distribution for an Energy and Mass Balance Snow-Cover Model. In: *International Conference on Snow Hydrology*, Brownsville, Vermont, USA, 6-9 October.
- Male D. H., and Granger, R. J. (1981), Snow surface energy exchange. *Water Resour. Res.*, 17(3):609-627.
- Martinec, J. (1980), Limitations in Hydrological Interpretations of the Snow Coverage. *Nordic Hydrology*, 11:209-220.
- Martinec, J. (1985), Snowmelt runoff models for operational forecasts. *Nordic Hydrology*, 16:129-136.
- Martinec, J., Rango, A., and Major, E. (1983), *The snowmelt-runoff model user's manual*. NASA Ref. Pub., 110, NASA, Washington, D.C., USA.
- Matzler C. (1994), Passive microwave signatures of landscapes in winter. *Meteorol. Atmos. Phys.* 54:241-260.
- Morris, E. M. (1985), Snow and ice, In *Hydrological Forecasting*, ed. M. G. Anderson and T. P. Burt, John Wiley & sons Ltd., pp 153-182.
- Obled, C., and Rosse, B. (1977), Mathematical models of a melting snowpack at an index plot. *J. Hydrol.*, 32 (1/2):139-163.
- Olyphant, G. A., and Isard, S. A. (1988), The role of advection in the energy balance of late-lying snowfields: Niwot. Ridge, Front Range, Colorado, *Water Resour. Res.*, 24(11):1962-1968.
- Ottle, C., and Vidal-Madjar, D. (1992), Estimation of land surface temperature with NOAA 9 data. *Remote Sens. Environ.*, 40:27-41.
- Pietroniro, A., Prowse, T. D., and Lalonde, V. (1995), Classifying terrain in a muskeg-wetland regime for application to GRU-type distributed hydrologic modelings. In: *Applications of Remote Sensing in Hydrology*, ed. G. W. Kite, A.

- Pietroniro, and T. Pults, Proc. Symp. No. 14, NHRI, Saskatoon, Canada, 275-286.
- Pomeroy, J. W., Gray, D. M., Shook, K. R., Toth, B., Essery, R. L. H., Pietroniro, A., and Hedstrom, H. (199-8), An evaluation of snow processes for land surface modeling, *Hydrol. Proc.*, 12(15):2339-2367.
- Pomeroy, J. W., Marsh, P., and Gray, D. M. (1997), Application of distributed blowing snow model to the Arctic. *Hydrol. Proc.*, 11:1451-1464.
- Pretula, B. R., and Ko, C. A. (1982), *Hydrogeology Paddle River Reservoir area near Mayerthorpe, Alberta*, Report prepared for Alberta Environment Protection (AEP), 107p.
- Price, J. C. (1984), Land surface temperature measurements from the split window channels of the NOAA 7 Advanced Very high resolution radiometer. *J. Geophys. Res.*, 89(D5):7231-7237.
- Qin Z., and Karnieli, A. (1999), Progress in the remote sensing of land surface temperature and ground emissivity using NOAA-AVHRR data. *Int. J. Remote Sensing*, 20(12):2367-2393.
- Quick, M. C., and Pipes, A. (1977), U.B.C. Watershed model. *Hydrol. Sci. Bull.*, 22(1):153-161.
- Running, S. W., Patterson, D. L., Spanner, M. A., and Teuber, K. B. (1986), Remote Sensing of coniferous forest leaf area. *Ecology*, 67:273-276.
- Sand, K. (1990), Modeling snowmelt runoff processes in temperate and arctic environments. *University of Trondheim, Norwegian Institute of Technology, IVB-rapport B-2-1990-1*, 176p.
- Shook, K. (1993), *Fractal geometry of snowpacks during ablation*. M. Sc. thesis, University of Sask., Saskatoon, Canada, 178p.
- Shook, K. (1995), *Simulation of the ablation of prairie snowcovers*. Ph. D. thesis, University of Sask., Saskatoon, Canada, 189p.

- Singh, P. R., and Gan, T. Y. (2000), Retrieval of snow water equivalent using passive microwave brightness temperature data. *Remote Sens. Environ.* 74(2): 275-286.
- Steffen, K., Abdalati, W., and Stroeve, J. (1993), Climate sensitivity studies of the Greenland ice sheet using satellite AVHRR, SMMR, SSM/I, and in situ data. *Meteor. Atmos. Phys.*, 51:239-258.
- Stroeve, J., and Steffen, K. (1998), Variability of a AVHRR-derived clear sky surface temperature over the Greenland ice sheet. *J. Appl. Meteorol.*, 37: 23-31.
- Sud, Y., and Fennessy, M. (1982), A study of the influence of surface albedo in July circulation in semi-arid regions using the GLAS GCM. *J. of Climatology*, 2:105-125.
- Tait A. (1998), Estimation of snow water equivalent using passive microwave radiation data. *Remote Sens. Environ.*, 64:286-291.
- Tao, T. and Kouwen, N. (1989), Remote sensing and fully distributed modeling for flood forecasting. *J. Wat. Resour. Plan. Manag. Div. ASCE*, 115(6): 809-823.
- Tarboton D. G., and Luce, C. H. (1996), *Utah Energy Balance Snow Accumulation and Melt Model (UEB), Computer model technical description and user's guide prepared by Utah Water Research Laboratory, Utah State University and USDA Forest Service, Intermountain Research Station, 64p.*
- Toll, D. L., Shirey, D., and Kimes, D. S. (1997), NOAA AVHRR land surface albedo algorithm development, *Int. J. Remote Sensing*, 18(18):3761-3796.
- Twardy, A. G., Lindsay, J. D. (1971), *Soil survey of the Chip Lake area, Alberta Soil Survey, No. 28:1-71.*
- Verseghy, D. L. (1991), Class-A Canadian land surface scheme for GCMs. I. Soil model. *Int. J. climatology*, 11:111-133.
- Vogt, J. V. (1996), Land surface temperature retrieval from NOAA AVHRR data. In: *Advances in the use of NOAA AVHRR data for land applications*, ed. G. D'Souza, A. S. Belward, and J. P. Malingreau, 125-151.

- Vukovich, F., Toll, D., and Murphy, R. (1987), Surface temperature and albedo relationships in Senegal derived from NOAA-7 satellite data. *Remote Sens. Environ.*, 22:413-421.
- Weisman, R. (1977), Snowmelt: a two-dimensional turbulent diffusion model. *Water Resour. Res.*, 13(2):337-342.
- Wigmosta, M. S., Lance, L. V., and Lettenmaier, D. P. (1994), A distributed hydrology-vegetation model for complex terrain. *Water Resour. Res.*, 30(6): 1665-1679.
- Winther, J. (1992), Landsat thematic mapper (TM) derived reflectance from a mountainous watershed during the snowmelt season. *Nordic Hydrology*, 23:273-290.
- Woo, M. K. and Waddington, J. M. (1990), Effects of beaver dams on subarctic wetland hydrology. *Arctic*, 43(3):223-230.
- Yamazaki, T. (1998), A multi-layer heat balance model of snowcover – simulations in Siberia and plans. In: *Proc. of second international workshop on energy and water cycle in GAME, Siberia*, 161-168.
- Ziverts, A., and Jauja, I. (1999), Mathematical model of hydrological processes METQ98 and its applications. *Nordic Hydrology*, 30(2):109-128.
- Zuzel, J. F., and Cox, L. M. (1975), Relative importance of meteorological variables in snowmelt. *Water Resour. Res.*, 11:174-176.

Table 1.1. Summary of data collection for the study

Topographic data	Mean altitude, aspect, flow direction, slope of the surface, drainage network, and topographic-soil index (derived from DEM data).
Land use and spatially distributed geophysical data	Spatial distribution of land use classes, surface albedo, vegetation index and surface temperature (Landsat image for land use classification and NOAA-AVHRR image for other geophysical parameters).
Hourly hydro-meteorological data	air temperature, ground temperature, precipitation (snow/rain), wind speed and wind direction, relative humidity, net radiation, short-wave radiation, ground heat flux data.
Snow course data	Snow depth and snow density along the transects in different land use.
Stream flow data	Stream flow data for the Paddle River Basin at Anselmo (hourly).

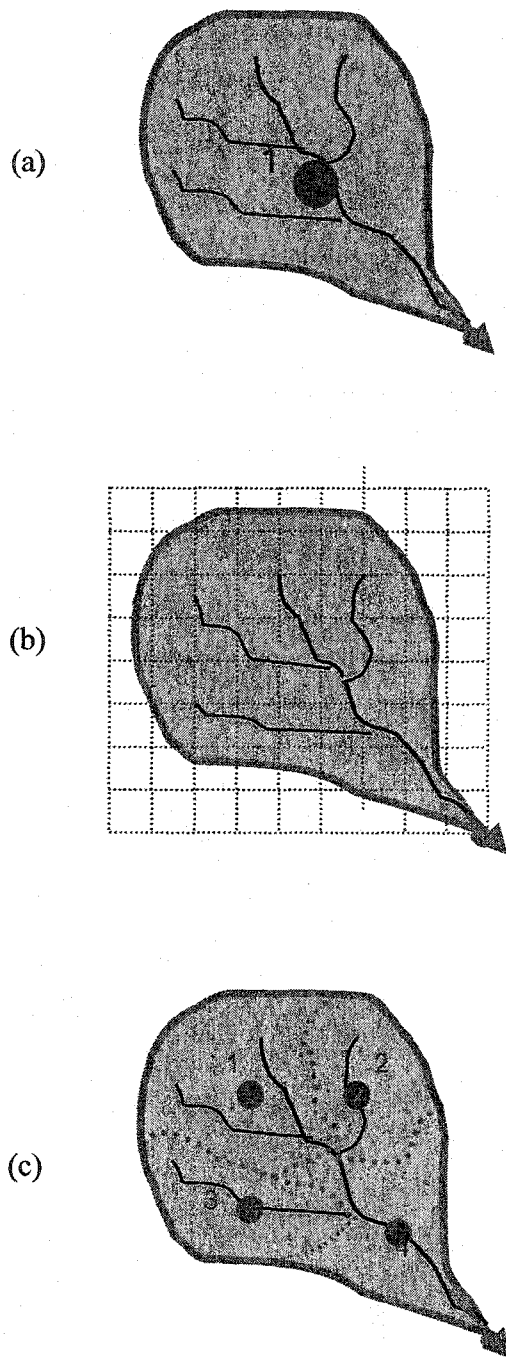


Figure 1.1 Modeling concepts in the field of snow hydrology (a) lumped or point model, (b) fully-distributed model, and (c) semi-distributed model.



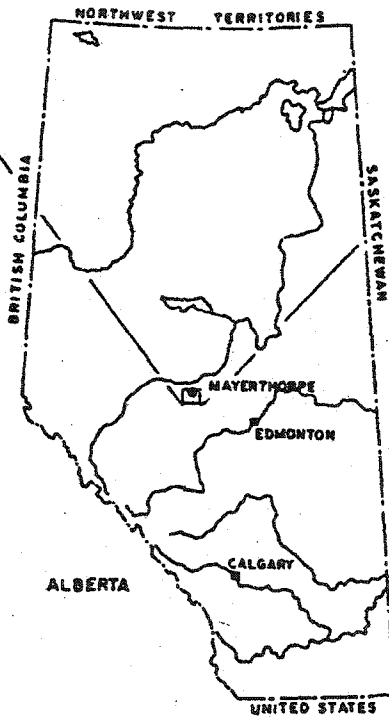
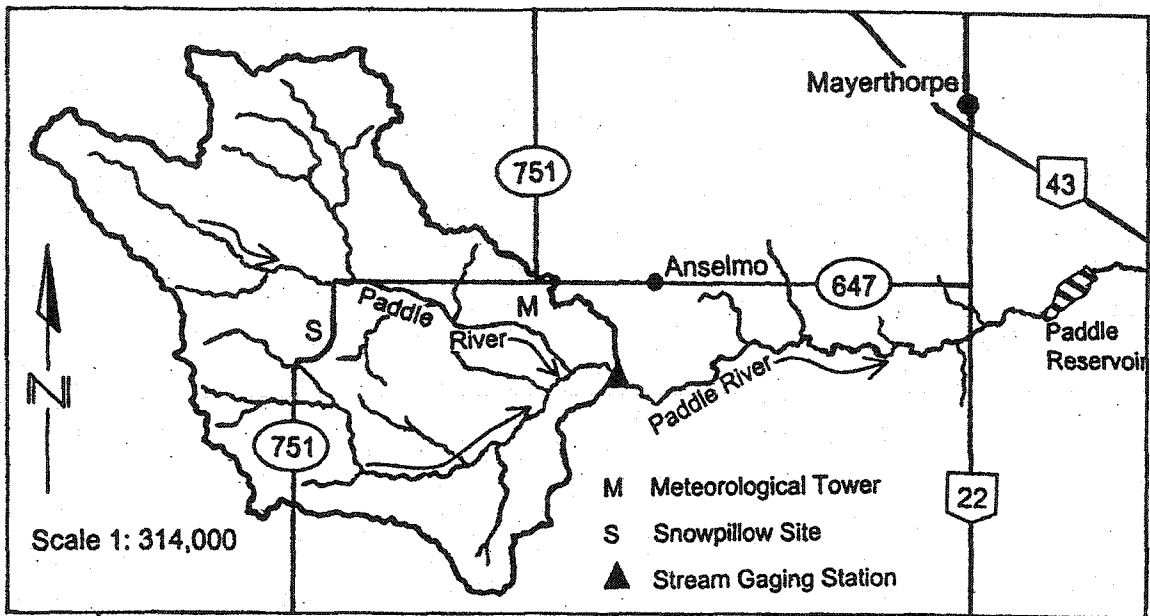


Figure 1.2 Location map of the Paddle River basin

## **Chapter 2**

# **Semi-Distributed Snowmelt Model (SDSM) using Remote Sensing Data, I. Model Development**

### **2.1 Introduction**

Water is a critical element of the earth's natural resources. Hydrology, which treats all phases of earth's water, is a subject of great importance for people and their environment. With the progress of civilization, human activities gradually intrude on the natural water environment, changing the dynamic equilibrium of the hydrological cycle and atmospheric processes. The implications of land use changes, agricultural practices, deforestation, urbanization, reservoir construction, etc. to our environment and to the world's water resources are of great concern to the society.

The land surface exerts a strong influence on atmospheric processes (Brass, 1999). Diurnal phenomena such as land and sea breezes are caused by uneven heating of

the earth's surface and result in atmospheric and oceanic circulation, causing the redistribution of heat and different forms of precipitation.

Snow accumulation and melting processes are critical components of land surface hydrology that influences energy transfer within the planetary boundary layer (Yeh et al., 1983). Snow influences the surface climate in three ways. First, snow has a high surface albedo and it reflects away a large proportion of solar radiation incident on the land surface. Second, snow has a low thermal conductivity, which acts as an insulating layer against heat transfer between the atmosphere and the ground. And third, snow cover has a distinct seasonality especially in the mid-latitudes, which exerts a large effect on the surface moisture budget. These features of snow influence the surface and near-surface heating both locally and regionally. Several studies using general circulation models (GCM) show that snow cover feedbacks have wide range of effects on the climate (Yeh et al., 1983; Marshall et al., 1994). Marshall et al. reported a significant improvement in an atmospheric GCM in modeling the annual surface moisture and energy budgets (e.g., shift in the runoff maximum from winter in the control run to spring in the snow hydrology run), when the GCM included the parameterization of snowfall and snow cover fraction, calculation of snow temperature, and the snow mass and hydrologic budgets.

Snow influences a drainage basin's response to the input of water equivalent because it is usually stored in a basin for a long time before running off by melting. At the end of winter, the seasonal snowcover may melt within a week to several months depending on the amount of snow, climatic factors, terrain features, and vegetation cover. Spring snowmelt provides water for many beneficial uses in the form of both surface and groundwater resources but it can also cause serious flooding and erosion during extreme flood events. The timing of spring snowmelt is therefore vital for their optimal use and the control of flooding.

The importance of snowmelt runoff in temperate and higher latitudes has been widely recognized for more than 50 years (Linsley, 1943). A systematic investigation of the fundamental issues of snow hydrology was started in 1956 by US Army Corps of Engineers (USACE, 1956). The World Meteorological Organization (WMO) conducted a survey of 11 snowmelt-runoff models that were built for forecasting snowmelt-induced runoff in watersheds (WMO, 1986). Since then, a great number of new snow models have appeared to accommodate various applications, both in the literature and in operation. The large scale impacts of snow accumulation and ablation warrant the need to account for the spatial and temporal variation in snowmelt runoff via distributed or semi-distributed instead of lumped or point snowmelt modeling (Bathurst and Cooley, 1996).

Point snowmelt models can be classified into two types. The first type of model concentrates on production of melt water from either conceptual (degree-day approach: Martinec, 1960, 1970, 1975; Riley et al., 1972; Martinec and Rango, 1986; Kane et al., 1997) or physically based methods (e.g., energy balance approach: Anderson, 1968; Obled and Rosse, 1977; Male and Granger, 1981; Braun, 1985; Bengtsson, 1986; Kondo and Yamazaki, 1990; Jordon, 1991; Kustas et al., 1994; Kuchment and Gelfan, 1996; Tarboton and Luce, 1996; Yamazaki, 1998). The second type concentrates on the percolation of meltwater through the snowpack (Colbeck, 1972, 1973, 1976, 1977; Colbeck and Davidson, 1973). However, meltwater routing through a snowpack by detailed physics offers little advantage over the simpler kinematic wave approach (Colbeck, 1977; Jordan, 1983). The meltwater routing time from the top to the bottom of the snowpack is typically less than one hour for a snowcover depth up to 55 cm (Bathurst and Cooley, 1996).

Two basic approaches to modeling the snowmelt rate are the degree-day and the energy balance methods. The degree-day method is entirely empirical that uses site-specific melt factors, while the energy balance method is more physics-based and so

is less site-restrictive. The disadvantage of the energy balance method is that it requires good quality meteorological measurements, which are scarcely available (Harding, 1986). While operational models tend to be simple to avoid data constraints, research-oriented models are often sophisticated, requiring massive amount of data. Furthermore, there are also problems in extending snowmelt runoff simulation at a point, to catchment, a regional scales (WMO, 1986; Levesley, 1989; Blöschl and Kirnbaur, 1991; Kirnbauer et al., 1994; Bales and Harrington, 1995; Blöschl and Sivapalan, 1995; Pomeroy et al., 1998; Blöschl, 1999; Liston, 1999). The research objective is to understand the physical processes of snowmelt in a Prairie environment and model them in a simplified yet physically realistic approach with minimum data requirements. Furthermore, such a model should not be site-specific and capable of assessing the effect of land use changes (Kirnbaur et al., 1994).

The development of hydrological models and remote sensing has progressed almost independently until the beginning of the 80's, when Peck et al. (1981) reported the potential benefit of remotely sensed data in hydrologic modeling, and Rango (1985) stressed the need to effectively assimilate remotely sensed data in hydrologic models. Progress in snow hydrology over the past two decades has been heavily dependent on the quality and resolution of remotely sensed data available for applications at local, regional, and continental scales (Bales and Harrington, 1995; Kite and Pietroniro, 1996; and Rango and Shalaby, 1998).

A basin-scale snowmelt runoff model typically simulates the processes of snow accumulation and melt, and transforms it to basin outflow. Snowmelt runoff modeling can be lumped or distributed, which accounts for the spatial variability of a basin's terrain and hydrological characteristics. Models that discretize a basin only in terms of elevation or sub-basins are referred to as semi-distributed models, while models with more detailed discretizations (fixed or variable length grids) are called

fully distributed models (Kirnbauer et al., 1994). The model complexity and data requirements increase substantially as one moves from a semi-distributed to a fully distributed approach particularly if energy balance is used to compute the snowmelt process.

With the advent of computer technology, models developed in the last two decades range from fully distributed hydrological models such as SHE (Abott et al., 1986; Bathurst and Cooley, 1996), HYDROTEL (Fortin et al., 1986 & 2001), IHDM (Beven et al., 1987), DHSVM (Wigmosta et al., 1994), MIKE SHE (Rafsgaard and Storm, 1995) to semi-distributed models such as SLURP (Kite, 1995 & 1996) and TOPMODEL (Beven et al., 1995).

Fully distributed models should theoretically perform better than lumped parameter models but the reverse could occur. Furthermore, besides excessive data demand, the use of small grid elements as an attempt to accurately represent heterogeneous terrain features involve many unresolved uncertainties (Kirnbaer et al., 1994). Besides these, modeling hydrological processes using rectangular grid scales can be artificial. Beven (1996) suggested using large scale rather than small-scale parameterization strategy. Blöschl (1999) suggested that the model element may in practice be dictated by data availability. Essentially, one must find a trade-off between the attainable resolution of processes to be modeled and the accuracy required. The resolution attainable depends mainly on the resolution of hydrological information retrievable from the satellite data.

A basin-scale semi-distributed snowmelt model (SDSM) is developed with the objective of making it a comprehensive, yet non-data intensive (relying on remotely sensed and limited ground data) model. Table 2.1 shows general features of various distributed and semi-distributed snowmelt runoff models including SDSM. The distributed surface information considered are such as the land use classification,

vegetation index, albedo, surface temperature, snow cover retrieved from, say, Landsat's Thematic Mapper (TM) and NOAA's Advanced Very High Resolution Radiometer (AVHRR), and snow water equivalent (SWE) from Special Sensor Microwave Imager (SSM/I) data. SDSM is assessed in a multi-criteria framework to avoid the possibility of obtaining satisfactory simulations mostly by curve-fitting, e.g., unrealistic or non-meaningful model parameters (Bathurst and Cooley, 1996), e.g., SDSM was assessed using the SWE, snow depth, snow surface temperature and basin outflow with observed values.

## 2.2 Model Components of the Semi-distributed Snowmelt Model (SDSM)

This section presents the components of SDSM, which is designed to simulate snowmelt using either the modified temperature index (SDSM-MTI) or the energy balance method (SDSM-EBM). SDSM can operate at hourly to daily time step.

### 2.2.1 Transformation of Precipitation into Rain and Snow

Transformation of precipitation into rain and snow is based on the air temperature.

$$P_s = P \quad (T_{\max} \leq T_{\text{thp}}) \quad (2.1a)$$

$$P_s = \frac{T_{\max} - T_{\text{thp}}}{T_{\max} - T_{\min}} P \quad (T_{\min} < T_{\text{thp}} < T_{\max}) \quad (2.1b)$$

$$P_s = 0 \quad (T_{\min} \geq T_{\text{thp}}) \quad (2.1c)$$

$$P_r = P - P_s \quad (2.1d)$$

Where  $P$  is the total precipitation,  $P_r$  and  $P_s$  are the water equivalent depths of rain and snowfall respectively,  $T_{\text{thp}}$  is the threshold temperature below which precipitation will be snow instead of rain, and  $T_{\max}$  and  $T_{\min}$  are the maximum and minimum observed temperature respectively for the simulation time step. An appropriate value for  $T_{\text{thp}}$  is close to  $0^\circ\text{C}$ . Precipitations expressed in terms of

equivalent water depth can be separately stored as rain and snow for each of the sub-basins in SDSM. For snow, the snow depth is dependent on the fresh snow density,  $\rho_s^f$  (kg/m<sup>3</sup>), which is estimated from the air temperature,  $T_a$  (Pomeroy et. al., 1998).

$$\rho_s^f = 67.9 + 51.3e^{(T_a/2.6)} \quad (2.2)$$

This relation gives values of  $\rho_s^f$  that varies from 68 kg/m<sup>3</sup> at -20 °C to 119 kg/m<sup>3</sup> at 0 °C. This is very close to the range of average density of newly fallen snow (50-120 kg/m<sup>3</sup>) for most part of Canada (Pomeroy et al., 1998) and is therefore used in SDSM.

### 2.2.2 Canopy and Snow Interception

Snow is intercepted and stored at different levels of vegetation until the maximum interception storage capacities are reached, which is determined from the leaf area index, LAI (Dickinson et al., 1984) retrievable from satellite data such as NOAA-AVHRR. Wigmosta et al. (1994) applied the LAI approach in the form of a two-layer vegetation canopy. Besides LAI, the amount of snow interception depends also on the forest types (Hardy and Bistow, 1990), the tree species and the prevailing forest structure (Golding and Swanson, 1986). While coniferous forests retain their canopy during winter, the leafless deciduous forests give rise to snow cones at the tree trunk (Sturm, 1992). The end result of snow interception of most forest canopies is a snowpack of spatially heterogeneous depth, snow water equivalent (SWE), and melt rate.

An experiment of the Canadian GEWEX Program on spruce and pine has indicated that intercepted snow behaves as a fractal (Pomeroy and Schmidt, 1993). The sublimation rate of intercepted snow is dependent on the degree of canopy's exposure to the atmosphere. They also observed SWE beneath the tree canopy to be about 65% of the undisturbed snow in the boreal forest (i.e., in the forest opening).



In contrast, Hardy et al. (1997) measured 60% less snow in boreal jack pine tree wells than in forest openings at maximum accumulation. Their study also indicated that generally as canopy density increased, the penetration of radiation and snowmelt rate decreases. However, sometimes snowmelt could increase under dense canopy due to decreased terrestrial radiative losses or outgoing longwave radiation (Yamazaki and Kondo, 1992). Under leafless deciduous canopies, the net radiation alone is a good predictor of snow ablation as the turbulent contribution to melt is minimal (Price, 1988). However, the net radiation alone was inadequate to estimate snowmelt in the boreal forest, possibly because of the complex processes involved in snowpack metamorphism (Metcalf and Buttle, 1995). It is therefore important to carefully consider the spatial, heterogeneous response of canopy to the snow accumulation and ablation process in a basin with a good proportion of forest cover.

A recent study by Pomeroy et al. (1998) recommended a snow interception model of Hedstrom and Pomeroy (1998) for the Canadian Prairies, where the interception,  $I$  ( $\text{kg}/\text{m}^2$ ) is related to a dimensionless snow unloading coefficient,  $c_{su}$ , the maximum snow load,  $I^*$ , initial snow load,  $I_o$  ( $\text{kg}/\text{m}^2$ ), an exponential function of snowfall,  $P_s$  ( $\text{kg}/\text{m}^2$  for a unit time), and the canopy density,  $C_c$ .

$$I = c_{su} (I^* - I_o) \left(1 - e^{-\frac{C_c P_s}{I^*}}\right) \quad (2.3)$$

$$I^* = S_p \text{LAI} \left(0.27 + \frac{46}{\rho_s^f}\right) \quad (2.4)$$

Where  $c_{su} = 0.678$  for hourly time step,  $S_p$  is a tree species coefficient ( $\text{kg}/\text{m}^2$ , e.g. 6.6 for pine, 5.9 for spruce) and  $\rho_s^f$  is fresh snow density ( $\text{kg}/\text{m}^3$ ). Equations (2.3) and (2.4) are used in SDSM to account for snow interception.  $C_c$  (or the forest cover fraction,  $f_c$ ) is related to NDVI (Kerr et al., 1992; Mecikalski et al., 1999) or LAI (Coudhury, 1987:  $f_c = 1 - e^{-0.5\text{LAI}}$ ). A similar LAI approach of Dickinson (1984) was used in the DPHM-RS for estimating rainfall interception by canopy (Biftu, 1998).

### 2.2.3 Snow Redistribution and Air Temperature Adjustment

Precipitation and air temperature are two of the most important variables in snowmelt/hydrologic modeling that need to be distributed or interpolated from observation points to each computational element (Kirnbaur et al., 1994). The redistribution of snow is important when vegetation is sparse. Recent development in distributed hydrological modeling has recognized the importance of redistributing snow within the basin for predicting basin snowmelt (Pomeroy et al., 1997; Luce et al., 1998a; Liston and Sturm, 1998; Hartman et al., 1999).

Snow redistribution is most prominent in open areas (or areas without vegetation canopy) and since forest dominates about 70% of the Paddle River Basin (PRB) study area, we will retain the precipitation distribution in SDSM as has been used in semi-distributed hydrologic models, e.g., DPHM-RS (Biftu, 1998) and HYDROTEL (Fortin et al., 1990a),

$$P_i = P_{st} \left[ 1 + \left( \frac{P_{dist}}{100} \right) (AMSL_i - AMSL_{st}) \right] \quad (2.5)$$

where,  $P$  is precipitation (snow or rain), the subscript 'i' refers to sub-basin number (1 to 5 for PRB), subscript 'st' refers to weather station, and AMSL is the altitude above mean sea level in meter.  $P_{dist}$  is the precipitation distribution factor based on Getu and Gan (2001). The  $P_{dist}$  for snowfall is however reduced because the influence of Topographic Similarity Index (TSI) on snow redistribution is to reduce the snow distribution according to the mean altitude for a given hill slope (i.e., more snow in the vicinity of pour point or stream channel in each of the sub-basin) (Hartman et al., 1999).

Air temperature adjustment essentially involves using the lapse rate but some researchers (Anderson, 1973; Moore and Owens, 1984) have indicated that the lapse rate along a vertical profile is not always the same as the gradient along a hillside. Lapse rates are either estimated from sounding data (e.g. WMO, 1986), physical considerations (adiabatic lapse rates) or a combination of both (e.g. Blöschl et al., 1990). Moore and Owens (1984), Braun (1985), and Blöschl (1991) provided some important discussions on the diurnal and seasonal variations of lapse rate. Using snowmelt season of 1988 and 1989 (March to July), Blöschl (1991) found the mean monthly lapse rates of about  $-0.65^{\circ}\text{C}/100\text{ m}$  (with standard deviations  $\sim 0.2\text{K}/100\text{ m}$ ) for the Austrian Alps. Kondo and Yamazaki (1990) also assumed a temperature lapse rate of  $-0.65^{\circ}\text{C}/100\text{ m}$  for a test basin of Japan, which is basically the saturated adiabatic lapse rate (Chow et al., 1988). Kawashima et al. (2000) reports a mean lapse rate of  $-0.6^{\circ}\text{C}/100\text{ m}$  (ranging from  $-0.398$  to  $0.8$ ) for the altitude ranging from 0 to 1500 m AMSL. As the Canadian Prairies is quite dry during winter, a lapse rate close to the dry adiabatic lapse rate ( $T_{\text{lapse}}$ ) of  $-1^{\circ}\text{C}/100\text{ m}$  is more appropriate from physical consideration point of view. Marks et al., (1992) and Hartman et al., (1999) have used  $-0.4^{\circ}\text{C}/100\text{ m}$  to obtain better model response in terms of basin discharge and snow distribution.

In SDSM, the hourly air temperature and ground temperature data for each of the sub-basin ( $T_i$ ) are distributed from the point data of weather station ( $T_{\text{st}}$ ) with a temperature lapse rate ( $T_{\text{lapse}}$ ) of  $-0.65^{\circ}\text{C}/100\text{ m}$  as,

$$T_i = T_{\text{st}} + \left( \frac{T_{\text{lapse}}}{100} \right) (\text{AMSL}_i - \text{AMSL}_{\text{st}}) \quad (2.6)$$

## 2.2.4 One-Dimensional Snowpack Energy and Mass Balance

The transfer of energy at the snow surface and snow/soil interface (see Figure 2.1 and 2.2) for melting the snow is determined from the one-dimensional, energy equation applied to a control volume of snow having upper and lower interfaces with air and ground respectively. The energy balance for the snowpack per unit area, can be written as,

$$\frac{dU}{dt} = \frac{d(\rho_w c_s W T_{sp})}{dt} = q_n + q_h + q_e + q_p + q_g + q_m \quad (2.7a)$$

where “ $dU/dt$ ” is the time rate of change of energy stored within the snowpack in the form of cold content ( $J m^{-2} s^{-1}$ ),  $\rho_w$  the density of water ( $1000 kg m^{-3}$ ),  $c_s$  the specific heat or heat capacity of snow ( $2093.4 J kg^{-1} ^\circ C^{-1}$ ),  $W$  the depth of snow water equivalent (m),  $T_{sp}$  the temperature of snowpack with respect to its cold content ( $^\circ C$ ),  $q_n$  the net radiation flux absorbed by snowpack ( $W m^{-2}$  or  $J s^{-1} m^{-2}$ ),  $q_h$  the convective or turbulent transfer of sensible heat flux between the air and the snow surface,  $q_e$  the convective flux of latent energy (evaporation, sublimation, condensation),  $q_p$  the advective energy flux from precipitation,  $q_g$  the energy flux across the snow-ground interface by conduction, and  $q_m$  the energy associated with the flux of melt water. The sign convention chosen is such that a positive flux is directed towards the surface into the pack.

With the assumption that specific heat,  $c_s$ , is a constant, we can develop the following equation,

$$\rho_w c_s \left[ W \frac{d(T_s)}{dt} + T_s \frac{d(W)}{dt} \right] = q_n + q_h + q_e + q_p + q_g + q_m \quad (2.8a)$$

Using finite difference scheme, Eq. (2.8a) can be rewritten as,

$$\rho_w c_s W (T_{sp}^{t+\Delta t} - T_{sp}^t) + \rho_w c_s T_{sp}^{t+\Delta t} \Delta W = (q_n + q_h + q_e + q_p + q_g + q_m) \Delta t \quad (2.8b)$$

It is noted that this approach includes any change in water equivalent depth ( $\Delta W$ ) in each time step ( $\Delta t$ ) and assumes that the specific heat  $c_s$  does not change with temperature,  $T_{sp}$ . Further simplification of Eq. (2.8b) leads to,

$$\rho_w c_s T_{sp}^{t+\Delta t} (W + \Delta W) = \rho_w c_s W T_s^t + (Q_n + Q_h + Q_e + Q_p + Q_g + Q_m) \quad (2.8c)$$

where the Q terms ( $Q_n$ ,  $Q_h$ ,  $Q_e$ ,  $Q_p$ ,  $Q_g$ , and  $Q_m$ ) are the corresponding energy exchange rates multiplied by the time step (or  $Q=q\Delta t$ ). Therefore, the Q terms can be referred to as heat fluxes, which are expressed in “ $J s^{-1} m^{-2} \times s$ ” or  $J m^{-2}$ . Further details on Eq. (2.8c) are discussed in section 2.2.4.2.

The internal energy of snowpack, U is also called the cold content, which is the heat required per unit area to raise the temperature of the snowpack to 0°C. In computing U, the heat capacity of the entrapped air is neglected.  $Q_n$  is the sum of net short wave ( $Q_{sn}$ ) and net long-wave fluxes ( $Q_{ln}$ ), the later being closely related to the temperature of the emitting surface and the emissivity of the medium through which it passes. The spatial distribution of albedo ( $\alpha$ ) of the snow-covered area is important to convert the incident short-wave radiation to  $Q_{sn}$ . The other important components of energy balance are  $Q_h$  and  $Q_e$ . Except for barren ground in the Arctic,  $Q_g$  is generally negligible. In this study,  $Q_n$ ,  $Q_s$ , and  $Q_g$  are measured by a Net Radiometer (0.25 to 60  $\mu m$ ), a LI200S Pyranometer (0.4 to 1.1  $\mu m$ ), and TCAV-Average Soil Thermocouple Probe respectively.

### 2.2.4.1 Energy Fluxes at the Snowpack

Among radiative ( $Q_{sn}$  and  $Q_{ln}$ ), advective ( $Q_p$ ), ground ( $Q_g$ ), and turbulent energy fluxes ( $Q_h$  and  $Q_e$ ), the turbulent energy fluxes are the most difficult to estimate or to measure using commercial sensors. Detailed discussion of snowpack energy fluxes can be found in Male and Granger (1981) and Nakawo & Hayakawa (1998).

#### 2.2.4.1.1 Radiative Flux

The net radiation  $Q_n$ , likely the most important component in the energy budget for snowmelt, can be expressed as

$$Q_n = Q_{sn} + Q_{in} = Q_s(1 - \alpha) + (Q_{li} - Q_{le}) \quad (2.9)$$

where  $Q_s$  is the incoming (global) short wave radiation flux,  $\alpha$  the areal albedo of the surface,  $Q_{li}$  and  $Q_{le}$  are incoming (downward) and outgoing (upward) long-wave radiation fluxes. Whenever possible,  $Q_n$  should be measured directly (Brutsaert, 1982). In the absence of direct measurements,  $Q_n$  can be estimated from Eq. (2.9) if  $Q_s$ ,  $Q_{li}$ ,  $Q_{le}$  are available. Otherwise  $Q_n$  is estimated by simpler empirical relationships. The  $Q_n$  thus obtained needs to be divided into canopy level ( $Q_{nc}$ ) and ground or soil level net radiation ( $Q_{ns}$ ), which is as discussed below.

The radiation transmission within the canopy depends more on the solar zenith angle ( $Z_s$ ) and LAI than albedo, since for a complete canopy cover, reflection back to the atmosphere originates near the vegetation tops, whereas transmission is controlled by the bulk canopy structure. The transmissivity  $\tau_c$  of the canopy is calculated using Beer's law of radiation transfer in a non-scattering media (Versegy et al., 1993),

$$\tau_c = \exp(-\kappa \text{LAI}) \quad (2.10)$$

where  $\kappa$ , the canopy attenuation or extinction coefficient, is

$$\kappa = \frac{\varepsilon \bar{O}}{\cos Z_s} \quad (2.11)$$

and  $\varepsilon$  ( $\leq 1$ ) accounts for the forward scattering of radiation and non-random leaf distributions. Considering the distribution of leaf angles to be spherical,  $\bar{O}=0.5$  (Choudhury and Monteith, 1988) and  $\cos Z_s$  is given as

$$\cos Z_s = \sin \delta \sin \theta + \cos \delta \cos \theta \cos \tau \quad (2.12)$$

where  $\delta$  is the solar declination angle that is dependent on the Julian date,  $\theta$  is the latitude, and  $\tau$  is the hour angle with respect to the local noon hour.

Beer's law can partition the  $Q_n$  received at the reference height into the net radiation at the ground (or soil) level,  $Q_{ns}$ , and vegetation canopy,  $Q_{nc}$ .

$$Q_n = Q_{ns} + Q_{nc} \quad (2.13)$$

such that

$$Q_{ns} = Q_n \tau_c \quad (2.14)$$

Using a two-source energy balance model and remotely sensed data, Kustas et al. (1998) proposed a modified exponential relationship to partition  $Q_n$  between  $Q_{ns}$  and  $Q_{nc}$  as

$$Q_{ns} = Q_n \exp\left(\frac{-\kappa' \text{LAI}}{\sqrt{2 \cos Z_s}}\right) \quad (2.15)$$

where  $\kappa'=0.6$  and other symbols are as defined in the early sections. Both Eqs. (2.14) and (2.15) give similar canopy attenuation effect on  $Q_n$ . Eq. (2.15) is used in SDSM.

#### (a) Shortwave Radiation ( $Q_s$ )

The  $Q_s$  incident at a surface is composed of direct, diffused, and terrain reflected components. The diffused component is associated with the interaction of the incoming solar radiation with water vapor, dust, and pollutants of the atmosphere. In a mountainous topography, a fairly dense network of radiation sensors is needed to capture most of the components or the surface variations of short wave radiation.

The snow surface albedo,  $\alpha_{sn}$  is computed using an albedo decay function similar to Riley et al. (1972)

$$\alpha_{sn}(t) = \alpha_{\text{fresh}} - \alpha_{\text{min}} (1 - e^{-k_a t}) \quad (2.16)$$

For an open area, the value of fresh snow albedo,  $\alpha_{\text{fresh}}$ , is generally around 0.85 and the value of minimum albedo varies from 0.5 to 0.7 (higher value in the early stage of snow accumulation) depending on the extent of liquid water present in shallow seasonal snowcover of Canada (Pomeroy et al, 1998). The value of time constant is about 0.2 and the number of days,  $t$  (taken as a real number for hourly time step), is counted from the day of snowfall. Once the new snowfall occurs, this "t" is reset to zero. Versegny et al. (1993) also used a similar albedo decay function with the range

from 0.84 for fresh snow to a lower limit of 0.7 for non-melting snow and 0.5 for melting snow.

In a forest-covered land-use, this albedo is modified to account for the effect of litter fall fraction ( $l_c$ ) (Hardy et al., 1998), which increases throughout the entire snow season as

$$l_c = 1.0 - (1.0 - l_r)^{t_c} \quad (2.17)$$

where  $l_r$  is the litter rate in fraction per day and  $t_c$  is the cumulative day from the first day of snowfall. A litter rate of 0.005 and 0.001 and a litter albedo value of 0.15 and 0.20 have been recommended for black spruce and aspen site respectively for the central Prairies (Hardy et al., 1998).

In addition to litter fall, the areal surface albedo ( $\alpha$ ) decreases as the snowcover ablates due to a decrease in the area of snowcover fraction ( $A_{sn}$ ). According to Gray and Landine (1987), the albedo decay of a Prairie snowcover can be divided into three time periods, premelt, melt, postmelt. In the premelt period, the snow albedo was observed to decline slowly at a fairly constant rate of 0.006 per day. During melt, the rate of decline in areal albedo (that of soil and snow patches) increased to approximately 0.071 per day. In the postmelt period, the albedo of the snow-free surface was relatively constant at 0.17.

The area of snowcover ( $A_{sn}$ ) is needed either to account for the local advection appropriately or to determine the type of energy exchange over snow/ground surface. Theoretically, the shape of the snowcover depletion curve (SDC, which relates  $A_{sn}$  with SWE) for a given unit of watershed or sub-basin should depend on the magnitude and distribution of variations in snowcover accumulation and snowmelt (Anderson, 1973). Luce et al. (1998b) attempted to generate the SDC,  $A_{sn}(W)$ , by parameterizing the SWE (or simply  $W$ ) probability distribution based on the basin's topography and vegetation, from a dimensionless depletion curve.



$$A_{sn}(W) = \Phi\left(\frac{W}{W_{max}}\right) \quad (2.18)$$

Where  $\Phi$  denotes a mathematical function that relates a dependent variable with an independent one. Donald (1992) indicated that a 3-parameter lognormal distribution can be used to represent the snowcover distribution within a given land class and a theoretical SDC can be derived from the lognormal representation. Similar forms of snowcover depletion curves were constructed by using an assumed mean snow water equivalent  $\overline{SWE}$  and coefficient of variation ( $CV_{SWE}$ ) for a natural snowcover (Shook, 1995). The spatial frequency distribution of the SWE in each of three landscapes in a prairie environment was approximated by the lognormal probability density function. However, any departure of SWE in the natural snowcover from the lognormal frequency distribution can cause measured curves to depart from the theoretical SDC (Shook, 1995).

A simple form of linear depletion curve proposed by Versegny (1991) is also available in SDSM, where the snow cover is assumed to be complete if the snow depth is greater than an assumed height, “h” (a threshold snow depth below which bare patches start to occur). Otherwise, the snow depth is fixed at “h”, and the fraction of snow covered area,  $A_{sn}$  is calculated from

$$A_{sn} = \frac{SD}{h} \quad (2.19)$$

where SD is snow depth in meter. Versegny (1991) used a value of h equal to 0.10 m in the CLASS model. Similarly Granberg et al. (1999) assumed a SD of 0.07 m before snowcover is complete, to account for the effects of incomplete snow cover and radiation reaching the ground during periods with a thin snow cover. The field observation of this study found SD ranging between 0.07 and 0.1 m as the cutoff for a partial snowcover. The simulated model parameters SD and SWE can be verified with field observations (e.g. snow course survey that provides both SD and SWE for different landuse). Besides a linear form (Eq. 2.19), non-linear depletion curves of

the form similar to Eq. (2.18) are also incorporated in SDSM. In SDSM, the ratio  $(W/W_{\max})$  is replaced by  $(SD/h)$ .

Shook (1993) showed an approximate linear relationship between snowpack albedo and snow-covered area in the central part of Canadian Prairies. This can lead to a simple expression for an areal albedo of a partially ablated snowcover ( $\alpha$ ), as a function of the albedo of snow ( $\alpha_{sn}$ , after litter fall consideration for forest covered area), the albedo of the ground surface ( $\alpha_g$ ), and the fraction of snow-covered area ( $A_{sn}$ ):

$$\alpha = \alpha_{sn} A_{sn} + \alpha_g (1 - A_{sn}) \quad (2.20)$$

This areal albedo value for different land use (open area, mixed forest, and coniferous forest) is compared with the interpolated albedo retrieved from the NOAA-AVHRR images for different landuse and the larger of two is used for the computation of net solar radiation. This is done because the snow pillow's precision is 1.9 mm SWE, and it is possible that SDSM may not be able to reflect the increase of albedo caused by a trace event of less than 1.9 mm SWE in some instances.

#### (b) Longwave Radiation ( $Q_{le}$ and $Q_{li}$ )

Any substance at a temperature above absolute 0 °K emits electromagnetic waves called thermal radiation. Terrestrial surfaces, including snow surfaces, emit thermal radiation in the wavelength range referred to as long-wave radiation (Nakawo and Hayakawa, 1998). The outgoing longwave radiation ( $Q_{le}$ ) emitted by a snow surface at temperature  $T_s$  (absolute temperature, expressed in °K) is

$$Q_{le} = \epsilon_s \sigma T_s^4 \quad (2.21)$$

where  $\epsilon_s$  is the surface emissivity (-0.97 for snow surface),  $\sigma$  is the Stefan-Boltzmann constant ( $5.6698 \times 10^{-8} \text{ Wm}^{-2}\text{K}^{-4}$ ) and  $T_s$  is the surface temperature (°K). The incoming longwave radiation is estimated based on the air temperature ( $T_a$ )

$$Q_{li} = \epsilon_{a,cls} \sigma T_a^4 \quad (2.22)$$

with a clear sky atmospheric emissivity,  $\epsilon_{\text{acls}}$ , estimated according to Satterlund (1979)'s

$$\epsilon_{\text{acls}} = 1.08 \left[ 1 - \exp\left(-e_a^{(T_a/2016)}\right) \right] \quad (2.23a)$$

where  $T_a$  is the air temperature in °K, and  $e_a$  is air vapor pressure in millibars. Satterlund (1979) showed superior estimates of  $\epsilon_{\text{acls}}$  than those obtained by Brutsaert (1975) at temperatures below freezing (Gray and Male, 1981), given as

$$\epsilon_{\text{acls}} = 1.24 \left( \frac{e_a}{T_a} \right)^{1/7} \quad (2.23b)$$

For a given cloud cover fraction ( $C_L$ ), the atmospheric emissivity ( $\epsilon_a$ ) is calculated according to Tarboton and Luce (1996).

$$\epsilon_a = C_L + (1 - C_L)\epsilon_{\text{acls}} \quad (2.24)$$

In literature, several methods have been proposed to estimate daily  $C_L$  [e.g., based on measured and potential solar radiation (Blöschl and Kirnbaur, 1991), and the range of maximum and minimum daily temperatures (Loukas and Quick, 1999)]. We have used an average range of maximum to minimum air temperature and/or clear NOAA-AVHRR images as an indication of clear days for three winter periods. However, the temporal variation of  $C_L$  (even within a day) and its dependence on several parameters limit its reliable estimation.

#### 2.2.4.1.2 Turbulent Heat Flux

The turbulent heat fluxes related to motion of air are comprised of the sensible heat flux ( $Q_h$ ) and the latent heat flux ( $Q_e$ ), which are difficult to predict (Kane et al., 1997) because they are sensitive to atmospheric stability and require the computation of reasonably accurate surface temperature.

**(a) Sensible Heat Flux ( $Q_h$ )**

When there is a temperature gradient between the snow surface and the atmosphere, heat will be transported towards or away from the snow surface mainly through convection,  $Q_h$  ( $J/m^2$ )

$$Q_h = K_a (T_a - T_s) \quad (2.25)$$

where  $K_a$  is the apparent thermal conductivity of air. Heat conduction with turbulent motion (as air actually moves up and down at rather high speeds) could also take place when small-scale air masses move in a macroscopic temperature gradient (Nakawo and Hayakawa, 1998). Therefore  $K_a$  is not a constant, but a function of wind speed, air density, the stability of the atmosphere etc., so that Eq. (2.25) is replaced by

$$Q_h = C_h \rho_a C_p V (T_a - T_s) \quad (2.26)$$

where  $\rho_a$ ,  $C_p$ , and  $V$  are air density, specific heat of air (1005 J/kg/°C), and wind velocity (m/s), respectively.  $C_h$  is the dimensionless bulk transfer coefficient, which depends on the reference, displacement, and roughness heights, and the stability of the atmosphere.

**(b) Latent Heat Flux ( $Q_e$ )**

Similar to  $Q_h$ , water vapor is also transported by the turbulent motion under a vapor pressure gradient between the snow surface and the atmosphere. In the wind swept environment of Canada, blowing snow provides an additional source of water vapor to the atmospheric boundary layer (Dery and Yau, 2001b). This leads to modification of surface energy budget. The latent heat flux ( $Q_e$ ) is thus partitioned into flux associated with surface sublimation/condensation ( $Q_{e,surf}$ ) and that associated with the blowing snow sublimation ( $Q_{e,bss}$ ) as,

$$Q_e = Q_{e,surf} + Q_{e,bss} \quad (2.27)$$

### Surface Sublimation/Condensation

When water vapor is transported to the snow surface, it changes phase to either liquid or solid, releasing latent heat flux at the snow surface,  $Q_{e,surf}$  ( $J/m^2$ ) where

$$Q_{e,surf} = \lambda_{(s \text{ or } v)} E = C_e \rho_a \left( \frac{\lambda_{(s \text{ or } v)} 0.622}{P_a} \right) V (e_a - e_s) \quad (2.28)$$

where  $E$  is the amount of vapor transported,  $C_e$  is the bulk transfer coefficient for water vapor transfer,  $\lambda$  is the latent of heat of sublimation (with subscript  $s$ ,  $2.836 \times 10^6$  J/kg) or the latent heat of vaporization (with subscript  $v$ ,  $2.501 \times 10^6$  J/kg),  $e_a$  and  $e_s$  are air vapor pressure and the vapor pressure at the snow surface (assumed saturated at  $T_s$ ) respectively and  $P_a$  is the standard atmospheric pressure (101.33 kPa). The saturated vapor pressure,  $e$  (in Pa), (Morton, 1978) is estimated using

$$e = 611 \exp \left[ \frac{17.27T}{237.3 + T} \right] \quad (T > 0) \quad (2.29a)$$

$$e = 611 \exp \left[ \frac{21.88T}{265.5 + T} \right] \quad (T \leq 0) \quad (2.29b)$$

The attenuation effect of forest cover on the wind speed around the snow surface is based on the study of Hardy et al. (1997 and 1998) conducted for North of Prince Albert, Saskatchewan (Eq. 2.30a and 2.30b) and northern Manitoba (Eq. 2.30c).

$$V_{aspen} = \max[(0.272 V) - 0.2384, 0] \quad (2.30a)$$

$$V_{spruce} = \max[(0.0761 V) - 0.0964, 0] \quad (2.30b)$$

$$V_{pine} = \max[(0.0420 V) - 0.0400, 0] \quad (2.30c)$$

where  $V_{aspen}$ ,  $V_{spruce}$ , and  $V_{pine}$  are sub-canopy wind speeds (m/s) in the aspen, black spruce, and jack pine forests respectively. According to Hardy et al., the range of wind speeds for black spruce was 0-0.4 m/s, for aspen was 0-1.8 m/s, and for jack pine was 0 to 0.3 m/s. Eq. (2.30a) is used in SDSM to determine the wind speed in the mixed forest area where aspen trees dominate. A factor proportional to the relative LAI is used on Eq. (2.30a) to attenuate the wind speed in the coniferous

forest area to avoid many instances of zero wind speed (as obtained from Eqs. 2.30b and 2.30c). Several studies in the energy balance study use LAI to attenuate the wind speed in the forest covered area (Tarboton and Luce, 1996; Kite, 1996).

### Blowing Snow Sublimation

Dery and Yau (2001a) developed a non-linear regression equation to compute sublimation due to blowing snow ( $Q_{e,bs}/\lambda_s$ ) for the Canadian Arctic environment using two parameters  $V$  and  $\xi$ :

$$\frac{Q_{e,bs}}{\lambda_s} = a_0 + a_1\xi + a_2\xi^2 + a_3\xi^3 + a_4V + a_5\xi V + a_6\xi^2 V + a_7V^2 + a_8\xi V^2 + a_9V^3 \quad (2.31)$$

where, the blowing snow sublimation rate (the left hand side of Eq. 2.31) is in mm/day of SWE,  $V$  is wind speed (m/s) at 10 m height,  $\xi$  is analogous to the condensation growth parameter (in  $-1 \times 10^{-2}$  m<sup>2</sup>/s) of Rogers and Yau (1989), and the regression coefficients  $a_0$  to  $a_9$  are given in Table 2.2.  $\xi$  is computed using following equations,

$$\xi = \frac{\left( \frac{q_v}{q_{is}} - 1 \right)}{2\rho_{ice}(F_k + F_d)} \quad (2.32)$$

$$F_k = \left( \frac{\lambda_s}{R_v T_a} - 1 \right) \frac{\lambda_s}{K_a T_a} \quad (2.33)$$

$$F_d = \frac{R_v T_a}{D_a e_i(T_a)} \quad (2.34)$$

Where,  $q_v$  and  $q_{is}$  = saturation mixing ratios with respect to vapor and ice respectively,  $\rho_{ice}$  = density of ice (kg/m<sup>3</sup>),  $F_k$  and  $F_d$  = conductivity and diffusion terms associated with the sublimation process (m.s/kg),  $R_v$  = gas constant for water vapor (461.5 J/kg/K),  $K_a$  = thermal conductivity of air (W/m/K),  $D_a$  = coefficient of diffusion of water vapor, and  $e_i(T_a)$  is given by Eq. (2.29b). Using  $K_a$  and  $D_a$  data

for the temperature range between  $-40^{\circ}$  and  $30^{\circ}$  °C (Rogers and Yau, 1989) for the given atmospheric pressure of 100 kPa, we found  $K_a$  (in  $1 \times 10^{-2}$  W/m/K) and  $D_a$  (in  $1 \times 10^{-5}$  m<sup>2</sup>/s) to be linearly related to  $T_a$  (with regression coefficient,  $R^2$  as shown in bracket),

$$K_a = 2.3960 + 0.0079T_a \quad (R^2=0.9993) \quad (2.35)$$

$$D_a = 2.2174 + 0.0152T_a \quad (R^2=0.9994) \quad (2.36)$$

In SDSM,  $\frac{q_v}{q_{is}}$  is approximately assumed as the relative humidity (RH).

### (c) Stability of the atmosphere

In a 1-D modeling, the turbulent flux at the surface boundary (a few meters in height) is assumed to be non-converging or diverging, and so it should have a constant bulk transfer coefficient independent of height. Kondo and Yamazawa (1986) obtained values of  $C_h=0.002$  and  $C_e = 0.0021$  over a flat snow surface at a reference height of 1 m and suggested that they are practically independent of wind speed. Kondo and Yamazaki (1990) and Yamazaki (1998) used these coefficients in their single and multi-layer snowmelt models respectively.

From comparing several turbulent transfer expression in a logarithmic boundary layer, Brutsaert (1982) derive the  $C_h$  (or  $C_e$ ) equation under neutral condition ( $C_n$ ),

$$C_h = C_e = C_n = \frac{k^2}{[\ln((z_r - d_o)/z_o)]^2} \quad (2.37)$$

where  $k$  is the von Karman's constant ( $=0.4$ ),  $z_r$  the reference height,  $d_o$  the zero-plane displacement height (assumed equal to snow depth in SDSM). The roughness height,  $z_o$  is related to the mean obstacle or the mean vegetation height,  $h_o$  by  $h_o/z_o=(7.35 \text{ to } 8)$  (Brutsaert, 1982). As an average,  $h_o/z_o$  is assumed 7.6 in SDSM.

Under neutral conditions, turbulent motion is essentially a combination of round shaped eddies. When subjected to a temperature gradient near the surface, these

eddies experience buoyancy effects that may enhance or dampen the turbulent transfers giving rise to unstable or stable atmospheric conditions respectively. For unstable conditions, the potential temperature decreases with height, and an uplifted air mass is subjected to the buoyancy force, since the moving air parcel has a lower density than the surrounding air. Similarly, an air mass moving downward is subjected to further acceleration. In stable conditions, the potential temperature decreases with height, and the velocity profile is compressed vertically since a vertically moving air mass is subjected to buoyancy generated restoring force (Nakawo and Hayakawa, 1998).

Unstable conditions often occur over open area under strong solar radiation and weak winds while stable conditions are frequently observed during nights with clear skies. The atmosphere is mostly stable throughout the day during melting season, since the surface temperature is not above 0°C. Enhanced or dampened vertical movement of air masses tends to increase or decrease turbulent fluxes, which can be quantified in terms of the Richardson number ( $R_{iB}$ ) or the Monin-Obukhov length ( $L_{mo}$ ). The most commonly used dimensionless  $R_{iB}$  without including the water vapor component is

$$R_{iB} = \frac{g}{T} \frac{dT/dz_r}{(dV/dz_r)^2} \approx \frac{g(T_a - T_s)z_r}{V^2 T_a} \quad (2.38)$$

where  $g$  is the acceleration due to gravity ( $m/s^2$ ) and temperatures ( $T_a$  and  $T_s$ ) are in K. There are three options available in SDSM to compute the adjusted bulk transfer coefficient  $C_{adj}$ . They are (1) Price and Dunne, 1976, (2) Louse, 1979, and (3) Morris, 1989 (see Appendix B).

SDSM has the option either to use the neutral bulk transfer coefficient (FSTAB=0) or full stability corrections (FSTAB =1) by adjusting FSTAB (stability factor, an integer variable) in the model.

$$C_{h \text{ or } e} = C_n + FSTAB(C_{adj} - C_n) \quad (2.39)$$



### 2.2.4.1.3 Advective Heat of Precipitation

Advective heat of precipitation,  $Q_p$  to the snowpack is given by

$$Q_p = \rho_w P_r (c_w T_a + \lambda_f) + \rho_w P_s c_s T_a \quad (T_s < 0) \quad (2.40a)$$

$$Q_p = \rho_w P_r c_w T_a + \rho_w P_s (c_s T_a - \lambda_f) \quad (T_s = 0) \quad (2.40b)$$

Where  $\lambda_f$  is the latent heat of melting/freezing ( $3.35 \times 10^5$  J/kg),  $P_r$  and  $P_s$  are rainfall and snowfall depth respectively.

### 2.2.4.1.4 Surface Temperature

Surface temperature is an important land surface variable that has been called ground surface temperature (Bhumralkar, 1975; Deardorff, 1978), surface temperature (Dickinson, 1988) and surface skin temperature (Blondin, 1991). According to Hu and Islam (1995), the ground surface temperature is the average temperature of the upper soil layer and the surface skin temperature is the temperature of the interface between the land surface and the atmosphere. Skin surface is a more general term, which can be used to describe any surface coming in contact with the atmosphere. The classical heat diffusion equation based on conduction and applicable to the snowpack surface is

$$\frac{\partial^2 T_{sp}}{\partial z^2} = \frac{1}{\kappa} \frac{\partial T_{sp}}{\partial t} \quad (2.41)$$

where  $z$  is snow depth (m),  $T_{sp}$  is the snowpack temperature ( $^{\circ}\text{C}$ ),  $\kappa$  is the thermal diffusivity of snow ( $\text{m}^2/\text{s}$ ), which is the ratio of thermal conductivity ' $\lambda$ ' to heat capacity ' $c$ ', and  $t$  is the time (s). Even though Eq. (2.41) can be solved using the laplace transform (Prasad, 1983), the ever changing thermal and physical properties of snowpack makes the mechanism of heat flow in snow much more complicated than that of a homogeneous solid. Further, a temperature change within the snowpack is also influenced by the freezing of both rainwater and melts at the snow surface in the snowpack.

Snow surface temperature can be estimated from a multi-layer snow model (Jordan, 1991; Yamazaki, 1998) or a single layer snow model (Kondo and Yamazaki, 1990; Tarboton and Luce, 1996). Leydecker and Melack (1999) used snow surface temperature as a function of air temperature and snow surface temperature at the previous time step. Their approach indicates the possibility of using the force-restore method in simulating snow surface temperature, which has been used in the prediction of soil surface temperature (Deardorff, 1978; Dickinson, 1988; Hu and Islam, 1995; Jacobs et al., 2000). Three methods are incorporated into SDSM to compute the snow surface temperature.

**(a) Force Restore Method (FRM)**

The heat conduction into the snow,  $Q$  can be approximately accounted for by two components: (1) a stationary mean diurnal temperature variation at the surface and (2) a near-steady-state heat flux of lower frequency variability. This is the force restore method (FRM) because the forcing by  $Q^*$  (net energy received by a control volume either by soil column or snowpack) is modified by a restoring term, the deep soil temperature (for soil column) or near-ground surface temperature (for snowpack). The FRM used by Hu and Islam (1995) for soil surface temperature is an approximation of the diffusion equation subjected to a periodic boundary forcing.

Considering a homogeneous layer, the classical heat diffusion equation (2.41) can be written as,

$$\frac{\partial T}{\partial t} = \left( \frac{\lambda}{c} \right) \frac{\partial^2 T}{\partial z^2} = k \frac{\partial^2 T}{\partial z^2} \quad (2.42)$$

subjected to the boundary condition

$$\left[ -\lambda \frac{\partial T}{\partial z} \right]_{z=0} = G(0, t) \quad (2.43)$$

For a periodic forcing (e.g. diurnal forcing) at the surface,

$$G(0, t) = G_1 e^{i(\omega_1 t + \varepsilon_1)} \quad (2.44)$$

where  $G(0, t)$  is the net energy entering the soil surface,  $G_1$  is the amplitude,  $\omega_1$  the fundamental frequency, and  $\varepsilon_1$  the initial phase of the surface forcing.

Different ways of approximating  $T(\delta, t)$  have resulted in different versions of FRM, but a general form suggested by Bhumalkar (1975), Blackadar (1976), Deardorff (1978) and Lin (1980) to estimate the ground surface temperature  $T_g$  (reviewed by Hu and Islam, 1995) is

$$\frac{dT_g}{dt} = C_1 G(0, t) - C_2 (T_g - \bar{T}) \quad (2.45)$$

where  $\bar{T}$  is the deep soil temperature. The first term of the RHS of Eq.(2.45) is the forcing term while the second term is the restoring term. The coefficients  $C_1$  and  $C_2$  of different versions of FRM are given in Table 2.3. The Deardorff (1978) version of FRM is used in SDSM because his work is applicable to predict temperature of different layer of snowpack.

In terms of the snow surface temperature,  $T_s$ , Eq. (2.45) can be written as

$$\frac{dT_s}{dt} = C_1 G(0, t) - C_2 (T_s - \bar{T}) \quad (2.46)$$

where  $\bar{T}$  is the near surface ground temperature ( $T_g$ ). Rearranging Eq.(2.46) and replacing  $\bar{T}$  with  $T_g$  gives,

$$G(0, t) = A_1 \frac{dT_s}{dt} + B_1 (T_s - T_g) \quad (2.47)$$

where  $A_1 = 1/C_1$  and  $B_1 = C_2/C_1$ .

$T_s$  can be solved using the simple finite difference scheme,

$$Q^* = G(0, t) = A_1 \left( \frac{T_s - T_{s-1}}{\Delta t} \right) + B_1 (T_s - T_g) \quad (2.48)$$

and solving for  $T_s$

$$T_s = \frac{\left[ Q^* + \left( \frac{A_1}{\Delta t} \right) T_{s-1} + B_1 T_g \right]}{\left[ \left( \frac{A_1}{\Delta t} \right) + B_1 \right]} \quad (2.49)$$

By setting the damping depth of the diurnal temperature wave,  $d_1$ , in terms of the diurnal frequency,  $\omega_1$ , [i.e.  $d_1 = \sqrt{2k/\omega_1}$  after Sellers (1965)],  $A_1$  and  $B_1$  become

$$A_1 = \sqrt{\frac{\lambda c}{2\omega_1}} \quad (2.50)$$

$$B_1 = \sqrt{\frac{\lambda c \omega_1}{2}} \quad (2.51)$$

where  $\omega_1 = \frac{2\pi}{86400}$ .

#### (b) Surface Conductance Method (SCM)

Tarboton and Luce (1996) computed  $T_s$  from a simple heat conduction ( $Q$ ) that is near steady state over an effective depth  $Z_e$  (or depth of penetration of diurnal surface temperature fluctuation) (Rosenberg, 1974), where thermal gradient acts. Following this simple approach and considering a uniform temperature gradient between  $T_s$  and temperature at the bottom of the snowpack (approximating with  $T_g$ ),

$$Q = \kappa \rho_s c_s \left( \frac{T_s - T_g}{Z_e} \right) = K_{sc} \rho_s c_s (T_s - T_g) \quad (2.52)$$

where  $\kappa$  is snow thermal diffusivity ( $m^2/s$ ) and  $Z_e$  (m) is an effective depth over which this thermal gradient acts. The ratio  $\kappa/Z_e$  is termed the snow surface conductance,  $K_{sc}$  (m/s), which can be used to fine-tune the simulated  $T_s$ . Eq. (2.52) is the simple form of Eq. (2.46), in which  $dT_s/dt$  is set equal to zero, thereby ignoring the diurnal cycle of surface temperature. Assuming equilibrium at the surface, the surface energy balance, given as a function of  $T_s$  (see Figure 2.2) is,

$$\dot{Q} = Q_{sn} + Q_{li} - Q_{lc}(T_s) + Q_h(T_s) + Q_e(T_s) + Q_p + Q_g \quad (2.53)$$

Analogous to Penman equation for evaporation, the above functions of  $T_s$  are

linearized about a reference temperature  $T^*$  (see Deardorff, 1978) and the equation can be solved for  $T_s$  for each time step.

$$T_s = \frac{Q_{sn} + Q_{li} + Q_p + KT_a \rho_a c_p - 0.6K\lambda_v \rho_a (e_s(T^*) - e_a - T^* \Delta) / P_a + 3\varepsilon_s \sigma T^{*4} + \rho_s c_s T K_{sc}}{\rho_s c_s K_{sc} + K \rho_a c_p + 0.6\Delta K \lambda_v \rho_a / P_a + 4\varepsilon_s \sigma T^{*3}} \quad (2.54)$$

where  $K$  ( $=C_h$  or  $e \times V$ ) is the heat/vapor conductance (m/s),  $\Delta = de_s/dT_a [= 4098 e_s / (237.3 + T_a)^2]$ , and temperature is solved iteratively with some initial guess. In each iteration,  $T^*$  (in °K or converted to °C wherever applicable) is replaced by the latest  $T_s$  until the difference between new  $T^*$  and  $T_s$  is very small. The saturated vapor pressure,  $e_s(T^*)$  is computed using Eq. (2.29) with  $T^*$  changed to °C. This method can also be called as a fixed surface conductance method as long as  $K_{sc}$  is fixed for the simulation period.

### (c) Kondo and Yamazaki Method (KYM)

This procedure relates the snow surface temperature ( $T_{s, n+1}$ ) at the present time step as a function of  $T_{s, n}$  of the previous time step, the change in freezing depth ( $Z_n - Z_{n+1}$ ) between the time step ( $\Delta t$ ), and the net energy received by snowpack  $Q^*$ ,

$$\frac{1}{2} c_s \rho_s [Z_n (T_o - T_{s, n}) - Z_{n+1} (T_o - T_{s, n+1})] + W_o \rho_s \lambda_f (Z_n - Z_{n+1}) + M_o \Delta t = Q^* \Delta t \quad (2.55)$$

where  $T_o = 0^\circ\text{C}$ ,  $W_o$  is the maximum water content in the snowpack, the subscripts  $n$  refers to time step, and other symbols are as defined previously. The first term on the left-hand side of Eq. 2.55 describes the energy of heating and cooling of the snow (shaded portion in Figure 2.3), and the second term accounts for the energy of melting or freezing of the liquid water remaining in snow layer (dotted portion in Figure 2.3). In the third term,  $M_o$  is the energy required to create runoff from the snow cover in excess of the maximum liquid water content. The net energy term  $Q^*$  on the right-hand side is similar to  $Q$  in Eq. 2.53.

Considering that the snow surface transmits solar radiation and the incoming long-

wave radiation ( $Q_{li}$ ) is measured, the energy balance equation of a snow surface with an infinitesimal thickness can be given according to Kondo and Yamazaki (1990) as

$$\varepsilon(Q_{li} - \sigma T_{s,n+1}^4) + Q_h(T_{s,n+1}) + Q_e(T_{s,n+1}) + \lambda \frac{T_o - T_{s,n+1}}{Z_{n+1}} = 0 \quad (2.56)$$

where  $\lambda$  is the thermal conductivity of snow. When the net radiation ( $Q_n$ ) and the global solar radiation ( $Q_s$ ) are measured instead of  $Q_{li}$ , the first term of Eq. 2.56 can be replaced by  $[Q_n - (1-\alpha)Q_s]$ .

Expanding  $(T_{s,n+1})^4$  around  $T_a$  to approximate a non-linear form of  $T_{s,n+1}$  to a linear form (Deardorff, 1978) such that  $(T_{s,n+1})^4 \approx T_a^4 + 4T_a^3(T_{s,n+1} - T_a)$ , and substituting the values of  $Q_h$  (using Eq. 2.26) and  $Q_e$  (using Eq. 2.28) in the Eq. 2.56 and solving this with Eq. 2.55, it is possible to obtain the snow surface temperature  $T_{s,n+1}$ . Solving  $T_{s,n+1}$  in each time step requires first solving  $Z_{n+1}$ , which is obtained by solving a quadratic equation (Kondo and Yamazaki, 1990).

In SDSM-EBM, the FRM, SCM and KYM methods are used to simulate  $T_s$ . If  $T_s > 0^\circ\text{C}$ , it means the energy input to the snow surface is partly for thermal conduction and partly for surface melt. The infiltration of meltwater will account for the energy difference and  $T_s$  is then reset to  $0^\circ\text{C}$ . In addition, channels 3 and 4 of cloud free NOAA-AVHRR images are used to obtain  $T_s$  and compare with the model-simulated values.

#### 2.2.4.2 Computation of Snowpack Water Balance

The snowpack water balance equations in SDSM are expressed in terms of water and ice at both canopy and ground level (see Eq. 2.8c and Figure 2.4) as

$$\rho_w c_s W^{t+\Delta t} T_{sp}^{t+\Delta t} = \rho_w c_s W^t T_{sp}^t + (Q_n + Q_h + Q_e + Q_g + Q_p) + Q_m \quad (2.57)$$

$W^{t+\Delta t}$  (or SWE for the next time step) accounts for both the addition of precipitation ( $P_r$  or  $P_s$ ) during the time step and the change in water and ice mass due to the latent

heat transfer (sublimation or freezing)  $Q_e$  depending on whether  $T_{sp}^t$  is isothermal at zero or less than zero,

$$\text{If } T_{sp}^t = 0: \quad W_{liq}^{t+\Delta t} = W_{liq}^t + P_r + \frac{Q_e}{\rho_w \lambda_v} \quad (2.58)$$

$$W_{ice}^{t+\Delta t} = W_{ice}^t + P_s \quad (2.59)$$

$$\text{and if } T_{sp}^t < 0: \quad W_{liq}^{t+\Delta t} = W_{liq}^t + P_r \quad (2.60)$$

$$W_{ice}^{t+\Delta t} = W_{ice}^t + P_s + \frac{Q_e}{\rho_w \lambda_s} \quad (2.61)$$

The net energy exchange in the snowpack ( $Q^*$ ) is then equal to

$$Q^* = (Q_n + Q_h + Q_e + Q_g + Q_p) \quad (2.62)$$

If  $Q^* < 0$ , the snowpack is losing energy to the atmosphere (cooling), and some liquid water (if available) may refreeze. The amount of energy released to the snowpack (positive value) by re-freezing liquid water is given by

$$Q_m = \min(-Q^*, \rho_w \lambda_f W_{liq}^{t+\Delta t}) \quad (2.63)$$

where  $\lambda_f$  is the latent heat of fusion of ice ( $3.35 \times 10^5 \text{ J kg}^{-1}$ ) and  $\rho_w \lambda_f W_{liq}^{t+\Delta t}$  the amount of energy that would be released to the snowpack by the re-freezing of available liquid water in the snowpack. The resulting change in the liquid and ice phases are given by

$$W_{liq}^{t+\Delta t} = W_{liq}^{t+\Delta t} - \frac{Q_m}{\rho_w \lambda_f} \quad (2.64)$$

$$W_{ice}^{t+\Delta t} = W_{ice}^{t+\Delta t} + \frac{Q_m}{\rho_w \lambda_f} \quad (2.65)$$

$$W^{t+\Delta t} = W_{liq}^{t+\Delta t} + W_{ice}^{t+\Delta t} \quad (2.66)$$

The snowpack temperature,  $T_{sp}^{t+\Delta t}$  (associated with its cold content), is then updated from Eq. (2.57).

If  $Q^* > 0$ , the snowpack is gaining energy from the atmosphere (heating), and in the process the negative snowpack temperature,  $T_{sp}^{t+\Delta t}$  (associated with its cold content) will increase until it just reaches the isothermal condition ( $T_{sp}^{t+\Delta t} \rightarrow 0$ ). When  $T_{sp}^{t+\Delta t}$  becomes positive, it is set equal to zero and the excess energy for melting the ice phase to liquid,  $Q_m$  is computed by Eq. (2.57) and applied to Eq.(2.64) and (2.65) to compute the new liquid and ice components of SWE.

At each time step, the compaction of snowpack,  $S_{comp}$  is calculated according to Riley et al. (1972), which use the present snowpack density  $\rho_{sp}$  ( $=W^{t+\Delta t} / SD^{t+\Delta t}$ , that includes the snow depth of fresh snow), maximum allowable density  $\rho_{s,max}$ , and a settlement constant,  $c_s$ .

$$S_{comp} = SD^{t+\Delta t} c_s \left( 1 - \frac{\rho_{sp}}{\rho_{s,max}} \right) \quad (2.67)$$

The depth of snowpack after compaction is the difference between  $SD$  and  $S_{comp}$ . The parameters  $\rho_{s,max}$  and  $c_s$  are obtained by manual calibration such that the model simulated  $SD$  match the corresponding snow course data for the given land-use. The effect of compaction due to rain on snow is also taken into consideration by Eq. (2.67), where  $SD^t$  replaces  $SD^{t+\Delta t}$  when precipitation is in the form of rain.

During melt,  $Q_m$  is negative, removing mass from the ice phase and increasing the liquid phase. Water is removed from the snowpack as meltwater ( $m_{ij}$ ) when  $T_{sp}^{t+\Delta t}$  is isothermal at  $0^\circ\text{C}$  and the liquid phase exceeds the current liquid water holding capacity (LWHC) of the snowpack.

$$m_{ij} = W_{liq}^{t+\Delta t} - (\text{LWHC})W^{t+\Delta t} \quad (2.68)$$

where 'i' is the sub-basin number and 'j' is the land cover type. LWHC of snow is the amount of water held within the pack at the time when snow surface melt first appears at the bottom of the snowpack and is a function of snowpack density and



several other factors (like shape, size and distribution of snow grain, presence of depth-hoar due to significant temperature gradient). For LWHC, U.S. Army Corps of Engineers (1956) recommends a value of 0.02W to 0.05W (2-5% of SWE) for a wide range of snow pack density. Riley et al. (1972) and others recommend a value of 0.05W for snowpack having density less than 400 kg/m<sup>3</sup>. Since the snow density in Prairies is less than 400 kg/m<sup>3</sup> in most cases, a value of 0.05W as LWHC is assumed in SDSM.

Meltwater routing within the pack is not considered in this present version of SDSM as the time of travel from the top to the bottom of the snowpack for a depth less than 0.55m is less than one hour (Bathurst and Cooley, 1996), which indicates that for a model simulation step of one hour or more, meltwater routing within the snowpack is not significant for a shallow seasonal snowcover. Thus, SDSM considers meltwater to be available at the bottom of snowpack for runoff production, thereby reducing the liquid water content of snowpack,  $W_{liq}^{t+\Delta t}$  as,

$$W_{liq}^{t+\Delta t} = W_{liq}^{t+\Delta t} - m_{ij} \quad (2.69)$$

and the final SWE of snowpack is computed from Eq. (2.66).

We have also included the heat budget in a thermally active soil layer ( $D_e$ ) beneath the snowpack. But, instead of considering this soil layer having the same temperature as that of snowpack (as used by Tarboton and Luce, 1996), we use the observed ground temperature data,  $T_g$  (assuming that the temporal change in  $T_g$  for a soil depth of about 10 cm measured at our study site does represent the temporal change in temperature for the thermally active soil layer). Thus  $\rho_g c_g D_e (T_g^t - T_g^{t+1})$  is added to the right hand side of Eq. (2.57), where  $\rho_g$  is the density of soil (assumed 1700 kg/m<sup>3</sup>), and  $c_g$  the soil specific heat. In SDSM,  $c_g$  is assumed to be 2090 J kg<sup>-1</sup> °C<sup>-1</sup>, which is also assumed by Tarboton and Luce (1996).

### 2.2.5 Snowmelt for each Sub-Basin

The local snowmelt for each time-step,  $M_i$  for each sub-basin is determined by summing the total melt from each land cover, weighted by their corresponding areal fraction  $\phi_j$  as

$$M_i = \sum_{j=1}^n \phi_j m_{ij} \quad (2.70)$$

where 'i', 'j' and 'n' are sub-basin number, land cover class and number of land cover class used in SDSM respectively.

## 2.3 Developing SDSM within DPHM-RS

SDSM is developed within the Semi-distributed, physically based, hydrological model using GIS and Remote Sensing or DPHM-RS (Biftu and Gan, 2001) to simulate basin-scale hydrological processes (see Figure 2.4 and 2.5: Flow chart of DPHM-RS model) during winter periods. When there is snow overlying the ground surface or snowfall, SDSM in DPHM-RS keeps track of the snow accumulation and ablation component of basin hydrology.

## 2.4 Division of a River Basin into Sub-Basins and Response Functions

In modeling basin-scale hydrology, some researchers propose a fully-distributed approach, e.g. the representative elemental area (REA) of Wood et al. (1998), which according to Fan and Bras (1995) is artificial, and does not exist in natural environment. Moreover, the limitation of input data and the difficulty in estimating effective model parameters values pose problems to the use of fully distributed models (Beven, 1996). On the other hand, semi-distributed models where a basin is divided into sub-basins called hydrological response units (HRU), or the group response units (GRU), or homogeneous hydrological units (HHU) is more practical

(Amerman, 1965; England and Stephenson, 1970; Kouwen, 1988; Fortin et al., 1990b; Martinec et al., 1992; Kite, 1995; Blöschl and Sivapalan, 1995).

SDSM follows the semi-distributed approach of DPHM-RS (Getu and Gan, 2001) where a study basin is divided into a number of sub-basins drained by a defined drainage network. The study site, Paddle River Basin (PRB) is divided into five sub-basins based on the digital elevation model (DEM) data and the strategic pour-point (sub-basin's lowest point or outfall) locations along the PRB drainage network using the WTRSHED module of PCI image processing software. For SDSM, the six land use types derived from Landsat TM image for each of the sub-basins are grouped into three: (1) coniferous forest, (2) mixed or deciduous forest, and (3) open area without vegetation canopy. The hydrological processes are evaluated for each land cover class at point scale and then aggregated according to the proportions of land cover areas present within the sub-basin. All the hydrological processes other than the snow accumulation and its ablation (e.g., infiltration, soil moisture, overland flow, base flow etc., also see Figure 2.5) are taken care of by calibrated model parameters of DPHM-RS. Finally, the surface runoff of each sub-basin is routed to the channel network based on an average response function derived for each sub-basin (see Figure 2.6).

## **2.5 Evaluation of Model Performance**

The classic approach in calibrating hydrologic parameters has been to minimize the deviation of simulated runoff from observed runoff. This approach has also been used in hydrological or snowmelt models: e.g., SRM (Martinec et al., 1992), UBC model (Micovic and Quick, 1999). However, the development of more physically based hydrological models to study the hydrological impact of land-use changes and land-atmospheric interaction with respect to climate change have changed the concept of calibration in hydrological models. Some authors even express doubt against the use of such a calibration criterion (difference between simulated and

observed runoff) in fully distributed hydrological models due to the large number of parameters involved in the hydrological processes (e.g. Beven, 1989; Rafsgaard, 1997). This traditional method of calibration is particularly inadequate with snow accumulation and ablation processes, where there is no runoff during snow accumulation period but variables such as snow depth, SWE, snow surface temperature etc change with time. To account for the distributed nature of internal processes within the model, a multi-objective calibration criterion was adopted (see Chapter 3).

In applying SDSM to the study site, Paddle River basin (PRB), some model parameters are calibrated with respect to snow course survey data, surface temperature retrieved from remotely sensed data, and basin outflow data. Model calibration is evaluated in terms of statistics like the Root Mean Square Error, RMSE; Coefficient of Determination,  $R^2$ ; and Nash-Shutcliffe Modeling Efficiency,  $E_f$  (see Table 2.4).

## 2.6 Model Organization

At each time step and for each of the land use options, the global parameters associated with SDSM are first accessed. Upon selection of energy balance method, the model first searches for the net radiation input file in the data directory. If net radiation data file is not available, then the global solar radiation input file is used to compute the various individual components of radiation budget in each of the landuse to determine the net radiation at the canopy and the ground levels. Three different heat conduction options are available in SDSM to simulate the snow surface temperature with respect to landuse. Wind speed is attenuated in the forest-covered area to reduce the turbulent heat fluxes, which in turn modifies the snow surface temperature. SDSM code is set up in such a manner that the major model

parameters can be changed for various scenarios with single compilation. This can be achieved by changing the parameters within SDSM menu prior to model run.

## 2.7 Summary

A semi-distributed snowmelt model (SDSM), developed to take advantage of the remotely sense data, models the basin-scale snow accumulation and ablation processes by sub-dividing a basin as a number of sub-basins, each with its own land cover types and terrain features, and drained by a network of stream channels. SDSM models the snowmelt processes using energy balance method, which considers (a) vertical energy exchange processes in open and forested area separately, (b) snowfall, canopy interception, fresh snow density, surface sublimation and blowing snow sublimation, refreezing, snow compaction, (c) snowmelt in terms of liquid and ice phases within the snowpack separately, (d) snow surface temperature simulation using force restore method, surface conductance method, and Kondo and Yamazaki method. This SDSM works within DPHM-RS (semi-distributed, physically based, hydrologic model using remotely sensed data), which accounts for the Hortonian, the saturation overland, and the subsurface runoff from each sub-basin, and routes them to the stream channel by an average, kinematic response function derived for each of the sub-basin, and then to the basin outlet using Muskingum-Cunge method.

As ground based point measurements are limited, SDSM is designed to take advantage of spatially distributed information such as topography (DEM data), land-use classification (using Landsat-TM data), and spatially and temporally distributed surface physical parameters (e.g., LAI, Albedo, and surface temperature data retrieved from NOAA-AVHRR data) that signify basin characteristics with respect to land use types of each sub-basin. This SDSM/DPHM-RS system can be used for studying the hydrological impact of land use changes and a land surface component of a meso-scale atmospheric model for climate change studies.

## References

- Abbott, M. B., Bathurst, J. C., Cunge, J. A., O'Connell P.E., and Rasmussen J. (1986), An introduction to the European Hydrological System-System Hydrologique Europeen, 'SHE', 1: History and philosophy of a physically-based, distributed modeling system. *J. Hydrol.*, 87(1/2):45-59.
- Amerman, C. R. (1965), The use of unit-source watershed data for runoff prediction. *Water Resour. Res.*, 1(4):499-507.
- Anderson, E. A. (1968), Development and testing of snowpack energy balance equations. *Water Resour. Res.*, 4(1):19-37.
- Anderson, E. A. (1973), *National Weather Service River Forecast System - Snow accumulation and ablation model*, NOAA Tech. Memorandum NWS Hydro-17, US Dept. of Commerce, Silver Spring, Maryland, USA.
- Anderson, E. A. (1979), Stream flow simulation models for use on snow covered watersheds. In: *Modeling of Snow Cover Runoff*, ed. S. C. Colbeck and M. Ray, Proc. Meeting, Hanover, New Hampshire, Sept. 1978, US Army Cold Regions Research and Engineering Laboratory, 336-350.
- Bales, R. C., and Harrington, R. F. (1995), Recent progress in snow hydrology. *Reviews of Geophysics*, Supplement, 1011-1020.
- Bathurst, J. C., and Cooley, K.R. (1996), Use of the SHE hydrological modeling system to investigate basin response to snowmelt at Reynolds Creek, Idaho, *J. Hydrol.*, 175:181-211.
- Bengtsson, L. (1986), Snowmelt simulation models in relation to space and time. *IAHS Publ. No. 155*:115-123.
- Beven, K. J. (1989), Changing ideas of hydrology: the case of physically-based models. *J. Hydrol.*, 105:157-172.
- Beven, K. J. (1996), A discussion of distributed hydrological modeling. In: *Distributed hydrological modeling*, ed. M. B. Abbott, and J. C. Refsgaard, Water Resources Publications, 255-278.

- Beven, K. J., Lamb, R., Quinn, P., Romanowicz, R., and Freer, J. (1995), TOPMODEL. In: *Computer models of watershed hydrology*, ed. V. P. Singh, Water Resources Publications, Colorado, 627-668.
- Bhumralkar, C. M. (1975), Numerical experiments on the computation of ground surface temperature in an atmospheric general circulation model. *J. Appl. Meteorol.*, 14:1246-1258.
- Biftu, G. F. (1998), *Semi-distributed, physically based hydrologic modeling using remotely sensed data and GIS*. PhD thesis, University of Alberta, Edmonton, Canada, 218 p.
- Biftu, G. F., and Gan, T. Y. (2001), Semi-distributed, physically-based, hydrological modeling of the Paddle River Basin, Alberta using remotely sensed data, *J. Hydrol.*, 244:137-156.
- Blackadar, A. K. (1976), Modeling the nocturnal boundary layer, In: *Proceedings of the Third Symposium on Atmospheric Turbulence, Diffusion and Air quality*, American Meteorological Society, Boston, Mass., pp. 46-49.
- Blondin, C. (1991), Parameterization of land surface processes in numerical weather prediction, In: *Land surface Evaporation: Measurement and parameterization*, edited by T.J. Schmugge and J.C. Andre, Springer-Verlag, New York, pp. 31-54.
- Blöschl, G. (1999), Scaling issue in snow hydrology. *Hydrol. Proc.*, 13: 2149-2175.
- Blöschl, G., and Kirnbauer, R.(1991). Point snowmelt models with different degree of complexity – internal processes. *J. Hydrol.*, 129:127-147.
- Blöschl, G., and Sivapalan, M. (1995), Scale issues in hydrological modeling: a review. *Hydrol. Proc.*, 9:251-290.
- Blöschl, G., Kirnbauer, R., and Gutknecht, D. (1990), Modeling snowmelt in a mountainous river basin on an event basis. *J. Hydrol.*, 113:207-229.
- Blöschl, G., R. (1990), The influence of uncertainty in air temperature and albedo on snowmelt. *Nordic Hydrology*, 22:95-108.

- Braun, L. N. (1985), *Simulation of snowmelt-runoff in lowland and lower alpine regions of Switzerland*. Zurich Geographische Schriften, Heft 21, Geographisches Institut ETH Zurich, 166p.
- Brutsaert, W. (1975), On a derivable formula for long-wave radiation from clear skies, *Water Resour. Res.*, 11:742-744.
- Brutsaert, W. (1982), *Evaporation into the Atmosphere*. D. Reidel Pub. Co., Dordrecht, Holland, 299p.
- Choudhury, B. J. (1987), Relationships between vegetation indices, radiation absorption, and net photosynthesis evaluated by a sensitivity analysis, *Remote Sens. Environ.*, 22:209-233.
- Choudhury, B. J., and Monteith, J. L. (1988), A four-layer model for the heat budget of homogeneous land surfaces. *Q.J.R. Meteorol. Soc.*, 114:373-398.
- Chow V. T., Maidment, D. R., and Mays, L. W. (1988), *Applied Hydrology*, McGraw-Hill International Editions, 572p.
- Colbeck, S. C. (1972), A theory of water percolation in snow. *J. Glaciol.*, 11:369-385.
- Colbeck, S. C. (1973), *Theory of metamorphism of wet snow*. USA Cold Regions Research and Engineering Laboratory (CRREL), Research Report 313.
- Colbeck, S. C. (1976), An Analysis of water flow in dry snow. *Water Resour. Res.*, 12(3):523-527.
- Colbeck, S. C. (1977), Short-term forecasting of water run-off from snow and ice. *J. Glaciol.*, 19(81):571-587.
- Colbeck, S. C., and Davidson, G. (1973), Water percolation through homogeneous snow, In: *The Role of Snow and Ice in Hydrology*. Proceedings of the Banff Symposium, September 1972, IAHS, Wallingford, Publ. No. 107:242-257.
- Deardorff, J. W. (1978), Efficient prediction of ground surface temperature and moisture, with inclusion of layer of vegetation. *J. Geophys. Res.*, 83(C4):1889-1097.



- Dery, S. J., and Yau, M. K. (2001a), Simulation of blowing snow in the Canadian Arctic using a double-moment model. *Boundary-Layer Meteorol.*, 99:297-316.
- Dery, S. J., and Yau, M. K. (2001b: in press), Simulation of Arctic ground blizzard using a coupled blowing snow - atmosphere model. *J. Hydrometeorology*.
- Dickinson, R. E. (1984), Modeling evapotranspiration for three-dimensional global climate models. In: Climate processes and climate sensitivity, ed. Hansen, J.E., and Takahashi, T., *Geophys. Monogr. Ser.*, 29, AGU, Washington D.C., 58-72.
- Dickinson, R. E. (1988), The force-restore model for surface temperature and its generalizations. *J. Climate*, 1:1086-1097.
- Donald, J. R. (1993), *Snowcover depletion curves and satellite snowcover estimates for snowmelt runoff modeling*. Ph. D. thesis, Univ. of Waterloo, Ontario, 232p.
- England, C. B., and Stephenson, G. R. (1970), Response units for evaluating the hydrologic performance of rangeland watersheds. *J. Hydrol.*, 11:89-97.
- Fan, Y., and Bras, R. (1995), On the concept of a representative elementary area in catchment runoff. *Hydrol. Proc.*, 9:821-832.
- Fortin J. P., Villeneuve, J. P., Benoit, J., Blanchette, C., Montminy, M., Proulx, H., Moussa, R., and Bocquillon, C. (1990a), *Hydrotel 2.1 user's guide*, Universite du Quebec, Institut national de la recherche scientifique, INRS- Eau, Sainte-Foy (Quebec), 171p.
- Fortin J. P., Turcotte, R., Massicotte, S., Moussa, R., Fitzback, J., and Villeneuve, J. P. (2001), Distributed watershed model compatible with remote sensing and GIS data. I: development of model. *J. Hydrologic Engrg.*, 6(2):91-92.
- Fortin J. P., Villeneuve, J. P., Bocquillon, C., Leconte, R. Harvey, K. D. (1990b), HYDROTEL, a hydrological model designed to make use of remotely sensed and GIS data. In: *Proceedings of the workshop on applications of remote in hydrology*, ed. G. W. Kite and A. Wankiewicz, Saskatoon, Saskatchewan, Feb 13-14, 177-185.
- Fortin J. P., Villeneuve, J. P., Guibot, A., and Seguin, B. (1986), Development of a modular hydrological forecasting model based on remotely sensed data, for

- interactive utilization on a microcomputer. In: *Hydrologic applications of space technology*, ed. A. I. Johnson, 307-319.
- Freeze, R. A., and Harlan, R. L. (1969), Blueprint for a physically-based, digitally simulated hydrologic response model, *J. Hydrol.*, 9(3):237-268.
- Gan T.Y., Dlamini, E. M., and Biftu, G. F. (1997), Effects of model complexity an structure, data quality, an objective functions on hydrological modeling, *J. Hydrol.*, 192:81-103.
- Gan, T. Y., and Biftu, G. F. (1996), Automatic calibration of conceptual rainfall-runoff models: optimization algorithms, catchment conditions, and model structure. *Water Resour. Res.*, 32(12):3513-3524.
- Garnier, B. J., and Ohmura, A. (1970), The evaluation of surface variations in solar radiation income. *Solar Energy*, 13:21-34.
- Golding, D. L., and Swanson, R. S. (1986), Snow distribution patterns in clearings and adjacent forest. *Water Resour. Res.*, 22:1931-1940.
- Granberg, G., Grip, H., Löfvenius, M. O., Sundh, I., Svensoon, B. H., and Nilsson, M. (1999), A simple model for simulation of water content, soil frost, and soil temperatures in boreal mixed mires, *Water Resour. Res.*, 35(12):3771-3782
- Granger, R. J., and Gray, D. M. (1990), A net radiation model for calculating daily snowmelt in open environments. *Nordic Hydrology*, 21:217-234.
- Gray, D. M., and Landine, P. G. (1987), Albedo model for shallow prairie snowcovers. *Can. J. Earth Sciences*, 25:1292-1303.
- Gray, D. M., and Male, .D. H. (Eds.), (1981), *Handbook of snow*, Pergamon Press Canada Ltd.
- Harding, R. J. (1986), Exchanges of energy and mass associated with a melting snowpack. In: *Modeling snowmelt processes*, ed. Morris, E.M., IAHS Publ., 155:3-15.
- Hardy, J. P. and Hansen-Bristow, K. J. (1990), Temporal accumulation and ablation patterns in forests representing varying stages of growth, In: *Proc. of the 58th Western Snow Conf.* Sacramento, CA, 23-34.

- Hardy, J. P., Davis, R. E., Jordan, R., Li, X., Woodcock, C., Ni, W., and McKenszie, C. (1997), Snow ablation modeling at the stand scale in a boreal jack pine forest, *J. Geophys. Res.*, 102(N24):29 397-29 406.
- Hardy, J. P., Davis, R. E., Jordan, R., NI, W., and Woodcock, C. (1998), Snow ablation modeling in a mature aspen stand of the boreal forest. *Hydrol. Proc.*, 12(10/11):1763-1778.
- Hartman M. D., Baron, J. S., Lammers, R. B., Cline, D. W., Band, L. E., Liston, G. E., and Tague, C. (1999), Simulation of sow distribution and hydrology in a mountain basin. *Water Resour. Res.*, 35(5):1587-1603.
- Hu Z., and Islam, S. (1995), Prediction of ground surface temperature and soil moisture content by the force-restore method. *Water Resour. Res.*, 31(10):2531-2539.
- Jackson, T. H. R. (1994), *A spatially distributed snowmelt-driven hydrologic model applied to Upper Sheep Creek*. Ph.D. thesis, Utah State University, Logan, Utah, USA.
- Jacobs, A. F. G., Heusinkveld, B. G., and Berkowicz, S. M. (2000), Force-restore technique for ground surface temperature and moisture content in a dry desert system. *Water Resour. Res.*, 36(5):1261-1268.
- Jordan, P., (1983), Meltwater movement in a deep snowpack. 2, Simulation model. *Water Resour. Res.*, 19(4):979-985.
- Jordan, R. (1991), *A one-dimensional temperature model for a snow cover: Technical documentation for SNTHERM.89*. Special Report 91-16, U.S. Army Cold Regions Research and Engineering Laboratory, Hanover, N.H., 49 p.
- Kane, D. L., Gieck, R. E., and Hinzman, L. D. (1997), Snowmelt modeling at small Alaskan arctic watershed. *J. Hydrologic Engrg.*, 2(4):204-210.
- Kawashima S., T. Ishida, M. Minomura, and T. Miwa. (2000), Relations between surface temperature and air temperature on a local scale during winter nights. *J. Appl. Meteorol.*, 39:1570-1579.

- Kerr, Y. H., Lagouarde, J. P., and Imbernon, J. (1992), Accurate land surface temperature retrieval from AVHRR data with use of an improved split window algorithm. *Remote Sens. Environ.*, 41:197-209.
- Kirnbauer, R., Blöschl, G., and Gutknecht, D. (1994), Entering the era of distributed snow models. *Nordic Hydrology*, 25:1-24.
- Kite G. W. (1995), Scaling of input data for macroscale hydrologic modeling. *Water Resour. Res.*, 31(11):2769-2781.
- Kite G. W. (1996), Manual for the SLURP Hydrological Model (Ver.10). *National Hydrology Research Institute (NHRI)*, Saskatoon, SK, Canada. 130p.
- Kite G. W., and Pietroniro, A. (1996), Remote sensing applications in hydrological modeling. *Hydrol. Sci. J.*, 41(4):563-591.
- Kondo J., and Yamazaki, T. (1990), A Prediction Model for Snowmelt, Snow Surface Temperature and Freezing Depth Using a Heat Balance Method. *J. of Appl. Meteorol.*, 29:375-384.
- Kondo J., and Yamazawa, H. (1986), Bulk transfer coefficient over a snow surface. *Boundary-Layer Meteorol.*, 34:123-135.
- Kouwen, N. (1988), WATFLOOD. A microcomputer based flood forecasting system based on real-time weather radar. *Can. Water Resour. J.*, 13(1):62-77.
- Kuchment, L. S., and Gelfan, A. N. (1996), The determination of the snowmelt rate and the meltwater outflow from a snowpack for modeling river runoff generation. *J. Hydrol.*, 179:23-36.
- Kustas, W. P., Jackson, T. J. (1999), The impact of area-averaged heat fluxes from using remotely sensed data at different resolutions: A case study with Washita '92 data. *Water Resour. Res.*, 35(5):1539-1550.
- Kustas, W. P., Rango, A., and Uijlenhoet, R. (1994), A simple energy budget algorithm for the snowmelt runoff model. *Water Resour. Res.*, 30(5):1515-1527.
- Kustas, W. P., Zhan, X., and Schmugge, T. J. (1998), Combining optical and microwave remote sensing for mapping energy fluxes in a semiarid watershed. *Remote Sens. Environ.*, 64:116-131.

- Leavesley, G. H. (1989), Problems of snowmelt runoff modeling for a variety of physiographic and climatic conditions. *Hydrol. Sci. J.*, 34(6): 617-634.
- Leydecker, A., and Melack, J. M. (1999), Evaporation from snow in the central Sierra Nevada of California. *Nordic Hydrology*, 30(2):81-108.
- Lin, J. D. (1980), On the force-restore method for prediction of ground surface temperature. *J. Geophys. Res.*, 85:3251-3254.
- Linsley, R. K. Jr. (1943), A simple procedure for the day-to-day forecasting of runoff from snowmelt. *Trans. Amer. Geophys. Union*, Part III:62-67.
- Liston, G. E. (1995), Local advection of momentum, heat, and moisture during the melt of patchy snow covers. *J. Appl. Meteorol.*, 34:1705-1715.
- Liston, G. E. (1999), Interrelationships between snow distribution, snowmelt, and snowcover depletion: implications for atmospheric, hydrologic, and ecologic modeling. *J. Appl. Meteorol.*, 38:1474-1487.
- Liston, G. E., and Sturm, M. (1998). A snow-transport model for complex terrain. *J. Glaciol.*, 44(148):498-516.
- Louice, J. F. (1979), A parametric model of vertical eddy fluxes in the atmosphere. *Boundary-Layer Meteorol.*, 66:281-301.
- Loukas A., and Quick, M. C. (1999), The effect of climate change of floods in British Columbia. *Nordic Hydrology*, 30:231-256.
- Luce, C. H., Tarboton D. G., and Cooley, K. R. (1998b), Sub grid parameterization of snow distribution for an energy and mass balance snowcover model. In: *International Conference on Snow Hydrology*, Brownsville, Vermont. USA, 6-9 October.
- Luce, C. H., Tarboton, D. G., and Cooley, K. R. (1998a), The influence of the spatial distribution of snow on basin-averaged snowmelt. *Hydrol. proc.*, 12 (10/11):1671-1683.
- Male D. H., and Granger, R. J. (1981), Snow surface energy exchange. *Water Resour. Res.*, 17(3):609-627.

- Marshall S., Roads, J. O., and Glatzmaier, G. (1994), Snow hydrology in a general circulation model. *J. Climate*, 7:1251-1269.
- Martinec, J. (1960), The degree-day factor for snowmelt runoff forecasting. IUGG General Assembly of Helsinki, IAHS Commission of Surface Water, *IAHS Publ.* 51:468-477.
- Martinec, J. (1970), Study of snowmelt runoff process in two representative watersheds with different elevation range. IAHS-UNESCO Symposium, Wellington, N.Z., *IAHS Publ.* 96:23-39.
- Martinec, J. (1975), Snowmelt-Runoff Model for stream flow forecasts. *Nordic Hydrology*, 6(3):145-154.
- Martinec, J., and Rango, A. (1986), Parameters values snowmelt runoff modeling, *J. Hydrol.*, 84:197-219.
- Martinec, J., Rango, A., and Roberts, R. (1992), *User's manual for the snowmelt-runoff model (SRM) (updated edition 1992, version 3.2)*. USDA, Hydrology Laboratory Technical report HL-17, Beltsville, Maryland, USA, 70p.
- Matcalfe, R. A., and Buttle, J. M. (1995), Controls of canopy structure on snowmelt rates in the boreal forest, In: *Proc. of the 52nd Eastern Snow Conf.*, Toronto, Ont., 249-257.
- Mecikalski, J. R., Diak, G. R., Anderson, M. C., and Norman, J. M. (1999), Estimating fluxes on continental scales using remotely sensed data in an atmospheric-land exchange model. *J. Appl. Meteorol.*, 38:1352-1369.
- Micovic, Z., and Quick, M. C. (1999), A rainfall and snowmelt runoff modeling approach to flow estimation at ungauged sites in British Columbia. *J. Hydrol.*, 226:101-120.
- Moore, R. D., and Owens, I. F. (1984), Modeling alpine snow accumulation and ablation using daily climate observations. *J. Hydrol. (NZ)*, 23(2):73-83.
- Morris, E. M. (1989), Turbulent transfer over snow and ice, *J. Hydrol.*, 105:205-223.

- Morton, F. I. (1978), Estimating evapotranspiration from potential evaporation: practicality of an iconoclastic approach. *J. Hydrol.*, 38(1/2):1-32.
- Nakawo M., and N. Hayakawa, (Eds.) (1998), *Snow and ice science in hydrology*, The IHP training course on snow hydrology, Institute of Hydrospheric-Atmospheric Sciences (IHAS), Nagoya University, 133p.
- Neumann, N., and Marsh, P. (1998), Local advection of sensible heat in the snowmelt landscape of Arctic tundra. *Hydrol. Proc.*, 12:1547-1560.
- Obled, Ch. (1990), Hydrological modeling in regions of rugged relief. In: *Hydrology in Mountainous Regions. I- Hydrological Measurements; the Water Cycle* (ed. H. Lang and A. Musy, Proc. Lausanne Symp., Aug. 1990), *IAHS Publ.*, 193:599-613.
- Obled, Ch., and Rosse, B. (1977), Mathematical models of a melting snowpack at an index plot. *J. Hydrol.*, 32:139-163.
- Olyphant, G. A. (1986), The components of incoming radiation within a mid-latitude alpine watershed during the snowmelt season, *Arctic Alpine Res.*, 18(2):163-169.
- Olyphant, G. A., and Isard, S. A. (1988), The role of advection in the energy balance of late-lying snowfields: Niwot. Ridge, Front Range, Colorado, *Water Resour. Res.*, 24(11):1962-1968.
- Peck, E. L., Keeper, T. N., and Johnson, E. R. (1981), Strategies for using remotely sensed data in hydrologic models. *NADA-CR-666729*, 77p.
- Pomeroy, J. W., and Schmidt, R. A. (1993), The use of fractal geometry in modeling intercepted snow accumulation and sublimation. In: *Proc. of the Joint Eastern and Western Snow Conf.*, Quebec City, P.Q., pp 1-10.
- Pomeroy, J. W., Gray, D. M., Shook, K. R., Toth, B., Essery, R. L. H., Pietroniro, A., and Hedstrom, N. (1998), An evaluation of snow accumulation and ablation processes for land surface modeling. *Hydrol. Proc.*, 12:2339-2367.
- Pomeroy, J. W., Marsh, P., and Gray, D. M. (1997), Application of distributed blowing snow model to the Arctic. *Hydrol. Proc.*, 11:1451-1464.

- Prasad, C. (1983), *Advanced mathematics for engineers*, Prasad Mudranalaya, Allahabad, India, 356p.
- Price, A. G. (1988), Prediction of snowmelt rates in a deciduous forest, *J. Hydrol.*, 101:145-157.
- Price, A. G. and T. Dunne, 1976. Energy balance computations of snowmelt in a subarctic area. *Water Resour. Res.*, 12(4):686-694.
- Qin Z., and Karnieli, A. (1999), Progress in the remote sensing of land surface temperature and ground emissivity using NOAA-AVHRR data. *Int. J. Remote Sensing*, 20(12):2367-2393.
- Rafsgaard, J. C. (1997), Parameterization, calibration, and validation of distributed hydrological models, *J. Hydrol.* 198:69-97.
- Rafsgaard, J. C., and Storm, B. (1995), MIKE-SHE. In: *Computer models in watershed hydrology*, ed. V. J. Singh, Water Resources Publications.
- Rango, A. (1985), Assessment of remote sensing input to hydrologic models. *Water Resources Bulletin*, 21(3):423-432.
- Rango, A., and Shalaby, A. I. (1998), Operational applications of remote sensing in hydrology: success, prospects and problems. *Hydrol Sci. J.*, 43(6):947-968.
- Riley, J. P., Israelsen, E. K., and Eggleston, K. O. (1972), Some approaches to snowmelt prediction. *AISH Publ.*, 2(107):956-971.
- Rogers, R. R., and Yau, M. K. (1989), *A Short Course in Cloud Physics*, Third Edition, Pergamon Press Canada Ltd, 293p.
- Rosenberg, N. J. (1974), *Microclimate the biological environment*, John Willey & Sons, Inc.
- Satterlund, D. R. (1979), An improved equation for estimating long-wave radiation from the atmosphere. *Water Resour. Res.*, 11:742-744.
- Sellers, W.D. (1965), *Physical Climatology*, Univ. of Chicago Press, Chicago, Ill.
- Shook, K. (1993), *Fractal Geometry of snowpacks during ablation*. M. Sc. thesis, Univ. of Saskatchewan, Saskatoon, Saskatchewan, Canada, 178p.



- Shook, K. (1995), *Simulation of the ablation of prairie snowcovers*. Ph. D. thesis, Univ. of Saskatchewan, Saskatoon, Saskatchewan, Canada, 189p.
- Shook, K., and Gray, D. M. (1997), Synthesizing shallow seasonal snow covers. *Water Resour. Res.*, 33(3):419-426.
- Sturm, M. (1992), Snow distribution and heat flow in the taiga, *Arctic and Alpine Res.* 24(2):145-152.
- Tarboton D. G., and Luce, C. H. (1996), *Utah Energy Balance Snow Accumulation and Melt Model (UEB), Computer model technical description and user's guide prepared by Utah Water Research Laboratory*. Utah State University and USDA Forest Service, Intermountain Research Station, 64p.
- U.S. Army Corps of Engineers (1956), *Snow Hydrology: Summary Report of the Snow investigations*. North Pacific Division, Corps of Engineers, U.S. Army, 210 Custom House, Portland, OR, 437p.
- Verseghy, D. L. (1991), Class-A Canadian land surface scheme for GCMs. I. Soil model. *Int. J. Climatology*, 11:111-133.
- Verseghy, D. L., Mcfarlane, N. A., and Lazare, M (1993), CLASS- A Canadian land surface scheme for GCMs, II. Vegetation model and coupled runs. *Int. J. Climatology*, 13:347-370.
- Weisman, R. (1977), Snowmelt: a two-dimensional turbulent diffusion model. *Water Resour. Res.*, 13(2):337-342.
- Wigmosta, M. S., Lance, L. V., and Lettenmaier, D. P. (1994), A distributed hydrology-vegetation model for complex terrain, *Water Resour. Res.*, 30(6):1665-1679.
- WMO (1986), *Intercomparison of modes of snowmelt runoff*. Operational Hydrology Report No. 23. WMO-No. 646, Secretariat of the World Meteorological Organization, Geneva, Switzerland.
- Woo, M., and Valverde, J. (1982), Ground and water temperatures of a forested mid-latitude swamp. In: *Proc. of the Canadian Hydrology Symposium '82, "Hydrological Processes of Forested Areas"*, Fredericton, N.B., 301-312.

- Wood, E. F., Sivapalan, M., Beven, K., and Band, L. (1988), Effects of spatial variability and scale with implications to hydrologic modeling. *J. Hydrol.*, 1020: 29-47.
- Yamazaki, T. (1998), A multi-layer heat balance model of snow cover – simulations in Siberia and plans. In: *Proc. of second international workshop on energy and water cycle in GAME, Siberia*, 161-168.
- Yamazaki, T., and Kondo, J. (1992), The snowmelt and heat balance in snow-covered forested areas, *J. of Appl. Meteorol.*, 31:1322-1327.
- Yeh, T. C., Wetherald, R. T. W., and Manabe, S. (1983), A model study of the short term climate and hydrologic effects of sudden snow-cover removal. *Mon. Wea. Rev.*, 111:1013-1024.

Table 2.1 General characteristics of selected distributed and semi-distributed snowmelt models (continued to next page).

Model Name	SHE	DHSVM	CLASS	UEB	SLURP	SDSM
Model basis	EBM & DDM	EBM	EBM	EBM	DDM	EBM & DDM
Operation mode	REA	MGC	MGC of GCM scale	MGC	ASA	Sub-Basin
Application/ purpose	Simulate hydrograph response	GCM/ snow processes and forecasting	GCM, RCM and NWPM	Understanding snow processes, for runoff, erosion, & water bal.	Forecasting runoff	Understanding snowmelt processes & runoff forecast
Forcing data needs	P, T <sub>a</sub> , V, RH, Q <sub>n</sub> or(Q <sub>s</sub> & Q <sub>i</sub> )	P, T <sub>a</sub> , V, RH, Q <sub>s</sub> , Q <sub>i</sub>	P, T <sub>a</sub> , V, RH, Q <sub>s</sub> , Q <sub>i</sub> , P <sub>a</sub>	P, T <sub>a</sub> , V, RH, D <sub>TR</sub> , Q <sub>s</sub> or Q <sub>n</sub>	Pr, T <sub>a</sub> , Q <sub>s</sub> , Q <sub>i</sub>	P, T <sub>a</sub> , T <sub>g</sub> , V, RH, Q <sub>n</sub> and/or Q <sub>s</sub> , Q <sub>g</sub> , LAI, A
Snow layers	1	2	1	1 + thermally active soil layer	1	1+ thermally active soil layer
Snowpack phases tracked by model	Only SWE	2 (ice & water)	1 (SWE)	1 (SWE)	1 (SWE)	2 (ice & water)
Retention/Perco.	Yes/Yes	Yes/No	Yes/No	Yes	No/No	Yes/No
Interception	No (below 0°C)		Yes	No	Yes	Yes
Refreezing	No	No	Yes	No	No	Yes
Snow density	No	No	Changing	Fixed	No	Changing
Snow Conductivity	No	Fixed	Changing	Fixed	Not tracked	Changing

Table 2.1 General characteristics of some distributed and semi-distributed snowmelt models (continued)

Model Name	SHE	DHSVM	CLASS	UEB	SLURP	SDSM
Surface temperature	Not computed	Not computed	Simulated	Simulated (fixed conductance)	Not computed	Simulated using 3-different methods
Vapor transfer	Yes	Yes	Changing		No	Changing
Ground-heat flux	Fixed	No	Yes	Yes, (in a rough way)	Yes	Yes
Heat convected by precipitation	Yes	Yes	Yes	Yes	No	Yes
Snow drifting	No	No	No	Yes	No	No
Sub-grid topography	Yes		Yes	Yes (with respect to $T_a$ )		
Frozen soil	No	No	Yes	Yes (through 'U')	No	No
RS data as input	No	No	No	No	Yes	Yes
Comparison with satellite data.	No	Yes, snowcover with AVHRR		No		Yes, ( $T_s$ with AVHRR derived)

EBM=Energy balance method; DDM=Degree-day method; REA=Representative elemental area; MGC=Model grid cell; HHU= Hydrologically homogeneous unit; ASA=Aggregated simulation area; GCM=Global climate model; RCM=Regional climate model; NWPM=Numerical weather prediction model; P=Precipitation;  $T_a$ =Air temperature;  $T_g$ =Ground temperature; V=wind speed; RH=Relative humidity;  $Q_s$ =short wave radiation flux;  $Q_l$ =Long-wave radiation flux;  $Q_n$ = net radiation flux;  $Q_g$ =Ground heat flux; Pa=surface pressure;  $D_{TR}$ =Daily temperature range.

Table 2.2 Coefficients of Eq. (2.31) (after Dery and Yau, 2001)

Coefficient	Value	Coefficient	Value
$a_0$	$3.78407 \times 10^{-1}$	$a_5$	$2.48430 \times 10^{-2}$
$a_1$	$-8.64089 \times 10^{-2}$	$a_6$	$-9.56871 \times 10^{-4}$
$a_2$	$-1.60570 \times 10^{-2}$	$a_7$	$1.24600 \times 10^{-2}$
$a_3$	$7.25516 \times 10^{-4}$	$a_8$	$1.56862 \times 10^{-3}$
$a_4$	$-1.25650 \times 10^{-1}$	$a_9$	$-2.93002 \times 10^{-4}$

Table 2.3 Coefficients of different versions of the force-restore method.

$C_1$	$C_2$	References
$[1/(1+2\delta/d_1)](2/cd_1)$	$[1/(1+2\delta/d_1)] \omega_1$	Bhumalkar (1975)
$(1/0.95)(2/cd_1)$	$1.18 \omega_1$	Blackadar (1976)
$2/cd_1$	$\omega_1$	Deardorff (1978)
$[1/(1+\delta/d_1)](2/cd_1)$	$[1/(1+\delta/d_1)] \omega_1$	Lin (1980)

Where,  $\delta$  = originally an upper soil thickness,

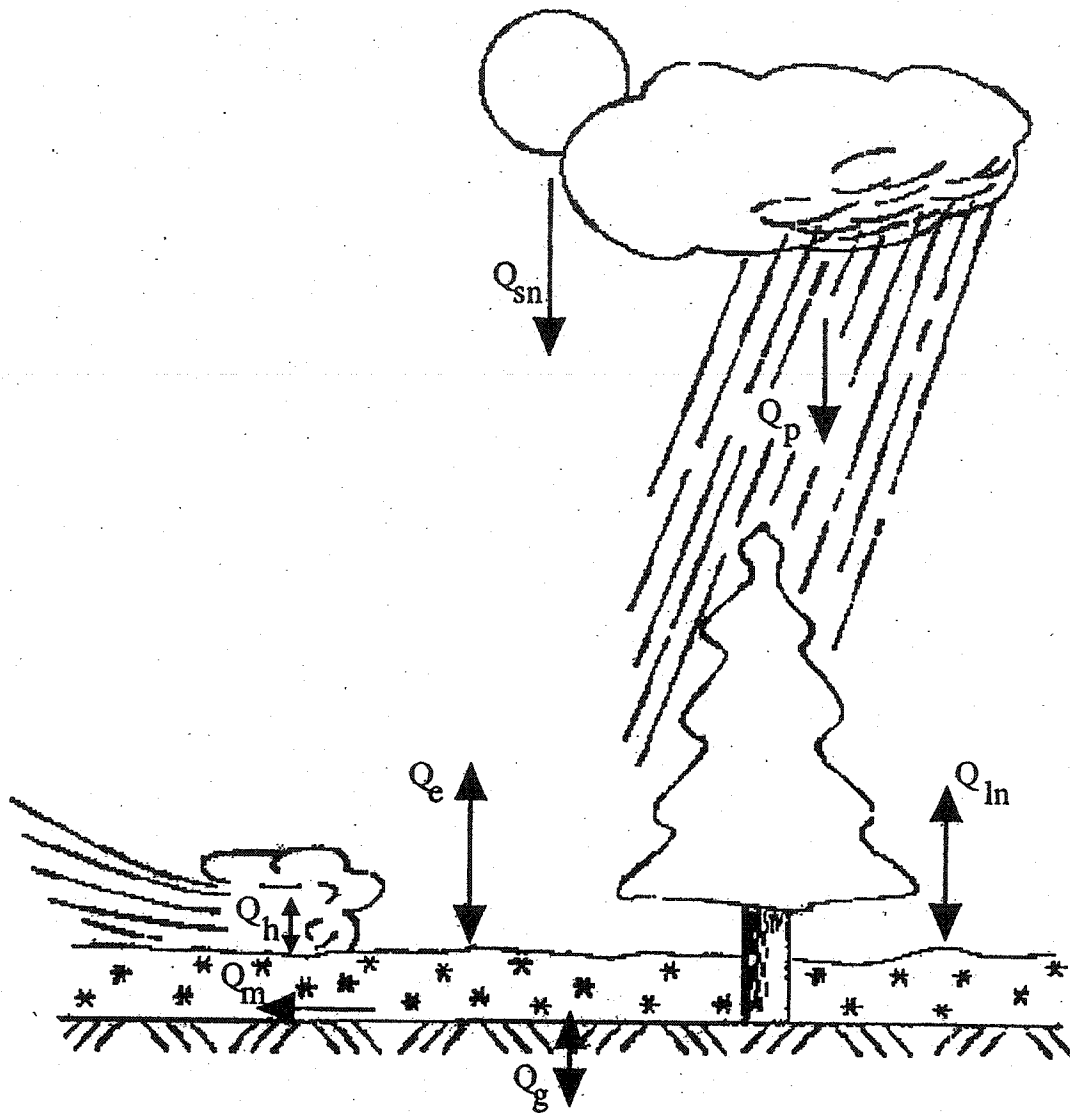
$d_1 = \sqrt{\frac{2k}{\omega_1}}$  is the damping depth of the diurnal temperature wave, and

$\omega_1$  = fundamental frequency.

Table 2.4 Statistical criteria used in SDSM to evaluate simulated basin outflows

Criteria	Equations <sup>1</sup>
1. Root Mean Square Error (RMSE)	$\left[ \frac{\sum_{k=1}^{M_k} (Q_{sk} - Q_{ok})^2}{M_k} \right]^{0.5} \times \left( \frac{1}{\bar{Q}_o} \right)$
2. Coefficient of Determination (R <sup>2</sup> )	$\frac{\sum_{k=1}^{M_k} (Q_{ok} - \bar{Q}_o)^2}{\sum_{k=1}^{M_k} (Q_{sk} - \bar{Q}_o)^2}$
3. Nash-Sutcliffe Coefficient (E <sub>f</sub> )	$\frac{\sum_{k=1}^{M_k} (Q_{ok} - \bar{Q}_o)^2 - \sum_{k=1}^{M_k} (Q_{sk} - Q_{ok})^2}{\sum_{k=1}^{M_k} (Q_{ok} - \bar{Q}_o)^2}$

<sup>1</sup>  $Q_{sk}$  = Simulated basin outflow,  $Q_{ok}$  = Observed outflow by WSC,  
 $\bar{Q}_o$  = mean of  $Q_{ok}$ , and  $M_k$  = number of observations.



$Q_{sn}$ - Net solar radiation;	$Q_e$ - Latent heat of sublimation;
$Q_{ln}$ - Net longwave radiation;	$Q_g$ - Ground heat flux;
$Q_p$ - Advective heat of precipitation;	$Q_m$ - Heat carried away by melt;
$Q_h$ - Sensible heat;	

Figure 2.1 Energy fluxes involved during snow accumulation and snowmelt processes considered in SDSM.

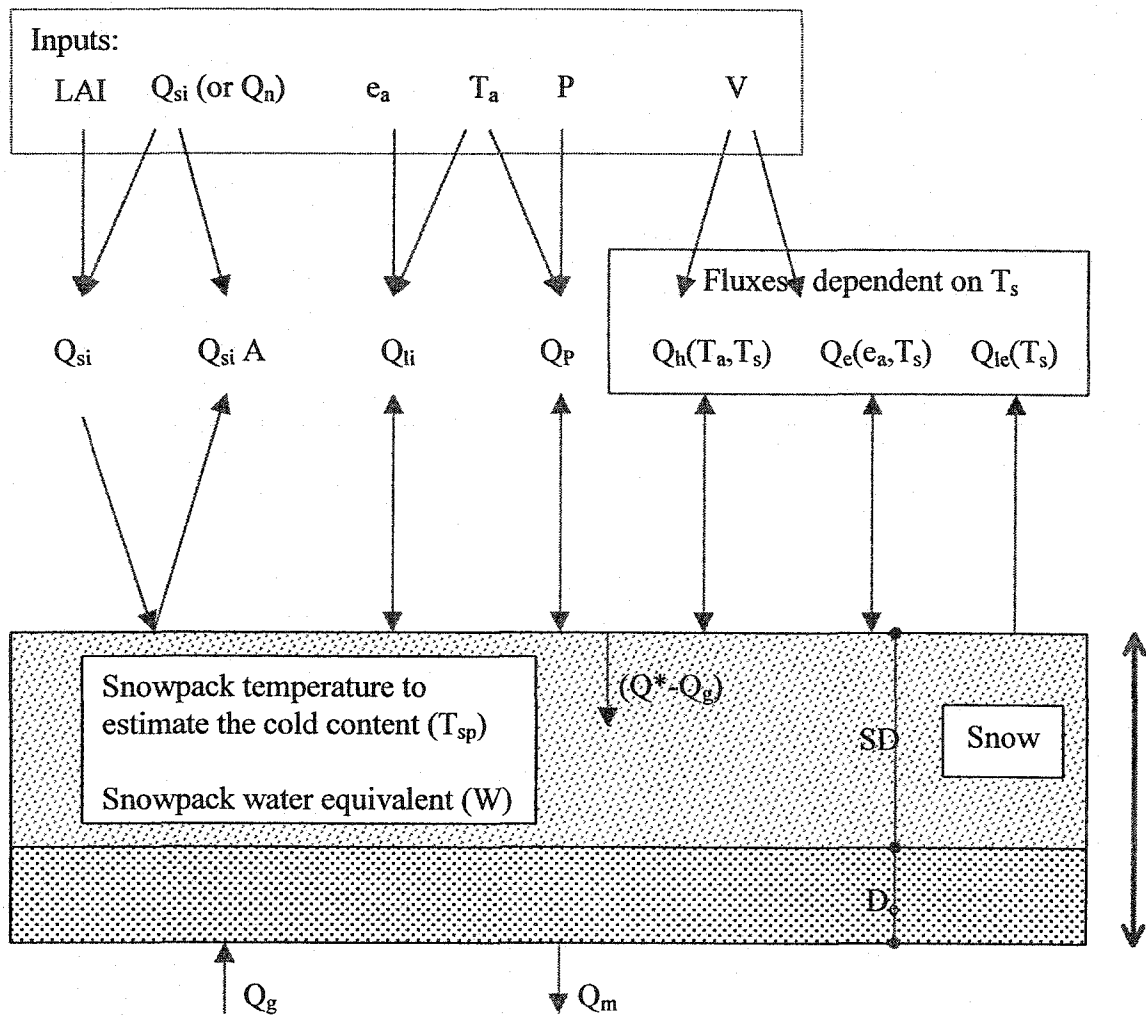


Figure 2.2 Snow model physics and parameterization in SDSM-EBM

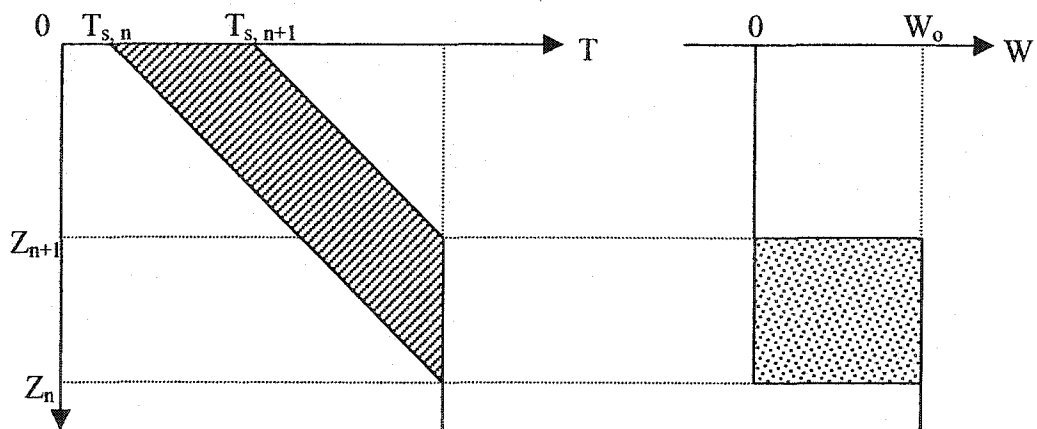


Figure 2.3 Schematic diagram of snow surface temperature ( $T_s$ ) and snowpack water content ( $W$ ) profiles in Kondo and Yamazaki Method (KYM)



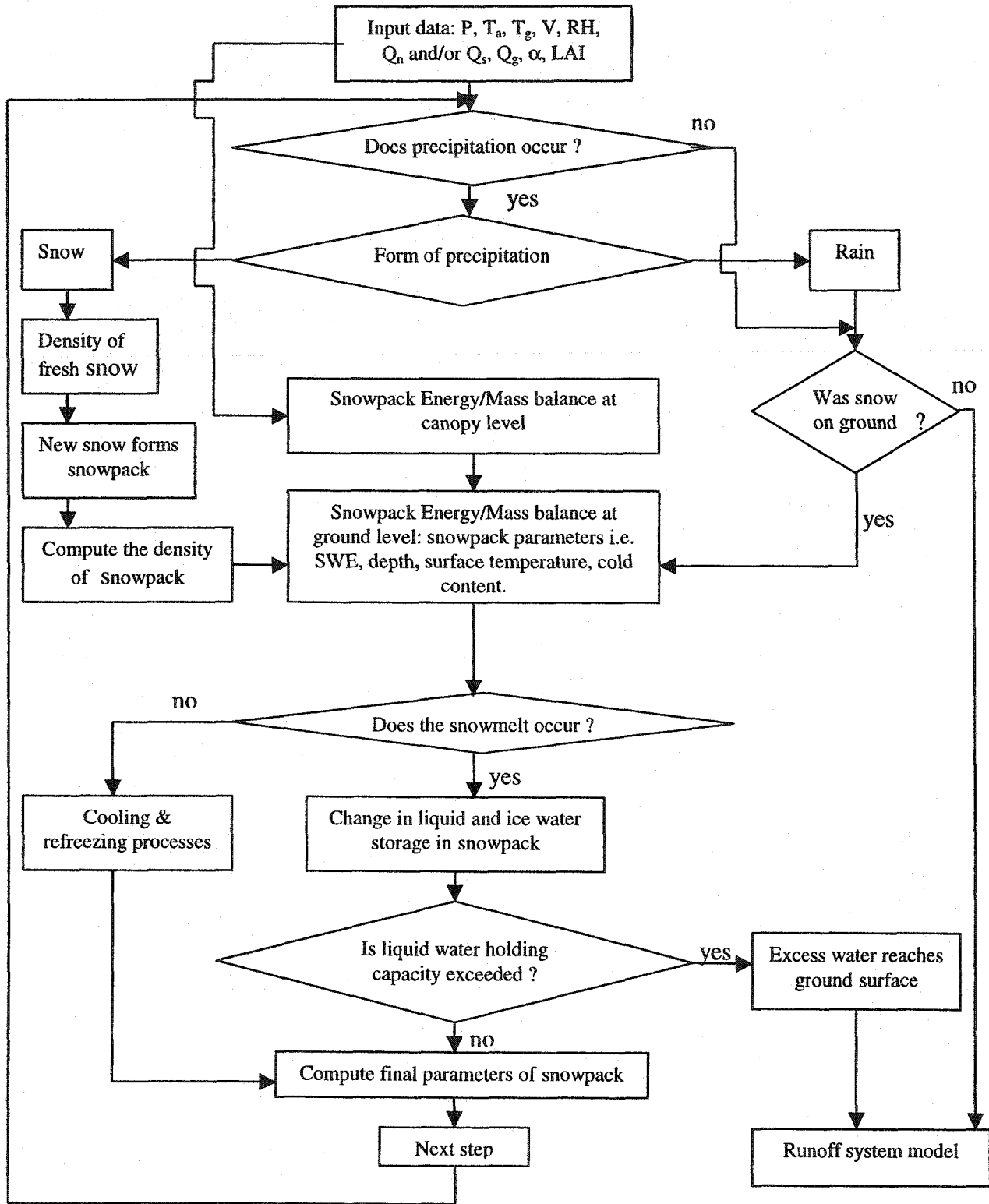


Figure 2.4 Schematic diagram of SDSM-EBM, a snow accumulation and ablation model

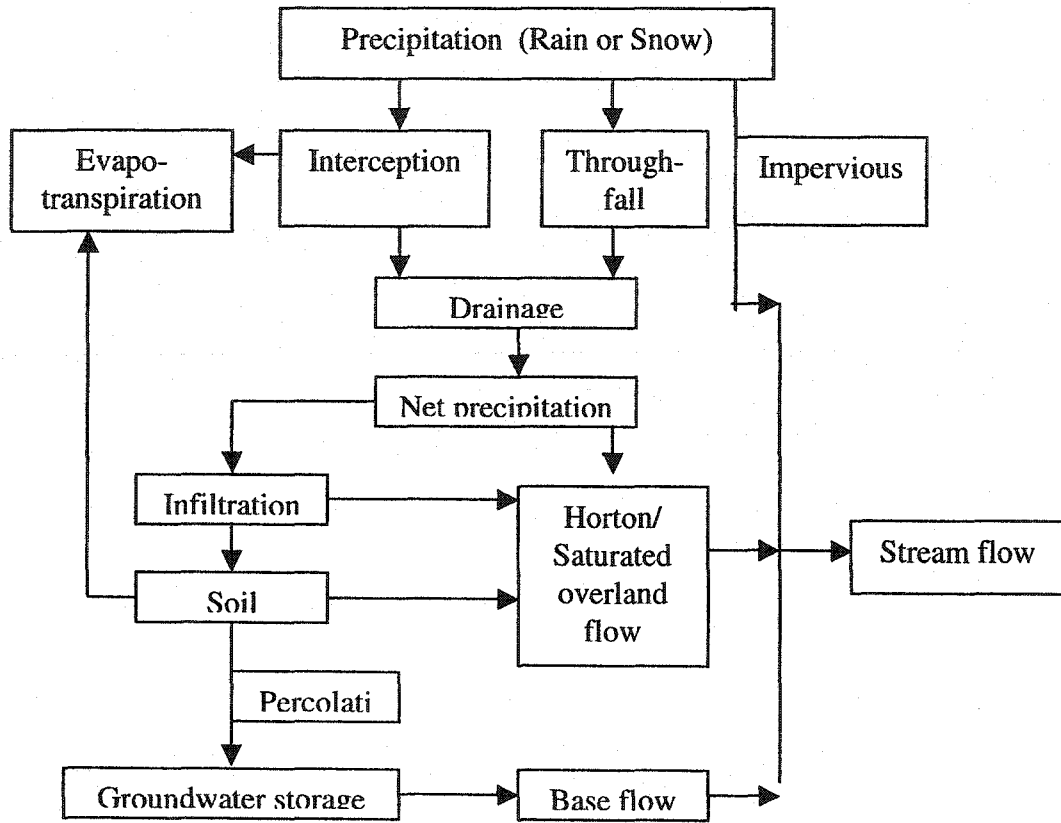
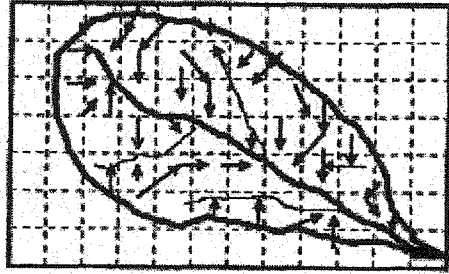
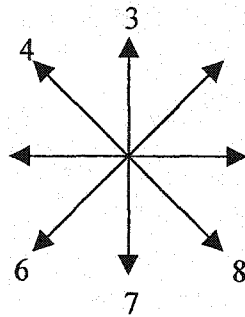


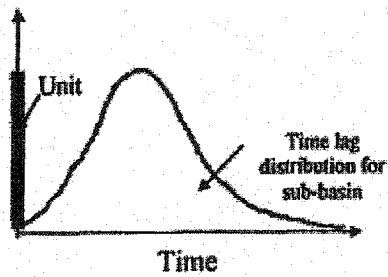
Figure 2.5 Flow chart of DPHM-RS model (adopted from Biftu, 1998)



(a) Grid-based kinematic wave flow in a sub-basin



(b) Eight-flow directions



(c) Average unit response function of a sub-basin

Figure 2.6. The average response function per unit rainfall or snowmelt excess for a sub-basin based on the kinematic wave theory and eight flow directions.

## **Chapter 3**

# **Semi-Distributed Snowmelt Model, Energy Balance Method (SDSM-EBM) using Remote Sensing Data, II. Application to the Paddle River Basin, Alberta**

### **3.1 Introduction**

Spring snowmelt is a dominant water source in Canada. The demand for more water and an improved hydrological knowledge of the snowcovered regions of the world are increasing. We need to improve our understanding of the role of snow cover on climate related to the land surface - atmosphere interactions. The large scale impact of snow accumulation and ablation processes in temperate and high latitude regions warrants the need to improve modeling the snowmelt runoff via distributed or semi-distributed instead of lumped or point snowmelt modeling.

Theoretically, fully distributed models should predict runoff more accurately than lumped parameter models but the reverse could occur. Furthermore, the former require large amounts of data because of its higher resolution approach to accurately represent heterogeneous terrain features though this approach still involves many unresolved uncertainties (Kirnbaer et al., 1994). Modeling basin hydrological processes using rectangular or square grid scales can be quite artificial. There are suggestions for using large scale than small scale parameterization strategy (Beven, 1996), choosing a model resolution according to the amount of data available and the predictive ability that is achievable (Blöschl, 1999). Conversely, one must find a trade-off between the resolution of processes to be modeled and the accuracy required. The maximum resolution attainable in such models depends mainly on the resolution of hydrological information retrievable from satellite data, that has played a significant role on the progress of snow hydrology (Rango and Shalaby, 1998).

An energy balance, semi-distributed snowmelt model (SDSM-EBM) was developed to optimize the joint application of spatial satellite data and ground point measurements. SDSM was applied to the Paddle River Basin (PRB: 265 km<sup>2</sup>) of Central Alberta (Figure 3.1), using distributed surface-physical data including land use classification, vegetation index, surface albedo, and surface temperature which were retrieved from space platforms such as Advanced Very High Resolution Radiometer (AVHRR) of National Oceanic and Atmospheric Administration of United States (NOAA), and Landsat-Thematic Mapper (TM). Topographic information such as mean elevation, ground slope, flow directions, sub-dividing PRB into sub-basins, and drainage systems were derived from digital elevation model (DEM) data. Retrieval of these spatial data was performed using the image analysis software EASY/PACE of PCI Geomatics. The performance of SDSM-EBM was evaluated against measured basin discharge, snow course data in terms of snow depth (SD) and snow water equivalent (SWE) and the surface temperature retrieved from AVHRR images.

## **3.2 Data Description**

The types of data used to drive the model can be broadly classified as ground based and remotely sensed data, which include topographic, land use, surface-physical data (e.g., vegetation index and albedo), meteorological and soil data (Table 3.1). The data used for model evaluation are streamflow data, snow course data, and surface temperature data. Three winters of data (1997/98, 1998/99, and 1999/2000) were collected for calibrating and validating SDSM-EBM.

SDSM-EBM was applied to the PRB using hourly hydrometeorological data collected from a 10-m meteorological tower set up in the basin, snow pillow data at the Paddle River Head Water, DEM, land cover class data (from Landsat -TM image), LAI and albedo data (retrieved from AVHRR images).

### **3.2.1 Ground Based Data**

Ground-based data consisted of meteorological data, snow course survey data, and the streamflow data collected for the study basin:

#### **3.2.1.1 Meteorological Data**

A 10-m meteorological tower was set up at the eastern edge of PRB (Figure 3.1) at an elevation of about 804 m AMSL to collect air temperature, relative humidity, wind speed, rainfall, net radiation, short-wave radiation, ground temperature, and ground heat flux at half-hourly interval. The sensors used to collect these data were: (1) CS500 temperature and relative humidity probe, (2) CR10TCR thermocouple reference, (3) MET ONE wind speed sensor, (4) TE525 tipping bucket rain gage, (5) Q-7 net radiometer, (6) LI200S pyranometer w/mount, (7) TCAV averaging soil temperature probe, and (8) HFT-3 soil heat flux plate. All sensors recorded data at 1-minute interval but stored as half hourly averages (with exception of rainfall,

which was stored as half hourly total) on a Campbell Scientific CR10X data-logger. The logger was powered by a MSX18 solar panel.

In addition, a 3-m tower was also set up with another set of a CR10X datalogger and a solar panel to collect the precipitation and wind direction using FS-100 four-season precipitation gauge and MET-ONE wind vane sensors respectively. Due to some technical problems in the data-logger, which was later also reported by Campbell Scientific Inc., the data from the second tower were lost. Instead, we used the snow pillow data from Paddle River Headwaters station 15V08 located in the central area of PRB at 855 m AMSL. The Data Management Group, Surface Water Monitoring Branch of Alberta Environment supplied the snow pillow data. Figures 3.2 to 3.4 show the temporal variation and diurnal pattern of six data types (taken at 6, 12, 18, and 24 hours) for the three winters: 1997-98, 1998-99, and 1999-00 respectively. Figure 3.5 shows the hourly precipitation data for the three winters.

### **3.2.1.2 Snow Course Data**

Snow course transects were measured on several occasions during the winters of 1998 (January 28 and February 6), 1999 (February 6 and March 14), and 2000 (January 23 and March 18) for selected land covers (agricultural, pasture and forest lands) of PRB, using a measuring stick for snow depths and an MSC snow sampler for snow density (see Plate F.1). Snow depths were measured at every 10 paces, while snow densities at about every 100 paces. The data management group of Alberta Environment also conducts the snow course survey near the Paddle River Headwaters snow pillow site (station 15V08, a forest covered area) since 1993 and near the Mayerthorpe snow pillow site (station: 07BB8099, an open area) since 1982 (see Table D.1 and D.2). The snow course data are summarized in Table 3.2.

### **3.2.1.3 Streamflow Data**

Streamflow data were measured at the Water Survey of Canada (WSC) gauging station 07BB011 (53° 51' 29" N and 115° 21' 45" W) established in October, 1979 and located near the Anselmo Hall at 749 m AMSL (marked "H" in Figure 3.1). Figure 3.6 shows the hourly streamflow data for 1998, 1999, and 2000 and the average daily streamflow data for 1980-1993.

#### **3.2.1.4 Soil Data**

Clay loam is the dominant soil type for the most part of PRB (Twardy and Lindsay, 1971). The soil parameters (e.g. saturated, critical, and residual soil moisture contents, soil moisture at permanent wilting point, saturated hydraulic conductivity, pore size index, etc.) for each sub-basin is based on the predominant soil type of the sub-basin. Most of the soil parameters for PRB were taken from Biftu and Gan (2001).

#### **3.2.1.5 Throughfall**

The throughfall coefficient ( $\tau_f$ ) indicates the percentage of precipitation reaching the surface without striking the vegetation canopy. Theoretically, such values can be obtained from field measurements of net precipitation and total precipitation (Rutter et al., 1971). In this study,  $\tau_f$  was derived according to past measurements for similar forest cover species (Leyton et al., 1967; Thompson, 1972), which gave  $\tau_f$  of 0.25 and 0.58 for the coniferous and mixed forests respectively.

### **3.2.2 Remote Sensing Data**

The use of remote sensing (RS) data in hydrology faces two challenges. First, the procedures to retrieve hydrologic information from RS data are not perfect and are at times ambiguous. Second, the spatial resolution and frequency of satellite data available from the current space platforms are still far from satisfactory. It is anticipated that higher resolution and more detailed information can be obtained



from the EOS-AM satellite of NASA that carries a number of sensors and one of them, the MODIS sensor provides global coverage of 36 spectral bands every one to two days. In this study, the land cover classifications were derived from Landsat-TM data of 30-120 m resolutions, and the surface albedo, vegetation index or LAI, and surface temperature from the 1-km resolution, NOAA-AVHRR High Resolution Picture Transmission (HRPT) data (see Table 3.3 and Appendix C).

### **3.2.2.1 Land Cover Class**

Most studies on the interaction between vegetation and snow accumulation examine forest and non-forest (short vegetative cover) ecosystems. A forest can be further divided according to tree species, which give rise to different snow accumulation and ablation processes. According to Anderson (1976), a forest cover restricts the penetration of wind and solar radiation, so that long-wave radiation dominates the energy exchange at the snow surface. The maximum accumulation of snow often occurs at the edges of a forest because snow is often blown in from adjacent open areas, but that highly depends on the density of the vegetation.

Given the highly exposed, relatively flat environment of the Canadian Prairies, the increased aerodynamic roughness resulting from meso- and micro-level differences in vegetation may produce a wide variation in snow accumulation pattern. Accumulations are most pronounced where sustained strong winds from one direction act on a long upstream fetch of loose snow, and less pronounced when wind frequently changes direction, especially at low speeds.

Biftu and Gan (2001) identified six landuse classes for PRB, namely: water/swamp, impervious, agricultural, pasture, coniferous forest and mixed or deciduous from a Landsat TM image of August 7, 1996 (see Figure 3.1). Since landuse influences the radiation budget and/or snowmelt computation for PRB, it forms part of the basis for the model parameter estimation for both SDSM-EBM and the Modified

Temperature Index snowmelt model (SDSM-MTI, which is described in Chapter 4). For SDSM-EBM, the above six landuse classes were reduced to three: open area, coniferous forest and deciduous or mixed forest, such that open area constitutes first four landuse classes (water/swamp, impervious, agriculture, and pasture). Table 3.4 shows the area of each land cover classes for each of the sub-basins. When coniferous and mixed forests are put together, it constitutes about 70 % of PRB's total drainage area. The remaining area of different landuse types constitutes an open area in SDSM-EBM model set-up.

### 3.2.2.2 Surface Albedo

Snow and ice are generally highly reflective. Therefore, seasonally snow covered areas show strong seasonal variations in surface albedo ( $\alpha$ ), which strongly influences the net solar energy at ground level. Ground measurements of  $\alpha$  are only representative spatially if the terrain is homogenous and fully snow-covered. Without freshly fallen snow, the surface albedo of a snowpack generally decreases with time as the snowpack ripens, snow grains coarsen and dirt accumulates (Riley, 1972; Pomeroy et al., 1998). Landsat-TM data can be used to estimate the surface albedo of snow cover but it has a 16-day cycle or frequency. The first two channels of NOAA-AVHRR have been extensively used to retrieve the surface albedo (Table 3.3) because the result is comparable to that of Landsat-TM but the data are available on a daily basis (Biftu and Gan, 2000). Moreover, NOAA-AVHRR data is readily available through the internet.

In this study, majority of the cloud free Level-1B AVHRR data of NOAA-14 spacecraft were downloaded from the satellite active archive of NOAA website (<http://www.saa.noaa.gov/>). Some NOAA-AVHRR data were also obtained from Environment Canada. These data were processed using the AVHRR Orbital Navigation package of PCI-Geomatics image analysis software. Using the following procedures: first, the solar zenith angle of channels 1 and 2 of AVHRR

images were radiometrically corrected to remove the associated spectral error. After radiometric correction, the pixel values were converted to albedo (reflectance) using the radiometric calibration of Rao and Chen (1996 and 1999) (see Table 3.5 and Appendix A). The images are then geometrically corrected using the GCPWorks of PCI-Geomatics and a master image of PRB, and finally the areal surface albedo in each sub-basin and each land cover class using the multi-layer modeling package of PCI-Geomatics. The weighting factor used to obtain  $\alpha$  from reflectance values of channels 1 and 2 for each of the pixel is based on that of Laine and Heikinheimo (1996),

$$\alpha = 0.322R_1 + 0.678R_2 \quad (3.1)$$

Where  $R_1$  and  $R_2$  are reflectance (or albedo) for AVHRR channels 1 and 2 respectively. The lack of information about cloud cover (Male and Granger, 1981) and atmospheric precipitable water is a possible source of error when estimating high  $\alpha$  values. However, for the winter periods of Prairies with precipitable water depth generally less than 2.0 cm (Singh and Gan, 2000), the error due to precipitable water should be negligible (Laine and Heikinheimo, 1996).

Table 3.6 shows the value of  $\alpha$  for the various land covers in each sub-basin for January 5, 1998, December 23, 1999, and for April 24, 1999 derived from NOAA-AVHRR images. More complete information of  $\alpha$  for coniferous forest, mixed forest, and open area are given in Table C.1. Though the range of  $\alpha$  values (high 0.8 during winter to low 0.2 during fall/spring) were comparable for different years, the frequency of  $\alpha$  attaining peak values after continued decay was remarkably large for 1998/99 winter compare to 1997/98 and 1999/00 winters. Based on the cloud-free images of NOAA-AVHRR, temporal variations of  $\alpha$  for three winter periods consistently showed a higher value of  $\alpha$  for an open area followed by the coniferous and the mixed forests. The higher value of  $\alpha$  in coniferous forest compared to mixed forest is believed to be due to its higher LAI, which causes greater snow

interception. Within the open area, the pastureland consistently showed a higher albedo value than the cultivated land.

### 3.2.2.3 Vegetation Index

Satellite data has been used extensively for large scale monitoring of land vegetation types (Running and Nemani, 1988; Pinty and Verstraete, 1992). The Normalized Difference Vegetation Index (NDVI) is often derived from channels 1 and 2 of geometrically corrected NOAA-AVHRR data (Deering et al., 1975),

$$\text{NDVI} = \frac{R_2 - R_1}{R_2 + R_1} \quad (3.2)$$

NDVI is then used to estimate LAI according to the vegetation using equations shown in Table 3.7. Table 3.8 shows the NDVI for different land cover in each sub-basin for January 5, 1998, December 23, 1999, and April 24, 1999. The average LAI for the three land cover classes are given in Table C.2.

In general LAI in each landuse gradually declines since the fall season, attaining a minimum value for most of the winter, and increases in late winter or early spring. The coniferous forest maintains a higher value of LAI compared to mixed forest throughout the fall and winter periods. The relatively long winter of 1998/99 (with respect to air temperature) caused a delay in the rise of LAI in the later part of winter by about two weeks compared to the winters of 1997/98 and 1999/2000. Based on the NOAA-AVHRR retrieved data, LAI of coniferous forest reached a value of 1.0 in October 22, 1998, reduced to 0.65-0.80 between November 26, 1998 and April 15, 1999, and then again increased to 1.15 in April 24, 1999. A similar trend was observed for 1997/98 and 1999/2000 winters. The maximum and minimum LAI obtained were 1.36 and 0.66 for the coniferous forest area and 0.76 and 0.34 for the mixed forest area respectively.

### 3.2.2.4 Surface Temperature

Snow surface temperature at ground level ( $T_s$ ) is one of the key factors in determining the exchange of energy between the land surface and the atmosphere. It can usually be determined by the use of a thermal infrared (IR) channel (Seguin and Itier, 1983). Price (1983) proposed a split-window algorithm that incorporates the effect of total precipitable water (TPW) to account for the atmospheric effect in retrieving  $T_s$  from the IR channels of NOAA-AVHRR data. A number of split-window algorithms for retrieving land surface temperature have been proposed (e.g., Qin and Karnieli, 1999; Kant and Badarinath, 2000), whereby the atmospheric radiation is eliminated by using two IR channels 4 and 5 of NOAA-AVHRR (Prince et al., 1998), and often with a reasonable accuracy over large areas (Cooper and Asrar, 1989).

The general form of split-window algorithm to estimate  $T_s$  in the open are is

$$T_s = TB_4 + \delta_1 (TB_4 - TB_5) + \delta_2 \quad (3.3)$$

Where  $TB_4$  and  $TB_5$  are brightness temperatures of NOAA-AVHRR channels 4 and 5,  $\delta_1$  and  $\delta_2$  are coefficients accounting for atmospheric effects, viewing angle and ground emissivity. Price (1984) provided  $\delta_1$  and  $\delta_2$  as 3.33 and 0 respectively in Eq. (3.3) assuming no variations in the emissivity of natural surfaces between channels 4 and 5. The derived  $T_s$  for the forest covered area using this equation is however the scene surface temperature,  $T_{scene}$ . The following paragraphs discuss the processes involved in retrieving brightness temperatures in each of the thermal channels of AVHRR ( $TB_4$  and  $TB_5$ ),  $T_{scene}$  and  $T_s$ .

If the surface radiation is transmitted through the atmosphere to the remote sensor unattenuated, then the ground surface or skin temperature can be theoretically determined from the emitted spectral radiance  $B_\lambda(TB)$  by inverting Planck's radiation equation as

$$TB_i = \frac{c_2}{\lambda \left( \ln \left[ \frac{c_1}{\lambda^5 B_\lambda(TB_i)} + 1 \right] \right)} \quad (3.4)$$

where  $c_1 = 2\pi^5 h^3 c^2 / 15 = 3.741771995 \times 10^{-16} \text{ W/m}^2$  and  $c_2 = hc/k = 1.43876869 \times 10^{-2} \text{ m} \cdot \text{K}$  ( $\epsilon_\lambda$ ,  $h$ ,  $c$ ,  $k$  are the emissivity, Planck's constant, speed of light and Boltzmann's constant respectively), and  $B_\lambda(TB)$  is the radiometrically corrected pixel values of the thermal channels. However,  $TB_i$  is also influenced by atmospheric attenuation, the radiance emitted by the atmosphere and the reflected component of the downward atmospheric radiance (Qin and Karnieli, 1999). Although there is usually only minor attenuation on the surface energy emitted in the infrared channels by the cloud free polar atmosphere (which is comparable with the clear sky winter atmosphere of Prairies with less than 2 cm precipitable water), the difference between actual and AVHRR TB can be as large as 3 °K in either direction (Stroeve and Steffen, 1998). The variability of surface (or snow) emissivity due to surface heterogeneity, failure to account for the viewing angle, and the changing grain size effect limits the use of infrared data in estimating TB to a greater accuracy.

In this study, the thermal channels (4 and 5) of cloud-free AVHRR raw data were directly converted to TBs ( $TB_4$  and  $TB_5$ ) using the slope ( $\delta_3$  in °K per count) and intercept ( $\delta_4$  in °K) values calibrated automatically by the AVHRR sensor.

$$TB_i = \delta_3 D_i + \delta_4 \quad (3.5)$$

where  $D_i$  is the digital count for the thermal channel "i". This was done using AVHRR Orbital Navigation package of PCI. Similar to channels 1 and 2, the radiometric calibration was followed by the geometric correction, the image registration, and finally the scene surface temperature in each sub-basin and each land cover class using the multi-layer modeling package of PCI. These scene surface temperatures ( $T_{scene}$ ) were then converted to  $T_s$  for different forest cover (coniferous and deciduous) fraction ( $f_c$ ) according to Kustas and Jackson (1999) as

$$T_{\text{scene}}^4 \approx f_c T_c^4 + (1 - f_c) T_s^4 \quad (3.6)$$

where  $T_c$  is the canopy temperature assumed equal to air temperature (Kustas and Jackson, 1999), and  $f_c$  is estimated from the LAI (Choudhury, 1987).

$$f_c = 1 - \exp(-\beta_{\text{lad}} \text{LAI}) \quad (3.7)$$

where  $\beta_{\text{lad}}$ , a function of the leaf angle distribution, is assumed equal to 0.5 for randomly distributed leaves (Choudhury et al., 1994).

The retrieved scene surface temperature,  $T_{\text{scene}}$  for the forest-covered landuse were generally higher than that for the open area, which indicates the influence of emission from the canopy layer, which is at a higher temperature than the snow surface temperature at ground level  $T_s$ . Except in the later part of winters (when bare patches start to dominate), the observed air temperatures were always higher than the corresponding surface temperature retrieved from AVHRR data, taken between 2-4 P.M. local time, generally by 4 to 7 °C. The evapotranspiration component of the semi-Distributed, Physically based, Hydrological Model using GIS and Remote Sensing (DPHM-RS) also simulated  $T_c$  that is quite close to  $T_a$  (Biftu, 1998) and therefore  $T_c$  was assumed equal to  $T_a$  in estimating  $T_s$  using Eq. (3.6). Furthermore, any error caused by the assumption of  $T_c$  (in Eq. 3.6) should be well within the range of error associated with a satellite derived  $T_s$ . Table 3.9 shows the  $T_s$  for different land cover in each sub-basin for January 5, 1998, December 23, 1999, and April 24, 1999 derived from the AVHRR images, and more detailed information are provided in Table C.3.

Although NOAA-AVHRR data lacks the spatial resolution (1-km) to track the spatial variability of  $T_s$ , its daily coverage provides the means to track its temporal variability. On the other hand, the Landsat-TM band 6 data can provide high resolution estimates of  $T_s$  (120m) but the 16-day, repeat cycle makes it useless for tracking the temporal variation of  $T_s$ . Values of  $T_s$  retrieved from cloud-free NOAA-AVHRR data using the split-window technique of Price (1984) were used to

evaluate the performance of SDSM-EBM.

### **3.2.2.5 Topographic Data**

Digital Terrain Elevation Data (DTED) from the US Defense Mapping Agency, which has a resolution of 100-m, was used to derive the drainage network and delineation of sub-basins for PRB (Figure 3.1). Other parameters derived from DTED are the mean altitude, aspect, flow direction, and slopes of each grid of the PRB using the watershed module of PCI-Geomatics.

### **3.2.3 General Characteristics of Winter Data**

Of the data used in this study (Table 3.1), most of the meteorological data were used as model inputs, while the streamflow and snow course data were used for calibrating model parameters at sub-basin scale and for validating the model outputs. SDSM-EBM operates within DPHM-RS, which together simulate basin hydrological processes such as evapotranspiration, soil moisture, snowmelt runoff and streamflow, etc. This simulated outflow discharge is compared with the observed stream flow data.

The meteorological data used to model spring snowmelt are shown in Figures (3.2, 3.3 and 3.4) for 1997/98, 1998/99 and 1999/2000 winters respectively. The hourly precipitation data for the study periods are shown in Figure (3.5), while the discharge data (gauging station 07BB011) are shown in Figure 3.6(a-c). Figure 3.6(d) shows the daily average flow at the basin's outlet for 1980-1993.

Among 8 years of snow course data at the Paddle River Headwaters site and 19 years of snow course data at Mayerthorpe Snow Pillow site, the winters of 1997/98 and 1999/00 were the driest (Table D.1 and D.2), while the winter of 1998/99 was one of the four wettest (Climate Trend and Variation Bulletin for Canada: 1948-2001). The sequence of winter regional temperature departures from normal ranked



from the warmest to the coolest is 1997/98, 1999/00, and 1998/99 out of 54 years of records for both Northwest Forest and Prairie region (Table D.3). The low snowfall winter of 1998 experienced a frequent rise in temperature (close to 10 °C) and radiation fluxes in the middle of winter (Jan 31, Feb 13, Feb 22), which caused metamorphic changes to the snowpack properties. The high snow accumulation winter of 1998/99 only experienced increases in temperature and radiation fluxes during late winters of 1999.

The hourly maximum wind speeds ( $U_{\max}$ ) for the winters of 1998, 1998/99, and 2000 were 6.5, 12.3, and 10.5 m/s respectively. Significant variation was also observed in wind speed for these winters ( $U_{\text{mean}}=1.9$  m/s and  $U_{\text{stdev}}=1.1$  m/s for the winter of 1998, and  $U_{\text{mean}}=2.3$  m/s and  $U_{\text{stdev}}=1.5$  m/s for the winters of both 1998/99 and 2000; also see Figures 3.2f, 3.3f, and 3.4f), which brought significant variations in snow distribution, snow densification and turbulent fluxes. Pomeroy et al. (1998) recommended using an increase in snow density at a rate of 9 kg/m<sup>3</sup>/h (or higher snow compaction) during the wind event for non-melting snow and hourly wind speed greater than 7 m/s. The field observation of 1998/99 winter snowpack indicated the presence of two thin ice layers (one near ground, and another at about 15 cm below the snow surface), which could be associated with the depth-hoar phenomenon caused by a large temperature gradient within the snowpack. Similar ice layer at near ground level (and also at near snow surface in some locations) was observed during 1999/00 winter. These observed variations were considered while selecting appropriate model parameters at the model calibration stage.

### 3.3 Model Parameter Estimation

The classic approach in calibrating hydrologic parameters has been to minimize the sum of least square of the difference between simulated and observed runoff. However, this traditional approach may not work with fully distributed physically-based models involving large number of model parameters. Model calibration is

problematic with the snow accumulation and ablation processes, which involve little or no runoff during the snow accumulation period but snow depth, SWE, snow surface temperature continue to change with time. Therefore to calibrate SDSM-EBM with PRB for the 1998/99 winter, a multi-objective calibration criterion was adopted.

The PRB consists of about 50% mixed forest, 21% coniferous forest, and 29% open area. In applying SDSM-EBM to PRB, some model parameters were taken from the literature and some calibrated from snow course data,  $T_s$ , and basin outflow (see Table 3.10). The parameters adopted from past findings were associated with either mass balance (e.g., canopy interception, throughfall, liquid water holding capacity, etc.) or energy balance (e.g., canopy attenuation of radiation and wind speed, range of albedo, etc.). Some physical parameters were also derived from different space platforms.

The number of model parameters required to run the 1-D, energy balance SDSM-EBM depends on the modeling options selected. Some parameters (e.g., temperature, rain/snow, threshold temperature for melt, maximum snowpack density, settlement constant, precipitation and temperature distribution factors etc.), can be changed while running the model but some parameters that are built into the model, if altered, will require the re-compilation of the computer code.

SDSM-EBM runs within the host model, DPHM-RS which accounts for the Hortonian, saturated overland, and the subsurface runoff from each sub-basin, and routes the flows to the stream channel by an average kinematic response function derived for each of the sub-basin, and then to the basin outlet using Muskingham-Cunge method. Most of the parameters required for running DPHM-RS are taken from Biftu and Gan (2001), who tested DPHM-RS to PRB for the summer periods of 1996-1998. However, most of the parameters of Biftu and Gan (2001) are still

applicable in this study. Other than the hydraulic conductivity of soil, which is very small at the frozen compared to unfrozen state, the other soil parameters used for the summer periods of Biftu and Gan (2001) were used in this study. The refreezing of infiltrating meltwater is reported to decrease infiltration, and a soil becomes impermeable if an ice lens forms on or near the ground surface (Gary and Landine, 1988). Formation of such ice lens was also observed during the snow course survey in the PRB. Another important parameter that determines the surface runoff response from each of the PRB's sub-basins is Manning's roughness 'n' values, which should not vary much between summer and winter on both open and forested area.

## **3.4 Discussion of the Results**

### **3.4.1 Model Calibration and Validation**

SDSM was calibrated using the hourly winter data of November 11, 1998 to May 16, 1999, and validated using the winter data of January 1 - April 30, 1998 and January 1- Apr 30, 2000. As mentioned in Section 3.2.3, these three winters experienced a wide range of snowfall (see Appendix D). We selected January 1<sup>st</sup> as the starting date of 1997-98 and 1999-00 winter data because major snowfall for both winters started very late. Moreover, in Alberta using January 1<sup>st</sup> as the starting date ensure that snow accumulation happened during sub-zero temperature.

SDSM-EBM was set up within the operating domain of DPHM-RS so that it can run with or without pre-specified unit response function (or the unit hydrograph) for each of the five sub-basins. While a typical SDSM-EBM model-run with a pre-specified unit hydrograph takes less than 10 minutes in a Pentium-200 PC, the same model run without such a unit hydrograph requires more than 2 hours because generating a unit hydrograph at 100 m × 100 m grid-scale based on the kinematic wave theory, eight flow directions, and Manning's roughness 'n' values in each of

the grids depending on the assigned land cover for each grid is time consuming. Unit hydrographs were generated for each of the sub-basins of PRB for several combinations of  $n$ -values for open and forested areas (within the range suggested in literature) and tested the ability of each to reproduce the basin's runoff response at the calibration stage (see Figure 3.6e). The unit hydrograph, which produced the optimum discharge hydrograph in terms of observed runoff volume and the time to peak was selected for further model runs at calibration and validation stages. The  $n$ -values selected from calibrating SDSM-EBM with the observed runoff data of PRB are 0.15 and 0.10 for forest cover and open area respectively (see Figure 3.6e(i)).

SDSM-EBM was evaluated with respect to the water balance (runoff hydrograph, snow depth, SWE) and energy balance ( $T_s$  of different land cover classes). This approach enables to assess most of the model performance at different stages of the snow accumulation and ablation processes. The basin water balance is checked against the surface runoff and channel routing schemes of DPHM-RS. In channel routing, the channel roughness parameters were adjusted within the theoretical range so as to match the time lag and magnitude of the simulated peak discharge with the observed values. Because the model is not concerned with the water level along the channel reach, the channel width is less significant and is assigned an average value obtained from site inspection.

#### **3.4.1.1 Basin Runoff Hydrograph**

The model was calibrated against hourly runoff data collected from November 11, 1998 to May 16, 1999 using graphical plots of observed and simulated hydrographs and statistics like the Coefficient of Determination ( $R^2$ ), the Nash-Shutcliffe Modeling Efficiency ( $E_f$ ), and the Root Mean Square Error (RMSE). The simplex algorithm of Nelder and Mead (1965) is built into SDSM-EBM for the automatic calibration of model parameters, but was unnecessary for this study.

Figures 3.7(a.1) and 3.7(a.2) compare simulated and observed runoff at the basin outlet using two methods of snow  $T_s$  simulation: (1) Force Restore Method (FRM), and (2) Snow Conductance Method (SCM) of SDSM-EBM for the 1998/99 calibration period (11/11/1998 to 5/16/99) based on the optimized parameters given in Table 3.10. In general, the simulated streamflow data are in good agreement with the observed for both FRM ( $R^2=0.82$ ,  $E_f=0.84$ , and  $RMSE=1.14$ ) and SCM ( $R^2=0.85$ ,  $E_f=0.87$ , and  $RMSE=1.01$ ). SCM did marginally better than FRM, which may be because it has an additional parameter  $K_{sc}$  (surface conductance) in addition to the iterative procedure adopted to balance the heat fluxes of snowpack at each time step. KYM did poorer than FRM and SCM ( $R^2=0.78$ ,  $E_f=0.80$ , and  $RMSE=1.25$ ) mainly because it did not iteratively balance the heat fluxes of snowpack but assumed that the snowpack has a linear temperature profile in the vertical direction. Besides  $T_s$ , some discrepancies between simulated and observed runoff can be partly attributed to input data collected from snow pillow at Paddle River Headwaters whose sensitivity to snowfall was about 1.8 mm, and to the lack of dense precipitation gauging network. Summer precipitation in PRB only varies spatially in a marginal manner, as reported by Biftu (1998). However, by comparing the precipitation of PRB with a nearby station east of PRB, it seems there is probably more spatial variability in winter precipitation. Including our Met tower, there are only two precipitation stations at PRB. Snowfall data is based on the snow pillow site at the Paddle River Headwaters. Beaver dams in PRB (see Plates F.2 and F.3) exerted some regulatory effects on the basin's observed streamflow, particularly during dry winters.

The validation results are less satisfactory for the 1998 winter (1/1/1998 to 4/1/1998) particularly with respect to total runoff volume and early spring snowmelt runoff ( $R^2= 0.5$ , Figure 3.7(b.1) for FRM and Figure 3.7(b.2) for SCM). The average model efficiency  $E_f$  for FRM between March 19 and 30 was 0.61 but it fell to 0.18 by March 31. The average  $E_f$  of SCM is similar but the range varies from 0.45 to

0.88. The overall RMSE value was  $3.5 \text{ m}^3/\text{s}$ , which is significantly high for the range of observed streamflow of 1998 winter.

It should be noted that the initial cold content used for the 1998 model run was higher than the 1998-99 (starting from 11/11/1998) model run because the soil surface for the former (starting from 1/1/1998) had already experienced sub-freezing temperature at the beginning of model run. Further, the lack of snowcover in the early part of a dry winter such as 1998 leads to deep permafrost in soil layers, which tend to increase the cold content of the snowpack after major snowfall began. For a wet winter such as 1998-99, the soil surface is usually insulated from the atmospheric forcing right from the beginning due to early snowfall.

The validation result of 1998 is less satisfactory with respect to basin runoff partly because during early part of the snowmelt season the water level was low, causing the observed streamflow to be relatively inaccurate. Figure 3.6(a) shows two versions of hourly streamflow data for the same 1998 winter. Further, the daily streamflow data for the same period of 1998 provided by Environment Canada (EC) was significantly different (smaller in values) when compared to that derived from the hourly streamflow data obtained from the same source. However, EC's daily streamflow data for the winters of 1999 and 2000 were very much similar to that derived from the hourly stream flow data ( $R^2=0.97$  and  $1.0$  for 1999 and 2000 respectively). A continued low flow for a prolonged period probably indicates the influence of beaver dams at strategic locations of the upper reach of PRB. These temporary structures alter the flow regime of a natural stream particularly during low spring snowmelt runoff. As a result, instead of prolonged low flow we could have got peak runoffs as simulated by the model if no beaver dams were present.

The validation result of the dry winter of 2000 also showed the presumed regulatory effects of beaver activities on the PRB streamflow, even though the model results

are slightly better than the 1998 results ( $R^2 = 0.58$  and  $0.6$  for the FRM and SCM respectively, (see Figures 3.7(c.1) and 3.7(c.2)), but  $E_f$  was maintained at  $0.75$  or higher for only three days between March 18-21, which then dropped to near zero. The hourly observed flows during this period were merely  $0.02$ - $0.04$   $m^3/s$ . The first major hourly snowmelt runoff peak simulated by SDSM-EBM for the winter of 2000 was  $2.45$   $m^3/s$  on March 22 (17:00 hour) while the corresponding observed peak was about  $0.42$   $m^3/s$  on March 23 (20:00), lagging by 27 hours. It is important to note that from March 23 to April 18, the observed hourly streamflow stayed at between  $0.3$ - $0.5$   $m^3/s$ , which is lower than the range of daily mean flows ( $0.5 - 2$   $m^3/s$ ) for this period of the year (see Figure 3.6d). Between 1/1/2000 and 4/30/2000, the maximum hourly peak flow observed from was only  $0.85$   $m^3/s$  on April 23. A near uniform observed flow for most part of the snowmelt season suggests that the PRB was not running under natural conditions. Woo and Waddington (1990) reported similar streamflow modifications due to the effects of underflow and overflow types of beaver dams.

Field observations of the major tributaries of Paddle River along Highway 751 to the south of the snow pillow site and along some access roads to the north of Highway 647 show evidence of watertight beaver dams of overflow types (e.g., Gurnell, 1998) that maintained a pool of water upstream and released only a small fraction of water to the downstream (see Plates F.2), particularly when the spring snowmelt is not large enough to overtop the beaver dams. Apparently, a beaver dam can easily stop a small tributary flow of PRB especially during dry periods (see Plate F.3). The beaver dam effect was relatively small during the calibration period because the spring snowmelt runoff was high, which can either overtop the dams fairly quickly or in extreme case can wash out such beaver dams.

It is beyond the scope of this research to account for the regulatory effects of such temporary control structures in PRB during those dry winters even though such

structures cause problems to our model results from SDSM-EBM. Partly because of this reason and partly because a multi-criteria assessment is more dependable, we also validate the model performance with respect to other variables.

#### **3.4.1.2 Snow Depth and Snow Water Equivalent**

Because the observed snow depth and snow water equivalent (SWE) are not affected by beaver dams, they are used as part of the mass balance assessment of SDSM-EBM. For most of the land cover classes of the sub-basins of PRB, SDSM-EBM's simulated SWE and snow depth generally agree well with the observed values obtained from winter snow course surveys conducted at PRB. Figures 3.8 (a.1-a.3: FRM) and 3.8 (b.1-b.3: SCM) show good agreements between the simulated and observed SWE and snow depth in the open (OA), mixed or deciduous (DF) and coniferous forest (CF) area of PRB based on two different maximum snow densities ( $\rho_{s,max}$ ) used at the calibration stage of 1998-99 winter. Figures 3.9(a.1) and 3.9(a.2) also show reasonably good agreements between simulated and observed data for both open and deciduous forest areas at the validation stage of 1997/98 winter using FRM and SCM respectively. All the parameters derived in the calibration stage were kept unchanged in the calibration stage except the initial cold content and  $\rho_{s,max}$ . This could be possibly the reason for some deviations in the simulated snow depth and SWE during the validation stage of 1997/98, which should have experienced very different snow metamorphism compared to 1998/99 wet and cold winter. Slightly better validation results of the 1999/2000 winter was obtained with respect to snow depth and SWE (Figure 3.9(b.1): FRM, and Figure 3.9(b.2): SCM) by fine tuning some of the parameters e.g. the snow surface conductance,  $K_{sc}$  in SCM and the wind speed modifications in the forest covered area (see Eq. 2.30).

Even though the snow course surveys were conducted in different parts of PRB, sub-basin or zone 4 was selected to show the results in Figures 3.8 and 3.9 partly



because the average altitude of this zone is close to the average altitude of PRB. SDSM's simulated snow depth and SWE for the calibration period using  $\rho_{s,max}=200 \text{ kg/m}^3$  agree closely with observed in the early part of snow accumulation, and that using  $\rho_{s,max}=250 \text{ kg/m}^3$  were in good agreement in the later part of snow accumulation process. As expected, snow density does not remain constant as has been assumed in many land surface schemes (e.g. Essery, 1997), but increases with time and usually attains a highest value at the end of the snow accumulation period. Gray and Prowse (1993) reported that dry snow densities for shallow snow (depth < 1 m) at forested environments reach an approximate maximum value of  $250 \text{ kg/m}^3$ . Though  $\rho_{s,max}$  is set for each model run in SDSM-EBM, the freshly fallen snow interacts with the existing snowpack and the resulting snow density continues to change based on the settlement constant and the fresh snow density (if any) until it attains the maximum density (as discussed in Chapter 2). The maximum snow densities used for both the calibration and validation periods agree closely with the measured values. Open areas (OA) tend to undergo more wind impacts and theoretically should have larger snow densities than the forested areas. Similar trend was found in general except few cases in 1998 winter. However,  $\rho_{s,max}$  observed in open and forested areas do not differ much. It is possible that the wind impact in the OA is partly compensated with the additional compaction received from the free falling wet snow (or melt water) from the canopy in the forested area. It is found that the variation of snow density in an OA from one winter to another corresponds to the wind velocity.

The under-estimation of simulated SWE and snow depth in sub-basin 3 and slightly over-estimation of these variables in sub-basin 2 with respect to the observed data at both calibrating and validation stages are attributed to the precipitation distribution factor applied to each of the sub-basins of PRB (see Table 3.4). The precipitation (snow or rain) at each of the sub-basins is distributed according to the elevation differences with the gauge station. Figures 3.10 (a.1-a.2 using FRM and b.1-b.2

using SCM) show such response for the OA and DF in zones 2 and 3, and Figure 3.8 (a.1– a.2 using FRM and b.1-b.2 using SCM) for the OA and DF in zone 4 at the calibration stage.

In summary, SDSM-EBM is capable of simulating dependable basin-scale SWE and snow depth, which demonstrates the integrity of the model, even though the simulated stream flows differ from the observed partly because of the effects of beaver dams during both validation periods of dry winters 1997/98 and 1999/2000. The calibration and validation results using SDSM-EBM were also in good agreement with the modified temperature index method (SDSM-MTI) described in Chapter 4.

### **3.4.1.3 Surface Temperature**

The energy component of SDSM-EBM was assessed by comparing its simulated surface/skin temperature ( $T_s$ ) using the Force Restore Method (FRM), the Snow Conductance Method (SCM), and the Kondo and Yamazaki Method (KYM) with that retrieved from NOAA-AVHRR for different land cover types of PRB by the split-window technique (Figures 3.11 to 3.13). Figures 3.14 and 3.15 show corresponding comparisons at validation stages of 1998 and 2000 winters respectively. The discrepancies between simulated and NOAA-AVHRR retrieved surface temperature were generally  $\pm 3^\circ\text{K}$  for the open area, which is about the error range of NOAA-AVHRR derived  $T_s$  due to atmospheric effects, surface emissivity, instrument calibration, etc. (Cooper and Asrar, 1989; Traore et al., 1997). The deciduous forest (DF) and coniferous forest (CF) areas generally showed higher fluctuations than the open areas (OA) attributed to either some of the simplifying assumptions used to compute  $T_s$  (e.g., KYM) or model parameters are inappropriate at the validation stage (e.g., FRM and SCM) because some model parameters related to snowpack metamorphism change from one winter to another and even within the same winter period, e.g., the partitioning of net radiation between canopy and bare

soil using Beer's law of radiation transfer, the modification of wind speed at the ground level in the forest-covered area, assuming canopy temperature as air temperature, etc.

In general,  $T_s$  of FRM and SCM exhibit higher level of fluctuations than that of YKM (Figures 3.11 to 3.13) which is a relatively simpler scheme than the formers. For FRM, the fluctuations are partly attributed to the build-in stationary-mean diurnal frequency (e.g., coefficients A1 and B1). The  $T_s$  of KYM also exhibits a certain degree of diurnal cycle which at times could disappear particularly for OA landcover type (Figures 3.13, 3.14(c.1) and 3.15(c.1)). However, for DF the fluctuations could be excessively high (e.g., Figure 3.14(c.2), also Figures 3.14(a.2 and b.2)) which likely has to do with the model parameters associated with the partitioning of net radiation (see Chapter 2). Another reason for KYM to perform poor is because in SDSM-EBM, values of  $T_s$  were simulated without performing iterations to keep the model in its original form.

In Figures 3.11 to 3.15, Sub-basin 4 was selected partly because its average altitude is close to the average altitude of PRB so that it will be more appropriate to compare the  $T_s$  of SDSM-EBM with that retrieved from NOAA-AVHRR data for PRB (or the weighted average  $T_s$  for all landuses in all sub-basins of PRB). Overall, these results show the general ability of three schemes to simulate the  $T_s$  in different land cover classes accurately.

$T_s$  simulated by FRM (Figure 3.11, 3.14a, and 3.15a) is similar to that using SCM (Figures 3.12, 3.14b, and 3.15b) but SCM requires the calibration of snow surface conductance ( $K_{sc}$ ), which was found to differ from year to year. Such a change in  $K_{sc}$  is possible because of the simplified approach of SCM that ignores the diurnal cycle of  $T_s$ , and the changes in snow depth and snowpack properties from one winter to the other. The calibrated value of  $K_{sc}$  is  $3.0 \times 10^{-6}$  m/s for 1998/99 and  $1.0 \times 10^{-6}$

m/s for 1999-00. The  $K_{sc}$  for 1997-98 was assumed to be the same as that for 1998-99. Theoretically FRM is likely better than SCM and KYM since it considers two aspects of heat conduction into snow, a stationary-mean diurnal temperature variation at the surface coupled to a near steady-state ground heat flux of relatively low frequency variability.

A reliable estimate of  $T_s$  is vital for accurate estimation of the outgoing long-wave radiation (when net radiation data is not available) and for the turbulent sensible ( $Q_h$ ) and the latent heat fluxes ( $Q_e$ ). It seems that FRM, SCM and KYM are credible schemes for computing  $T_s$ , particularly FRM. More extensive research is recommended to test these three schemes over a wide range of climatic and landuse conditions.

### **3.5 Summary and Conclusions**

A semi-distributed, snowmelt model, energy balance model (SDSM-EBM) was developed and applied to the seasonally snowcovered, Paddle River Basin (PRB) of central Alberta. SDSM-EBM is a physics-based, energy balance model developed to model basin-scale snow accumulation and ablation processes by considering (a) vertical energy exchange processes in open and forested area separately; (b) snowmelt processes that include liquid and ice phases separately within the snowpack and that takes canopy interception, fresh snow density, sublimation, refreezing, snow compaction etc into consideration. SDSM-EBM is also set up to simulate snow surface temperature using the force-restore, snow surface conductance, and the Kondo and Yamazaki Methods. Other than the “regulatory” effects of beaver dams that affected the validation results on simulated runoff, on a whole SDSM-EBM was able to simulate reasonably accurately water (snowmelt runoff, a snow depth, SWE) and energy (snow surface temperature) fluxes in PRB. This demonstrates that it is capable of modeling basin-scale snow accumulation and ablation processes.

## References

- Anderson, E. A. (1976), *A point energy and mass balance model of a snow cover*. Tech. Memo. NWS-HYDRO 19, National Oceanic Atmos. Admin.(NOAA), Washington, D.C.
- Beven, K. J. (1996), A discussion of distributed hydrological modeling. In: *Distributed hydrological modeling*, ed. M. B. Abbott, and J. C. Refsgaard, Water Resources Publications, 255-278.
- Biftu, G. F. (1998), *Semi-distributed, physically based hydrologic modeling using remotely sensed data and GIS*. PhD thesis, University of Alberta, Edmonton, Canada, 218p.
- Biftu, G. F. (1998), *Semi-distributed, physically based hydrologic modeling using remotely sensed data and GIS*, PhD thesis, University of Alberta, Edmonton, Canada, 218p.
- Biftu, G. F., and Gan, T.Y. (2000), Assessment of evapotranspiration models applied to a watershed of Canadian Prairies with mixed land-uses, *J. Hydrol. Process.*, 14:1305-1325.
- Biftu, G. F., and Gan., T. Y. (2001), Semi-distributed, physically based, hydrologic modeling of the Paddle River Basin, Alberta, using remotely sensed data, *J. Hydrol.*, 244:137-156.
- Blöschl, G. (1999), Scaling issue in snow hydrology. *Hydrol. Process.*, 13: 2149-2175.
- Choudhury, B. J. (1987), Relationships between vegetation indices, radiation absorption, and net photosynthesis evaluated by a sensitivity analysis. *Remote Sens. Environ.*, 22:209-233.
- Choudhury, B. J., Ahmad, N. U., Idso, S. B., Reginato, R. J., and Daughtry, C. S. T. (1994), Relations between evaporation coefficients and vegetation indices studied by model simulations, *Remote Sens. Environ.*, 50:1-17.

- Cooper, D., and Asrar, G. (1989), Evaluating atmospheric correction models for retrieving surface temperature from the AVHRR over a tall grass prairie, *Remote Sens. Environ.*, 27:93-102.
- Deering, D. W., Rouse, J. W., Haas, R. H., and Schall, J. A. (1975), Measuring forage production of grass units from Landsat MSS data. Environment, Ann Arbor, MI, 1169p.
- Essery, R. L. H. (1997), Seasonal snow cover and climate change in the Hadley Center GCM, *Ann. Glaciol.*, 25:362-366.
- Gary D. M. and Landine, P.G. (1988), An energy budget snowmelt model for the Canadian Prairies, *Canadian J. Earth Science*, 25(8):1292-1303.
- Gray, D. M., and Prowse, T. (1993), Snow and floating ice, In: *Handbook of Hydrology*, ed. D. R. Maidment, McGraw-Hill Inc., New York, 7.1-7.58.
- Gurnell, A. M. (1998). The hydrogeomorphological effects of beaver dam-building activity. *Progress in Physical Geography*, 22(2): 167-189.
- Kant, Y., and Badarinath, K. V. S. (2000), Studies on land surface temperature over heterogeneous area using AVHRR data. *Int. J. Remote Sensing*, 21(8):1749-1756.
- Kirnbauer, R., Blöschl, G., and Gutknecht, D. (1994), Entering the era of distributed snow models. *Nordic Hydrology*, 25:1-24.
- Kondo J., and Yamazaki, T. (1990), A Prediction Model for Snowmelt, Snow Surface Temperature and Freezing Depth Using a Heat Balance Method. *J. Appl. Meteorol.*, 29:375-384.
- Kuchment, L. S., Gelfan, A. N., Demidov, V. N. (2000), A distributed model of runoff generation in the permafrost regions. *J. Hydrol.*, 240:1-22.
- Kustas W. P., Rango, A., and Uijlenhoet, R. (1994), A simple energy budget algorithm for the snowmelt runoff model. *Water Resour. Res.*, 30(5):1515-1527.
- Kustas, W. P., Jackson, T. J. (1999), The impact of area-averaged heat fluxes from using remotely sensed data at different resolutions: A case study with Washita '92 data. *Water Resour. Res.*, 35(5):1539-1550.

- Laine, V., and Heikinheimo, M. (1996), Estimation of surface albedo from NOAA AVHRR data in high latitudes. *Tellus*, 48A:424-441.
- Leyton, L., Reynolds, E. R. C., and Thompson, F. B. (1967), Rainfall interception in forest and moorland. In: *Forest Hydrology*, ed. W. E. Sopper and H. W. Lull, Pergamon Press, Oxford, 163-168.
- Pinty, B., and Verstraete, M. M. (1992), GEMI: a non-linear index to monitoring global vegetation from satellite. *Vegetation*, 101:15-20.
- Pomeroy, J. W., Gray, D. M., Shook, K. R., Toth, B., Essery, R. L. H., Pietroniro, A., and Hedstrom, N. (1998), An evaluation of snow accumulation and ablation processes for land surface modeling. *Hydrol. Proc.*, 12:2339-2367.
- Price, J. C. (1983), Estimated surface temperature from satellite thermal infrared data—a simple formulation for the atmospheric effect. *Remote Sens. Environ.*, 13:353-361.
- Price, J. C., 1984. Land surface temperature measurements from the split window channels of the NOAA 7 Advanced Very high resolution radiometer. *J. Geophys. Res.*, 89(D5):7231-7237.
- Prince, S. D., Goetz, S. J., Dubayah, R. O., Czajkowski, K. P., and Thawley, M. (1998), Inference of surface and air temperature, atmospheric precipitable water and vapor pressure deficit using advanced very high resolution radiometer satellite observations: comparison with field observations, *J. Hydrol.*, 212-213:230-249.
- Qin Z., and Karnieli, A. (1999), Progress in the remote sensing of land surface temperature and ground emissivity using NOAA-AVHRR data. *Int. J. Remote Sensing*, 20(12):2367-2393.
- Rao, C. R. N., and Chen, J. (1996), Post-launch calibration of the visible and near-infrared channels of the Advanced Very High Resolution Radiometer on the NOAA-14 spacecraft. *Int. J. Remote Sensing*, 17:2743-2747.

- Rao, C. R. N., and Chen, J. (1999), Revised post-launch calibration of the visible and near-infrared channels of the Advanced Very High Resolution Radiometer (AVHRR) on the NOAA-14 spacecraft, *Int. J. Remote Sensing*, 18:3485-3491.
- Riley, J. P., Israelsen, E. K., and Eggleston, K. O. (1972), Some approaches to snowmelt prediction. *AISH Publ.*, 2(107):956-971.
- Running, S. W., and Nemani, R. R. (1988), Relating seasonal patterns of the AVHRR vegetation index to simulated photosynthesis and transpiration of forests in different climates. *Remote Sens. Environ.*, 24:347-367.
- Rutter, A. J., Kershaw, K. A., Robins, P. C., and Morton, A. J. (1971-72). A predictive model of rain interception in forests, 1. Derivation of the model from observations in a plantation of Corsican Pine. *Agric. Meteorology*, 9:367-384.
- Seguin, B. and Itier, B. (1983), Using mid-day surface temperature to estimate daily evaporation from satellite thermal infrared data. *Int. J. Remote Sensing*, 4:371-383.
- Singh, P. R., and Gan, T. Y. (2000), Retrieval of snow water equivalent using passive microwave brightness temperature data. *Remote Sens. Environ.*, 74:275-286.
- Stroeve, J., and Steffen, K. (1998), Variability of AVHRR derived clear-sky surface temperature over the Greenland ice sheet. *J. Appl. Meteorol.*, 37:23-31.
- Thompson, F. B. (1972), *Rainfall interception by oak coppice (Quercus robur, L.)*. Research paper in Forest Meteorology, ed. J. A. Taylor, Cambrian News Ltd., Aberystwyth, 59-74.
- Traore, P. C. S., Royer, A., and Goita, K. (1997), Land surface temperature time series derived from weekly AVHRR GVI composite datasets: Potential and constraints for northern latitudes. *Canadian J. Remote Sens.*, 23(4):390-400.
- Twardy, A. G., and Lindsay, J. D. (1971), *Soil survey of the Chip Lake area, Alberta soil survey, report No. 28*, 71p.



- Woo, M., and Valverde, J. (1982), Ground and water temperatures of a forested mid-latitude swamp. In: Proc. of the Canadian Hydrology Symposium '82, *Hydrological Processes of Forested Areas*, Fredericton, N.B., 301-312.
- Woo, M., and Waddington, J. M. (1990), Effects of beaver dams on subarctic wetland hydrology. *Arctic*, 43(3):223-230.

Table 3.1 Summary of data used in SDSM-EBM

Topographic data	Mean altitude, aspect, flow direction, slope of the surface, drainage network, & topographic-soil index derived from DEM.
Land use & spatially distributed surface-physical data	Spatial distribution of land use classes, surface albedo, vegetation index and surface temperature (Landsat image for land use classification and NOAA-AVHRR image for other surface-physical parameters).
Hourly hydro-meteorological data	air temperature, ground temperature, precipitation (snow/rain), wind speed and wind direction, relative humidity, net radiation, short-wave radiation, ground heat flux data.
Snowcourse Data	Snow depth & density along the transects in different land use.
Stream flow data	Stream flow data for the Paddle River Basin at Anselmo.

Table 3.2a Summary of snow course survey (SCS) data for 1998, 1999, and 2000 winters (snow depth in cm and SWE in mm).

Date	Coniferous forest	Mixed forest	Agriculture & Pasture land	<sup>4</sup> PRHW S.P.	Mayerthorpe S.P.
	SCS conducted for this research work <sup>1</sup>			SCS conducted by AE <sup>2</sup>	
1/29/1998 <sup>1,2</sup>	18.0/17.0 <sup>3</sup>	14.9/21.7	18.0/20.2	15/21	-
2/06/1998 <sup>1</sup>	17.1/22.4	15.2/21.5	-	-	-
2/25/1998 <sup>2</sup>	-	-	-	11/15	12/15
3/31/1998 <sup>2</sup>	-	-	-	7/15	0/0
1/28/1999 <sup>2</sup>	-	-	-	54/112	-
2/06/1999 <sup>1</sup>	59.3/119.8	57.3/112.3	57.5/114.2	-	-
3/02/1999 <sup>2</sup>	-	-	-	63/137	55/118
3/14/1999 <sup>1</sup>	60.8/131.3	63.5/127.5	60.5/136.8	-	-
3/30/1999 <sup>2</sup>	-	-	-	64/155	46/112
1/23/2000 <sup>1</sup>	N/A	11.0/10.1	10.8/12.4	-	-
2/01/2000 <sup>2</sup>	-	-	-	9/13	-
2/28/2000 <sup>2</sup>	-	-	-	11/15	13/18
3/18/2000 <sup>1</sup>	24.0/39.1	17.6/29.2	13.9/27.6	-	-
3/28/2000 <sup>2</sup>	-	-	-	4/10	3/8

Notes: <sup>1</sup> Snow course survey dates conducted for this research work

<sup>2</sup> Snow course survey dates conducted by Alberta Environment (AE)

<sup>3</sup> 18.0/17.0 means the snow depth was 18.0 cm and SWE was 17.0 mm

<sup>4</sup> PRHW S. P. is Paddle River Headwaters Snow Pillow site

Table 3.2b Standard deviation of observed snow depth data for three winters.

Year	Range of Standard Dev. (cm)		Average Standard Dev (cm)	
	Open area	Forest area	Open area	Forest area
1998	1.2-4.6	1.2-8.2	2.3 (4 SCS sites*)	3.6 (4 SCS sites)
1999	2.3-4.5	3.4-7.2	3.4 (7 SCS sites)	5.7 (5 SCS sites)
2000	1.1-3.2	0.6-5.0	1.9 (7 SCS sites)	2.9 (3 SCS sites)

\* Each of the SCS sites has 15 to 40 samples taken at every 10 paces for snow depth and 1 to 3 snow density measurements.

Table 3.3 Characteristics of NOAA-AVHRR satellite data.

Ground resolution	1.1 km at nadir
Ground swath	2700 km wide
Spectral Bands	
Channel 1 (visible)	0.58 – 0.68 $\mu\text{m}$
Channel 2 (near infrared)	0.72 – 1.10 $\mu\text{m}$
Channel 3 (thermal infrared)	3.55 – 3.93 $\mu\text{m}$
Channel 4 (thermal infrared)	10.3 – 11.3 $\mu\text{m}$
Channel 5 (thermal infrared)	11.5 – 12.5 $\mu\text{m}$

Table 3.4 Five zones (sub-basins) of Paddle River Basin (Figure 3.1a), their land use classification and corresponding area used in the SDSM.

Zone	Mean altitude (meter AMSL)	Total area ( $\text{km}^2$ )	Area ( $\text{km}^2$ ) for each of the Land Cover Classes		
			Coniferous forest	Mixed forest	Open area
1	872.5	55.02	9.83	32.99	12.20
2	884.5	49.91	12.36	25.88	11.67
3	807.5	56.97	11.41	15.60	29.96
4	862.5	88.68	18.25	53.02	17.41
5	768.5	11.13	2.53	1.93	6.67
Total landuse ( $\text{Km}^2$ )		261.71	54.38	129.42	77.91
Landuse fraction (%)		100.00	20.78	49.45	29.77

Table 3.5 Equations to retrieve albedo and spectral radiance from NOAA-AVHRR (NOAA-14 spacecraft) satellite data.

Albedo/Radiance	Equation	Reference
Albedo from channel 1	$(0.0000135d + 0.111) * (C_{10} - 41)$	Rao and Chen (1999)
Albedo from channel 2	$(0.0000133d + 0.134) * (C_{10} - 41)$	
Radiance from channel 1	$(0.0000690d + 0.566) * (C_{10} - 41)$	
Radiance from channel 2	$(0.0000435d + 0.440) * (C_{10} - 41)$	

Where  $d$  is the elapsed time in orbit, expressed in days after the day of launch (30 December, 1994) and  $C_{10}$  is the corresponding channel's AVHRR signal in counts on a 10-bit scale.

Table 3.6 Surface albedo retrieved from NOAA-AVHRR for different land cover classes in each sub-basins of PRB.

SB#	Coniferous	Deciduous	Water	Agriculture	Pasture	Impervious
Date: January 5, 1998						
1	0.651	0.656	0.670	0.708	0.695	0.678
2	0.597	0.623	0.564	0.644	0.673	0.599
3	0.726	0.669	0.643	0.831	0.870	0.839
4	0.590	0.607	0.592	0.648	0.649	0.636
5	0.842	0.900	0.705	0.884	0.900	0.900
WA	0.642	0.634	0.602	0.743	0.792	0.744
Date: December 23, 1999						
1	0.738	0.702	0.728	0.825	0.769	0.856
2	0.640	0.651	0.616	0.658	0.673	0.613
3	0.784	0.729	0.722	0.867	0.886	0.884
4	0.634	0.639	0.639	0.655	0.658	0.638
5	0.789	0.848	0.676	0.823	0.881	0.900
WA	0.693	0.671	0.656	0.774	0.805	0.790
Date: April 24, 1999						
1	18.37	18.13	18.27	18.66	18.57	18.67
2	17.62	17.63	17.78	17.58	17.90	17.71
3	18.49	17.95	17.80	19.12	19.39	19.44
4	17.28	17.21	17.34	17.55	17.87	17.32
5	19.11	19.46	19.26	19.48	19.60	20.34
WA	0.179	0.177	0.178	0.185	0.189	0.186

SB#=sub-basin number; and WA = weighted average value.

Table 3.7 Relationship between NDVI and Leaf Area Index (LAI) for different landuse classes.

	Land cover type	Equation	Reference
1.	Agriculture	$LAI = -2.5 * \ln(1.2 - 2 * NDVI)$	Kanemasu et al., 1977
2.	Pasture	$LAI = 0.21 * \exp(NDVI/0.264)$	Kite and Spence, 1995
3.	Mixed forest	$LAI = \left( 0.52 * \left( \frac{NDVI + 1}{1 - NDVI} \right) \right)^{1.715}$	Petersen et al., 1987
4.	Coniferous forest	$LAI = 0.65 * \exp\left(\frac{NDVI}{0.34}\right)$	Nemani and Running, 1989

Where, Normalized Difference Vegetation Index (NDVI) is  $[(\text{Channel 2} - \text{Channel 1}) / (\text{Channel 2} + \text{Channel 1})]$  with channel values as the corresponding reflectance.

Table 3.8 AVHRR derived NDVI for different land cover classes in each sub-basins of PRB.

SB#	Coniferous	Deciduous	Water	Agriculture	Pasture	Impervious
Date: January 5, 1998						
1	0.0906	0.0924	0.0974	0.0889	0.0899	0.0875
2	0.0962	0.0917	0.1051	0.0889	0.0880	0.0889
3	0.0854	0.0841	0.0867	0.0824	0.0824	0.0826
4	0.0886	0.0874	0.0883	0.0848	0.0833	0.0836
5	0.0835	0.0810	0.0887	0.0820	0.0809	0.0741
WA	0.0898	0.0890	0.0972	0.0849	0.0843	0.0837
Date: December 23, 1999						
1	0.0856	0.0871	0.0869	0.0839	0.0858	0.0805
2	0.0861	0.0820	0.0918	0.0789	0.0828	0.0778
3	0.0747	0.0742	0.0774	0.0732	0.0741	0.0753
4	0.0803	0.0765	0.0815	0.0747	0.0751	0.0739
5	0.0686	0.0679	0.0660	0.0686	0.0660	0.0631
WA	0.0809	0.0798	0.0866	0.0757	0.0763	0.0751
Date: April 24, 1999						
1	0.1906	0.1798	0.1919	0.1820	0.1802	0.1834
2	0.2015	0.1921	0.2050	0.1918	0.1878	0.1857
3	0.1833	0.1811	0.1890	0.1770	0.1736	0.1738
4	0.1932	0.1770	0.1891	0.1774	0.1856	0.1817
5	0.1839	0.1768	0.1902	0.1794	0.1723	0.1714
WA	0.1921	0.1812	0.1964	0.1799	0.1782	0.1803

SB#=sub-basin number; and WA = weighted average value.



Table 3.9 Scene surface temperature ( $T_s$  in °K) retrieved from NOAA-AVHRR for different land cover classes in each sub-basins of PRB.

SB#	Coniferous	Deciduous	Water	Agriculture	Pasture	Impervious
Date: January 5, 1998						
1	246.06	245.05	246.00	245.93	245.91	245.49
2	244.73	243.20	245.55	243.52	243.11	244.66
3	245.80	246.45	246.71	244.48	244.15	244.40
4	245.35	244.85	245.17	244.25	244.87	244.69
5	242.79	242.50	246.00	242.61	242.14	243.73
WA	245.33	244.76	245.65	244.40	244.17	244.63
Date: December 23, 1999						
1	248.93	248.96	249.01	248.78	249.18	248.10
2	248.78	248.77	248.56	248.45	249.00	249.78
3	249.22	249.37	250.11	247.64	247.83	248.34
4	249.31	248.88	249.02	248.59	249.79	250.28
5	249.44	248.18	251.00	249.05	247.85	245.73
WA	249.11	248.93	248.93	249.11	248.93	248.82
Date: April 24, 1999						
1	297.81	300.82	299.18	300.00	299.91	300.17
2	295.95	297.33	293.53	298.48	299.02	298.41
3	300.55	300.97	299.55	302.14	302.31	302.26
4	298.70	299.79	298.63	299.52	299.34	300.52
5	301.07	301.02	301.66	301.38	301.08	301.96
WA	298.41	299.74	296.70	300.59	300.93	301.06

SB#=sub-basin number; and WA = weighted average value.

Table 3.10 Model parameters used in SDSM-EBM (1-16), and some of the important parameters used in DPHM-RS (17-19).

Description of Model Parameters	SDSM-EBM
1. Rain to snow threshold temperature, $T_{th}$ ( $^{\circ}\text{C}$ )	1.1
2. Threshold temperature for melt, $T_m$ ( $^{\circ}\text{C}$ )	0
3. Throughfall coefficient for CF, $\tau_{f,cf}$	0.25
4. Throughfall coefficient for MF, $\tau_{f,mf}$	0.58
5. Tree species coefficient for CF, $S_{p,cf}$ ( $\text{kg}/\text{m}^2$ )	0.00625
6. Tree species coefficient for MF, $S_{p,mf}$ ( $\text{kg}/\text{m}^2$ )	0.00313
7. Snow unloading coefficient, $c$	0.678
8. Maximum density of snow pack, $\rho_{s,max}$ ( $\text{kg}/\text{m}^3$ )	150-250
9. Settlement constant, $c_s$	0.05
10. Liquid water holding capacity (LWHC)	0.05
11. Stability factor (FSTAB)	0
12. Thermally active soil layer ( $D_e$ , m)	0.40
13. Surface Conductance, $K_{sc}$	1.0E-6 - 3.0E-6
14. Snowfall distribution factor (%/100 m)	0.20
15. Rainfall distribution factor (%/100 m)	0.80
16. Temperature lapse rate ( $^{\circ}\text{C}/100$ m)	-0.65
17. Relative water content ( $\theta/\theta_s$ )	0.80 for both layers
18. Depth of each layer (m)	0.2
19. Manning's roughness coefficients, $n$	0.15 (forest) & 0.1 (open area)

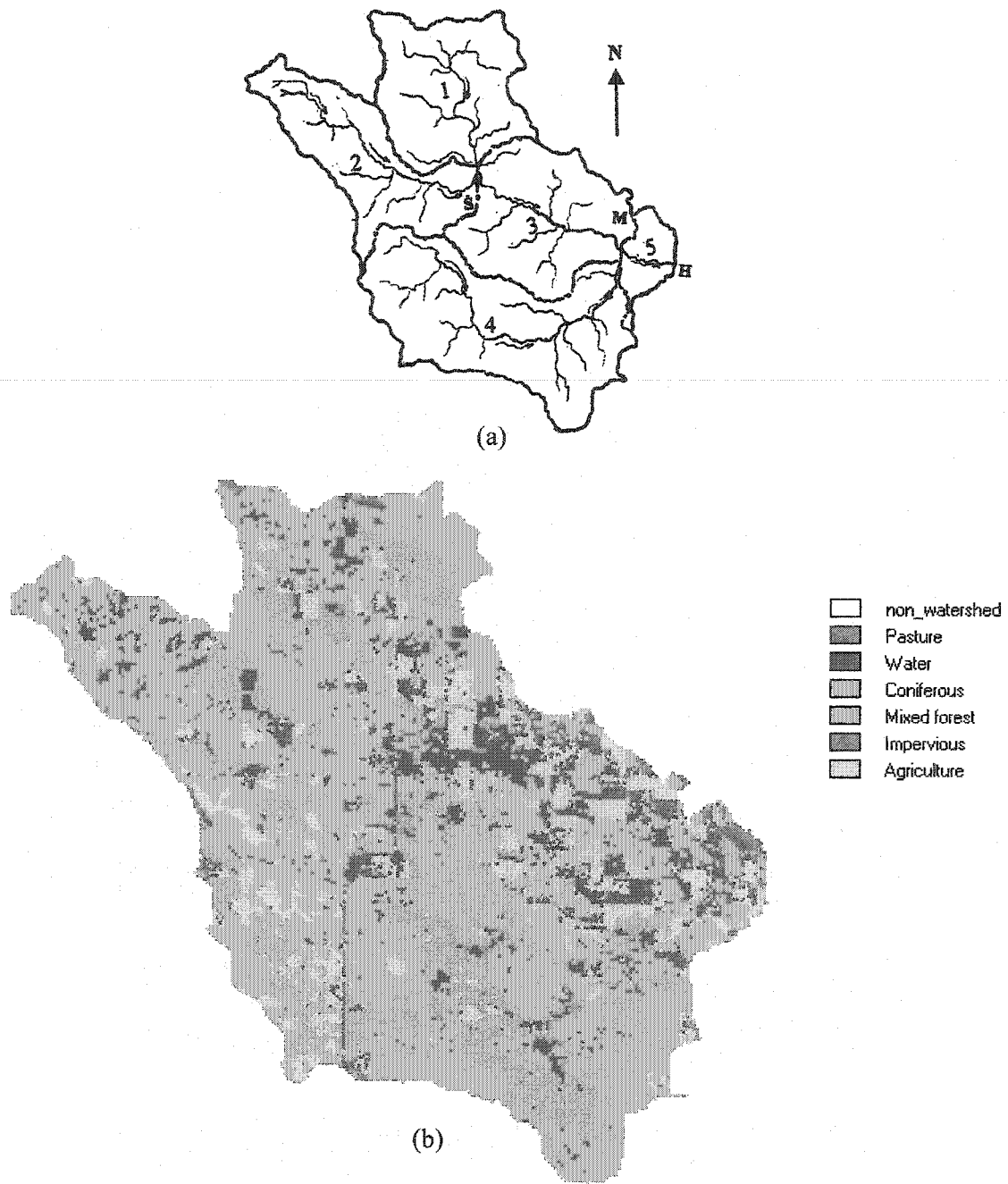


Figure 3.1 (a) Five sub basins (1 to 5) of Paddle River Basin and its drainage network derived from DTED. H, M, and S are locations of streamflow gauge at the basin outlet, meteorological tower, and snow pillow site respectively; (b) Landuse classification of PRB derived from Landsat TM image of August 7, 1996.

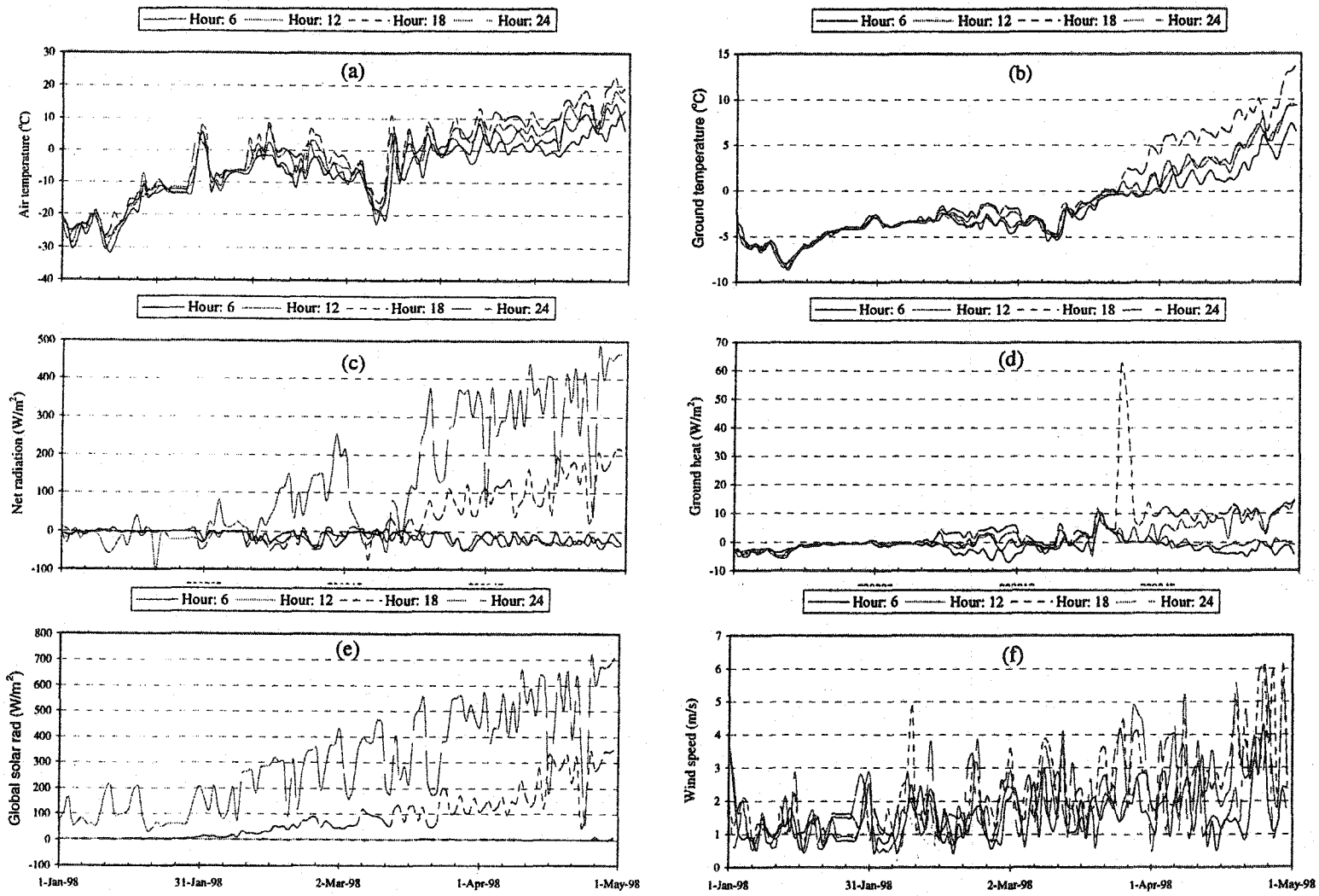


Figure 3.2 Diurnal pattern of meteorological data: (a) air temperature, (b) ground temperature, (c) net radiation, (d) ground heat flux, (e) global solar radiation, and (f) wind speed measured at Paddle River Basin for 1998 winter from January 1 to April 30, 1998.

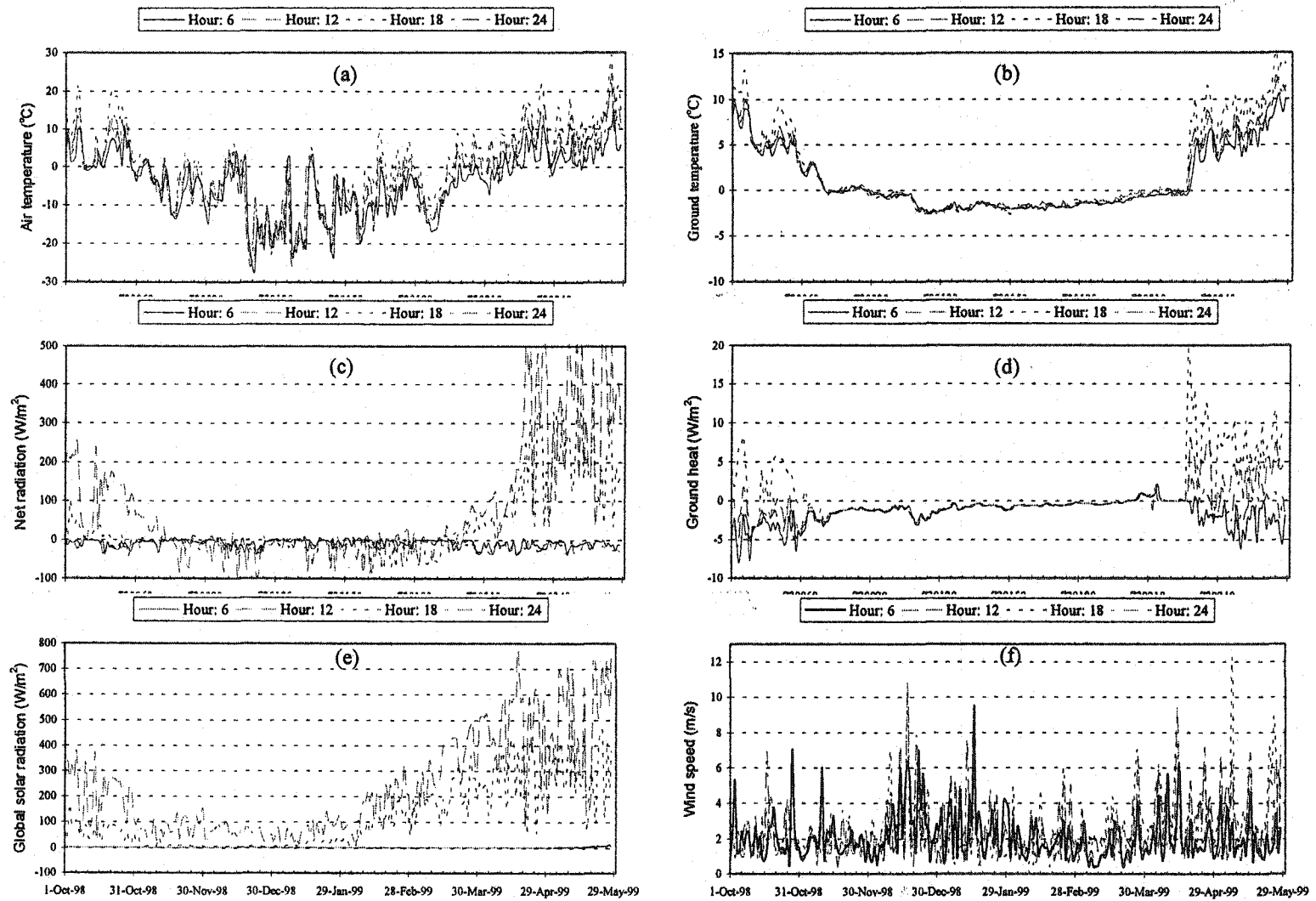


Figure 3.3 Diurnal pattern of meteorological data: (a) air temperature, (b) ground temperature, (c) net radiation, (d) ground heat flux, (e) global solar radiation, and (f) wind speed measured at Paddle River Basin for the 1998-99 winter from October 1, 1998 to May 28, 1999.

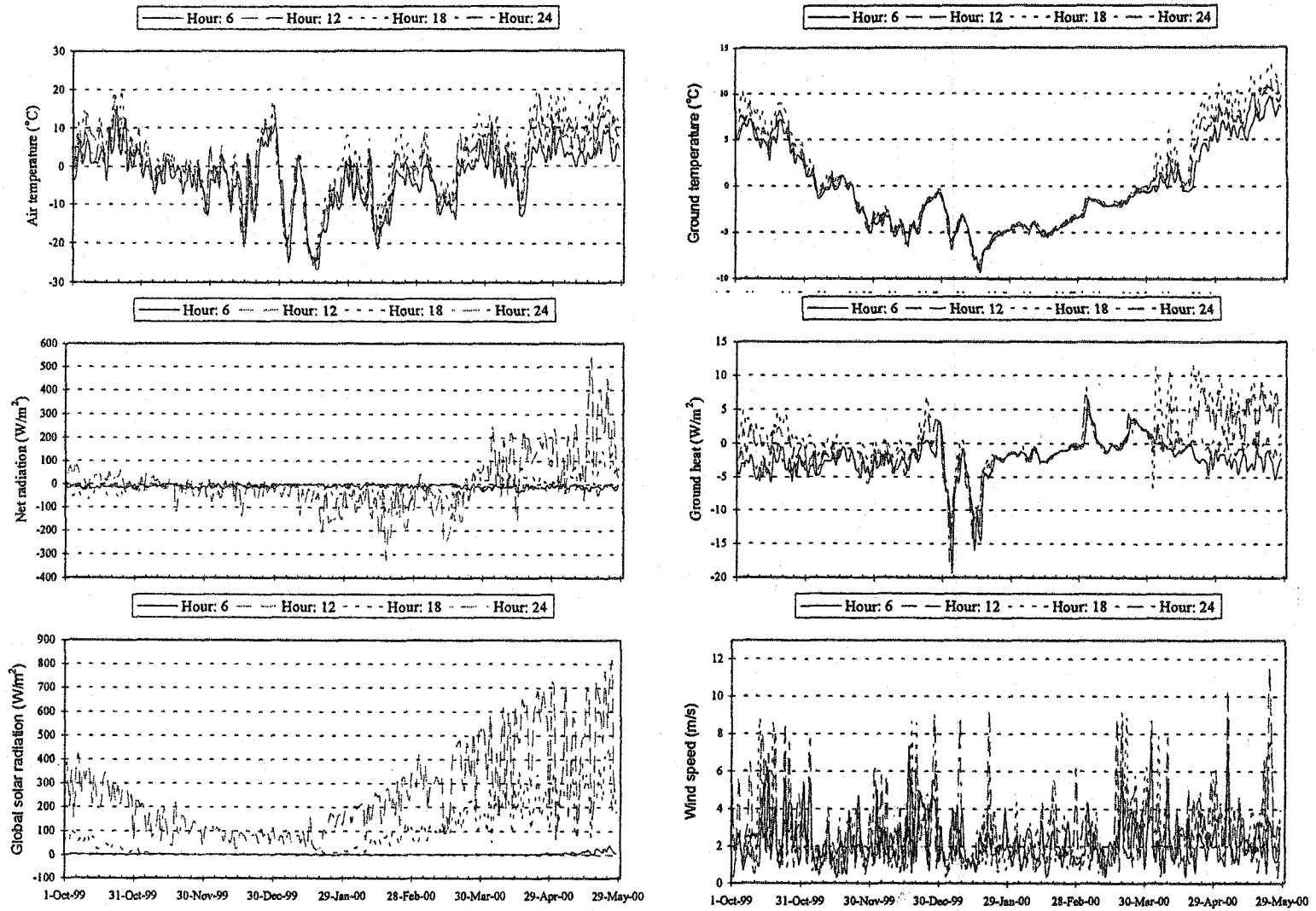


Figure 3.4 Diurnal pattern of meteorological data: (a) air temperature, (b) ground temperature, (c) net radiation, (d) ground heat flux, (e) global solar radiation, and (f) wind speed measured at Paddle River Basin for the 1999-2000 winter from Oct 1, 1999 to May 28, 2000.

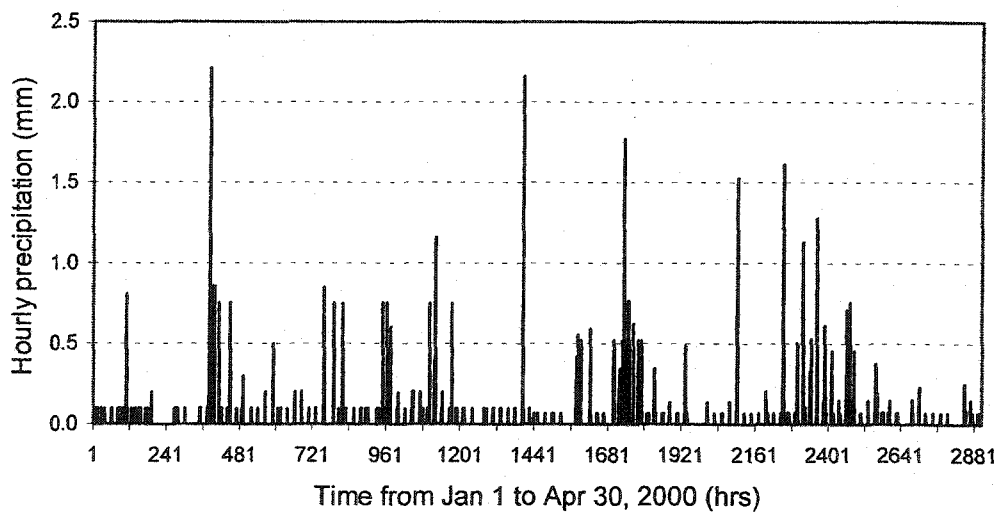
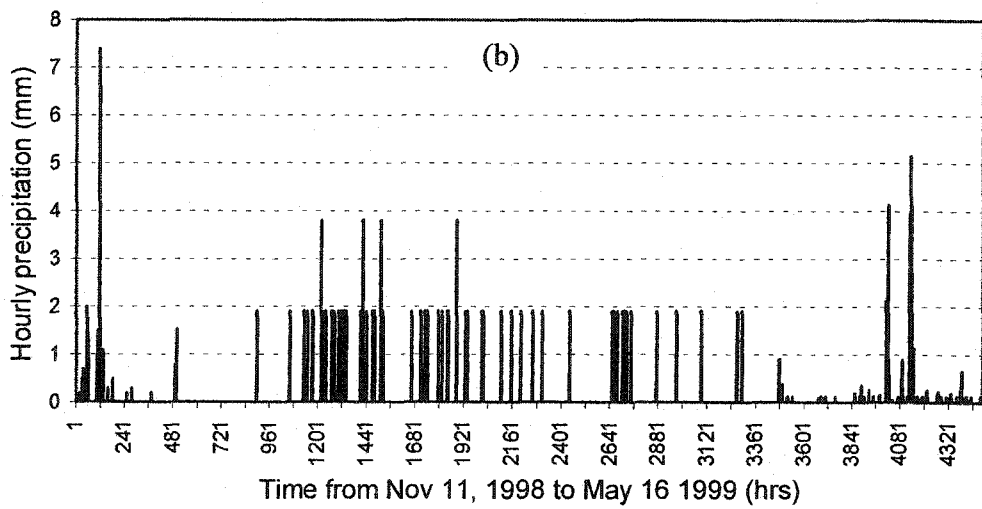
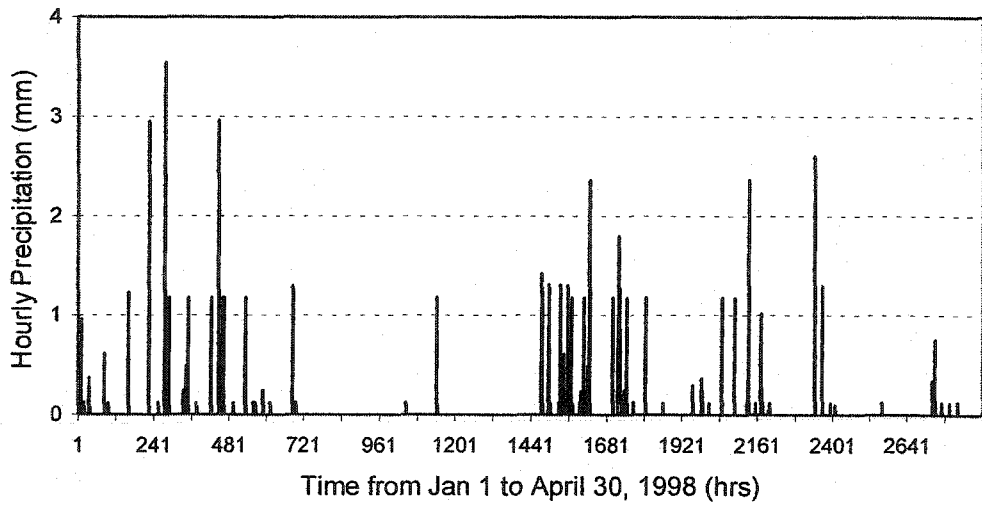


Figure 3.5 PRB's precipitation data (water equivalent) for three winters.

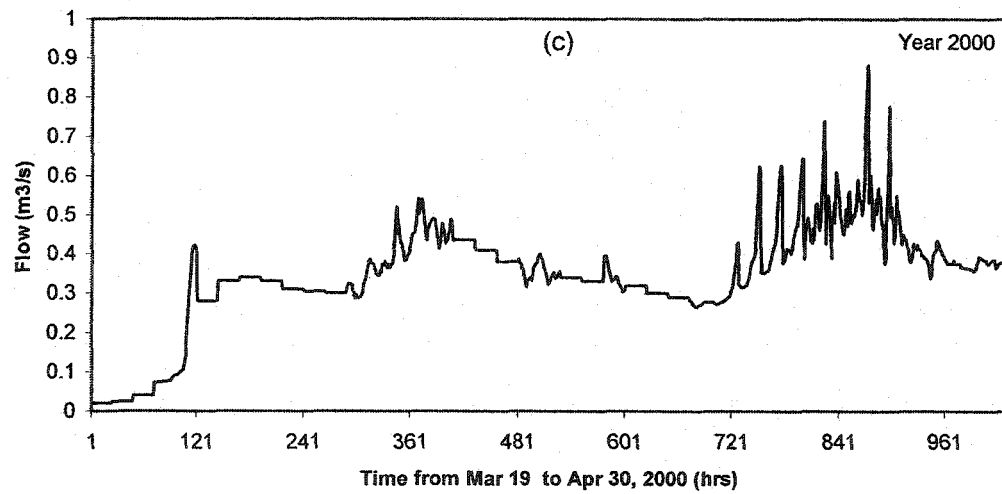
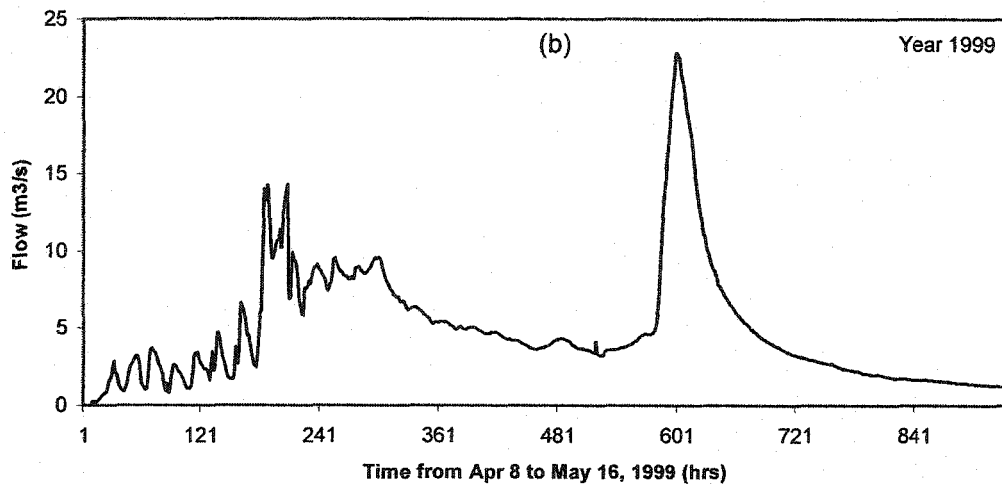
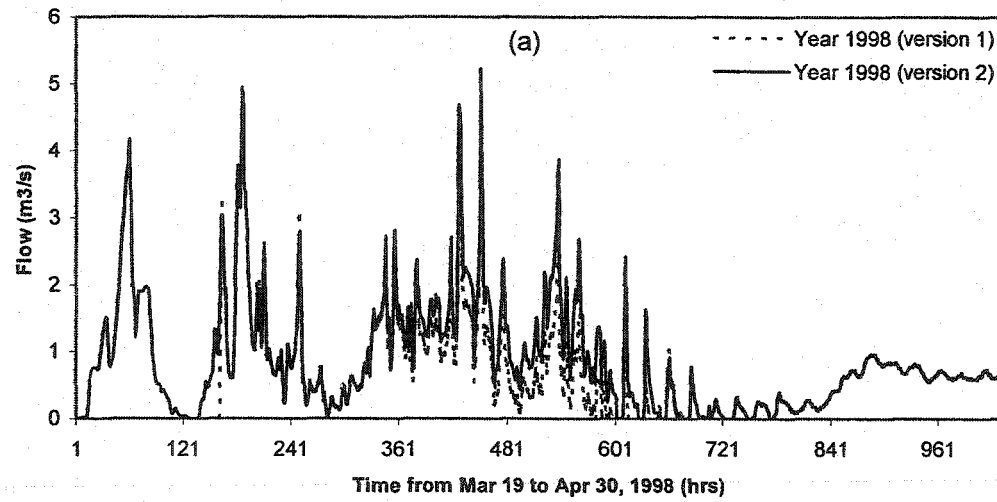


Figure 3.6 PRB's hourly streamflow hydrographs at the WSC station 07BB011 near Anselmo for (a) 1998, (b) 1999, (c) 2000 winters.



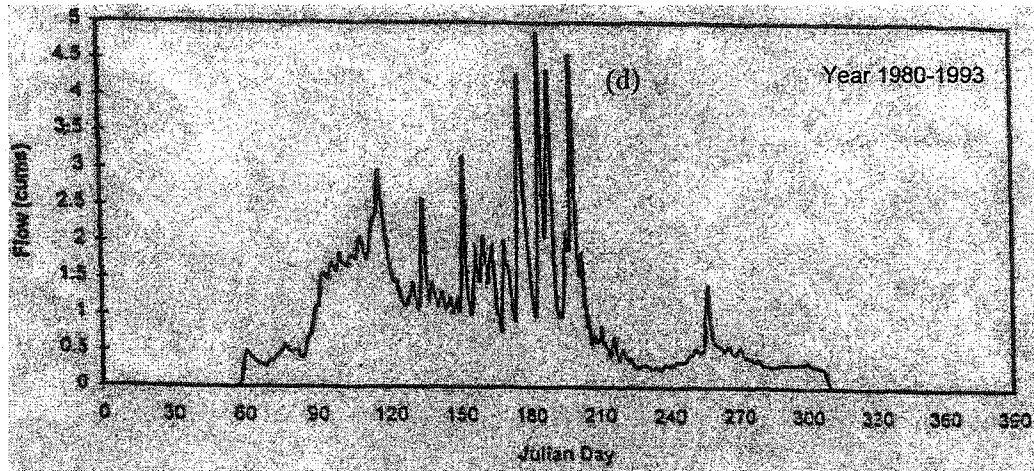


Figure 3.6(d) PRB's daily average streamflow hydrograph at the WSC station 07BB011 near Anselmo for 1980-1993.

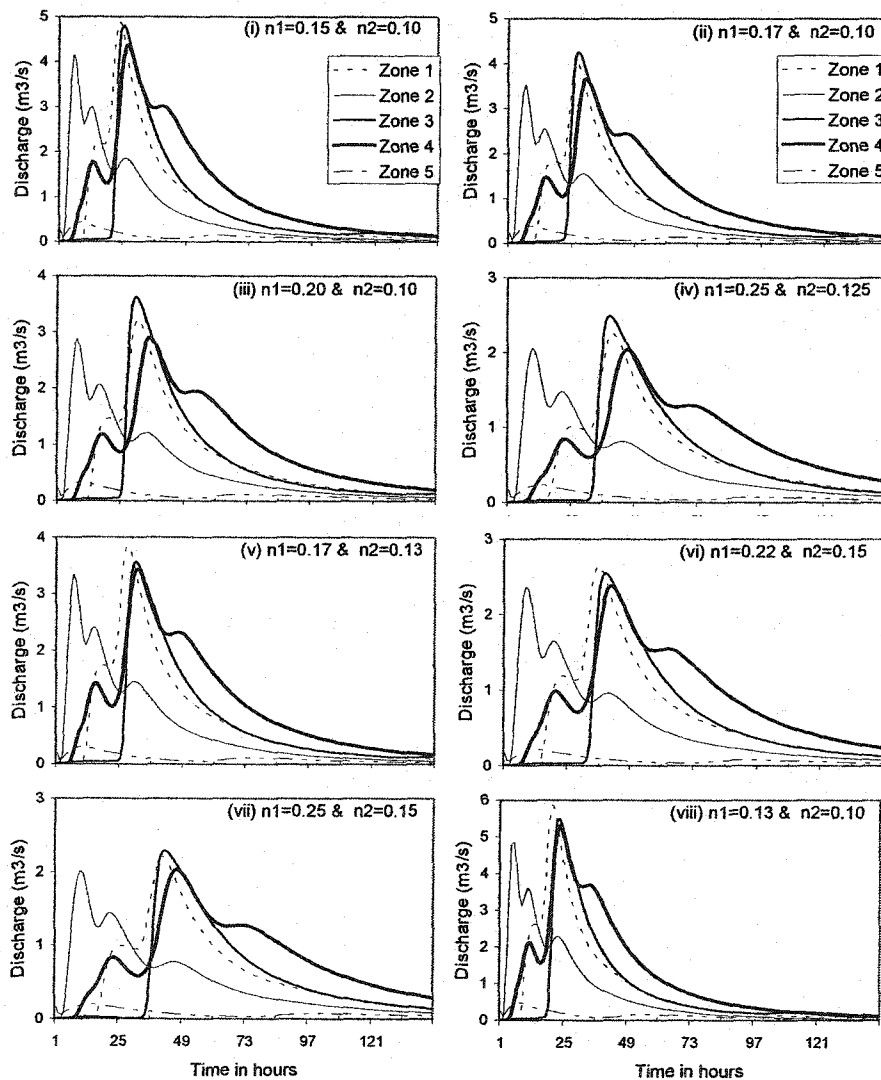
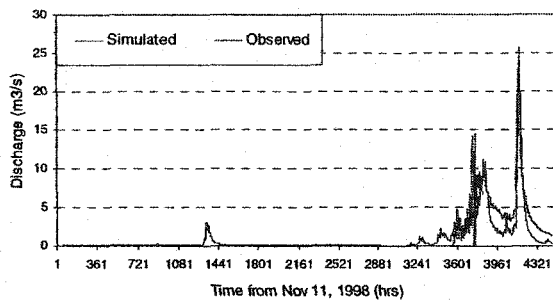
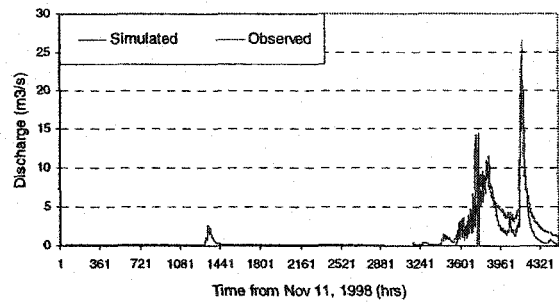


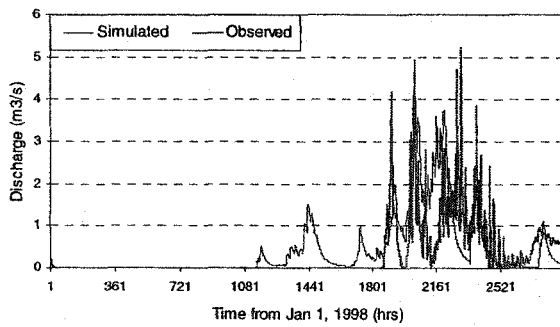
Figure 3.6(e) Unit hydrographs for each of the five zones of PRB for different combinations of Manning's roughness: 'n1' for the forest and 'n2' for open area.



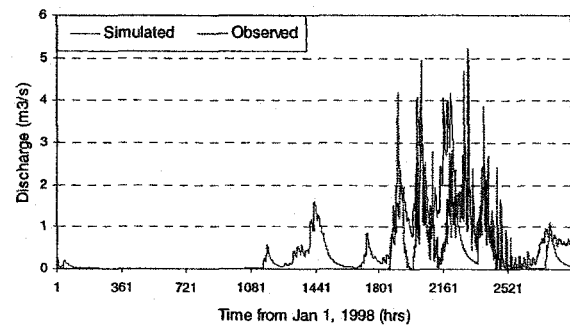
(a.1)



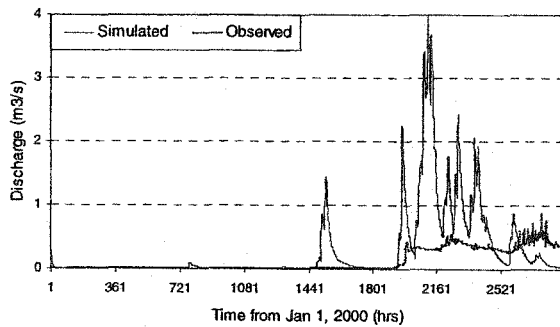
(a.2)



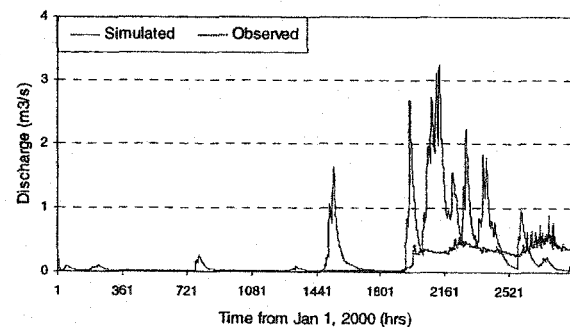
(b.1)



(b.2)



(c.1)



(c.2)

Figure 3.7 Comparison of SDSM-EBM simulated and observed runoff at the outfall of Paddle River basin (PRB): (a) for the calibration stage (Nov. 11, 1998 to May 16, 1999) using (a.1) Force Restore Method (FRM) and (a.2) Snow Conductance Method (SCM); (b) for the validation stage (Jan. 1, 1998 to Apr. 30, 1998) using (b.1) FRM and (b.2) SCM; and (c) for another validation stage (Jan. 1, 2000 to Apr. 30, 2000) using (c.1) FRM and (c.2) SCM.

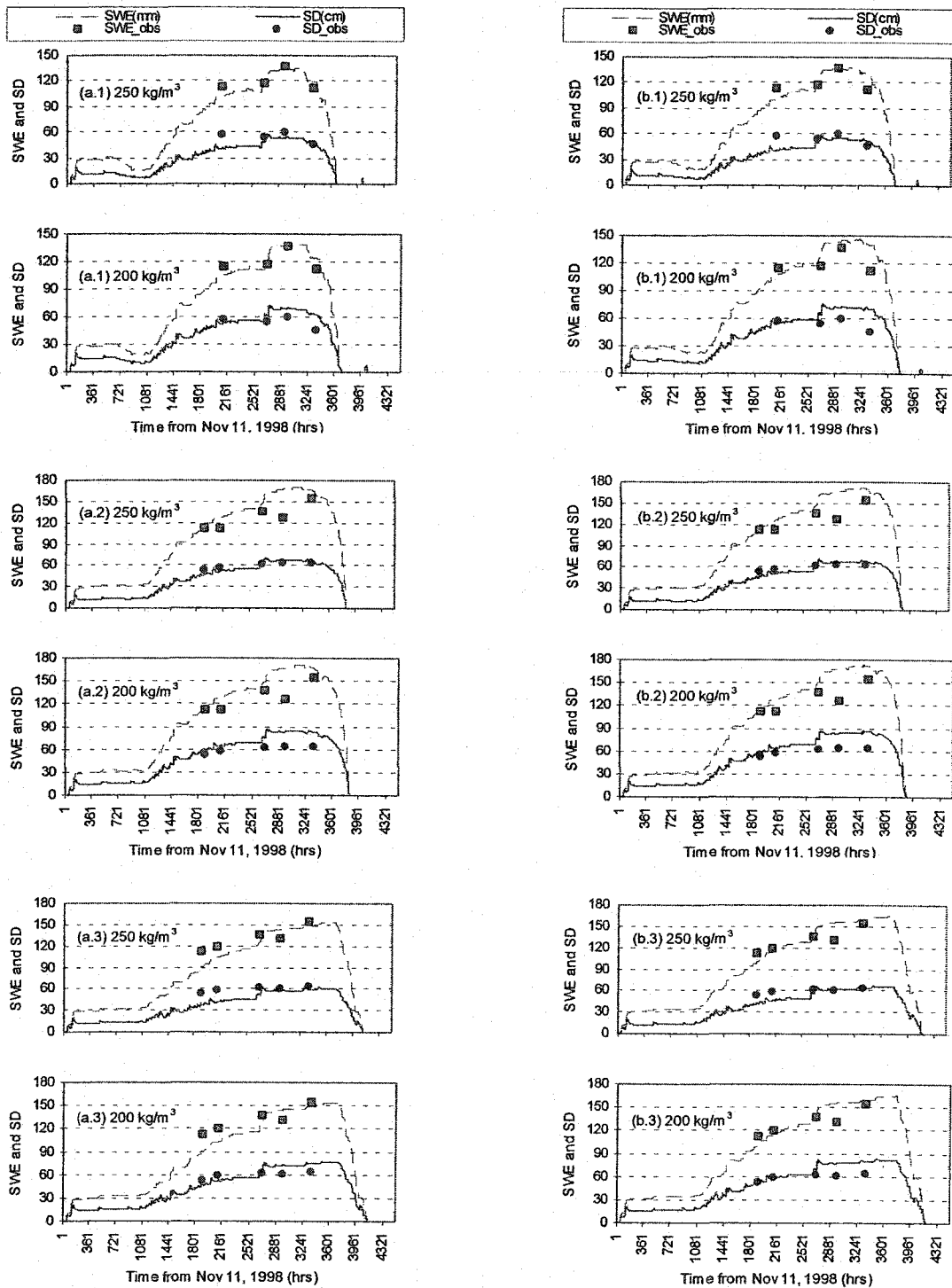


Figure 3.8 Comparison of SDSM-EBM simulated and observed SWE and snow depth (SD) for Zone 4 at the calibration stage (Nov. 11, 1998 to May 16, 1999) with maximum snow density  $\rho_{\max} = 250$  and  $200 \text{ kg/m}^3$  using: (a) Force Restore Method or FRM for (a.1) Open Area (OA), (a.2) Deciduous Forest (DF), and (a.3) Coniferous Forest (CF); and (b) Snow Conductance Method or SCM for (b.1) OA, (b.2) DF, and (b.3) CF.

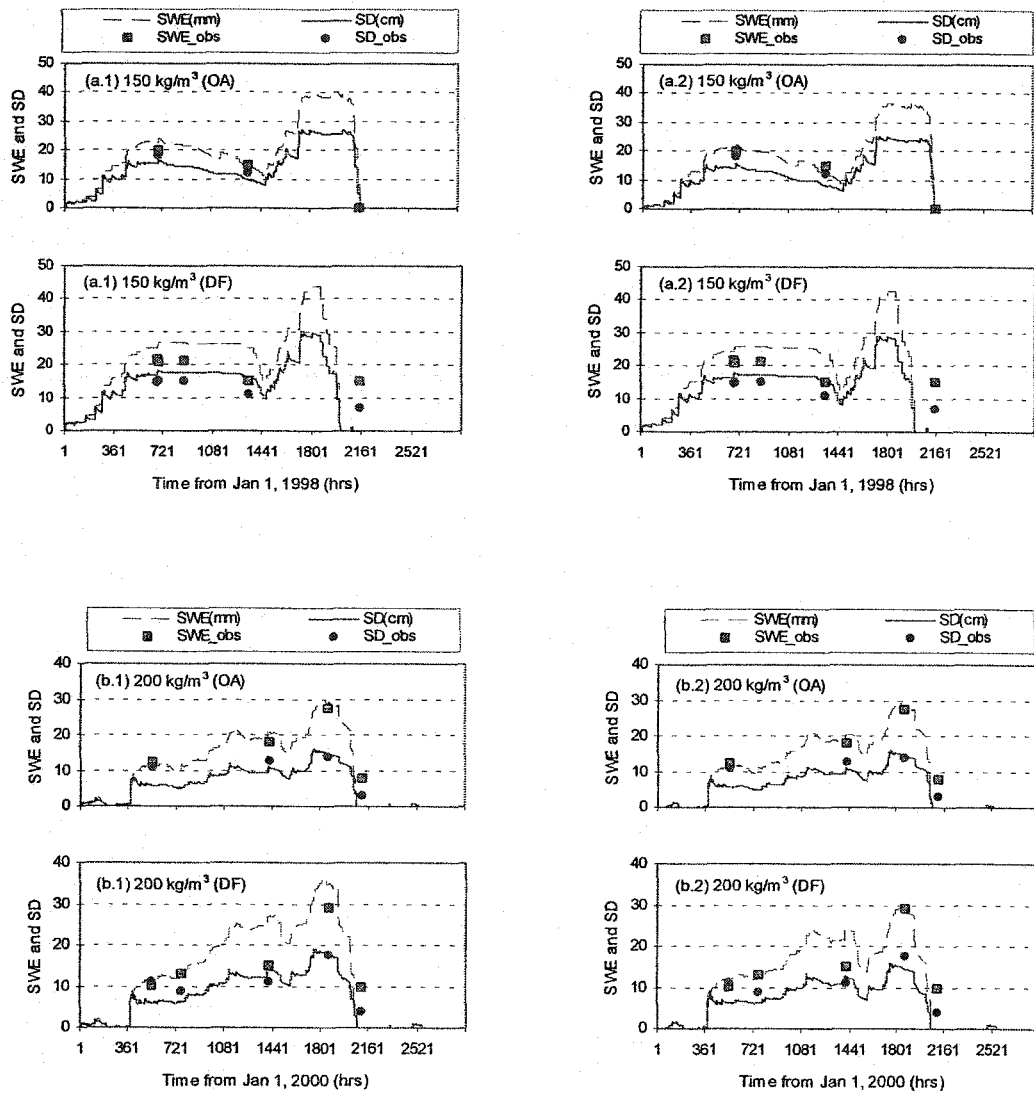


Figure 3.9 Comparison of SDSM-EBM simulated and observed SWE and snow depth (SD) for Zone 4 with maximum snow density  $\rho_{\max} = 200 \text{ kg/m}^3$  for the Open Area (OA), and Coniferous Forest (CF) at the validation stages: (a) Jan. 1, 1998 to Apr. 30, 1998 using (a.1) Force Restore Method or FRM, and (a.2) Snow Conductance Method or SCM; and (b) Jan. 1, 2000 to Apr. 30, 2000 using (b.1) FRM, and (b.2) SCM.

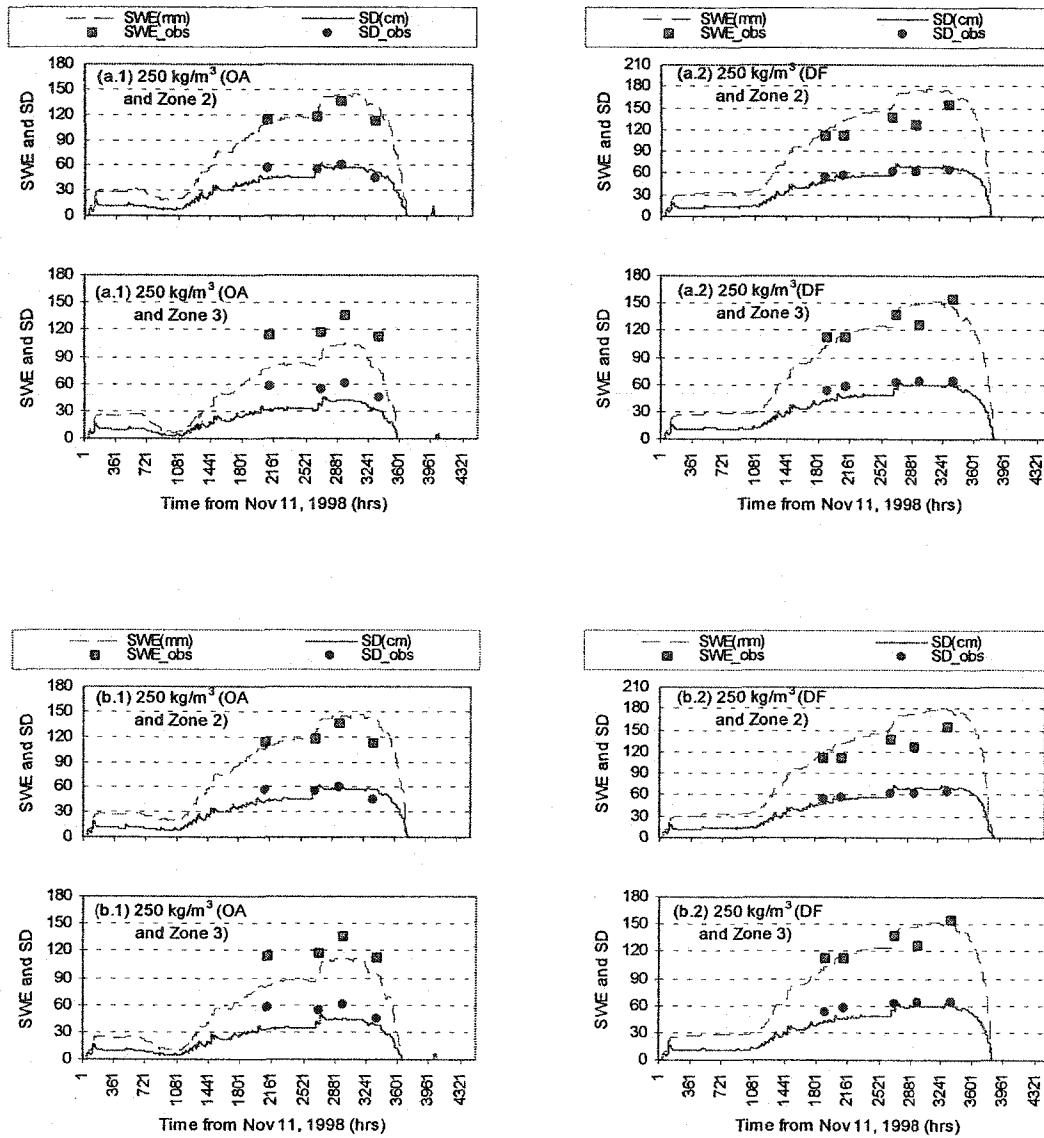


Figure 3.10 Comparison of SDSM-EBM simulated and observed SWE and snow depth (SD) for Zones 2 and 3 with maximum snow density  $\rho_{\max} = 250 \text{ kg/m}^3$  for the Open Area (OA), and Deciduous Forest (DF) at the calibration stage (Nov. 11, 1998 to May 16, 1999) using (a) Force Restore Method or FRM, and (b) Snow Conductance Method or SCM.

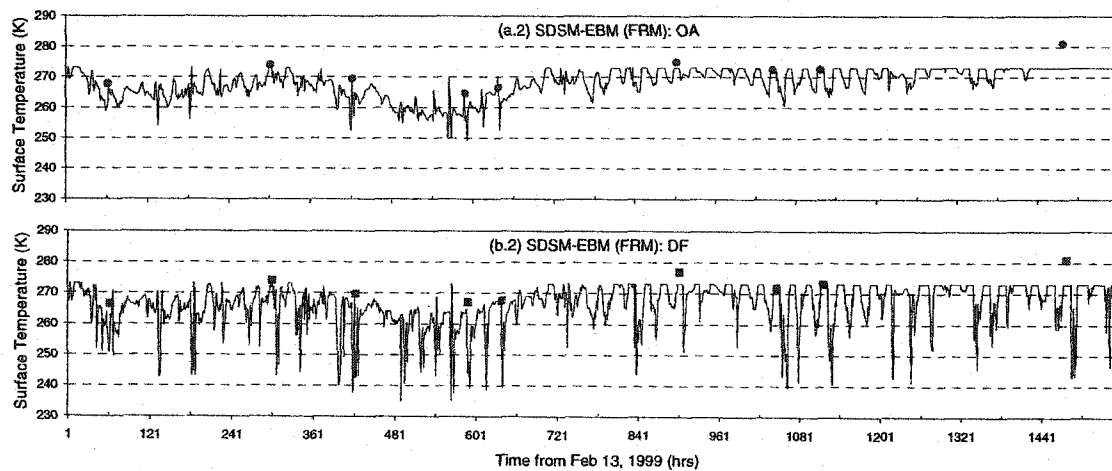
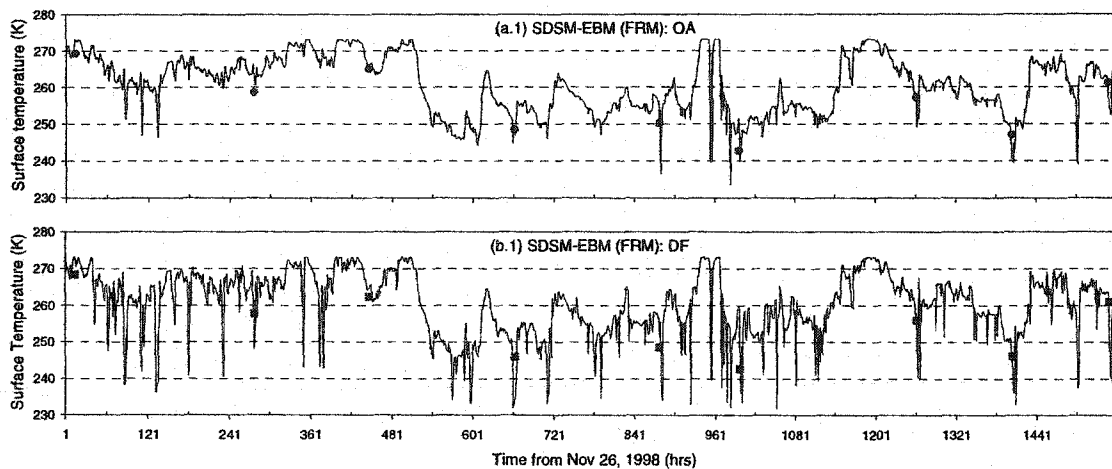


Figure 3.11 Comparison of snow surface temperature ( $^{\circ}\text{K}$ ) retrieved from NOAA-AVHRR images in different land cover classes (Open Area or OA and Deciduous Forest or DF) of PRB with simulated counterparts of SDSM-EBM (FRM) for the calibration period in hours (a.1 and b.1) Early part of winter from Nov 26, 1998 to Jan 29, 1999 and (a.2 and b.2) later part of winter from Feb 13 to Apr 18, 1999.

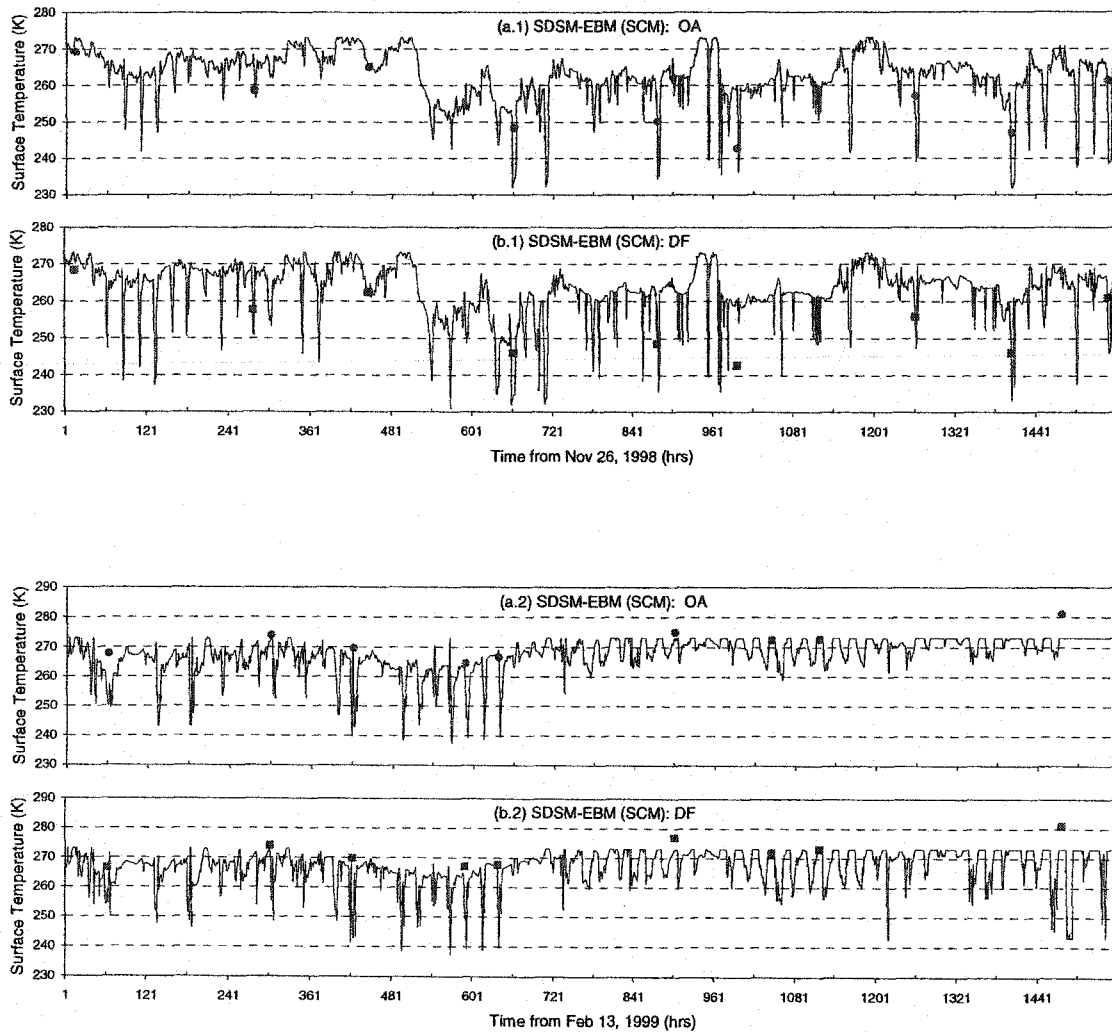


Figure 3.12 Comparison of snow surface temperature ( $^{\circ}\text{K}$ ) retrieved from NOAA-AVHRR images in different land cover classes (Open Area or OA and Deciduous Forest or DF) of PRB with simulated counterparts of SDSM-EBM (Surface Conductance Method or SCM) for the calibration period in hours (a.1 and b.1) Early part of winter from Nov 26, 1998 to Jan 29, 1999 and (a.2 and b.2) later part of winter from Feb 13 to Apr 18, 1999.

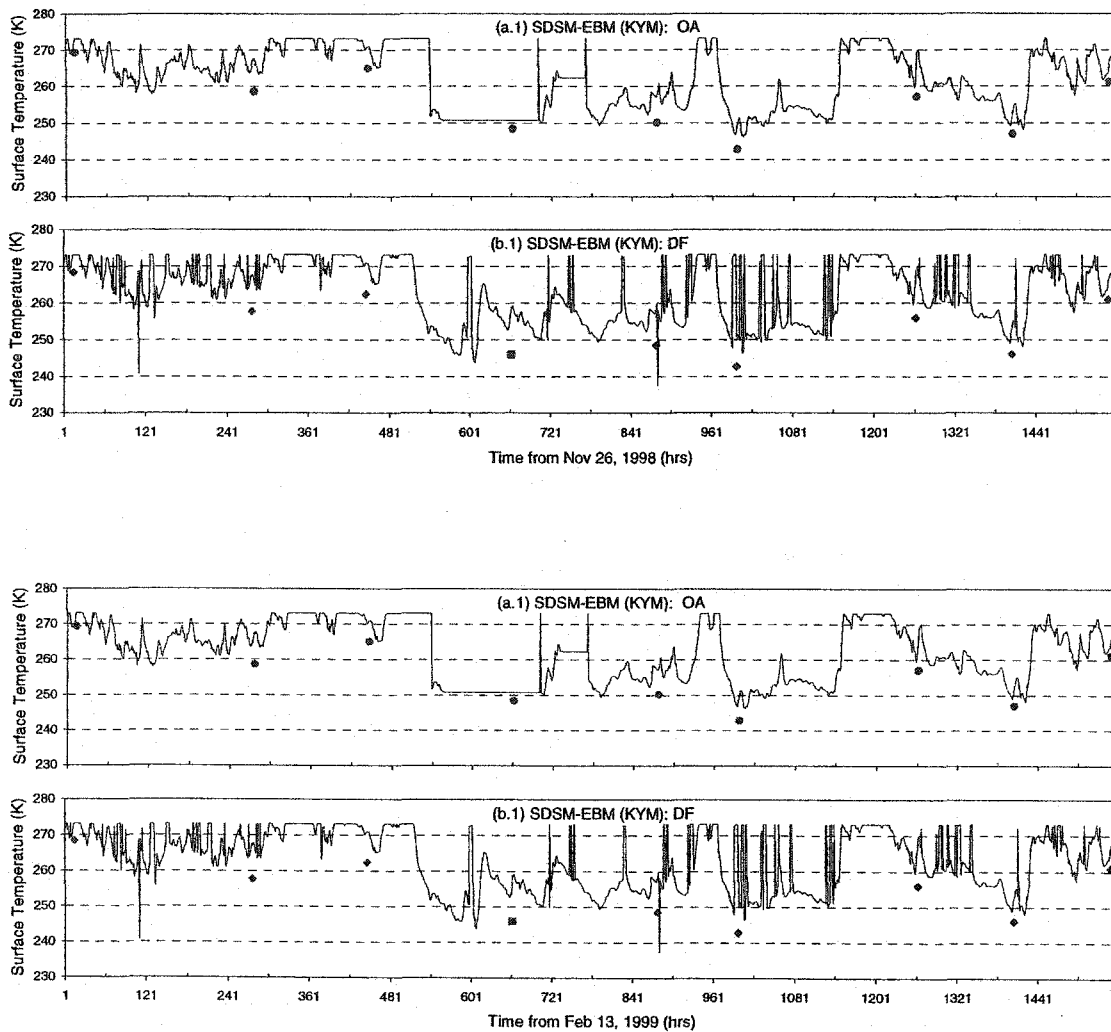


Figure 3.13 Comparison of snow surface temperature ( $^{\circ}\text{K}$ ) retrieved from NOAA-AVHRR images in different land cover classes (Open Area or OA and Deciduous Forest or DF) of PRB with simulated counterparts of SDSM-EBM (Kondo and Yamazaki Method or KYM) for the calibration period in hours: (a.1) and (b.1) Early part of winter from Nov 26, 1998 to Jan 29, 1999; and (a.2) and (b.2) later part of winter from Feb 13 to Apr 18, 1999.



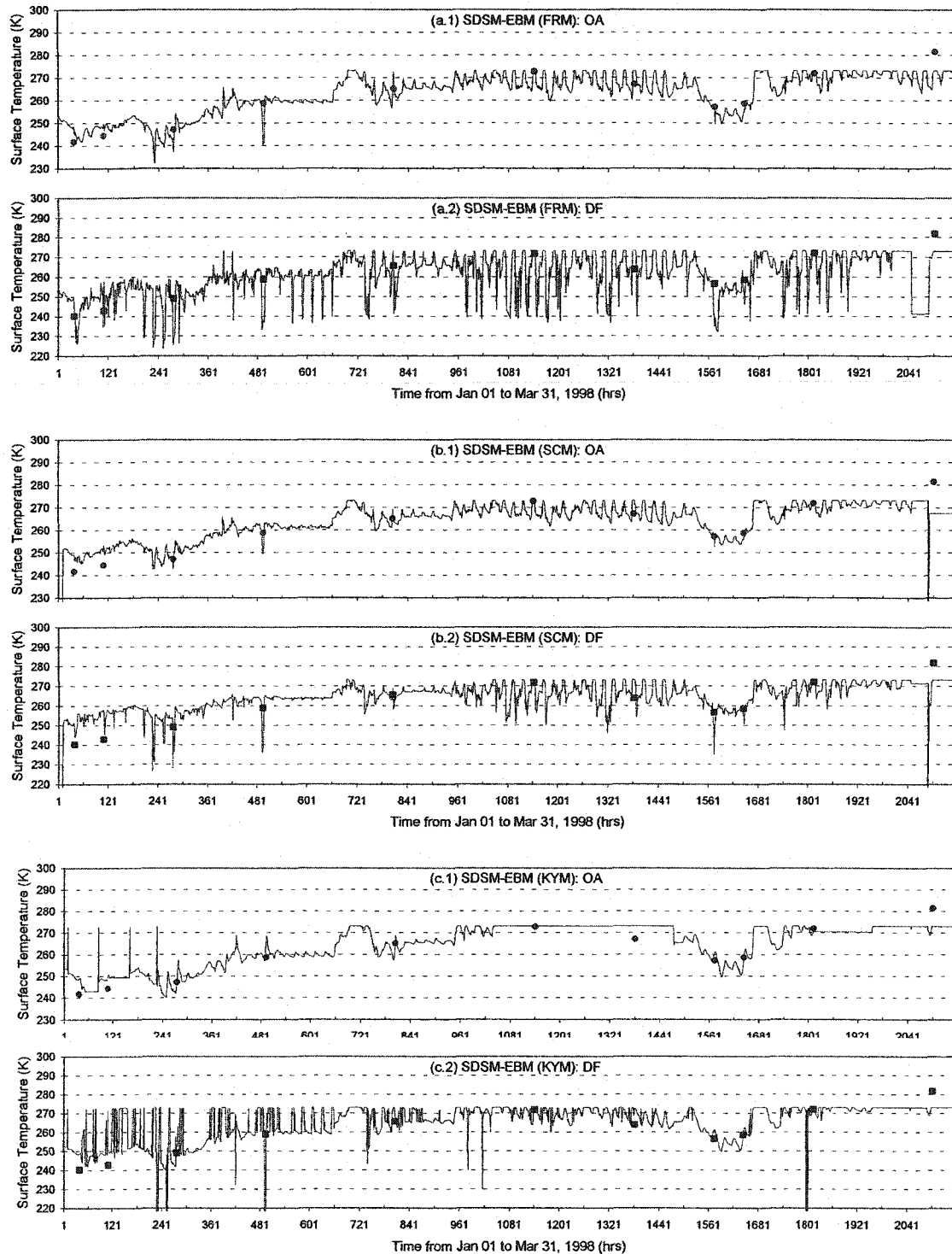


Figure 3.14 Comparison of snow surface temperature ( $^{\circ}\text{K}$ ) retrieved from NOAA-AVHRR images in different landuse classes of PRB with model simulated counterparts of SDSM-EBM using different methods: (a.1 and a.2) FRM; (b.1 and b.2) SCM; and (c.1 and c.2) KYM in the validation winter year 1998.

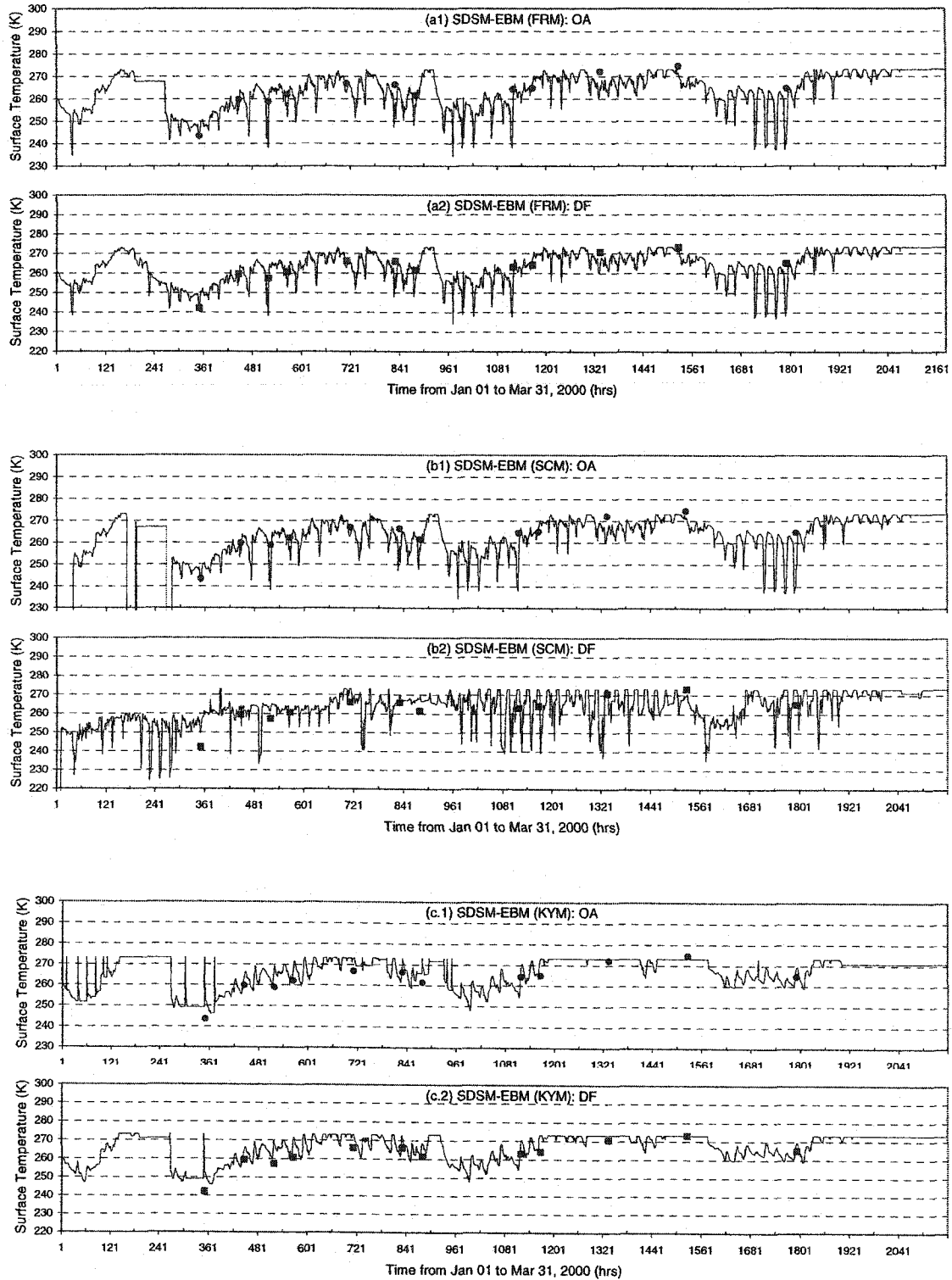


Figure 3.15 Comparison of snow surface temperature ( $^{\circ}\text{K}$ ) retrieved from NOAA-AVHRR images in different landuse classes of PRB with model simulated counterparts of SDSM-EBM using different methods: (a.1 and a.2) FRM; (b1 and b2) SCM; and (c.1 and c.2) KYM in the validation winter year 2000.

## **Chapter 4**

# **A Semi-distributed, Modified Temperature Index Approach for Modeling Snowmelt in the Canadian Prairies using Near Surface Soil and Air Temperature**

### **4.1 Introduction**

Seasonal snow covers that dominate the landscape of North America particularly during winters exert a significant influence on its climate. Snow is usually stored in a basin for a long time, but at the end of winter major snowmelt usually happens within several weeks, depending on the amount of snow, climatic factors, terrain features, and vegetation cover. About 1/3 of the Canadian Prairies' annual precipitation occurs as snowfall, but the spring snowmelt generates up to 80% of its annual surface runoff (Granger and Gray, 1990). It is important to model the spring snowmelt of the Prairies accurately, as has been widely recognized almost 60 years ago for temperate and higher latitude regions (e.g., Linsley, 1943).

The standard temperature index (TINX) or degree-day approach is the most widely used method for snowmelt computations in most operational snowmelt models today, e.g., National Weather Service River Forecast System, NWSRFS or Sacramento snowmelt model (Anderson, 1973), HBV (Bergstorm, 1975), UBC (Quick and Pipes, 1977), CEQUEAU (Charbonneau et al., 1977) and the Snowmelt Runoff Model, SRM (Martinec et al., 1983). This approach is popular partly because it can approximate the heat transfer processes associated with the melting of snow to accuracy comparable to those determined from a detailed energy balance method (USACE, 1971; Martinec et al., 1983; Sand, 1990; Kane et al., 1997). Moreover, air temperatures are generally the most readily available climate data even in the remote, mountainous areas. According to Anderson (1973), it is the best single index to estimate the amount of energy available for snowmelt.

As early as 1887, Finsterwalder and Schunk applied a TINX approach in the Alps. The TINX method for snowmelt-runoff calculations has been in use for almost 70 years (e.g., Collins, 1934), in different geographic locations and in various time steps, e.g., daily in Himalayas (Singh et al., 2000), 6-hourly at south Saskatchewan (Granger and Male, 1978) and hourly at Alaska (Kane et al., 1997). It is often used when a simpler model is preferred or where only limited climate data are available, such that the snowmelt rate estimated depends on the daily air temperature, some optimized melt factors, and a depletion curve that relates the mean areal snow water equivalent to the extent of snow cover empirically.

The melt factor that varies from basin to basin depends on a basin's climatic zone, latitude, altitude, and other factors. Some models such as the UBC, CEQUEAU, NWSRFS, and METQ98 (Ziverts and Jauja, 1999) allow the melt factor to vary throughout the melt season. Melt factors generally increase as the melt season progresses because of the seasonal increase in the radiation flux. Besides climate,

the snowmelt process also depends on factors like terrain characteristics, vegetation types, and even the fraction of snow cover on ground that can be updated using satellite images, e.g., SRM of Martinec et al. (1992). For a Northern Swedish catchment, Bengtsson (1982) even presented the importance of nighttime refreezing on the diurnal snowmelt cycle. Gray and Landine (1988) proposed an energy budget snowmelt runoff model (EBSM) that worked better than the TINX method for the Canadian Prairie, where energy fluxes were related empirically to standard climatological data. Sand (1990) applied a TINX and data-intensive surface energy models to both temperate and Arctic regions and found that only the energy balance is applicable to all the test regions. Among three models tested in a small Arctic watershed of 2.2 km<sup>2</sup>, surface energy balance, TINX, and the combined temperature and radiation index, Kane et al. (1992) found that the accuracy of the energy balance approach decreases as the variability of the surface energy increases in the watershed. They also found the TINX method reliable for a watershed with a strong influence of sensible heat transfer. This research concluded that the net radiation has a strong impact upon timing and rate of snowmelt, however the combined temperature and radiation index method could not do much better than TINX.

By solely dependent on the air temperature, TINX may not adequately account for many climatic factors related to snowmelt. For example, the dominant short wave radiation in open non-forested areas was poorly related to air temperature (Male and Granger, 1979) but in forested areas where wind and solar radiation cannot penetrate freely, the dominant longwave radiation is closely correlated to air temperature (Anderson, 1976). Therefore TINX generally requires the melt factor to be calibrated to adequately reflect the influence of a basin's physical characteristics and climate on snowmelt. Under normal climatic conditions, TINX may give good results but under extreme conditions, it could produce significant errors. Complex energy balance models require less calibration effort and may be more accurate than TINX, but they require a large amount of good quality data which are usually not

available due to several reasons such as: large investment associated with instrumentation and operation and maintenance, instrumental errors, human errors, etc. Irrespective of the techniques used, snowmelt modeling is usually complicated by factors such as: (1) changing responses of the underlying soil layer insulated by a snow layer, (2) changes in snow metamorphism due to the influence of temperature gradients within the snow layer, (3) temporal and spatial variation of melt water refreezing, etc. Attempts have been made to account for the varying responses of the underlying soil layer by introducing either frozen ground index (Molnau and Bissell, 1983) or the infiltration model (Granger et al., 1984) to simulate the occurrence of frozen ground and its effects on percolation and runoff (Landine et al., 1988).

Variables other than air temperature had been included in a modified TINX framework. Under sub-zero air temperature, Granger and Male (1978) compared energy fluxes (for eighty-four 6-hour periods) in southern Saskatchewan (Canadian Prairie) with various combinations of snow surface and air temperatures but failed to find any correlation between them, partly because the dominant net longwave radiation at night was not related to air temperature to significant extent. Besides air temperature, Kane et al. (1997) also used wind speed and net radiation but could not improve modeling the snowmelt for an Alaskan watershed. They found the optimized melt factors and base temperatures for the same watershed to differ in six consecutive years because climate varied from year to year. Granberg et al. (1999) introduced soil surface heat flow component into the TINX approach of Anderson (1973) as a component of their model to predict the water table and soil temperature profiles to a 3-m depth in a small boreal mixed mire system (study basin of 6.5 km<sup>2</sup>) of Sweden using the readily available climate data on air temperature and precipitation as derivable variables. The mean standard deviation of simulated and measured surface temperature at 10-cm depth during the periods of snowcover was 0.3±0.3°C in 1996/97 and 0.5±1.1°C in 1997/98.

Even though a close correlation can be interpreted between near surface soil temperature and snowmelt from the observed data of Woo and Valverde (1982) and Kutchment et al. (2000), none of the TINX models has attempted to assess the combined use of air and the near surface soil temperatures, partly because of the lack of near surface soil temperature data.

## **4.2 Research Objective**

The primary objective is to develop a semi-distributed snowmelt model – modified TINX (acronym as SDSM-MTI) method where the near surface soil temperature ( $T_g$ ) is used together with air temperature ( $T_a$ ) to model basin snowmelt in a Prairie environment.

Three winters of data were collected for the study site, Paddle river basin (PRB). SDSM-MTI was calibrated using the winter data of 1998/99 (Nov 11, 1998 to May 16, 1999) and validated using the winter data of 1998 ((Jan 1 to Apr 30, 1998) and 2000 (Jan 1 to Apr 30, 2000). SDSM-MTI was calibrated and validated against the observed basin streamflow, and the snow course data collected in different landuses for PRB. It operates within the domain of a semi-distributed, physically based, hydrologic model called DPHM-RS (Biftu and Gan, 2001) in order to simulate other closely related hydrologic variables (see Figure 3.4).

## **4.3 Paddle River Basin (PRB)**

The study site, PRB (53° 52' N, 115° 32' W) is a tributary of Athabasca River basin of central Alberta, which is located at the southern tip of the Mackenzie River Basin, the Canadian GEWEX site called MAGS (Figure 4.1). PRB has a basin area of about 265 km<sup>2</sup> and elevations ranging from 749 m at the basin outlet) to about 1000 m above the mean sea level (AMSL) at the western end. With an average land

slope of 3-5%, PRB has a moderate hydrological response. It consists of about 49% mixed forest, 21% coniferous forest, and remaining 30% agriculture and pasture land as open area during winters. Located at the Northwestern edge of the Prairies (Alberta Plains) and adjacent to the Northwestern Forest (see Table D.3 for the climate trends in the region), PRB lies in the “short, cool summer” koeppen climatic zone (Longley, 1968; Hare and Thomas, 1974), where the mean temperature in January is  $-15.5\text{ }^{\circ}\text{C}$  and that in July is  $+15.6\text{ }^{\circ}\text{C}$ . The annual mean precipitation is approximately 508 mm (Pretula and Ko, 1982), and about one-fourth of which falls between December and April. The average April 1<sup>st</sup> basin average snow water equivalent (SWE) for the PRB is 70 mm with a record maximum SWE of about 200 mm in 1974 (AENR, 1986). Its major soil group is the Hubalta series associated with Onoway and Modeste (Twardy and Lindsay, 1971) characterized by strongly developed Orthic Gray Wooded features, and the dominant clay loam soil texture under moderately well drained conditions.

PRB's deciduous or mixed and coniferous forest play an important role in controlling the spring melt runoff from its Headwaters area. The area close to the stream channels in the Headwaters reach has the greatest potential for contributing to flood runoff (AENR, 1986). However, the recent intervention in the Headwaters reach of PRB both by human beings (road construction and logging of forest resources) and that by beaver activities (damming of natural streams; see Woo and Waddington, 1990; Gurnell, 1998) could affect its runoff to the extent that PRB discharge at the outlet may no longer be natural particularly during low flow years.

PRB was selected for the study mainly because of the relatively natural stream flow of Paddle River up to the basin outlet (749 meters AMSL), where Water Survey of Canada has been operating a permanent gauging station since October 1979. Moreover, there is little influence of the Paddle reservoir (located about 30 km downstream of basin outlet) in any extreme event because the probable maximum



flooding level is about 711 m AMSL (Alberta Environment, 1982).

## 4.4 Modified Temperature Index Method

In its simplest form, TINX equates snowmelt to a melt factor ( $M_r$  in mm/hr or d/°C) multiplied with the difference between the average daily temperature ( $T_a$ ) and a threshold-melt temperature ( $T_{thm} \approx 0$ ),

$$m = \Phi(T_a) = M_r(T_a - T_{thm}) \quad (4.1)$$

Where,  $m$  is the snowmelt in mm/hr or mm/day, and  $\Phi$  a mathematical function.  $M_r$  depends on the slope, aspect of the land surface (Frank and Lee, 1966; Lee, 1963), vegetation cover and climatic region. On a regional basis,  $T_a$  is a good index of available energy at particular elevations (Riley et al., 1972). In TINX,  $\Phi(T_a)$  represents the total melt energy. As a simple method, TINX only works well when there is a strong correlation between the air temperature and the dominant energy fluxes responsible for snowmelt. Some different forms of modified TINX snowmelt algorithms are

$$m = M_r \left( \frac{R_s}{R_h} \right) (T_a - T_{thm})(1 - \alpha) \quad (4.2)$$

$$m = [M_r + (M_w u)](T_a - T_{thm}) \quad (4.3)$$

$$m = M_r(T_a - T_{thm}) + M_s(1 - \alpha)Q_{si} \quad (4.4)$$

$$m = M_r(T_a - T_{thm}) + \frac{Q_{gs}}{\rho_w \lambda_f} \quad (4.5)$$

In Eq (4.2),  $R_s$  and  $R_h$  = radiation indices on sloping and horizontal surface, respectively, and  $\alpha$  is the surface albedo (Riley et al., 1972). In Eqs. (4.3) and (4.4),  $M_w$ ,  $M_s$  are melt rates associated with the wind speed “ $u$ ” and the incoming short-wave radiation “ $Q_{si}$ ” respectively (Kane et al., 1997). In Eq. (4.5),  $Q_{gs}$  = soil surface heat flow,  $\rho_w$  = density of water, and  $\lambda_f$  = latent heat of fusion (Granberg et al., 1999). Granger and Male (1978) found  $M_r$  ranging from 3 to 8 (in mm/d/°C) for an open area in the Canadian Prairies (about 51°N), which are within the range

reported by Singh et al. (2000), who based on 19 references on the TINX method, reported  $M_r$  ranging from 2.5 to 8 mm/d/°C for snow and 3.2 to 13.8 mm/d/°C for ice.

The SDSM-MTI proposed is similar to Eq. 4.2 without the terms  $R_s$  and  $R_h$  that are more suitable for fully distributed models, where the radiation indices of each grid element are available.  $R_s$  and  $R_h$  are not suitable to include in a semi-distributed model like SDSM-MTI because it is based on the sub-basin approach, where at sub-grid level indices associated with the north and/or east-facing could cancel with that of the south and/or west facing or vice-versa. Similarly, the use of the near surface soil temperature ( $T_g$ ) in the proposed algorithm (Eq. 4.6) takes care of albedo term in Eq. 4.2. Though radiation indices and albedo options are available in SDSM-MTI, these terms are not included in the proposed algorithm,

$$m = M_r (M_{rf})^\psi (T_r - T_{thm}) \quad (4.6)$$

where  $M_r$  “or melt rate” depends on the land use types (open area, coniferous and mixed or deciduous forest),  $M_{rf}$  is the melt rate factor,  $\psi$  is an exponent of  $M_{rf}$  and  $T_r$  is the reference temperature (Eq. 4.7), or a weighted average of the near surface soil and air temperature ( $T_g$  and  $T_a$ ) observed in PRB (see Figures 4.2 to 4.4, and Table 4.1).

$$T_r = \chi T_a + (1 - \chi) T_g \quad (4.7)$$

where  $\chi$  is the coefficient obtained from calibration (Figure 4.5).  $M_{rf}$ , introduced to modify  $M_r$  to capture the timing of initial snowmelt and set with an upper limit of one, is assumed to be a tangent function of  $T_g$  (Figure 4.6) as

$$M_{rf} = 0.599 + (0.438 \tan(T_g) + 0.844) \quad (4.8)$$

Eq. 4.8 was based on a regression of  $M_{rf}$  with  $T_g$  towards 0 °C. The tangent function was used to reflect a significant drop in  $M_{rf}$  with an incremental decrease in  $T_g$  below 0 °C . It is expected that  $T_r$  (weighted average of  $T_g$  and  $T_a$ ) is a better index representing the amount of energy available for snow melt than  $T_a$  alone used in a

standard TINX. Based on the extreme climate conditions of the Canadian Prairies during 1997/98 and 1999/2000 winters, it seems that  $T_g$  is better correlated with solar and net radiation than  $T_a$  (see Table 4.1 and 4.2). If reliable values of  $T_g$  are available, this modified TINX is expected to perform better than the standard TINX, but it requires a calibration of three parameters, namely,  $\chi$ ,  $\psi$ , and  $M_r$  (see Table 4.3)

Similar to the energy balance method, the operation of SDSM-MTI also requires the separation of precipitation into rain and snow, the fresh snow density (see Eqs. 2.1 and 2.2), the redistribution of precipitation and temperature (see Eqs. 2.5 and 2.6), and the compaction of snowpack (see Eq. 2.67) described in Chapter 2.

## 4.5 Semi-Distributed Approach

A lumped conceptual snowmelt model almost totally ignores spatial variability by simplifying complex physical processes at a point. In conceptual modeling, complex physical processes are simplified, but such models are still widely applicable and preferred over regression models. On the other hand, a distributed snowmelt model accounts for spatial variability by modeling details of complex processes at grid scales of high resolution. The latter are often too ambitious, suffer from excessive data demand, and yet assume no interaction between adjacent grid elements. Therefore such models may be useful for theoretical quest but have little practical value. To find a trade-off between modeling resolution, complexity and data availability, we adopted a semi-distributed approach (e.g., Kite and Kouwen, 1992) where PRB is divided into 5 sub-basins or zones (Figure 3.1a). At sub-basin scale, the local snowmelt ( $M_i$ ) at each time-step is the sum of melt from each land cover, weighted by their corresponding drainage area fraction  $\phi_j$  as

$$M_i = \sum_{j=1}^n \phi_j m_{ij} \quad (4.9)$$

where 'i', and 'n' are sub-basin number and the total number of land cover classes

considered. The semi-distributed model is preferred over the fully distributed approach because it is less computationally intensive, requires less data, and yet could achieve similar or even better results.

## 4.6 Description of Data

A brief description of the hydrometeorological, snow pillow, snow course, streamflow and land cover class data collected for PRB is herein given (see Table 1.1 for the list of data collected and Plate F.1 for PRB's meteorological tower, snow pillow site, and snow course survey). The hourly meteorological data were collected for PRB using a 10 m meteorological tower located at an elevation of about 806 m AMSL (marked "M" in Figure 4.1, also see Plate F.1(a)). The hourly precipitation data were supplemented with the snow pillow data at Paddle River Head Water (station: 15V08), located in the central area of PRB at 855 m AMSL (marked by "S" in Figure 4.1, also see Plate F.1(b)). Figures 3.2 to 3.4 show the temporal variation and diurnal pattern of the meteorological data (taken at 6, 12, 18, and 24 hours of each day) for the winter periods of 1997-98, 1998-99, and 1999-00. Figure 3.5 shows the temporal variation of hourly precipitation data for the corresponding period. Among the meteorological data collected, only  $T_a$ ,  $T_g$ , and the precipitation data were used as input to SDSM-MTI. The hourly variation of  $T_a$  and  $T_g$  for three winter periods is shown in Figure 4.2 to 4.4.

Transects of snow course data were taken on several occasions during the winters of 1998 (January 28 and February 6), 1999 (February 6 and March 14), and 2000 (January 23 and March 18) at selected land covers (open area, mixed forest and coniferous forest) of PRB using a measuring stick for the snow depth and a MSC snow sampler for the snow density (see Plate F.1(b)). Snow depths have been recorded at every 10 paces, while snow density at, say, every 100 paces. The Alberta Environment (AE) also conducted the snow survey near the Paddle River Headwaters snow pillow (SP) site (station: 15V08, a forest covered area) since 1993

and near the Mayerthorpe SP site (station: 07BB809, an open area) since 1982 (see Tables D.1 and D.2). The AE snow course data and ours (both snow depth and SWE) were used to evaluate the performance of SDSM-MTI in both calibration and validation years.

The streamflow data at PRB outfall is taken from the Water Survey of Canada (WSC) gauging station 07BB011 (53 51' 29" N and 115 21' 45" W), established near the Anselmo Hall at 749 m AMSL (marked "H" in Figure 4.1, also see Plate F.3(c)) since October 1979. Figure 3.6 shows the hourly streamflow data for 1998, 1999, and 2000 and the average daily data for 1980-1993.

Biftu and Gan (2001) identified six landuse classes for PRB, namely: water/swamp, impervious, agricultural, pasture, deciduous or mixed forest, and coniferous forest using the Landsat TM image of August 7, 1996. In applying SDSM-MTI to PRB, the first four landuse classes were lumped together under one class called open area. Table 3.4 shows the area of each land cover class for each of PRB's five sub-basins.

#### **4.6.1 General Characteristics of Meteorological Data**

Among 8 years of snow course data at the Paddle River Headwaters site and 19 years of snow course data at Mayerthorpe Snow Pillow site, the 1997/98 and 1999/00 winters were the driest (Table D.1 and D.2), while the 1998/99 winter was one of the four wettest. Climate Trend and Variation Bulletin for Canada (1948-2001) also ranked the 1998/99 as the wettest, and 1999/00 and 1997/98 as the driest winter precipitation for both Northwest Forest and Prairie region. However, the sequence is different in the Mackenzie District. In direct contrast, the sequence of winter regional temperature departure ranked from the warmest to the coolest is 1997/98, 1999/00, and 1998/99 for both Northwest Forest and Prairie region, but again the sequence is slightly different for the Mackenzie District. The ranking of these three years of winter data (out of 54 years of records) are summarized in Table

### D.3.

Kane et al. (1997) demonstrated the importance of sensible and radiant heat transfer for spring snowmelt in an Arctic watershed where the net radiation ( $R_n$ ) became more important as snowmelt progressed. In the Emerald Lake basin of California, Mark (1992) found the radiation to dominate over other energy fluxes for melt. Shook (1996) reported that  $R_n$  generally dominated the spring snowmelt in the Canadian Prairies, where the large scale advection usually was not significant. The meteorological data for PRB were assessed to determine the existence of any close correlation between the net radiation data and other weather data. Three years of winter data in PRB revealed that the daily  $R_n$  is correlated well with the daily  $T_g$  with correlation coefficients equal to 0.92, 0.78, and 0.78 for 1997/98, 1998/99, and 1999/00 data respectively. The data also revealed that both the hourly cumulative  $R_n$  and solar radiation were better correlated with the corresponding hourly  $T_g$  than  $T_a$  when the soil temperature was below or near freezing temperature (see Table 4.1), except for the wet winter of 1998/99 when  $R_n$  was slightly better correlated with  $T_a$  than  $T_g$  partly due to the insulating effect of large snowfall in that winter. Sarratt et al. (1992) reported that a snow depth of 42.5 cm was required to maintain steady  $T_g$ . Sudden drops in correlations were also obtained with respect to both  $T_a$  and  $T_g$  when the data periods were extended beyond the major melt (Table 4.2).

Woo and Valverde (1982) showed that the  $T_g$  of the Beverly Swamp of southern Ontario (43° 22N, 80° 27' W) was a reliable variable to indicate snow accumulation and melt processes irrespective of the landuse, and particularly when the ground is snow covered (Figure 2 in Woo and Valverde, 1982). They found that the observed  $T_g$  for open and forest sites agreed closely with each other and followed a definite pattern (a smooth curve near or below the freezing mark with very little diurnal variation) when the ground was covered with snow. This is also observed in PRB (Figure 3.2b and 4.2a for 1997 winter, Figure 3.3b and 4.3a for 1999 winter; and

Figure 3.4b and 4.4a for 2000 winter). A significant rise in  $T_g$  from below to above the freezing and/or significant diurnal variation is indications of active snowmelt processes that increases the size of bare patches at the expense of snow-covered area. The energy consumed by melting decreases after peak snowmelt (thereby increasing the ground temperature of bare patches) and so is the correlation between  $R_n$  and  $T_g$  (Table 4.2). A similar trend of ground heat flux (see Figures 3.2d, 3.3d and 3.4d) for the three winters further supports the importance of  $T_g$  measurements for snowmelt modeling. The hydrometeorological and surface physical data (precipitation, ground thawing and snow depths,  $T_g$ ,  $T_a$ , and basin runoff) collected from Kolyma water balance station of Russia ( $60^\circ$ - $63^\circ$ N latitude and 1000-2000 m AMSL), between May 1 and July 31 of 1968 to 1972 also revealed a close correlation between the basin snowmelt runoff and  $T_g$  (Figures 1-5 in Kutchment et al., 2000).

For PRB, the low snowfall during the winter of 1998 experienced a frequent rises in air temperature (close to  $10^\circ\text{C}$ ) and radiation fluxes in the middle of winter (Jan 31, Feb 13, Feb 22), which is expected to be causing metamorphic changes to the snowpack. The high snow accumulation of 1998/99 winter only experienced such rise in temperature and radiation during late winters of 1999. The  $T_a$  of the 2000 winter was similar to that of 1998 but its radiative fluxes were similar to that of 1999 (Figures 4.2, 4.3, and 4.4).

The hourly wind speed varied widely in these winters (e.g., the maximum hourly wind speed was 5 m/s in 1998, 11 m/s in 1999 and 10 m/s in 2000 winters), which brought significant variations in snow distribution, snow densification and turbulent fluxes. The snow density observed was less in the winter of 1997/98 than in 1998/99 and 1000/2000. Pomeroy et al. (1998) recommended using a higher snow compaction rate if the wind speed exceeds 7 m/s. The field observation of 1998/99 winter snowpack indicated the presence of two thin ice sheet (one near ground, and

another at about 15 cm below the snow surface), which could be associated with the depth-hoar phenomenon caused by a large temperature gradient within the snowpack. These observed variations in snowpack properties could lead to different model parameters obtained from model calibrations.

## **4.7 Discussion of Results: Model Calibration and Validation**

SDSM-MTI was calibrated using the hourly winter data of November 11, 1998 to May 16, 1999, and validated using the winter data of January 1 - April 30, 1998 and January 1 - April 30, 2000. These three winters experienced a wide range of snowfall, with 1998-99 as a record wet while 1997-98 and 1999-00 as record dry winters. We selected the start of 1997-98 winter from January 1, 1998 because snowfall started late that year. Though 1999-00 winter had some snow in the later part of November, the following month of December experienced an air temperature as high as near 20 °C bringing  $T_g$  to 0 °C (Figure 4.4). Further, late starting dates were chosen so that this ensures the winter snowpack accumulation process happened with  $T_g$  at near or below the freezing level.

SDSM-MTI is built within DPHM-RS of Biftu and Gan (2001). It can run with or without a pre-specified unit response function (unit hydrograph) for each of the sub-basins of PRB. A SDSM-MTI model run with unit hydrographs as an input data takes less than 10 minutes in a Pentium-200 PC; the same model run without unit hydrographs requires more than 2 hours. This is because, developing an unit hydrograph from an exhaustive, grid-based (100 m × 100 m), eight flow directions routing technique based on the kinematic wave theory (see Figure 2.4) and Manning's roughness ( $n$ ) is time consuming. The routing of surface runoff is based on the response functions of a unit snowmelt or rainfall excess in each of the sub-basins. The unit hydrograph for each of the sub-basins of PRB was generated using



several combinations of  $n$ -values for open and forested areas (see Figure 3.6e) and comparing the calculated basin outlet discharge with the observed runoff hydrograph. The unit hydrograph that produced a basin discharge hydrograph closest to the observed in terms of mass balance and the time to peak flow was then selected. The corresponding  $n$ -values are 0.1 and 0.15 for open and forest covered areas respectively. To adequately account for the distributed nature internal processes, besides basin runoff the calibration and validation of SDSM-MTI was also done with respect to observed snow depth and SWE in different land covers, a multi-criteria approach. Such a multi-criteria approach helps to ensure SDSM-MTI adequately modeled different stages of snow accumulation and ablation processes. The statistics used to assess model performance are the Coefficients of Determination ( $R^2$ ), the Nash-Sutcliffe coefficient ( $E_f$ ), and the Root Mean Square Error (RMSE).

#### 4.7.1 Runoff at Basin Outlet

The calibration result of SDSM-MTI (Figure 4.4(a.1)) using optimized values of the parameters,  $\chi$ ,  $\psi$ , and  $M_r$  (see Table 4.3) shows the observed runoff at the basin outlet agrees well with that simulated by SDSM-MTI ( $R^2 = 0.79$ ,  $E_f = 0.76$ ,  $RMSE=1.24$ ). It is believed that some of the discrepancies between simulated and observed runoff at the calibration stage occur partly because the spatial variation in winter precipitation was not properly accounted for in this study. There were only two precipitation gauge stations at PRB including our meteorological station. The winter precipitation in the form of snow however, was obtained only from snow pillow site at Paddle River Headwaters. Furthermore, beaver dams in PRB (see Plates F.2- F3) also exerted some “regulatory” effects on the basin’s streamflow, which is less significant during wet than during dry winters.

The validation result for the 1998 winter (January 1 to April 30, 1998) with respect to early spring snowmelt runoff is better ( $R^2= 0.63$ , Figure 4.7(d.1)) if we change  $M_r$

for coniferous forest to 0.075 mm/hr/°C and  $\psi = 1.0$ , than if we keep all the calibrated model parameters unchanged for the 1998 winter ( $R^2 = 0.50$ , Figure 4.7(b.1)). However, a better  $R^2$  for the 1998 winter means a less representative SWE data for the open area (Figure 4.7(d.1)). Further, the result deteriorates with time, e.g.  $E_f$  changes from 0.38 in March 20 to 0.80 in March 22 and remains at or above 0.74 until March 25. Then it suddenly falls to 0.45 in March 26, which continues to drop to 0.24 by March 31. The validation result is less satisfactory partly because during early snowmelt season the water level was low, causing the observed streamflow to be relatively inaccurate, and the part of the snowmelt season the water level was low, causing the observed streamflow to be relatively inaccurate (see Figure 3.6(a) with two versions of streamflow data for the same 1998 winter), and the beaver dams located at strategic, upper reach locations of PRB to exert more significant influence on the natural flow regime.

The validation result of another dry winter (year 2000) once again shows the regulatory effects of beaver activities on the PRB streamflow at some locations on Paddle River tributaries (Figure 4.7(c.1)), e.g., a very uniform flow between 0.3-0.5 m<sup>3</sup>/s for most part of the snowmelt season, which should not be the case under natural conditions. Woo and Waddington (1990) reported similar streamflow modifications due to both underflow and overflow types of beaver dams. According to Climate Trends and Variations Bulletin for Canada, both 1998 and 2000 winters also happened to be record warm (Table D.3).

A careful observation of different strategic locations along the major tributaries of PRB that cross the highway or access roads (along highway 751 to south of the snow pillow site, and some access roads to the north of highway 647, and upstream of the PRB gauging station as shown in photographs of Plate F.2) show ample evidence of watertight beaver dams of overflow types (Woo and Waddington, 1990; Gurnell, 1998) that by effectively maintaining a pool of water upstream, only release

a very small fraction of water to the downstream side, particularly when the spring snowmelt is not large enough to flush out the obstruction made by beaver or to overtop the dam crest, e.g. see photographs of Plate F.3. For PRB, the 1998 and 2000 happened to be winters of record low snowpack susceptible to beaver dam effects. However, the spring snowmelt of a wet year (e.g., 1998/1999) could easily wash out such temporary dams or overtop the dam crest fairly quickly. Therefore, it is possible to see some unlikely extreme events occurring during wet winters because of the sudden failure of beaver dams, as noted by Hillman (1998). It is beyond the scope of this study to give a full account of the complicating effects of beaver dams on snowmelt runoff of PRB. Without such effects, the validation results of SDSM-MTI based on basin runoff would have been better. To substantiate our assessment of SDSM-MTI at both calibration and validation stage, we also compared the model simulated SWE and snow depth at different land covers of PRB with the observed (Section 4.7.2).

To assess the contribution of  $T_g$  by adjusting model parameters  $\chi$ ,  $M_{rf}$  and  $\psi$  (see Eqs. 4.6-4.8) on the simulated snowmelt runoff, several sensitivity runs were conducted. When  $\chi$  was set to 1 (which means  $T_g$  is partially ignored) and other calibrated parameters left unchanged,  $R^2$  dropped from 0.79 to 0.71 and  $E_f$  dropped from 0.76 to 0.71 for the calibration period of 1998-99 (see Figure 4.7(a.2)). However, when  $\chi$  was set to 1 and  $\psi$  set to 0 (thereby setting  $T_g$ -dependent  $M_{rf} = 1$ , which means  $T_g$  is totally ignored),  $R^2$  and  $E_f$  suddenly dropped to 0.3 and 0.25 respectively (see Figure 4.7(a.3)). Similar results were observed for the validation year 1997-98 (see Figures 4.7(b.2) and 4.7(b.3)). Apparently  $\psi$  (or  $M_{rf}$  exponent) exerts a more significant role on the influence of  $T_g$  than  $\chi$  in SDSM-MTI. Our results confirm the contribution of  $T_g$  in modeling basin-scale snowmelt runoff.

#### **4.7.2 Snow Water Equivalent and Snow Depth**

For most of the landcover classes of the sub-basins of PRB, SDSM-MTI's simulated

SWE and snow depth generally agree well with the observed values obtained from winter snow course surveys conducted at PRB. Figures 4.8(a.1 and a.2) show good agreements between the simulated and observed SWE and snow depth in the open area (OA) and coniferous forest (CF) of PRB based on two different maximum snow densities ( $\rho_{\max}$ ) used at the calibration stage of 1998/99 winter. Figure 4.8(b1, b2) also shows good agreements between simulated and observed data for both OA and CF at the validation stage of 1997/98 winter, and similarly Figure 4.8(c1, c2) for 1999/2000 winter.

Even though the snow course survey was conducted in different parts of PRB, sub-basin or zone 4 was selected to show the results in Figures (4.7 and 4.8(a to c)) partly because the average altitude of this zone is close to the average altitude of PRB. SDSM's simulated snow depth and SWE for the calibration period using  $\rho_{\max}=200 \text{ kg/m}^3$  agree closely with observed in the early part of snow accumulation, and that using  $\rho_{\max}=250 \text{ kg/m}^3$  were in good agreement in the later part of snow accumulation process. As expected, snow density does not remain constant as has been assumed in many land surface schemes (e.g. Essery, 1997), but increases with time and usually attains a highest value at the end of the snow accumulation period. Gray and Prowse (1993) also reported that dry snow densities for shallow snow (depth < 1 m) at forested environments reach an approximate maximum value of  $250 \text{ kg/m}^3$ . Though  $\rho_{\max}$  is set for each model run in SDSM-TIM, the freshly fallen snow interacts with the existing snowpack and the resulting snow density continues to change based on the settlement constant and the fresh snow density (if any) until it attains the maximum density (as discussed in Chapter 2). The maximum snow densities used for both the calibration and validation periods agree closely with the measured values. Open areas tend to undergo more wind impacts and therefore theoretically should have larger snow densities than the forested areas. Similar trend was found in general except few cases in 1998 winter. However,  $\rho_{\max}$  observed in open and forested areas do not differ much. It is possible that the wind impact in the

open area is partly compensated with the additional compaction received from the free falling wet snow (or melt water) from the canopy in the forested area. The variation of snow density in the open area from one winter to another also corresponds to the wind velocity as explained in section 4.6.5.

The under-estimation of simulated SWE and snow depth in sub-basin or zone 3 and slightly over-estimation of these variables in zone 2 with respect to the observed data at both calibrating and validation stages are attributed to the precipitation distribution factor applied to each of the sub-basins of PRB (see Table 4.3). The precipitation (snow or rain) at each of the sub-basins is distributed according to the elevation differences with the gauge station. Figure 4.8(d) shows such response for the open area (zone 2 and 3) when compared to open area in zone 4 (Figure 4.8(a.1)) in the calibration stage. Similar comparison can be made between Figures 4.8(e) and 4.8(a.2) for the coniferous forest.

The contribution of  $T_g$  with respect to SWE and snow depth simulated by SDSM-MTI at both the calibration (Figures 4.9(a.1, a.2)) and validation stages (Figures 4.9(b.1, b.2) and 4.9(c.1, c.2)) was again assessed by adjusting parameters  $\chi$  and  $\psi$ . Similar to runoff simulation, this sensitivity analysis once again showed that when  $\psi$  was set to zero and  $\chi$  to 1 (meaning  $T_g$  is completely ignored), the result became much poorer than when only  $\chi$  was set to 1 (which means  $T_g$  is partially ignored).

In summary, SDSM-MTI is capable of simulating dependable basin-scale SWE and snow depth when both  $T_a$  and  $T_g$  are part of the input data. The simulated stream flows differ from the observed partly because of the effects of beaver dams during both validation periods of dry winters, 1997/98 and 1999/2000. The calibration and validation results using SDSM-MTI are also in good agreement with the energy balance model of SDSM (SDSM-EBM), which is discussed in Chapter 2 and 3 (also see Figure 4.10).

## 4.8 Summary and Conclusions

We propose a semi-distributed, modified temperature index method for modeling snowmelt (SDSM-MTI) using a weighted average ( $T_r$ ) of near surface soil ( $T_g$ ) and air temperature ( $T_a$ ) data (Eqs. 4.6 to 4.8) and successfully tested it at the seasonally snow-covered, Paddle River Basin (PRB) of the Canadian Prairies. Other than the “regulatory” effects of beaver dams that affected the validation results on simulated runoff, overall SDSM-MTI was able to simulate reasonably accurate snowmelt runoff, SWE and snow depth in PRB. The advantage of using both  $T_a$  and  $T_g$  is partly attributed to  $T_g$  showing a stronger correlation with solar and net radiation at PRB than  $T_a$ . We also demonstrated the negative effect of partially and completely ignoring  $T_g$  in SDSM-MTI by setting parameters  $\chi$  to 1, or  $\chi$  to 1 and  $\psi$  to 0 while other parameters left unchanged respectively. By using a combination of  $T_a$  and  $T_g$ , SDSM-MTI avoids the excessive demand for detailed data required by physics-based, energy-balance snowmelt models. Our results show that if reliable  $T_g$  data is available, they should be utilized to model the snowmelt processes particularly if the degree-day or TINX approach is adopted. The approach of SDSM-MTI should be applicable to other parts of the world subjected to seasonally snow covers, but more work needs to be done to determine the optimum or adequate number of soil temperature and air temperature gauge stations needed to model the snowmelt processes reliably under various climatic conditions (e.g., Dickinson, 1988; Granberg et al., 1999; Riseborough, 2001).

## References

- Alberta Energy and Natural Resources, AENR (1986), *Watershed management in the Paddle River Headwaters*, Alberta Energy and Natural Resources, Edmonton, ENR No. T/104, 60p.

- Anderson, E. A. (1973), *National Weather Service River Forecast System - Snow accumulation and ablation mode*, NOAA Tech. Memorandum NWS Hydro-17, US Dept. of Commerce, Silver Spring, Maryland, USA.
- Anderson, E. A. (1976), *A Point Energy and Mass Balance Model for a Snowcover*, NOAA Technical Report, NWS 19, US Dept. of Commerce, Silver Spring, Md, 150p.
- Bengtsson, L. (1982), The importance of refreezing on diurnal snowmelt cycle with application to a Northern Swedish catchment. *Nordic Hydrology*, 13:1-12.
- Bergstrom, S. (1975), The development of snow routine for the HBV-2 Model. *Nordic Hydrology*, 3:73-92.
- Biftu, G. F., and Gan, T. Y. (2001), Semi-distributed, Physically Based, Hydrologic Modeling of the Paddle River Basin, Alberta using Remotely Sensed data, *J. Hydrol.*, 244:137-156.
- Charbonneau, R., Fortin, J. P. and Morin, G. (1977), The CEQUEAU model: description and examples of its use in problems related to water resources management. *Hydrol. Sci. Bull.*, 22(1):193-203.
- Collins, E. H. (1934), Relationship of degree-days above freezing to runoff, *Eos Trans. AGU*, 15:624-629.
- Dickinson, R. E. (1988), The force-restore model for surface temperature and its generalizations. *J. Climate*, 1:1086-1097.
- Essery, R. (1997), Modeling fluxes of momentum, sensible heat and latent heat over heterogeneous snow cover. *Quart. J. Roy. Meteor. Soc.*, 123:1867-1883.
- Finsterwalder, S., and Schunk, H. (1887), *Der Suldenferner*, Seitschrift des Deutschen und Österreichischen Alpenvereins. 18:72-89.
- Frank, E. C., and Lee, R. (1966), *Potential solar beam irradiation on slopes*. Res. Paper RM-18, U.S. Forest Service, Washington, D.C.
- Granberg, G., Grip, H., Löfvenius M. O., Sundh, I., and Svensson, B. H. (1999), A simple model for simulation of water content, soil frost, and soil temperatures in boreal mixed mires. *Water Resour. Res.*, 35(12):3771-3782.

- Granger R. J., Gray, D. M., and Dyck, G. E. (1984), Snowmelt infiltration to frozen Prairie soils. *Can. J. Earth Sci.*, 21:669-677.
- Granger, R. J., and Gray, D. M. (1990), A net radiation model for calculating daily snowmelt in open environments. *Nordic Hydrology*, 21:217-234.
- Granger, R. J., and Male, D. H. (1978), Melting of a prairie snowpack. *J. Appl. Meteorol.*, 17: 1833-1842.
- Gray, D. M., and Landine, P. G. (1988), An energy-budget snowmelt model for the Canadian Prairies. *Can. J. Earth Science*, 25:1292-1303.
- Gurnell, A. M. (1998). The hydrogeomorphological effects of beaver dam-building activity. *Progress in Physical Geography*, 22(2):167-189.
- Hare, T. K., and Thomas M. K. (1974), *Climate Canada*, Wiley Publications of Canada Ltd., Toronto.
- Hillman, G. R. (1998), Flood wave attenuation by a wetland following a beaver dam failure on a second order boreal stream, *Wetlands*, 18(1): 21-34.
- Kane, D. L., Gieck, R. E., and Hinzman, L. D. (1997), Snowmelt modeling at small Alaskan arctic watershed. *J. Hydrologic Engrg.*, 2(4): 204-210.
- Kite, G. W., and Kouwen, N. (1992), Watershed modeling using land classifications. *Wat. Resour. Res.*, 28(12): 3193-3200.
- Kuchment, L. S., Gelfan, A. N., Demidov, V. N. (2000), A distributed model of runoff generation in the permafrost regions. *J. Hydrol.*, 240:1-22.
- Landine, P. G., Granger, R. J., and Gray, D. M. (1988), Evaluation of snowmelt models for application in permafrost environments. *NHRI Contract Report No. 88001*, National Hydrology Research Institute, Environment Canada, Saskatoon, Saskatchewan, Canada.
- Lee, R. (1963), *Evaluation of solar beam irradiation as a climatic parameter of mountain watersheds*. Hydrology Papers No. 2, Colorado State University, Fort Collins, Colorado, USA, 50p.
- Linsley, R. K. Jr. (1943), A simple procedure for the day-to-day forecasting of runoff from snowmelt. *Trans. Amer. Geophys. Union*, Part III: 62-67.



- Longley, R. W. (1968), *Climatic maps for Alberta*, University of Alberta, Edmonton, Canada.
- Male D. H., and Granger, R. J. (1979), Energy and mass fluxes at the snow surface in a prairie environment, In: *Proc. Modeling of Snow Cover Runoff*, ed. S. C. Colbeck and M. Ray, CREEL, Hanover New Hampshire, 101-124.
- Marks, D., and Dozier, J. (1992), Climate and energy exchange at the snow surface in the alpine region of the Sierra Nevada, 2, Snow surface energy balance, *Water Resour. Res.*, 28(11):3043-3054.
- Martinec, J., Rango, A., and Major, E. (1983), *The snowmelt-runoff model user's manual*. NASA Ref. Pub., 110, NASA, Washington, D.C., USA.
- Martinec, J., Rango, A., and Roberts, R. (1992), *User's manual for the snowmelt-runoff model (SRM) (updated edition 1992, version 3.2)*. USDA, Hydrology Laboratory Technical report HL-17, Beltsville, Maryland, USA, 70p.
- Molnau, M. and Bissell, V. (1983), A continuous frozen ground index for flood forecasting. In: *Proc. Western Snow Conf.*, 51<sup>st</sup> Annual Meeting, Washington, USA, 153-190.
- Pietroniro, A., Prowse, T. D., and Lalonde, V. (1995), Classifying terrain in a muskeg-wetland regime for application to GRU-type distributed hydrologic modeling. In: *Applications of Remote Sensing in Hydrology*, ed. G. W. Kite, A. Pietroniro, and T. Pults, Proc. Symp. No.4, NHRI, Saskatoon, Canada, 275-286.
- Pretula, B. R., and Ko, C. A. (1982), *Hydrogeology of Paddle River Reservoir area near Mayerthorpe*, Alberta, Report prepared for Alberta Environment Protection (AEP), 107p.
- Quick, M. C., and Pipes, A. (1977), U.B.C. Watershed model. *Hydrol. Sci. Bull.*, 22(1):153-161.
- Riley, J. P., Israelsen, E. K., and Eggleston, K. O. (1972), Some approaches to snowmelt prediction. *AISH Publ.*, 2(107):956-971.
- Riseborough, D. W. (2001), An analytical model of the ground surface temperature under snowcover with soil freezing. Paper presented In: *52<sup>nd</sup> ECS conference*,

Ottawa, May 12-15, 2001.

- Sand, K. (1990), *Modeling snowmelt runoff processes in temperate and arctic environments*. University of Trondheim, Norwegian Institute of Technology, IVB-rapport B-2-1990-1, 176p.
- Sarratt, B. S., Baker, D. G., Wall, D. B., Skaggs, R. H., and Ruschy, D. L. (1992), Snow depth required for near steady-state soil temperatures, *Agric. For. Meteorol.*, 57:243-251.
- Singh, P., Kumar, N., and Arora, M. (2000), Degree-day factors for snow and ice for Dokriani Glacier, Garhwal Himalayas. *J. Hydrol.*, 235:1-11.
- Twardy, A. G., Lindsay, J. D. (1971), *Soil survey of the Chip Lake area*, Alberta Soil Survey, No. 28:1-71.
- US Army Corps of Engineers, USACE (1971), *Runoff evaluation and streamflow simulation by computer, Part-II*, US Army Corps of Engineers, North Pacific Division, Portland, Oregon, USA.
- Woo, M., and Valverde, J. (1982), Ground and water temperatures of a forested mid-latitude swamp. In: Proc. of the Canadian Hydrology Symposium '82, *Hydrological Processes of Forested Areas*, Fredericton, N.B., 301-312.
- Woo, M., and Waddington, J. M. (1990), Effects of beaver dams on subarctic wetland hydrology. *Arctic*, 43(3):223-230.
- Ziverts, A., and Jauja, I. (1999), Mathematical model of hydrological processes METQ98 and its applications. *Nordic Hydrology*, 30(2):109-128.

Table 4.1 Comparison of correlation coefficients ( $\rho$ ) between cumulative air temperature ( $\Sigma T_a$ ), cumulative near surface soil temperature ( $\Sigma T_g$ ), measured net ( $\Sigma R_n$ ) and solar radiation ( $\Sigma R_{sol}$ ) for selected winter periods in PRB such that  $T_g$  was at or below freezing temperature.

Winter		$\Sigma T_a$	$\Sigma T_g$	$\Sigma R_n$	$\Sigma R_{sol}$
1997/98 Jan 1 - Mar 31, 1998	$\Sigma T_a$	1.0	0.98	-0.36	0.81
	$\Sigma T_g$	0.98	1.0	-0.48	-0.90
1998/99 Nov 11, 1998 - Apr 30, 1999	$\Sigma T_a$	1.0	0.98	0.98	-0.81
	$\Sigma T_g$	0.98	1.0	0.95	-0.89
1999/2000 Jan 1, 2000 - Mar 31, 2000	$\Sigma T_a$	1.0	0.98	0.92	-0.83
	$\Sigma T_g$	0.98	1.0	0.97	-0.91
1999/2000 Nov 21, 2000 - Mar 31, 2000	$\Sigma T_a$	1.0	0.99	0.95	-0.88
	$\Sigma T_g$	0.99	1.0	0.97	-0.91

Table 4.2 Comparison of correlation coefficients ( $\rho$ ) between cumulative air temperature ( $\Sigma T_a$ ), cumulative near surface soil temperature ( $\Sigma T_g$ ), measured net ( $\Sigma R_n$ ) and solar ( $\Sigma R_{sol}$ ) radiation for selected winter periods in PRB used for calibrating and validating SDSM-MTI such that  $T_g$  was either below, at or above freezing temperature.

Winter		$\Sigma T_a$	$\Sigma T_g$	$\Sigma R_n$	$\Sigma R_{sol}$
1997/98 Jan 1 - Apr 31, 1998	$\Sigma T_a$	1.0	0.98	-0.20	-0.49
	$\Sigma T_g$	0.98	1.0	-0.24	-0.54
1998/99 Nov 11, 1998 - May 16, 1999	$\Sigma T_a$	1.0	0.91	0.29	-0.63
	$\Sigma T_g$	0.91	1.0	0.57	-0.42
1999/2000 Jan 1, 2000 - Apr 30, 2000	$\Sigma T_a$	1.0	0.96	0.90	-0.58
	$\Sigma T_g$	0.96	1.0	0.97	-0.72
1999/2000 Nov 21, 2000 - Apr 30, 2000	$\Sigma T_a$	1.0	0.99	0.94	-0.72
	$\Sigma T_g$	0.99	1.0	0.97	-0.79

Table 4.3 Model parameters used in SDSM-MTI (1-12), and some of the important parameters used in DPHM-RS (13-15).

Description of Model Parameters	SDSM-MTI
1. Melt factor for coniferous forest, $M_{r,cf}$ (mm/hr/°C)	0.10
2. Melt factor for mixed forest, $M_{r,mf}$ (mm/hr/°C)	0.15
3. Melt factor for open area, $M_{r,oa}$ (mm/hr/°C)	0.30
4. Melt-rate-factor exponent ( $\psi$ )	2.0
5. Rain to snow threshold temperature, $T_{th}$ (°C)	1.1
6. Threshold temperature for melt, $T_m$ (°C)	0
7. Maximum density of snow pack, $\rho_{s,max}$ (kg/m <sup>3</sup> )	250
8. Settlement constant, $c_s$	0.05
9. Liquid water holding capacity (LWHC)	0.05
10. Snowfall distribution factor (%/100m)	0.20
11. Rainfall distribution factor (%/100m)	0.80
12. Temperature lapse rate (°C/100m)	-0.65
13. Relative water content ( $\theta/\theta_s$ )	0.80 for both layers
14. Depth of each layer (m)	0.2
15. Manning's roughness coefficients, n	0.15 (forest) & 0.1 (open area)

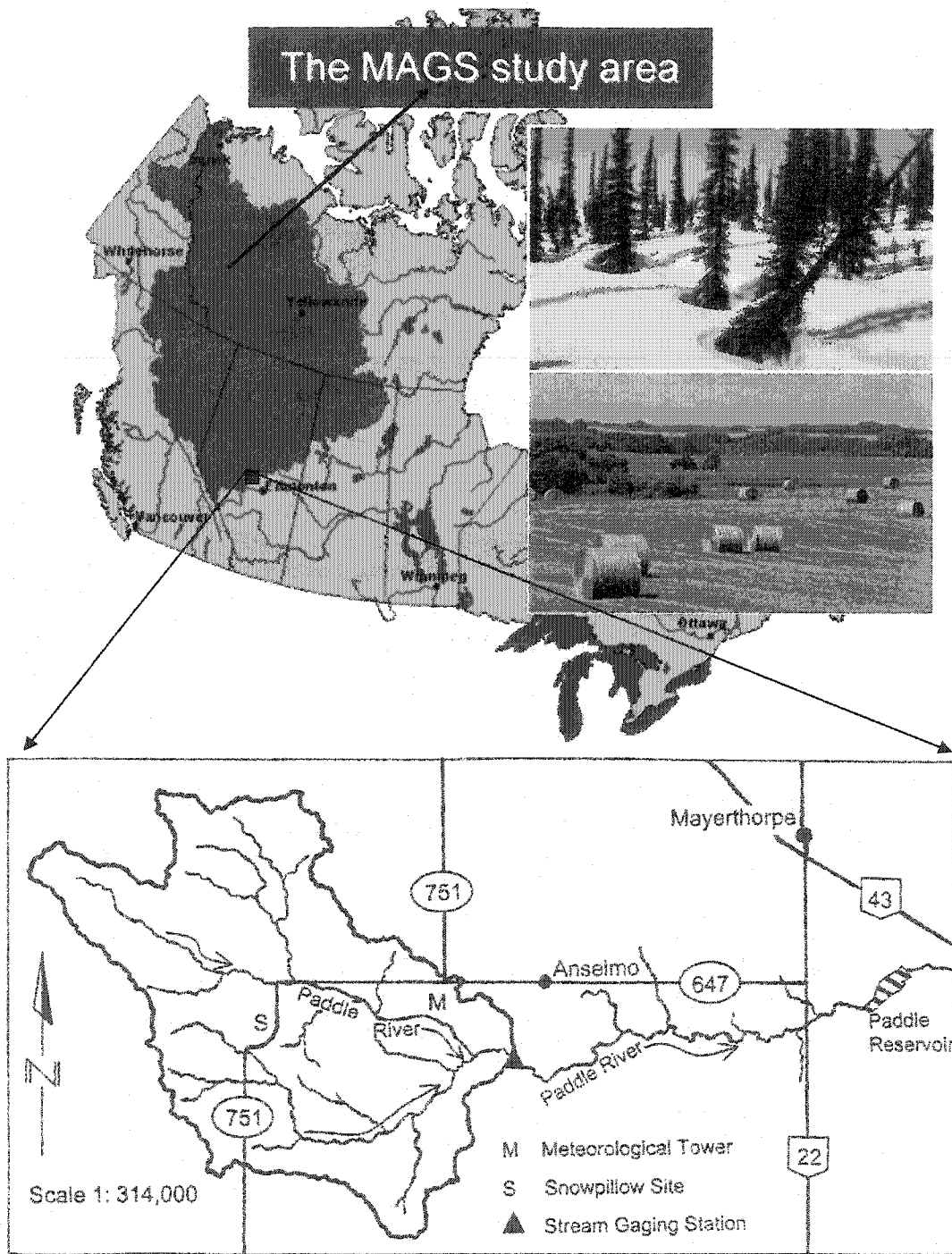


Figure 4.1 Location map of Paddle River basin in the Mackenzie GEWEX Study area (MAGS).

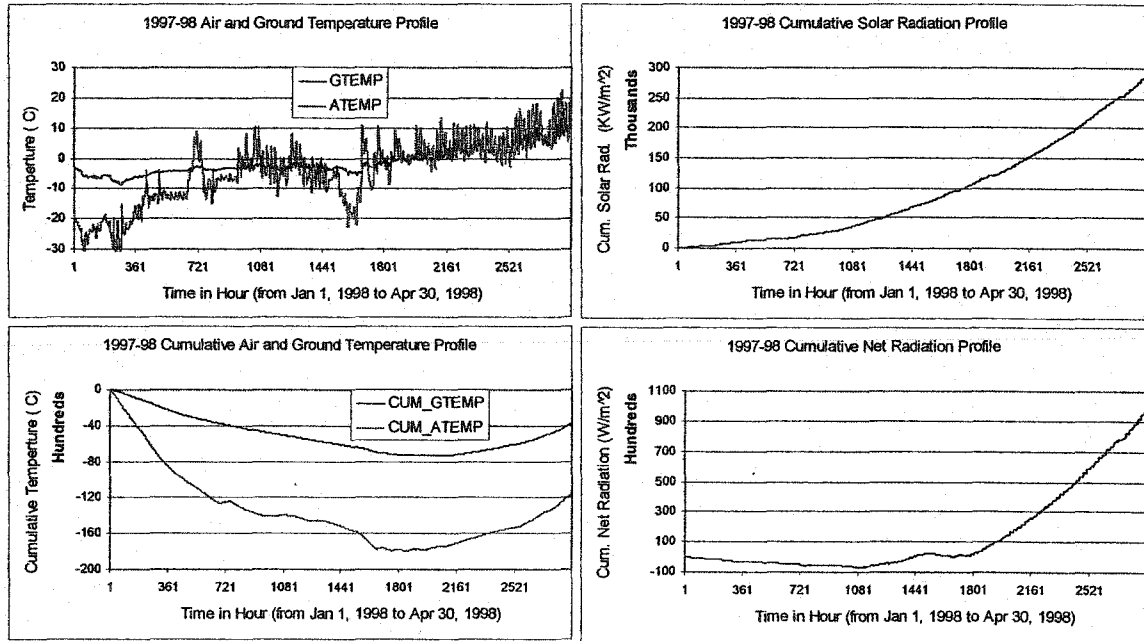


Figure 4.2 PRB's meteorological data during the validation period of 1997/98 winter

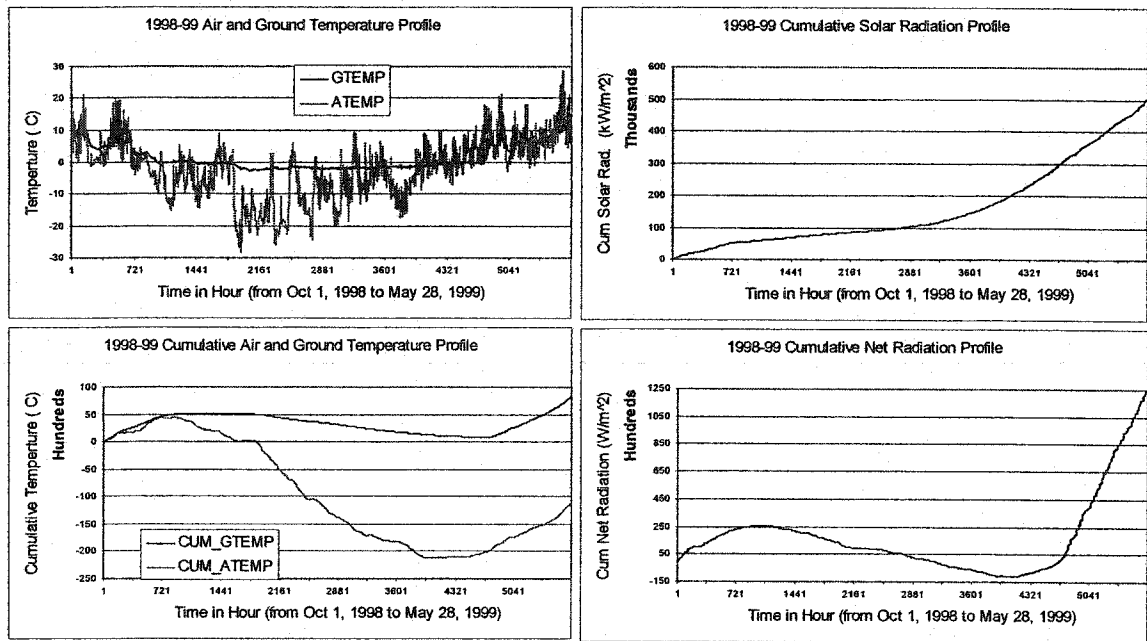


Figure 4.3 PRB's meteorological data during the calibration period of 1998/99 winter

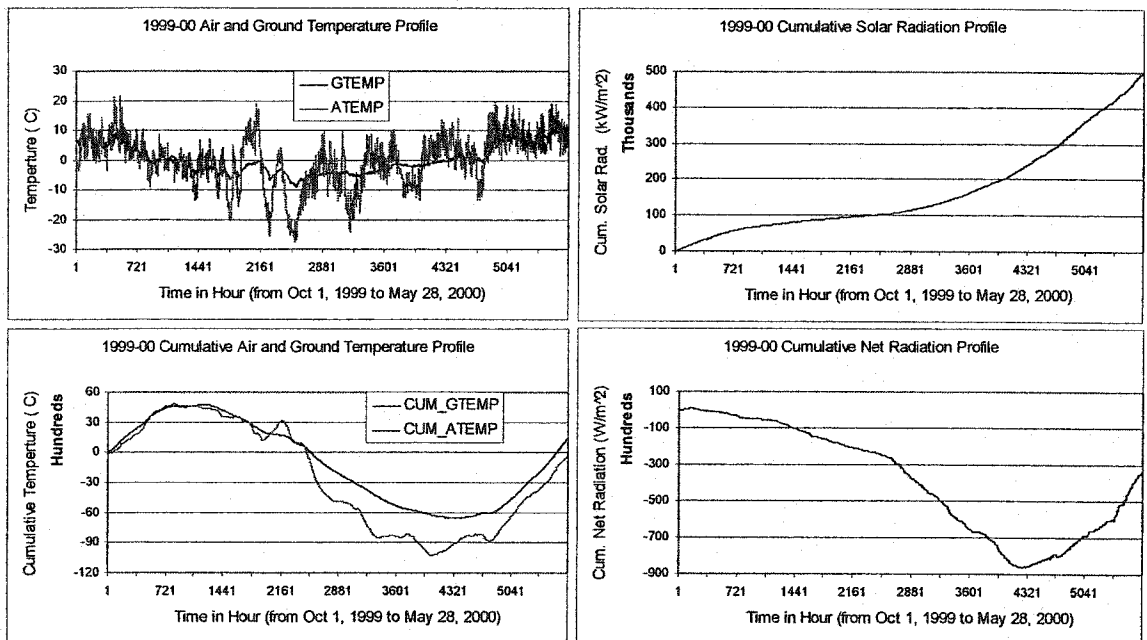


Figure 4.4 PRB's meteorological data during the validation period of 1999/00 winter

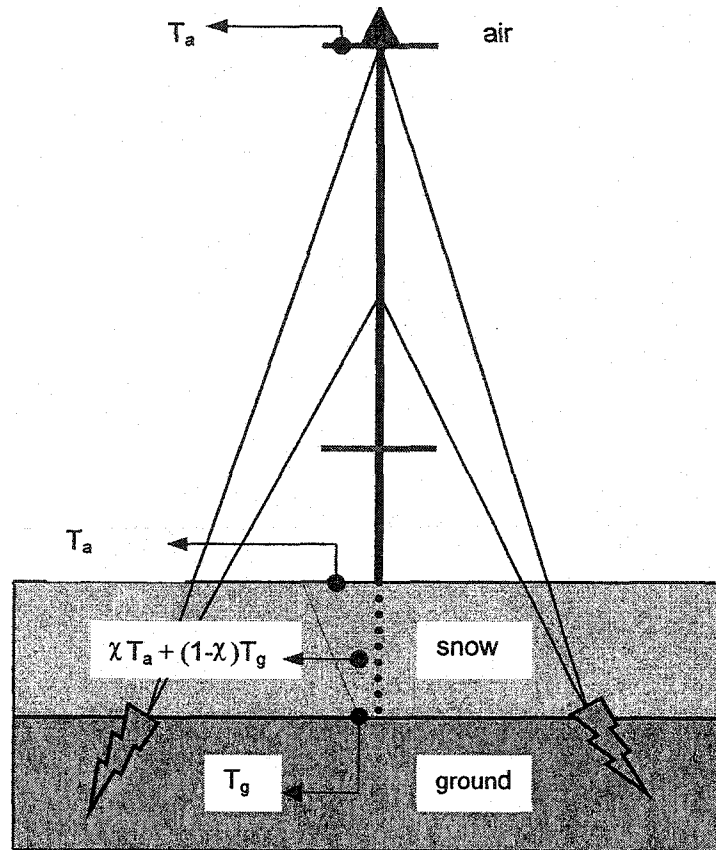


Figure 4.5 The concept of reference temperature, " $T_r = \chi T_a + (1-\chi)T_g$ " used in the modified temperature index method of SDSM (or SDSM-MTI).

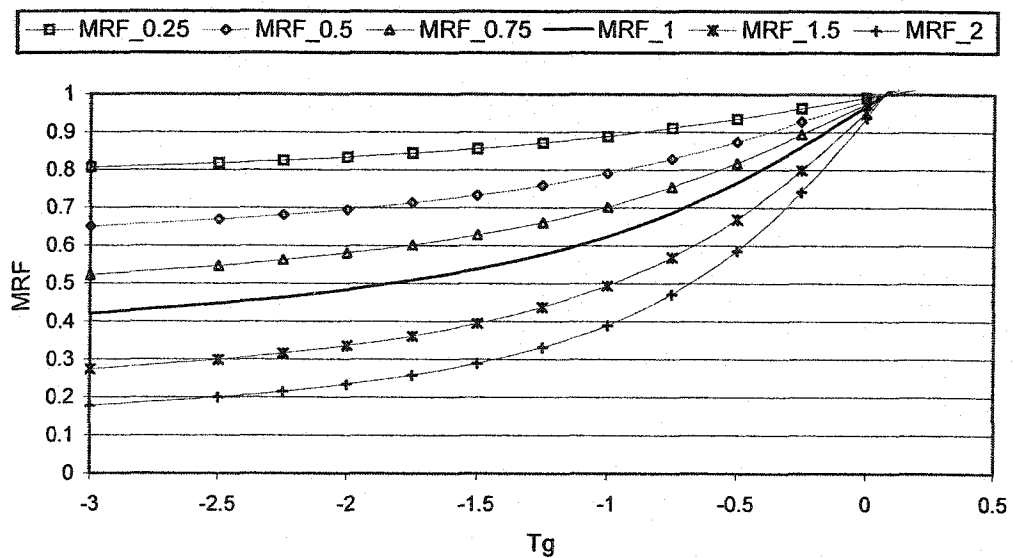


Figure 4.6 Melt Rate Factor ( $MRF = (M_{rf})^\psi$ ) for different near surface soil temperature ( $T_g$  in °C) and  $M_{rf}$  exponent  $\psi = 0.25, 0.5, 0.75, 1, 1.5, \& 2.0$ .



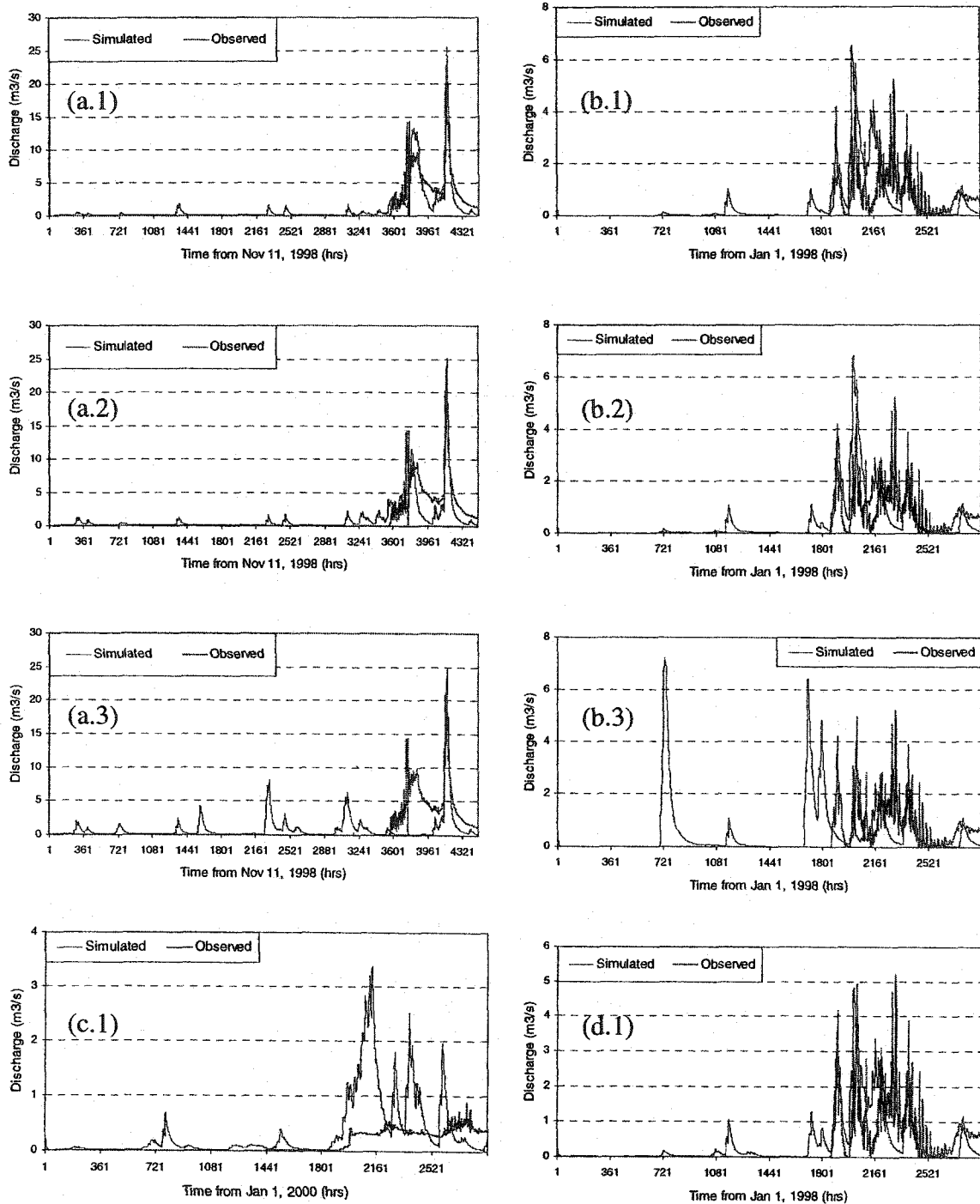


Figure 4.7 Comparison of SDSM-MTI simulated and observed streamflow for PRB at the calibration (*Cal*) (Nov. 11, 1998 to May 16, 1999) and the validation (*Val*) stages (Jan. 1, 1998 to Apr. 30, 1998 and Jan. 1, 2000 to Apr. 30, 2000), such that there is no change of calibrated parameters: (a.1) for *Cal* and (b.1 and c.1) for *Val*; with  $\chi$  set to 1 but other parameters unchanged (i.e.  $T_g$  is partially ignored): (a.2) for *Cal* and (b.2) for *Val*; with  $\chi$  set to 1 and  $\psi$  set to 0 but other parameters unchanged (i.e.  $T_g$  is completely ignored): (a.3) for *Cal* and (b.3) for *Val*; and (d.1) is similar to (b.1) but with slightly reduced melt factors and  $\psi$  set to 1.

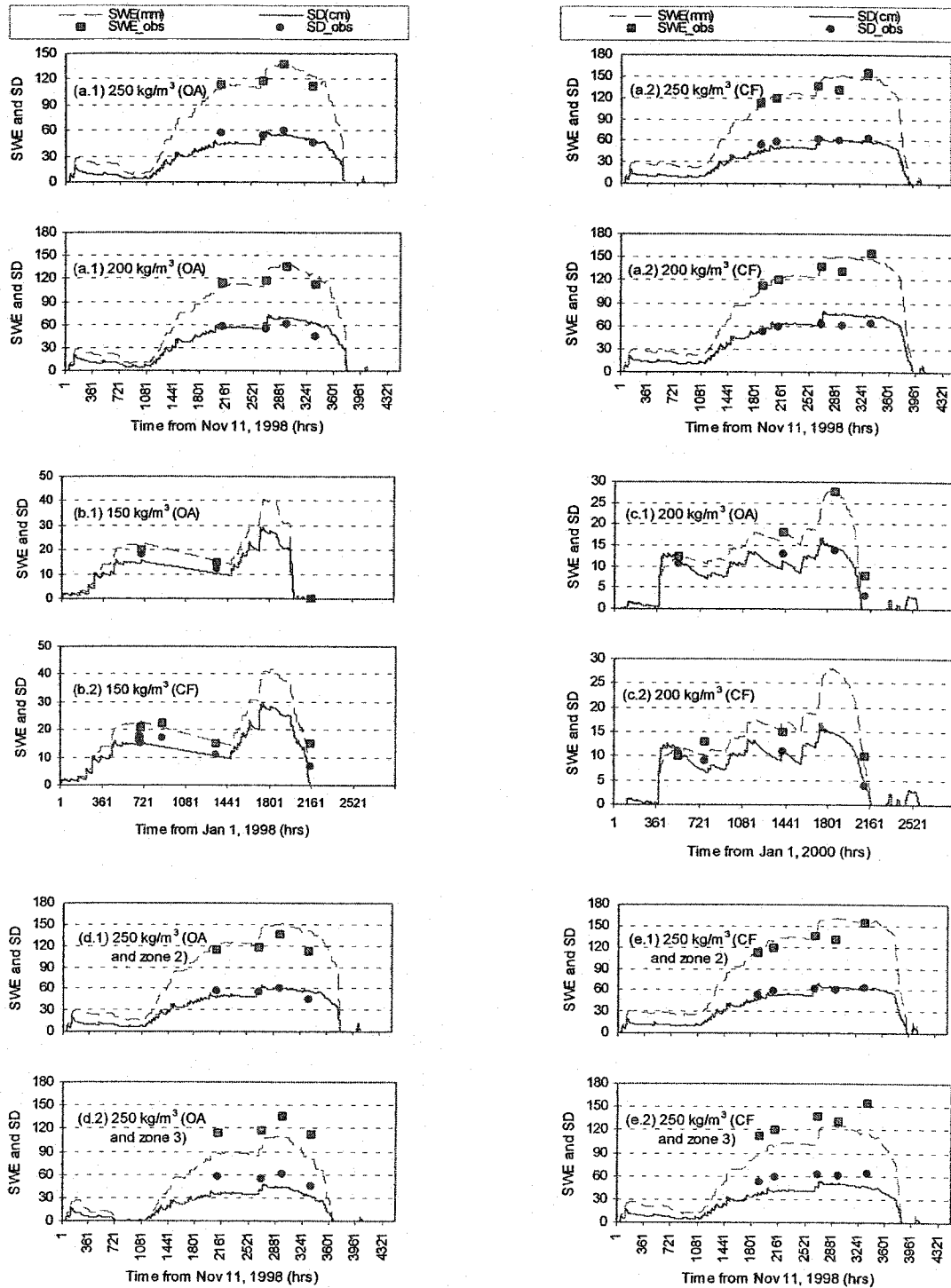


Figure 4.8 Comparison of SDSM-MTI simulated and observed SWE and snow depth (SD) for Zone 4: at the calibration stage (Nov. 11, 1998 to May 16, 1999) with maximum snow density  $\rho_{\max} = 250$  and  $200 \text{ kg/m}^3$  for (a.1) Open Area (OA) and (a.2) Coniferous Forest (CF); at the validation stages (Jan. 01 to Apr. 30) for OA and CF (b) 1998 with  $\rho_{\max} = 150 \text{ kg/m}^3$  and (c) 2000 with  $\rho_{\max} = 200 \text{ kg/m}^3$ ; and zone 2 and 3 at calibration stage with  $\rho_{\max} = 250$  for (d) OA and (e) CF.

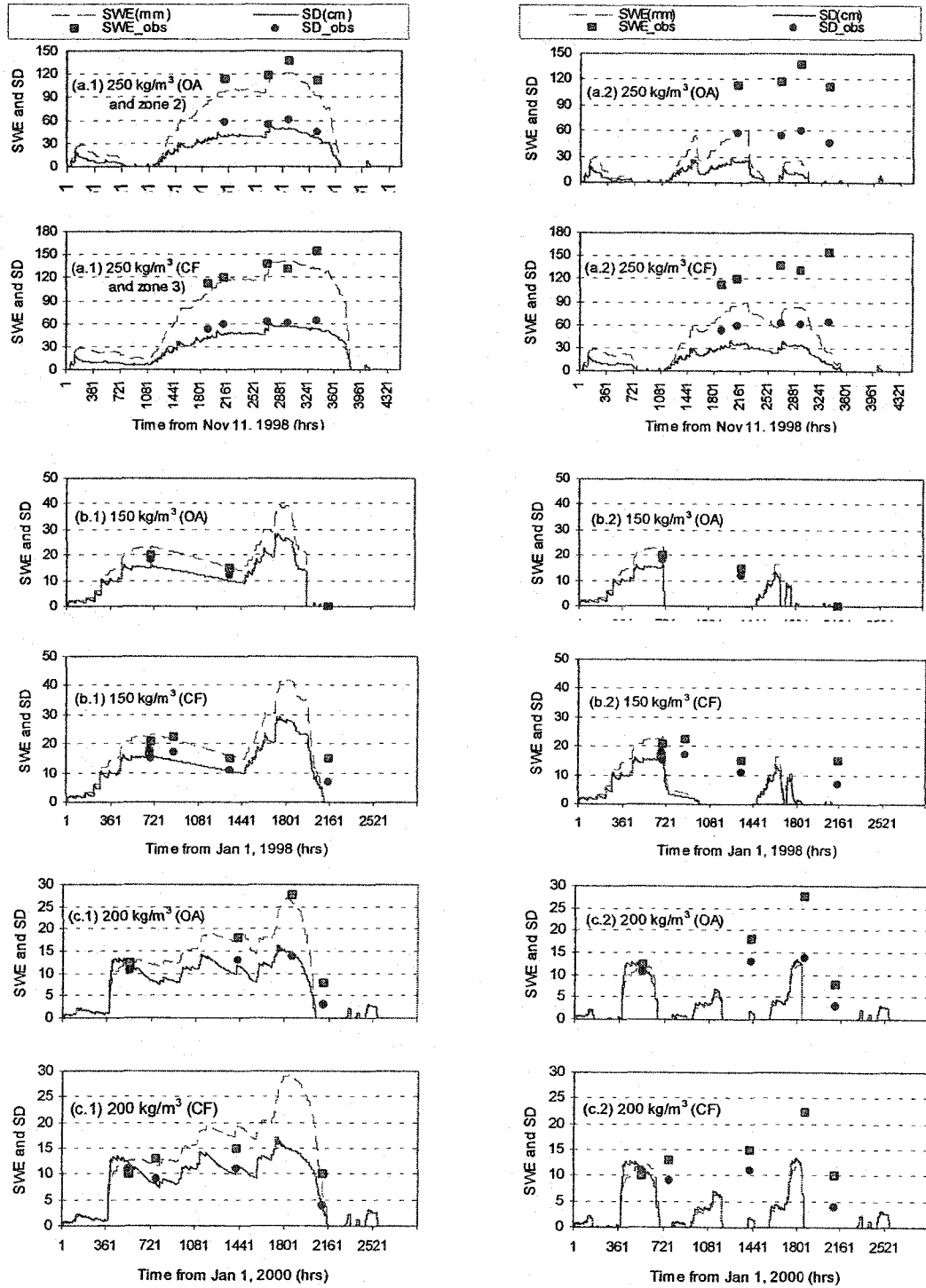


Figure 4.9 Comparison of SDSM-MTI simulated and observed SWE and snow depth (SD) in zone 4: at the calibration stage (Nov. 11, 1998 to May 16, 1999) with  $\rho_{max} = 250$  and  $200 \text{ kg/m}^3$  for (a.1)  $\chi=1$  and  $\psi=2$ , and other parameters unchanged, (a.2)  $\chi=1$  and  $\psi=0$ , and other parameters unchanged; similar results at the validation stages: (b) Jan. 01 to Apr. 30, 1998, and (c) Jan. 01 to Apr. 30, 2000.

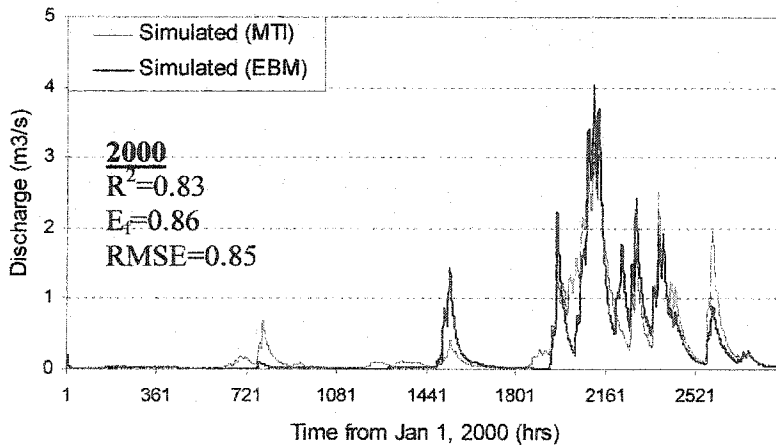
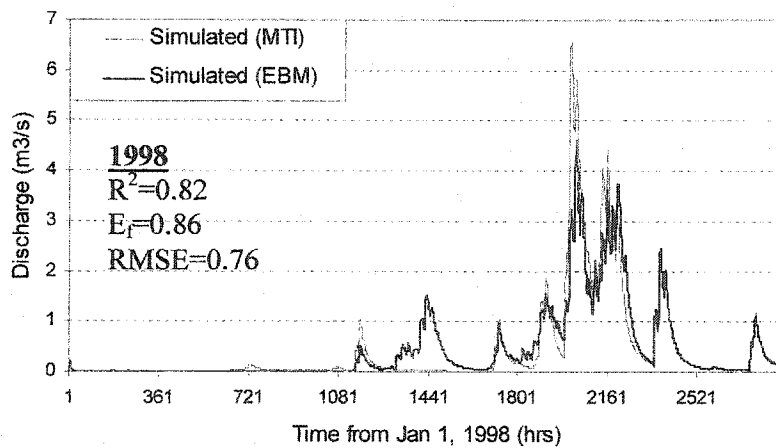
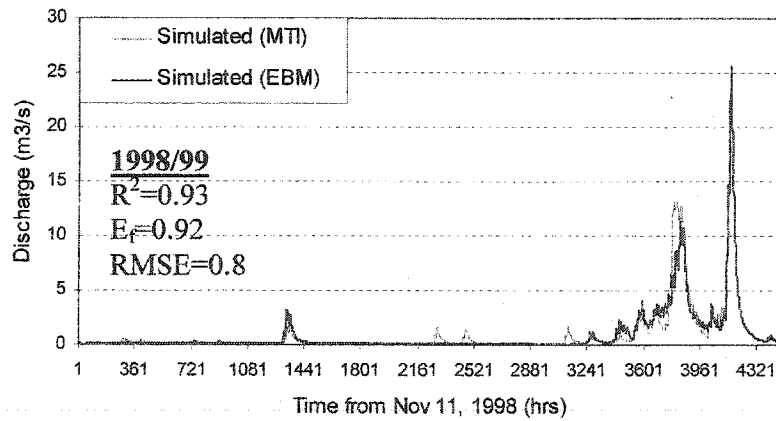


Figure 4.10. Comparison of PRB's simulated streamflow using SDSM-MTI and SDSM-EBM in both calibration stage of 1998/99 winter (Nov. 11, 1998 to May 16, 1999) and validation stages of 1998 and 2000 winters (Jan. 1 to Apr. 30).

## **Chapter 5**

# **Retrieval of Snow Water Equivalent Using Passive Microwave Brightness Temperature Data**

### **5.1 Introduction**

In the northern hemisphere, the mean monthly land area covered by snow ranges from 7 to 40% during the annual cycle, making snow cover [in terms of area extent and snow water equivalent (SWE)] the most rapidly varying surface-feature on Earth. Snow is a dominant source of water supply in Canada and some parts of the United States. In the Canadian Prairies, the shallow snow cover generates as much as 80% of the annual surface runoff from some local areas (Granger and Gray, 1990). In the Colorado Rockies and Sierras of California, snowfall accounts for up to 90% of the annual water supply. During spring, snowmelt fills reservoirs and groundwater systems that provide water for agricultural and municipality use and hydropower generation. Thus, knowing the seasonal variations of SWE is critical for an effective management of water resources. However, the only way to adequately

estimate the spatial coverage and temporal changes of snow cover in a regional scale is via remote sensing.

Space borne data have been utilized since the mid-1970s in water resources management. The advent of airborne gamma ray spectrometry and microwave remote sensors are keys to passive microwave snow research (e.g. Goodison et al., 1986; Chang et al., 1987; Hallikainen, 1989). For example, the Office of Hydrology, National Weather Service of USA has been measuring SWE using airborne gamma radiation with as many as 1,578 flight lines distributed in 32 states/provinces of the United States and southern Canada (see NWS, 1992). Unfortunately, very high operational cost involved with such airborne survey restricts its application globally.

England (1975), Chang et al. (1976), and others reported the scattering of microwave radiation by snow crystals. This scattering effect, which redistributes the upwelling radiation according to snow thickness and crystal size, provides the physical basis of microwave detection of snow. In spite of its coarse resolution (about 25 km), the ability of passive microwave to penetrate dry snow, clouds, and to provide dual polarization information at different frequencies at night makes it attractive for snow studies on a global basis. Earlier studies (between 1978 and 1987) were mainly based on the microwave brightness temperature (TB) data from the Scanning Multi-channel Microwave Radiometer (SMMR) aboard the Nimbus-7 satellite. After 1987, such studies use TB data from the Special Sensor Microwave/Imager (SSM/I) aboard the Defense Meteorological Satellite Program (DMSP) spacecraft. In this study, past retrieval algorithms (e.g., Hallikainen, 1989; Goodison and Walker, 1994; Gan, 1996; Chang et al., 1996; Foster et. al., 1997; Tait, 1998) are reviewed and new algorithms proposed. Due to a lack of detailed field data on snow properties, most of these SWE retrieval algorithms from microwave TB data are statistically, rather than physically, based.

Hallikainen (1989) found that vertically polarized TB of 37 GHz (V37) emitted from snow-covered terrain has the most sensitive diurnal variation, with a range as high as 100 K. The diurnal variation of TB from a snow layer is associated with both temporal and spatial variation of snow structure at the influence of atmospheric forcing (e.g., air temperature, solar radiation, etc.) within the SSM/I footprint. Because of this diurnal variation of TB, it becomes necessary to develop retrieval algorithms with respect to satellite overpass time (e.g., morning/night time overpasses or afternoon/evening overpasses from DMSP-F8, F10 and F13). The SSM/I data used in this study were of morning and night overpasses. Differences between satellite TB are also partly attributed to differences in satellite calibration, satellite geo location, and data processing methods (Table 5.1).

Essentially, TB data reflect the scattering behavior of a snow layer on the incident microwave in terms of the combined effect of grain size (depth-hoar), snow density, liquid water content, degree of metamorphism, nocturnal crust development, and ice lenses that also affect the dielectric property of the snow layer. Although microwave radiation at less than 40 GHz can penetrate through typical packs of dry seasonal snow, the estimation of SWE by microwave radiometry is hindered by the presence of wet snow, varying grain size, the layering of the snowpack, and other considerations (Matzler, 1994). With increasing liquid water content in snow (which also means an increase in the dielectric constant), the absorption of microwave radiation will slowly dominate over scattering as the major loss mechanism, to the extent that TB becomes independent of SWE for wet snow (Hallikainen, 1989). For a snowpack with a liquid water exceeding 1%, the penetration depth reduces to about 10 cm for 19 GHz emission and even less for 37 GHz emission, which limits the amount of information that is retrievable (Ulaby et al., 1986).

For dry snow cases, theoretical analysis and field data show that the scattering of the 37 GHz microwave radiation is directly related to snow depth and grain size (Chang

et al., 1976). Using data from high latitude regions, Zwally (1977) found that for a given average surface temperature, the snow grain size profile increases with depth from top to bottom. On the other hand, the average grain size was found to also decrease with an increase in the overall snow depth (Armstrong et al., 1993; Matzler, 1994). Snow grain size not only changes within the snowpack, but also with time. Shallower winter snowpacks are more susceptible to produce large grains of depth-hoar near the bottom due to a generally larger temperature gradient than that for a deep snowpack (SWE > 25 cm). In a study on microwave emissivity (5 to 100 GHz) with reference to the estimation of SWE of dry snow, Matzler (1994) found the need of using seasonal parameters on a regional scale. Root and Aschbacher (1989) suggested possible improvements in SWE retrieval if the effect of atmospheric attenuation could be included in the algorithms. However, Tait (1998) did not see much improvement from incorporating total precipitable water (TPW) into his algorithms, which may be partly because TPW data is available at low resolution, and the magnitude of TPW is generally less than 2 cm during winter seasons.

## **5.2 Research Objective**

This research has two primary objectives: (1) to develop and validate new SWE retrieval algorithms using conventional (multivariate regression) and new (projection pursuit regression) statistical techniques using SSM/I data (of different spacecrafts), physiographic and climate data for a prairielike environment of North America; and (2) to establish criteria to eliminate SSM/I footprint data that are affected by large water bodies and depth-hoar.

## **5.3 Study Site and Data**

The US portion of the Red River basin (between geographical coordinates 100°W-49°N and 95°W-46°N) that forms the study site is located in eastern North Dakota



and northwestern Minnesota (Figure 5.1). The study site has an area of approximately 120,000 km<sup>2</sup> and elevations ranging from 237 m at the outlet near U.S.-Canada international boundary to 552 m above the mean sea level (AMSL) near Sheyenne lake, which forms one of the longest and largest tributaries of the Red River (i.e., Sheyenne River). Precipitation falls in smaller amounts to the west and larger amounts to the east of the Red River valley. Out of an average annual precipitation of 520 mm (based on 100 years of data), about one-fifth falls between December to April. The October to April precipitation total for 1996-1997 was 268 mm, the largest value ever recorded in the Red River. The predominantly flat terrain, open farmland (forest cover only dominates the northeastern portion), and strong winds combined with light snow give rise to drifting and blowing snow.

This portion of the Red River basin was selected for the study mainly because of the large number of airborne flight lines repeatedly conducted by the Airborne Gamma Radiation Survey Program of NWS-USA SWE data were collected using a gamma-ray spectrometer (NWS, 1992) during the winter periods of 1988, 1989 and 1997 (see Table 5.2). Furthermore, these 3 years experienced a wide range of snowfall (Figure 5.2). The details of SSM/I data used in this research are shown in Table 5.1 and that of physiographic and climate data shown in Table 5.3.

## 5.4 Existing Algorithms

In dry snow, volumetric scattering is the dominant loss mechanism for microwave radiation above 15 GHz. As a result, the difference between a high scattering channel (37 or 85 GHz) and a low scattering channel (18 or 19 GHz) of vertical or horizontal polarization has been considered in most SWE retrieval algorithms. While Goodison et al. (1986), and Hallikainen (1989) developed SWE algorithms using vertical polarization channels (V19 and V37 GHz), the majority of other algorithms employed horizontal polarization channels (e.g., H19 and H37 GHz).

Foster et al. (1997) found that the sensitivity of horizontal polarization is more than that of vertical polarization in some vegetated areas. The following equations represent the primary forms of past SWE retrieval algorithms developed for passive microwave data [see Eqs. (5.1) through (5.5),

$$\text{SWE} = K_1 + K_2(\text{V19} - \text{V37}) \quad (5.1)$$

$$\text{SWE} = K_3 + K_4(\text{H19} - \text{H37})(1 - A_F) \quad (5.2)$$

$$\text{SWE} = K_5 + K_6[(\text{V18}_{\text{SWE}} - \text{V37}_{\text{SWE}}) - (\text{V18}_{\text{SWE}=0} - \text{V37}_{\text{SWE}=0})] \quad (5.3)$$

$$\text{SWE} = K_7(A_{\text{TUNDRA}})(\text{H19} - \text{H37}) + K_8(A_W)(T_a) + K_9 \quad (5.4)$$

$$\text{SWE} = K_{10}(\text{H18} - \text{H37})/(1 - A_F) \quad (5.5)$$

where,  $K_1$  to  $K_{10}$  are coefficients,  $\text{V18}_{\text{SWE}}$  and  $\text{V18}_{\text{SWE}=0}$  are vertically polarized TB of 18 GHz at snow-covered and snow-free areas,  $A_F$  is the fraction of forest cover,  $T_a$  is the air temperature, and  $A_{\text{TUNDRA}}$  and  $A_W$  are fraction of tundra and water body area within each SSM/I footprint respectively. It should be noted that SSM/I provided 19.35 (referred to here as 19) GHz while SMMR provided 18 GHz frequencies.

For SSM/I data, values of  $K_1$  and  $K_2$  in Eq. (5.1) provided by Goodison and Walker (1994) are  $-2.07$  cm (offset) and  $0.259$  cm/K (slope), and  $K_3$  and  $K_4$  in Eq. (5.2) by Chang et al. (1996) are  $-2.5$  cm and  $0.48$  cm/K under the negligible forest fraction ( $A_F \approx 0$ ). Chang et al. (1996) found that  $K_4$  tends to increase slowly with an increase in the forest fraction, by about 7 % for an  $A_F$  of 10%, and  $K_4$  reaches a value as high as  $0.96$  cm/K for an  $A_F$  of 50%. A detailed analysis of the results of Chang et al. (1996) showed that  $K_4$  is exponentially related to  $A_F$  [e.g.,  $K_4 = \exp(A_F)^\alpha + \beta$ , where we found  $\alpha$  and  $\beta$  to be 1.434 and  $-0.522$ , respectively.

Hallikainen (1989) developed Eq. (5.3) for northern and southern Finland, where  $K_5$  and  $K_6$  for northern Finland are  $-10.87$  cm and  $0.87$  cm/K, and those for southern Finland are  $-9.8$  cm and  $1.01$  cm/K, respectively. The increase in the value of  $K_6$  is

associated with an increase of forest cover in southern Finland. Gan (1996) developed Eq. (5.4) based on the assumption that microwave emission from frozen water bodies is related to air temperature ( $T_a$ ). Comparison of SWE estimated from Eqs.(5.1) to (5.4) with ground measurements showed a better estimate of SWE from Eq. (5.4). Using a mean snow density of  $300 \text{ kg/m}^3$  (as given in Chang et al., 1996), Foster et al. (1997) proposed Eq. (5.5), where  $K_{10}$  is  $0.477 \text{ cm/K}$  for North America and  $0.234 \text{ cm/K}$  for the interior area of Eurasia. Tait (1998) developed several algorithms, one of which is similar to Eq. (5.2) for a non-forested, non-mountainous terrain of no depth-hoar and no melting snow, with  $K_3$  and  $K_4$  equal to  $1.29 \text{ cm}$  and  $0.31 \text{ cm/K}$ , respectively ( $R = 0.754$ ). However, for a forested basin, and with SWE as a function of (V19-H37), Tait (1998) found  $K_3$  and  $K_4$  to be  $2.64 \text{ cm}$  and  $-0.13 \text{ cm/K}$ , respectively ( $R=0.407$ ).

To calibrate the above algorithms, it has been found necessary to identify and separate SSM/I data that represent snowpacks affected by wet snow and depth-hoar. The use of air temperature alone to achieve this purpose (e.g., Tait, 1998) may not be sufficient, especially for large study areas. Goodison et al. (1986) set certain limits on TB and TB difference [e.g.,  $V37 \geq 241 \text{ K}$  and  $(V19-V37) \geq 9 \text{ K}$ ] as the wet snow elimination criteria. The polarization difference at 37 GHz ( $V37-H37 \geq 10 \text{ K}$ ) was also defined as a threshold to discriminate wet snow from snow-free land if the estimated SWE was close to zero (Goodison and Walker, 1994). Goodison and Walker estimated that  $(V37-H37)$  could range from 3 to 11 K for snow-free open prairies, 9 to 24 K for wet snow, and 8 to 33 K for dry snow areas. After the work of Neale et al. (1990), the NOAA-NASA SSM/I Pathfinder (NNSP) program also uses SSM/I data to derive land surface classifications, and to establish dry snow based on the following criteria:  $V22-V19 \leq 4$ ;  $V19-H19+V37-H37 > 8$ ;  $V19-V37 > 7.8$ ;  $225 < V37 < 257$ ;  $V19 \leq 266$ ; and  $H85-H37 < 10.5$ . The polarization factor ( $p\_factor$ ), the ratio of polarization difference and its sum, has also been used to reflect the different surface conditions (Chang et al., 1982).

So far, only a few studies have included the validation of algorithms using different passive microwave data or SSM/I data from different spacecraft, such as Chang et al. (1996), who used Eq. (5.2) to retrieve SWE from both airborne radiometer and SSM/I (DMSP-F10 and F11) data, and compared them with ground data. They found the retrieved SWE using airborne radiometer data (at 3 and 4 P.M. local time) to be less than that using DMSP-F10 SSM/I data (10 and 10 P.M. local time as reported) for agricultural and forested grids. They attributed this difference to be the presence of wet snow in the former because of its overpass time of 3 and 4 P.M. (local time). Besides the satellite overpass time, the diurnal variation of microwave data (H37 or V37; Hallikainen, 1989) or the algorithm itself could make a difference to the amount of SWE estimated from satellite data. Surprisingly, despite this diurnal variation effect Chang et al. (1996) found that the SWE ( $< 5\text{cm}$ ) retrieved from DMSP-F11 data (acquired at 6 P.M. local time or evening overpass) agrees well with that of DMSP-F10 data. This could be partly attributed to a shallow snowpack (SWE  $< 5\text{cm}$ ), because using their algorithm and our data (SWE  $> 5\text{cm}$ ), the results we obtained are not as encouraging [see Figure 5.4(j) through 5.4(l)]. To avoid the effect of diurnal variation, it seems necessary to use different algorithms for satellite data of different overpass time, as was done in this study.

## 5.5 Proposed Algorithms

The SSM/I data for 1988 and 1989 are from DMSP-F8, while that for 1997 are from DMSP-F10 and DMSP-F13 respectively. All three satellites have a different equatorial overpass time (Table 5.1). The following two retrieval algorithms (Eqs. 5.6 and 5.7) are proposed and tested with the Red River basin for morning/night time overpass (between 10:30 pm and 10:30 am of the following day) SSM/I data only. Algorithm parameters and some criteria were identified using the regression tree technique, the stepwise multiple regression and the linear and non-linear

regression techniques. Similar criteria of Goodison et al. (1986) ( $V37 < 250$  K,  $V19 - V37 \geq 9$  K), Walker and Goodison (1993) ( $V37 - H37 \geq 10$  K) and the  $p\_factor$  (which equals  $(V37 - H37)/(V37 + H37)$  and  $> 0.026$ ) were used to establish dry snow conditions. Also, additional criteria used include  $V37 > 225$  K (a criterion of NNSP mentioned in Section 5.3) for DMSP-F8, and  $p\_factor < 0.041$  (proposed in this study) for DMSP-F10 and DMSP-F13 data.

$$SWE = K_{11}(V19 - H37) + K_{12}AMSL + K_{13}(1 - A_F) + K_{14}(1 - A_w)T_a + K_{15}TPW \quad (5.6)$$

$$SWE = K_{21}(TB\_V19 - TB\_V37) + K_{22}(TB\_H19) + K_{23}AMSL + K_{24}A_F \quad (5.7)$$

In these algorithms we introduced new variables such as that with the prefix  $TB\_$  (which represent surface brightness temperature) and  $AMSL$  (average elevation above mean sea level). The conversion of surface  $TB$  from SSM/I data was based on Choudhury (1993)'s atmospheric attenuation model (Appendix: E), which accounts for the attenuation of atmosphere water vapor (based on  $TPW$  in cm) on SSM/I  $TB$  data at 19 and 37 GHz. The model requires sky temperature,  $T_{sky}$  that according to Choudhury (1993), was estimated from the air temperature ( $T_a$ ), the atmospheric transmission ( $t_a$ ), the optical thickness ( $\tau$ ), and  $TPW$ . Other than using  $TPW$  indirectly to correct  $TB$  for atmospheric attenuation via Choudhury's model (Eq. 5.7),  $TPW$  is also used directly as an independent variable in Eq. 5.6.

Eq. (5.6), which is nonlinear, and Eq. (5.7), which is linear, were respectively developed from the 1989 and 1988 ascending (morning overpass) data of DMSP-F8. All data sets were first screened from footprints affected by wet snow and depth-hoar, and then used to calibrate the algorithms using multivariate regression.

In a prairie-like environment, the Red River Basin is predominantly open-ground with scattered vegetation (except north eastern part of basin), which means that the effect of wind on snow metamorphism and re-distribution is often significant. As

snow is generally blown from high grounds to low-lying area, we would expect less snow at higher grounds. But there are exceptions, such as a northwesterly/southwesterly wind blowing past a south/north facing basin slope. In this case, the lower portion of the basin would not necessarily collect snow from the higher portion of the basin. The effect of wind is significant at high altitudes, but its effect decreases with increasing forest cover ( $A_F$ ). In addition, the distribution of forest cover in various altitude bands modifies the distribution of SWE differently. Therefore, snowpack metamorphism caused by wind could be partly explained by the combined effect of AMSL and  $A_F$ . The calibration process involving AMSL and  $A_F$  is complicated by the non-uniform distribution of SWE data (retrieved from airborne gamma ray) across the study site.

In addition to multivariate regression, the non-parametric Projection Pursuit Regression (PPR) of Friedman and Stuetzle (1981) was introduced to estimate SWE (response variable) from several predictor variables that consist of SSM/I TB data (19 & 37 GHz dual polarization), physiographic and atmospheric data. PPR models the response variable as a sum of functions of linear combinations of predictor variables. Suppose  $y$  and  $x$ 's denote response and predictor vectors respectively, PPR finds the number of terms  $M_0$ , direction vectors ( $\alpha_1, \alpha_2, \dots, \alpha_{M_0}$ ) and nonlinear transformations ( $\phi_1, \phi_2, \dots, \phi_{M_0}$ ) as shown in Eq. (5.8),

$$\hat{y} \approx \bar{y} + \sum_{m=1}^{M_0} \beta_m \phi_m(\alpha_m^T x) \quad (5.8)$$

The model parameters  $\beta_m$  (the response linear combinations),  $\alpha_m$  (the direction vectors),  $\phi_m$  (the predictor functions),  $m=1,2, \dots, M_0$  in Eq. (5.8) are obtained from minimizing the expected distance or mean square error between  $y$  (e.g., observed SWE) and  $\hat{y}$  (estimated SWE) given by,

$$L_2(\beta, \alpha, \phi, x, y) = E[y - \hat{y}]^2 \quad (5.9)$$

As the name implies, the "projection" part of PPR means that the independent vectors  $x$  are projected onto the direction vectors  $\alpha_1, \alpha_2, \dots, \alpha_{M_0}$  to get the lengths  $\alpha^T x$ , and the "pursuit" part indicates that an optimization technique is used to find good direction vectors. The use of PPR essentially consists of choosing an appropriate number of terms  $M_0$ . Friedman (1985) suggested starting the algorithm with a large  $M_0$  and then decreasing  $M_0$  such that the increase in accuracy due to an additional term is not worth the increased complexity. The discrepancy of each PPR model for a given  $M_0$ ,  $U$ , is measured in terms of the fraction of variance it cannot explain (Friedman and Stuetzle, 1981; Morton, 1989). Based on Eq. (5.9), this unexplained variance,  $U$  is defined as

$$U = \frac{L_2(\beta, \alpha, \phi, x, y)}{\text{Var}(y)} \quad (5.10)$$

The plot of  $M_0$  versus  $U$  in Figure 5.3 suggests that the number of terms that will give a superior response lie between 3 and 5. However, Figure 5.3 is based on the assumption that the amount of data available is large and representative of the population. If the amount of data available is limited, using a model of many terms (big  $M_0$ ) may lead to an over fit at the calibration stage, which happens at the expense of the physical basis of calibrated parameters, leading to poor results at the validation stage. In this study, an over fit results as soon as  $M_0$  was set to 3. Therefore we set  $M_0$  to 2.

## 5.6 Discussion of Results

The discussion first focuses on the proposed criteria to eliminate SSM/I footprints affected by large water bodies and depth-hoar, and then on snow retrieval from existing and proposed algorithms. A careful inspection of six such airborne flight lines of 1989 and 1997 reveal that these flight lines fall in three SSM/I footprints, of which the central footprint has 12.7% of surface areas covered by water bodies (two others have 6.1% and 4%). The high dielectric constant of water bodies (due to the presence of unfrozen water underneath or the presence of liquid water in snowpack)

tend to reduce the brightness temperature gradient between low and high scattering channels because of a higher extinction loss (absorption) in parts of the SSM/I footprint affected by water. The use of  $p\_factor$  ( $>0.026$ ) proposed in this study, removed footprints with a fair proportion of frozen lake and wet snow, which could cause the predicted SWE to be under-estimated. For footprints somewhat affected by the high dielectric constants of water bodies, the effect is accounted for by the area of water bodies,  $A_w$ . The coefficient associated with  $A_w$  in Eq. (5.6) is positive (Table 5.4), indicating its positive feedback to SWE.

The lower limit of V37 ( $>225$  K) was found to be sensitive for SSM/I data from DMSP-F8 spacecraft in eliminating dry snowpacks influenced by depth-hoar, which could also overestimate SWE. This is also one of the criteria used for selecting dry snow in the NOAA-NASA SSM/I Pathfinder (NNSP) program. The 1997 data from DMSP-F10 and F13 that supposedly represent dry snow cases only (e.g., data associated with wet snow already eliminated by other criteria) are further screened by the  $p\_factor$  ( $>0.041$ ) to eliminate dry snow cases affected by depth-hoar. Figure 5.5 shows that if depth-hoar affected data were not eliminated both existing (Eqs. 5.1 and 5.2) and proposed algorithms (Eqs. 5.6 and 5.7) would consistently produce poor validation results for 1997 data of DMSP-F10 and DMSP-F13. The need to eliminate data affected by depth-hoar can also be inferred from the work of Abdalati and Steffen (1998). They found that unless depth-hoar formation can be adequately parameterized, it would be impossible to estimate snow depth and/or detect its interannual variations successfully using passive microwave data. For future research, parameterization schemes for depth-hoar affected snowpacks (such as snow crystal growth model of Josberger and Mognard, 1998) should be tested to see if we can use such schemes to avoid eliminating depth-hoar affected footprints in developing our retrieval algorithms.



The amount of data so eliminated were 31 and 38 data points for the ascending and descending overpasses of DMSP-F10, and 24 data points for the descending overpass of DMSP-F13. The relatively severe weekly air temperature data in Table 5.5 for 1997 February & March ( $\approx -14^{\circ}\text{C}$  to  $-22^{\circ}\text{C}$ ) probably implies a large temperature gradient in the snow pack at this period. As temperature-gradient metamorphism is the primary mechanism that makes snow grains at the bottom of a snowpack grow (particularly for shallow snow), it is not surprising to see many data points eliminated because of depth-hoar influences. Tait (1998) also found that the inclusion of depth-hoar affected snow data lead to poor results, e.g.,  $R < 0.5$ .

The calibration and validation results of proposed and existing algorithms using 3 years of diverse data (from below the 100-year normal for 1988 to the 100-yr precipitation of 1997, see column “D-M” and “O-A” in Table 5.6 & Figure 5.2) are shown in Figure 5.4. The first three rows of Figure 5.4 (a) to (i) compare the calibration and validation results of the existing algorithms (Eqs. 5.1, 5.2 and 5.5) with the proposed algorithms (Eqs. 5.6, 5.7 and 5.8) for morning/night satellite overpasses. The last row of Figure 5.4 shows a very poor correlation with existing algorithms (Eqs. 5.1, 5.2 and 5.5) for evening satellite overpass. To obtain good results at the validation stage, Figure 5.4 (a to i) shows that it was necessary to add shift parameters to the proposed algorithms, irrespective of whether the algorithms were calibrated by multivariate regression or projection pursuit regression. The amount of shifts (in cm of SWE) used in the algorithm and the associated improvements to the validation results (measured in terms of  $R^2$  and RMSE) are shown in Table 5.7. The relative shift parameters were kept unchanged for all the proposed algorithms.

Perhaps the most important finding of this study is the necessity to add a shift parameter or an “offset” (see Table 5.7) to the calibrated algorithms in the validation stage in order to obtain good validation results (e.g., compare Figure 5.4b with 5.5c,

5.5e with 5.5f, and 5.5h with 5.5i). Apparently, these “offsets” are data dependent and their basis can be taken from the work of England (1975) that illustrated the theory of radio emission from dielectric layers containing Raleigh scatterers. The application of microwave radiometry to dry snow based on the scattering parameters of a dielectric snow layer (a function of size parameter, which is the ratio of average grain size and microwave wavelength denoted as  $\bar{d}/\lambda_0$ ) shows that scattering albedo ( $\omega_0$ ) is related to the scatter-induced darkening,  $\Delta TB_0$  (which means a reduction in TB in the scattering channel) of the snow layer and  $D/\lambda_0$  (see Figure 5.6). Scattering albedo (the snow layer's property responsible for this darkening) is related not only to the snowpack thickness but also to its metamorphism and grain size that changes from year to year.

It is therefore conceivable to obtain a difference in the scatter-induced darkening or scattering albedo for snowpacks of the same thickness, because snowpacks likely undergo different metamorphism in different years. Figure 5.6 shows a series of curves representing the change of  $\Delta TB_0$  with respect to  $\omega_0$  for snowpacks of various thicknesses ( $D$ ) (assuming the microwave wavelength,  $\lambda_0$ , remains constant). For an average grain size, England (1975) also showed that  $\omega_0$  could increase with an increasing volume fraction of enlarged ice grains in the snowpack. This implies that a formation of depth-hoar at the bottom layer would affect  $\omega_0$ , which in turn could change the degree of scatter-induced darkening significantly.

The direction (e.g., positive or negative) and magnitude of the shift parameter have been found to be closely related to the relative amount of winter precipitation between calibration and validation stages (see Figure 5.2, Table 5.2 and 5.7). For example, the shift parameter applied to Eq. (5.6) calibrated with 1989 data (mean SWE = 9.25 cm) turns out to be -5 cm for the 1988 validation data (mean SWE = 3.43 cm) but +4 cm for the 1997 validation data (mean SWE = 13.55 cm). Similarly,

Eq. (5.7) calibrated with 1988 data requires a shift parameter of +5 cm for 1989 and +9 cm for 1997 validation data, respectively.

The performance of existing algorithms (Eqs. 5.1, 5.2, and 5.5) also improved significantly if appropriate shift parameters are included at the validation stages, e.g., Eq. (5.1) of Goodison and Walker (1994) shows marked improvement when the same shift parameters applied to Eq. (5.7) for 1989 and 1997 data were also used (compare Figure 5.4(a) (no shift parameter) with Figure 5.7(c.1) (with shift parameter)). Similar improvement is obtained between the existing (Eqs. 5.1, 5.2 and 5.5) and the proposed algorithm (Eq. 5.6) if appropriate shift parameters are consistently applied at the validation stage (Figure 5.7b.1 to 5.7b.3). However, distinct differences between existing (Eqs. 5.1, 5.2, and 5.5) and proposed (Eq. 5.6) algorithms are found if shift parameters are only applied to the latter (see Figure 5.7a.1 to 5.7a.3). It is observed that accounting for the atmospheric attenuation by including TPW on the algorithm is not fruitful probably because of very coarse TPW data ( $1^\circ$  resolution) that cannot account for the possible variable effect of water vapor within the footprint size of SSM/I. As it may be beneficial to see the combined effect of both basin and atmospheric parameters on the retrieval algorithm (using SSM/I TB data), a careful investigation was done for one of the algorithms (Eq. 5.6). The contribution of basin and atmospheric parameters in SWE retrieval algorithm is significant for SWE less than 7 cm but diminishes for increasing SWE (more than 10 cm).

Finally, encouraging results are also obtained from Projection Pursuit Regression (PPR) (Eq. 5.8). However, the performance of PPR depends on the number of terms  $M_0$  in the algorithm. It was found that a better calibration fit (1989 data) to the PPR algorithm is achieved using  $M_0=3$  rather than  $M_0=2$ . However, a better calibration could be achieved at the expense of poorer validation results (1988 and 1997 data), e.g.,  $M_0=2$  produces better validation results than  $M_0=3$ . In applying PPR using Eq.

(5.8), the necessity of adding an appropriate shift parameter at the validation stage is once again demonstrated. Overall, PPR produced better calibration results than the multivariate regression but performed slightly poorer in the validation stage (see Table 5.7).

## 5.7 Summary and Conclusions

Existing snow retrieval algorithms from SSM/I data were assessed and new algorithms were proposed in this study. Algorithm development and validation were done using airborne gamma-ray measurements of SWE for 1989, 1988, and 1997 as the ground truth. Encouraging calibration results are obtained for the proposed algorithms using multivariate regression technique and dry snow cases of the 1989 and 1988 SSM/I data (from DMSP-F8). Similarly, validation results for data not used in calibration, e.g., 1988 (1989 as calibration data), 1989 (1988 as calibration data), and 1997 (from DMSP-F10 and F13), are also encouraging.  $R^2$  values are equal to 0.79 for 1988 SSM/I data and 0.71 for 1997 SSM/I data, respectively. The non-parametric, Projection Pursuit Regression (PPR) algorithm also gave good results in both stages. Overall, PPR produces better calibration results than multivariate regression but performed slightly poorer in the validation stage.

Apparently by including land-cover categories, average elevation of footprint and atmospheric opacity, the above regression techniques can produce meaningful relationships between SWE and TB data. However, a key step towards reliable SWE estimate from passive microwave data is also using screening criteria such as those proposed in this study (and existing criteria) to eliminate SSM/I footprints affected by wet snow, large water bodies and depth-hoar. Lastly, for the validation stage, adding a shift parameter to all retrieval algorithms was found to be always necessary because of possibly different scatter-induced darkening (caused by

scattering albedo), which could arise even for snowpacks of the same thickness because snowpacks undergo different metamorphism in different years.

### *Acknowledgements*

*This project is partly funded by NSERC of Canada. A University of Alberta Ph.D. Scholarship also supports the first author. Dr. T. Carroll of the Airborne Gamma Radiation Survey Program of NWS-USA provided the gamma-ray spectrometer SWE data. The National Snow and Ice Data Center, University of Colorado, Boulder provided the 1988 and 1989 EASE-Grid SSM/I data of DMSP-F8; and the Global Hydrology Resource Center (GHRC) of USA provided the 1997 Swath SSM/I data of DMSP-F10 and F13. The High Plains Climate Center (HPCC), University of Nebraska provided the climate data for the study basin. Similarly, the total precipitable water vapor data was obtained from TIROS Operational Vertical Sounder and the land use and DEM data from USGS.*

## **References**

- Abdalati, W., and Steffen, K. (1998), Accumulation and hoar effects on microwave emission in Greenland and ice-sheet dry-snow zones. *J. Glaciol.* 44(148):523-531.
- Armstrong R., Chang, A., Rango, A., and Josberger, E. (1993), Snow depths and grain size relationships with relevance for passive microwave studies. *Ann. Glaciol.* 17:171-176.
- Chang, A., Foster, J. L. and Hall, D. K. (1996), Effects of forest on the snow parameters derived from microwave measurements during the boreal. *Hydrol. Proc.* 10:1565-1574.
- Chang, A.T.C., Foster, J. L., and Hall, D. K. (1987), Nimbus-7 SMMR derived global snow cover parameters. *Ann. Glaciol.* 9:39-44.

- Chang, A.T.C., Foster, J. L., Hall, D. K., Rango, A., and Hartline, B. K. (1982), Snow water equivalent accumulation by microwave radiometry. *Cold Regions Science and Technology*. 5(3):259-267.
- Chang, A. T. C., Gloersen, P., Schmugge, T., Wilheit, T. T., and Jwally, H. J. (1976), Microwave emission from snow and glacier ice. *J. Glaciol.* 16(74):23-39.
- Choudhury, B. J. (1993), Reflectivities of selected land surfaces types at 19 and 37 GHz from SSM/I observations. *Remote Sens. Environ.* 46:1-17.
- England A. W. (1975), Thermal microwave emission from a scattering layer. *J. Geophys. Res.* 80(32):4484-4496.
- Foster J. L., Chang, A. T. C., and Hall, D. K. (1997), Comparison of snow mass estimates from a prototype passive microwave snow algorithm, a revised algorithm and snow depth climatology. *Remote Sens. Environ.* 62:132-142.
- Friedman J. H., and Stuetzle, W. (1981), Projection pursuit regression, *Journal of the American Statistical Association*. 82:249-266.
- Friedman J. H. (1985), Classification and multiple regression through projection pursuit. *Technical Report LCS012*, Department of Statistics, Stanford University.
- Gan T. Y. (1996), Passive microwave snow research in Canadian high arctic. *Canadian Journal of Remote Sensing*. 22(1):36-44.
- Goodison B. E., and Walker, A. E. (1994), Canadian development and use of snow cover information from passive microwave satellite data. *ESA/NASA International Workshop*, 245-262.
- Goodison B. E., Rubinstein, I., Thirkettle, F. W., and Langham, E. J. (1986), Determination of snow water equivalent on the Canadian prairies using microwave radiometry. *IAHS Publ.* 155:163-173.
- Granger, R. J., and Gray, D. M. (1990), A net radiation model for calculating daily snowmelt in open environments. *Nordic Hydrology*. 21:217-237.

- Hallikainen M. T. (1989), Microwave radiometry on snow. *Adv. Space Res.* 9(1):267-275.
- Josberger, E. G., and Mognard, N. M.(1998), A passive microwave snow depth algorithm with a proxy for snow metamorphism. In: *Proceedings of the 4th International Workshop on Applications of Remote Sensing in Hydrology*, Santa Fe, New Mexico, USA.
- Matzler C. (1994), Passive microwave signatures of landscapes in winter. *Meteorol. Atmos. Phys.* 54:241-260.
- Morton S. C. (1989), *Interpretable projection pursuit*. Ph.D. thesis, Stanford University, USA, 109p.
- Neale C. M. U., McFarland, M. L., and Chang, K. (1990), Land-surface-type classification using microwave brightness temperatures from the special sensor microwave/imager. *IEEE Trans. Geosci. Remote Sens.*, 28(5):829-837.
- NWS (1992), Airborne gamma radiation snow survey program and satellite hydrology program: user's guide version 4.0. *Office of Hydrology, National Weather Service, NOAA, US Department of Commerce, Minneapolis, Minnesota.* 54p.
- Root H., and Aschbacher, J. (1989), On the use of satellite microwave radiometers for large-scale hydrology, *IAHS Publ.* 186:21-30.
- Tait A. (1998), Estimation of snow water equivalent using passive microwave radiation data. *Remote Sens. Environ.* 64:286-291.
- Ulaby, F. T., Moore, R. K., and Fung, A. K. (1986), *Microwave remote sensing: active and passive (Vol. III)*, Artech House, Inc., Dedham, Mass.
- Walker A. E., and Goodison, B. E. (1993), Discrimination of a wet snow cover using passive microwave satellite data. *Ann. Glaciol.* 17:307-311.
- Zwally H.J. (1977), Microwave emissivity and accumulation rate of polar firn. *J. Glaciol.*, 18(79):195-215.

Table 5.1. Ascending and descending equatorial overpass (local) times of the SSM/I data of three DMSP satellites used in this study.

Year	SSM/I	Overpass Time		Data Source/ Projection
		Ascending	Descending	
1988& 1989	DMSP F8	6:13	18:13	NSIDC, EASE-Grid
1997	DMSP F10	22:24	10:24	MSFC, Swath Data
1997	DMSP F13	17:46	5:46	MSFC, Swath Data

Table 5.2. Details of SWE estimated from airborne gamma-ray data

Year	1988	1989	1997
Total number of airborne data	65	241	192
Total gridded airborne data	52	175	197
Maximum SWE (cm)	11.80	15.70	21.8
Minimum SWE (cm)	0.00	3.30	1.00
Mean (cm)	3.49	9.29	12.44
Standard Deviation (cm)	2.73	2.43	4.02
Dry snow (screened) data <sup>+</sup>			
Total number	16	121	119
Maximum SWE (cm)	7.00	15.70	19.50
Minimum SWE (cm)	0.60	4.60	7.20
Mean (cm)	3.43	9.25	13.55
Standard Deviation (cm)	2.12	2.18	3.05

<sup>+</sup> Dry snow cases based on four criteria ( $V37 < 250$  K;  $V19 - V37 \Rightarrow 9$  K;  $V37 - H37 \Rightarrow 10$  K;  $p\_factor > 0.026$ )



Table 5.3. Physiographic and atmospheric data used in this study.

Data Type	Resolution/Climate division	Source
Land use Classification	1 km	USGS
DEM	1 km	USGS
Precipitation (100 yrs) (Table 4)	5 climate divisions (CD) of North Dakota and 3 CD of Minnesota	State Climatology Office, Minnesota
Air Temperature (Table 5.5) and snowfall (Figure 2) for 30 climate stations		High Plains Climate Center, University of Nebraska
Total Precipitable Water Vapor (TPW)	1 degree	TIROS Operational Vertical Sounder

Table 5.4. Coefficients derived for the Proposed Algorithms [Eqs. (5.6) and (5.7)].

Equation	Coefficients				
	1 <sup>st</sup>	2 <sup>nd</sup>	3 <sup>rd</sup>	4 <sup>th</sup>	5 <sup>th</sup>
6	0.2357	0.0064	4.0399	-0.0287	1.0825
7	0.1680	0.0052	-0.0028	11.9938	

Table 5.5. Weekly maximum and minimum air temperature (°C) of Red River Basin study area covering the airborne SWE data collection periods of 1988, 1989 and 1997.

Year	Month->	February				March				April			
		Week ->	1	2	3	4	1	2	3	4	1	2	3
1988	Max	-17.6	-13.3	-0.5	2.7								
	Min	-28.6	-24.6	-15.0	-10.3								
1989	Max	-19.0	-5.2	-13.5	-6.4	-11.7	1.5	-5.9	2.3	6.0			
	Min	-28.3	-17.6	-26.0	-18.7	-23.5	-5.5	-19.2	-5.3	-3.4			
1997	Max	-4.6	-7.5	-3.1	-5.3	-7.6	-4.4	-1.5	4.6	3.8	-0.5	10.2	
	Min	-14.9	-21.4	-16.4	-18.5	-20.0	-15.8	-14.3	-4.2	-4.9	-10.7	-1.7	

Table 5.6. Mean monthly and annual precipitation (cm) of Red River Basin.

Year / Month	Oct	Nov	Dec	Jan	Feb	Mar	Apr	D-M*	O-A#	Annual
100 yr.(Normal)	3.72	2.02	1.47	1.47	1.33	2.30	4.12	6.56	16.42	52.07
1987/88	0.94	1.22	1.35	2.26	0.41	2.39	0.58	6.40	9.14	40.13
1988/89	1.07	2.72	2.24	3.00	0.69	3.68	3.10	9.60	16.48	45.21
1996/97	5.82	4.50	2.72	3.53	0.97	3.23	5.99	10.44	26.75	56.64

\* D-M stands for December through March, and # O-A stands for October through April precipitation.

Table 5.7. Summary of calibration and validation results of proposed algorithms [Eqs. (5.6) to (5.8)]

Test Cases	Calibration(C)	Validation (V)		C & V (with SP)	C & V (without SP)
1. [Eq. 6]	Year: 1989	1988	1997	1989, 1988, 1997	1989, 1988, 1997
$R^2$	0.778	0.792	0.708	0.905	0.602
RMSE	1.121	1.123	3.467	2.273	10.969
SP	0	-5.00	+4.00	0, -5.00, 4.00	0, 0, 0
2. [Eq. 7]	Year: 1988	1989	1997	1988, 1989, 1997	1988, 1989, 1997
$R^2$	0.440	0.300	0.735	0.855	0.537
RMSE	2.110	4.088	3.161	3.480	12.387
SP	0	+5.00	+9.00	0, 5.00, 9.00	0, 0, 0
3. [Eq. 8]	Year: 1989	1988	1997	1989, 1988, 1997	1989, 1988, 1997
$R^2$	0.857	0.532	0.623	0.886	0.697
RMSE	0.735	2.147	4.428	3.263	8.090
SP	0	-5.00	+4.00	0, -5.00, 4.00	0, 0, 0

$R^2$  = Coefficient of Determination; RMSE = Root Mean Square Error (cm); and SP = Shift Parameter (cm)

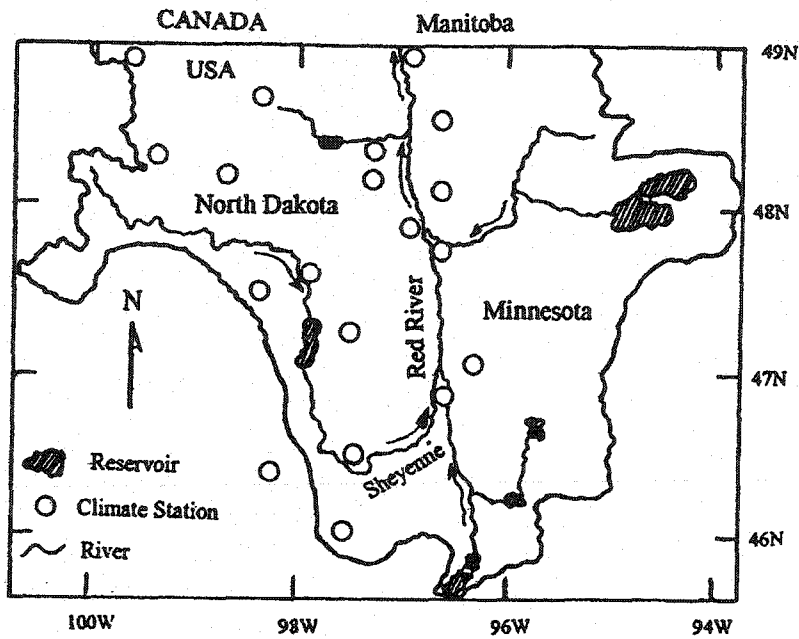


Figure 5.1 The Red River basin study area of eastern North Dakota and northwestern Minnesota

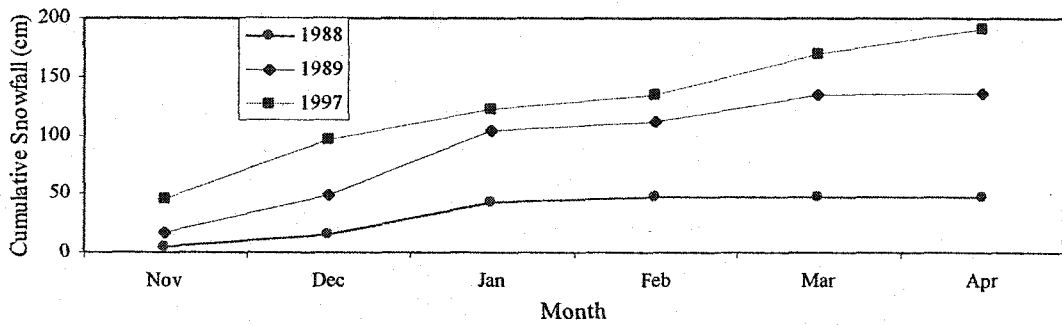


Figure 5.2 Cumulative snowfall at the end of each month for three winter periods of Red River Basin.

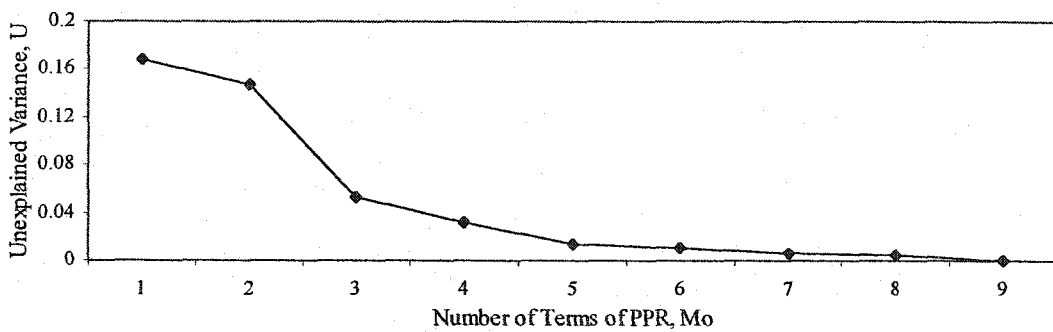


Figure 5.3 The calibration results for the projection pursuit regression model expressed in terms of the fraction of unexplained variance (U) versus the number of terms (Mo) using screened, ascending overpass SSM/I data of 1989.

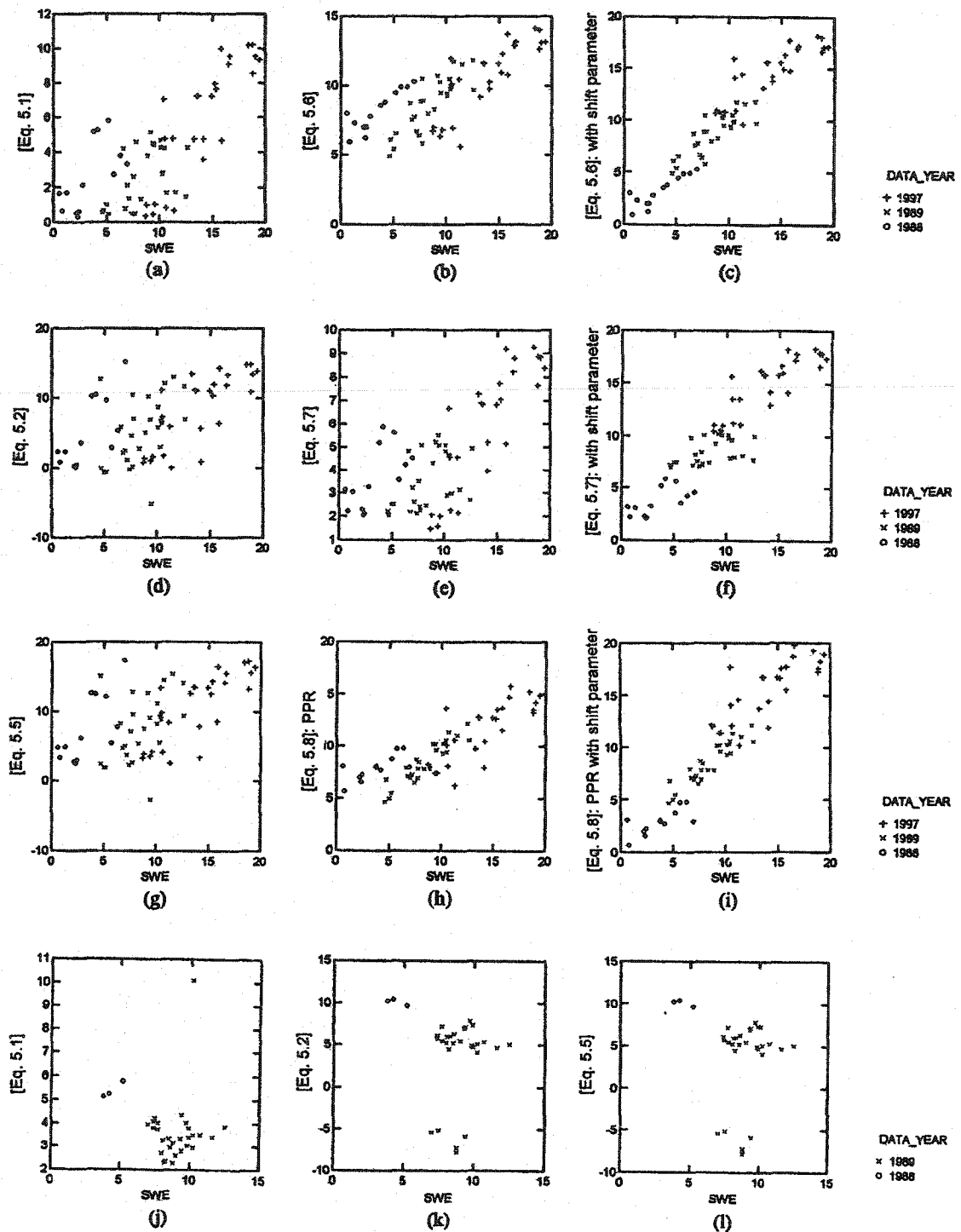


Figure 5.4 Plots of combined results (calibration and validation) of proposed algorithms without (b, e, h) and with shift parameters (c, f, i), and their comparisons with existing algorithms (a, d, g) based on screened, morning/nighttime overpass SSM/I data of 1988, 1989, and 1997. The three plots (j, k, l) of SWE derived from existing algorithms based on screened, evening overpass SSM/I data show very poor correlation with observed SWE.

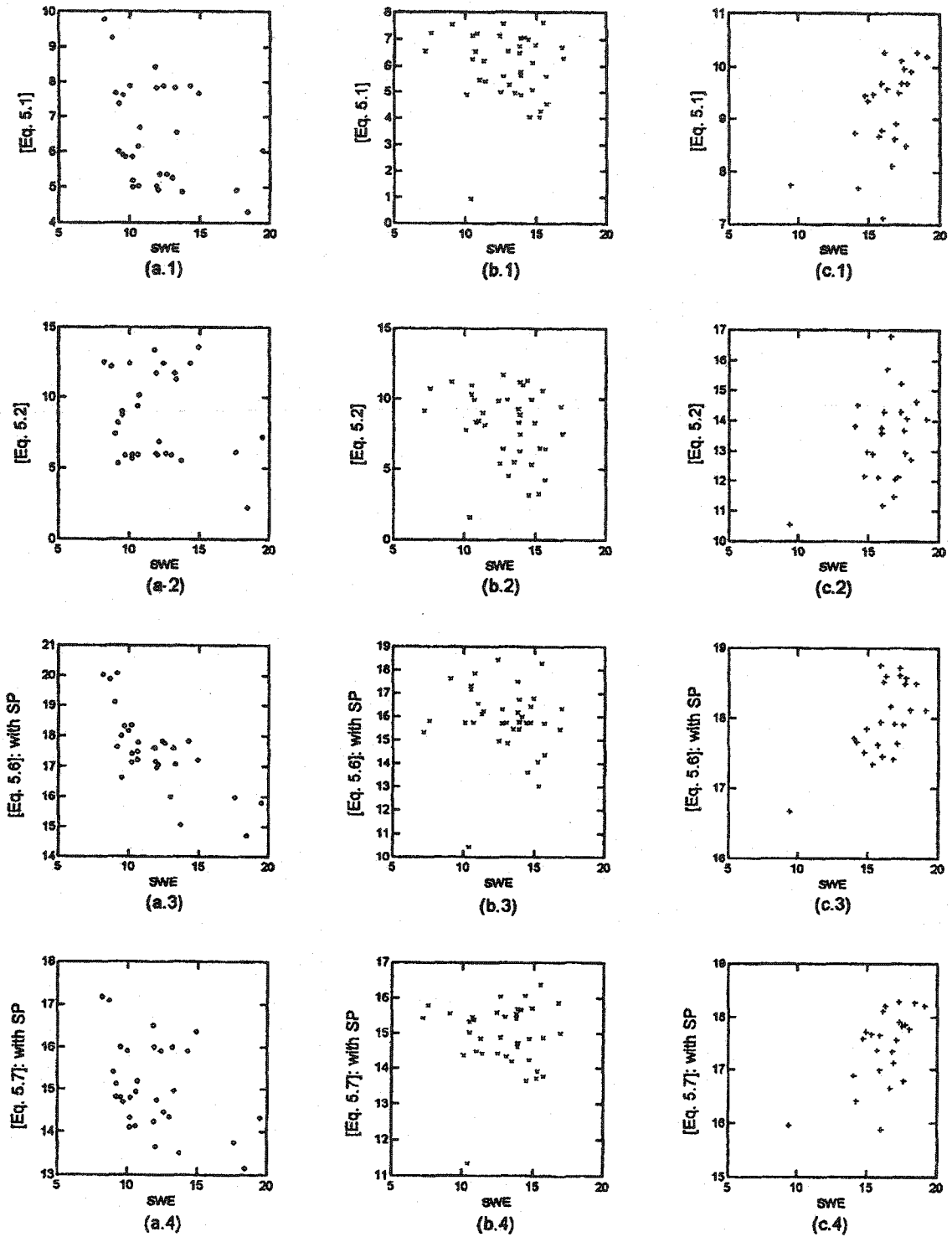


Figure 5.5 Scatterplots of observed SWE versus retrieved from 1997 TB data of DMSF F10, ascending (a.1 to a.4) and descending (b.1 to b.4), and DMSF-F13 descending (c.1 to c.4), based on existing (Eqs. 5.1 and 5.2) and proposed (Eqs. 5.6 and 5.7) algorithms. The fairly significant scatters found in all the plots are mainly attributed to SSM/I data only screened from wet snow cases but not cases affected by depth-hoar.

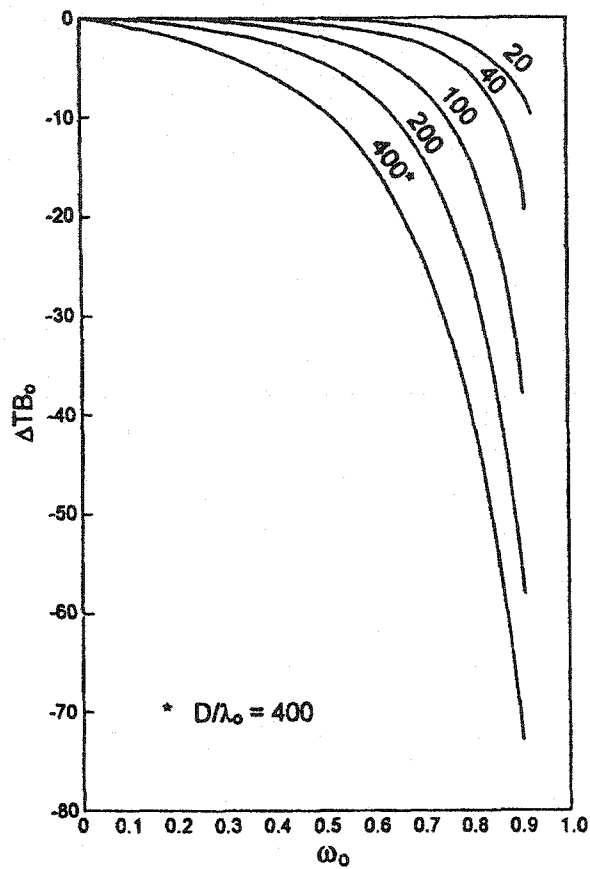


Figure 5.6 Scatter induced darkening ( $\Delta TB_0$ ) versus scattering albedo ( $\omega_0$ ) for various thicknesses ( $D$ ) of dry fresh snowpack at 273 K, a case of free space microwave wavelength ( $\lambda$ ) of 10 cm (adapted from England, 1975).

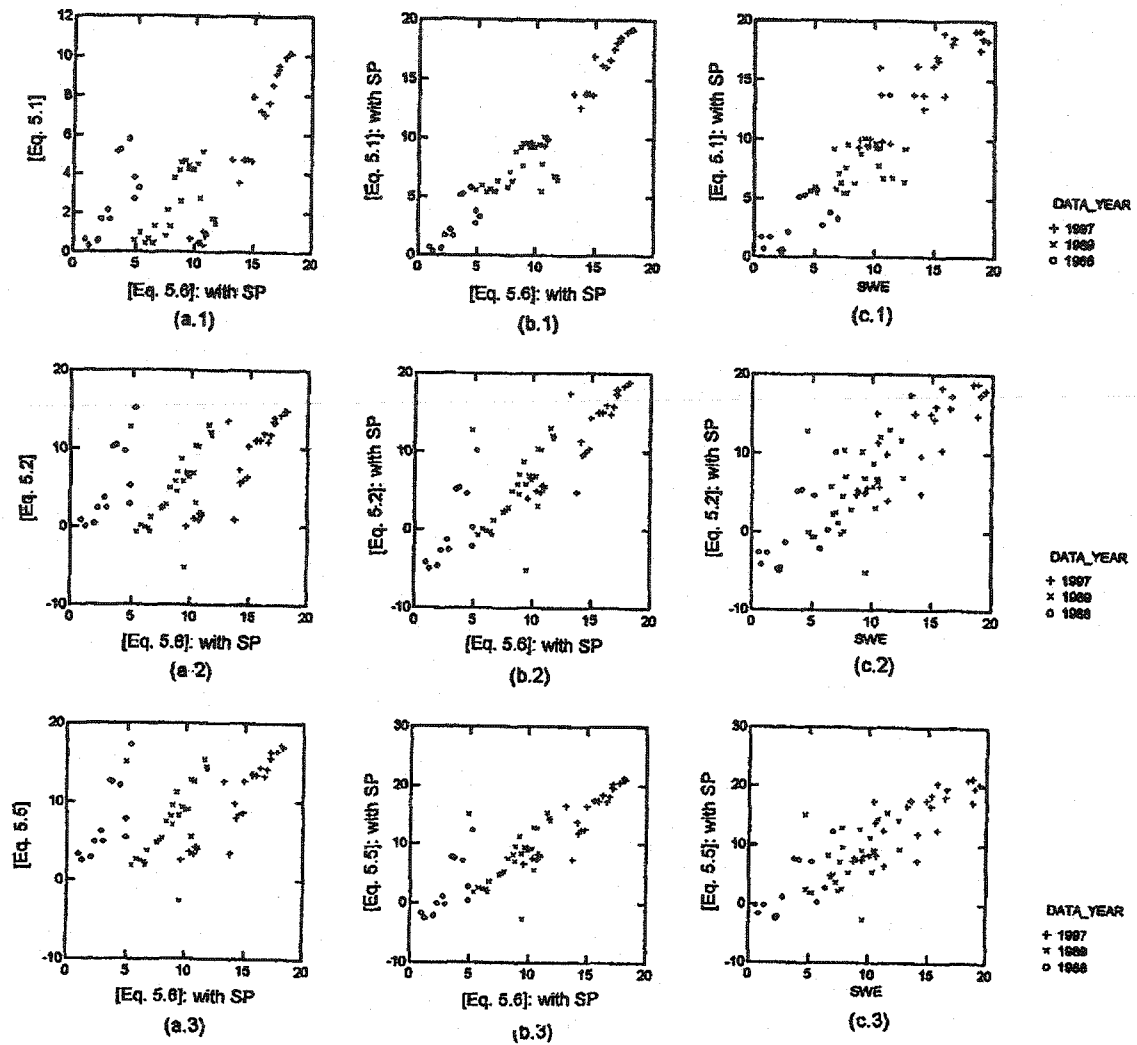


Figure 5.7 A marked improvement in the retrieved SWE of existing algorithms (Eqs. 5.1, 5.2 and 5.5) results when appropriate shift parameters (SP) are added (compare a.1 to a.3 with b.1 to b.3 plotted against Eq. 5.6, and c.1 to c.3 plotted against observed SWE). The SP used for Eq. (1) are 5cm for 1989 and 9cm for 1997 (as in Eq. 5.7) and that for Eqs. (5.2) & (5.5) are -5cm for 1988 and 4cm for 1997 (as in Eq. 5.6).



## **Chapter 6**

# **Summary, Conclusions and Recommendations for Future Works**

### **6.1 Summary and Conclusions**

Semi-distributed snowmelt model (SDSM), utilizing remotely sense data, models the basin scale snow accumulation and ablation processes by sub-dividing a basin as a number of sub-basins, each with its own land cover types and terrain features, and drained by a network of stream channels. SDSM models the snowmelt processes in either of the two methods, (1) the energy balance method (or SDSM-EBM), and (2) the modified temperature index method (or SDSM-MTI). The energy balance model considers (a) vertical energy exchange processes in open and forested area separately, (b) snowfall, canopy interception, fresh snow density, sublimation, refreezing, snow compaction, (c) snowmelt in terms of liquid and ice phases within the snowpack separately, (d) snow surface temperature simulation using either the force restore method, the surface conductance method, or the Kondo and Yamazaki method. A modified temperature index method (SDSM-MTI) using near surface soil and air temperature data was also developed to avoid the general excessive demand for data required by energy-balance snowmelt models. These SDSMs

(SDSM-EBM and SDSM-MTI) work within DPHM-RS (semi-distributed, physically based, hydrologic model using remotely sensed data), which accounts for the Hortonian, the saturation overland, and the subsurface runoff from each sub-basin, and routes them to the stream channel by an average, kinematic response function derived for each of the sub-basin, and then to the basin outlet using the Muskingum-Cunge method.

Both SDSM-EBM and SDSM-MTI were tested at the Paddle River Basin (PRB) of Alberta using three consecutive years of winter data 1997-98, 1998-99, and 1999-00. The models were calibrated using 1998-99 winter data (Nov 11, 1998 to May 16, 1999) and validated using the 1997-98 (Jan 1 to Apr 30, 1998) and 1999-00 (Jan 1 to Apr 30, 2000) winter data. Other than the “regulatory” effects of beaver dams (Woo and Waddington, 1990) that affected the validation results on simulated runoff, overall both SDSM-EBM and SDSM-MTI were able to simulate snowmelt runoff reasonably accurately at the basin outlet, SWE and snow depth in different land cover classes of PRB. In addition, SDSM-EBM could simulate reasonably accurate surface temperature in different land cover classes. The multi criteria results for both calibration and validation periods demonstrated that the SDSMs proposed in this study are capable of modeling basin-scale snow accumulation and ablation processes.

Although SDSM-EBM is relatively data intensive, it keeps track of both mass and energy components during both accumulation and ablation periods of snow melting. As ground-based point measurements are limited, SDSM-EBM was designed to take advantage of spatially distributed physiographic information such as the topography (DEM data), the land-use classification (using Landsat-TM data), and the spatially and temporally distributed geophysical parameters (e.g., LAI, albedo, and surface temperature data retrieved from NOAA-AVHRR data) that signify basin characteristics with respect to land use types of each sub-basin. This SDSM-EBM/DPHM-RS system can be used for studying the hydrological impact of land use changes and serves as a land surface component of a meso-scale atmospheric

model for climate change studies.

On the other hand, a less data intensive SDSM-MTI, also simulated accurate mass balance (snow depth, SWE, and runoff) during both accumulation and ablation periods of snowmelt. It seems that besides air temperature, the addition of near surface soil temperature in SDSM-MTI significantly improves the performance of the standard degree-day method to estimate snowmelt processes, thus eliminating the need for more detailed data needed in recent operational snowmelt models such as updating the depletion curve or the snowcovered area by remotely sensed data, or other site specific information, or the use of energy-budget method. Our results show that if reliable near surface soil temperature data are available, they should be utilized to model the snowmelt processes particularly if the degree-day approach is adopted.

Existing algorithms for retrieving snow water equivalent (SWE) from the Special Sensor Microwave/Imager (SSM/I) passive microwave brightness temperature data were also assessed and new algorithms that include physiographic and atmospheric data developed for the Red River basin of North Dakota and Minnesota (Singh and Gan, 2000). The frequencies of SSM/I data used are 19 and 37 GHz in both horizontal and vertical polarization. The corresponding airborne gamma-ray measurements of SWE for the years 1989, 1988, and 1997 provided the ground truth data for the algorithm development and validation. Encouraging calibration results are obtained for the algorithms using multivariate regression technique and dry snow cases of the 1989 and 1988 SSM/I data (from DMSP-F8). Similarly, validation results for data not used in calibration, e.g., 1988 (1989 as calibration data), 1989 (1988 as calibration data), and 1997 (from DMSP-F10 and F13), are also encouraging. The non-parametric, Projection Pursuit Regression (PPR) technique also gave good results in both stages. However, for the validation stage, adding a shift parameter to all retrieval algorithms was always necessary because of possibly different scatter-induced darkening (caused by scattering albedo), which could arise even for snowpacks of the same thickness because snowpacks undergo

different metamorphism in different winter years. Screening criteria are also proposed to eliminate SSM/I footprints affected by large water bodies and depth-hoar, another key step towards reliable SWE estimate from passive microwave data.

## 6.2 Recommendation for Future Works

Even though SDSM-EBM gave encouraging results in PRB of Alberta, fine-tuning important winter phenomena such as blowing snow, patchy snow cover etc. can further improve its performance in a Prairie environment. To adequately account for these phenomena, we need to collect certain meteorological data (e.g., wind speed, precipitation, net radiation) at different sub-basin and land cover classes. Some data, such as the surface temperature data could be retrieved from platforms such as NOAA-AVHRR. If substantial amount of the aforementioned data are available, parameterization schemes such as listed below could be developed or improved:

- (1) Develop plausible statistical relationships of wind speed between open area and forest areas in terms of LAI or the forest cover fraction ( $F_c$ ) in each of the forest types for the Prairies. This will be useful for simulating surface temperature in the forest cover area;
- (2) Test Beer's law for partitioning net radiation between canopy and bare soil observed in the open area. Most of the algorithms proposed are obtained using summer data where the net radiation data are always positive;
- (3) Develop functional relationships between the cold content of snowpack and patchy snowcover with the near surface soil temperature in each of the land cover classes separately.
- (4) Develop analytical procedure to account for possible refreezing of meltwater before it reaches the sub-basin or basin outlet.
- (5) Apply certain linear mixing models to determine the percentage composition of pixels in the image (snow, cloud, land fractions).
- (6) Test the blowing snow sublimation model of Dery and Yau (2001), built into SDSM-EBM for the Prairie environment.

These proposed efforts would be useful to better model the snow accumulation and ablation processes by the energy budget approach for the Prairies. The proposed modified degree-day approach (SDSM-MTI) should also be tested in other parts of the world subjected to seasonally snow covers particularly in regions of temperate climate. Furthermore, more work should be done to determine the optimum or adequate number of soil temperature and air temperature gauge stations needed to model the snowmelt processes reliably using SDSM-MTI under various climatic conditions (e.g., Dickinson, 1988; Granberg et al., 1999).

Lastly, it will be beneficial to validate the algorithms proposed to retrieve SWE from passive microwave SSM/I radiometry using data from various DMSP spacecrafts for different parts of the world. Similarly, the proposed screening criteria to eliminate SSM/I footprints affected by large water bodies and depth-hoar needs to be validated with extensive field observations.

## References

- Dickinson, R. E. (1988), The force-restore model for surface temperature and its generalizations. *Journal of Climate*, 1:1086-1097.
- Granberg, G., Grip, H., Löfvenius M. O., Sundh, I., and Svensson, B. H. (1999), A simple model for simulation of water content, soil frost, and soil temperatures in boreal mixed mires. *Water Resour. Res.*, 35(12):3771-3782.
- Singh, P. R., and Gan, T. Y. (2000), Retrieval of snow water equivalent using passive microwave brightness temperature data. *Remote Sens. of Environment*. 74(2): 275-286.
- Woo, M., and Waddington, J. M. (1990), Effects of beaver dams on subarctic wetland hydrology. *Arctic*, 43(3):223-230.
- Dery, S. J., and Yau, M. K. (2001), Simulation of blowing snow in the Canadian Arctic using a double-moment model. *Boundary-Layer Meteorol.*, 99:297-316.

## Appendix A

### Calibration of NOAA-AVHRR Data in Channels 1 and 2 for Albedo Retrieval

The visible (Channel 1,  $\approx 0.58\text{-}0.68\ \mu\text{m}$ ) and near-infrared (Channel 2,  $\approx 0.72\text{-}1.1\ \mu\text{m}$ ) channels of the AVHRR on the NOAA-14 spacecraft (launched on December 30, 1994) have no onboard calibration devices. This requires some other means of calibration to obtain the parameters like albedo or reflectance and radiance from the AVHRR level-1b image signal in counts on a 10-bit scale (also called  $C_{10}$ ). One of the calibration methods used is that of Rao and Chen (1996 and 1999), who proposed several algorithms to estimate albedo and radiance based on a 3-year (1995-1997) top-of-atmosphere albedo data over a calibration site. The algorithms proposed by Rao and Chen (1999) were used to calibrate channels 1 and 2 to obtain the albedo or reflectance in each of the channels. These reflectance values of channels 1 and 2 were also used to compute the NDVI and finally the LAI of land cover and corresponding forest cover fraction ( $f_c$ ) for the Paddle River Basin.

Albedo (%) from channel  $i$  ( $i = 1, 2$ ) is represented as,

$$\alpha_i = S_i (C_{10} - C_0) \rho_\alpha^2 \quad (\text{A.1})$$

where  $S_i$  is the slope and  $\rho^2$  is the square of earth-sun distance in astronomical units.  $S_i$  depends on the revised calibration, which is a function of elapsed time in orbit, expressed in days 'd' after the day of launch (Dec 30, 1994 for the NOAA-14 spacecraft).  $C_{10}$  is the AVHRR signal in counts on a 10-bit scale and the offset and  $C_0$  is the offset set equal to 41 in both channels 1 and 2.

$$\rho_\alpha^2 = (1.00011 + 0.34221\cos\theta + 0.001280\sin\theta + 0.000719\cos 2\theta + 0.000077\sin 2\theta)^{-1} \quad (\text{A.2})$$

Where,  $\theta$  (in degrees) =  $0.9863 \times n$ ,  $n$  being the Julian day of the year and the slopes  $S_1$  and  $S_2$  are,

$$\text{Channel 1: slope, } S_1 = 0.0000135d + 0.111 \quad (\text{A.3})$$

$$\text{Channel 2: slope, } S_2 = 0.0000133d + 0.134 \quad (\text{A.4})$$

Where,  $d$  is days after the launch of AVHRR onboard NOAA-14 spacecraft (Dec 30, 1994).

Alternatively, we could use the calibration coefficients given in the AVHRR Level-1b tape for channel 1 and 2 (between November 1996 until December 8, 1998) and then apply the correction factors  $CF_1$  and  $CF_2$  for each of the channels according to,

$$\text{Channel 1: } CF_1 = (1.015 - 8.8 \times 10^{-5}d + 1.3 \times 10^{-8}d^2) \quad (\text{A.5})$$

$$\text{Channel 2: } CF_2 = (1.037 - 1.8 \times 10^{-4}d + 3.2 \times 10^{-8}d^2) \quad (\text{A.6})$$

## References

- Rao, C. R. N. and Chen, J. (1996), Post-launch calibration of the visible and near-infrared channels of the Advanced Very High Resolution Radiometer on the NOAA-14 spacecraft. *Int. J. Remote Sensing*, 17:2743-2747.
- Rao, C. R. N. and Chen, J. (1999), Revised post-launch calibration of the visible and near-infrared channels of the Advanced Very High Resolution Radiometer (AVHRR) on the NOAA-14 spacecraft. *Int. J. Remote Sensing*, 20:3485-3491.

## Appendix: B

### Stability of the Atmosphere

In a 1-D modeling, the turbulent flux at the surface boundary (a few meters in height) is assumed not converging or diverging, and so it should have a constant bulk transfer coefficient independent of height and based on the measured vertical fluxes Kondo and Yamazawa (1986) obtained values of  $C_h = 0.002$  and  $C_e = 0.0021$  over a flat snow surface at a reference height of 1 m and suggested that they are practically independent of wind speed. Kondo and Yamazaki (1990) and Yamazaki (1998) use these coefficients in their single and multi-layer snowmelt models respectively.

From comparing several turbulent transfer expression in a logarithmic boundary layer, Brutsaert (1982) derive the  $C_h$  (or  $C_e$ ) equation under neutral condition ( $C_n$ ),

$$C_h = C_e = C_n = \frac{k^2}{[\ln((z_r - d_o)/z_o)]^2} \quad (\text{B.1})$$

where  $k$  is von Karman's constant ( $\approx 0.4$ ),  $z_r$  the reference height,  $d_o$  the zero-plane displacement height (assumed equal to snow depth in SDSM). The roughness height,  $z_o$  is related to the mean obstacle or the mean vegetation height,  $h_o$  by  $h_o/z_o = (7.35 \text{ to } 8)$  (Brutsaert, 1982). In SDSM,  $h_o/z_o$  is assumed as 7.6.



Under neutral conditions, the turbulent motion is essentially a combination of round shaped eddies, when subjected to a temperature gradient near the surface, these eddies would experience buoyancy effects that may enhance or dampen the turbulent transfers giving rise to unstable or stable atmospheric conditions respectively. For unstable conditions, the potential temperature decreases with height, and an uplifted air mass is subjected to the buoyancy force, since the moving air parcel has a lower density than the surrounding air. Similarly, an air mass moving downward is subjected to further acceleration. In stable conditions, the potential temperature increases with height, and the velocity profile is compressed vertically since a vertically moving air mass is subjected to a buoyancy generated restoring force (Nakawo and Hayakawa, 1998).

Unstable conditions often occur over open area under strong solar radiation and weak winds while stable conditions are frequently observed during nights with clear skies. The atmosphere is mostly stable throughout the day during melting season, since the surface temperature is not above 0°C. Enhanced or dampened vertical movement of air masses tends to increase or decrease turbulent fluxes, which should be considered in hydrological models. This effect can be quantified in terms of the Richardson number ( $R_{iB}$ ) or the Monin-Obukhov length ( $L_{mo}$ ). The most commonly used dimensionless  $R_{iB}$  is

$$R_{iB} = \frac{g}{T} \frac{dT/dz_r}{(dV/dz_r)^2} \approx \frac{g(T_a - T_s)z_r}{V^2 T_a} \quad (B.2)$$

where  $g$  is the acceleration due to gravity ( $m/s^2$ ) and temperatures are in °K. Though  $R_{iB}$  is one of the most widely used stability parameter, there is no single criteria in its application.

Following three approaches are found to be extensively used for stability correction in snowmelt models. Price and Dunne (1976) proposed the following adjustment for

the atmospheric stability, which is used by Bathurst and Cooley (1996) in their snowmelt component of distributed hydrologic model "SHE".

$$C_{adj} = C_n (1 - 10 R_{iB}) \quad (R_{iB} < 0, \text{ Unstable condition}) \quad (\text{B.3a})$$

$$C_{adj} = \frac{C_n}{(1 + 10 R_{iB})} \quad (R_{iB} > 0, \text{ Stable condition}) \quad (\text{B.3b})$$

Application of this approach gave some unreasonable correction factors in Tarboton and Luce (1996). Kane et al. (1997) used the same correction factor but there was no discussion on its effectiveness.

Another stability correction factor proposed by Louise (1979) has also been used in some snowmelt models (e.g. Liston, 1995) as given below,

$$C_{adj} = C_n \left( 1 - \frac{9.4 R_{iB}}{1 + \gamma |R_{iB}|^{1/2}} \right) \quad (R_{iB} < 0, \text{ Unstable condition}) \quad (\text{B.4a})$$

$$C_{adj} = C_n (1 + 4.7 R_{iB})^{-2} \quad (R_{iB} > 0, \text{ Stable condition}) \quad (\text{B.4b})$$

$$\gamma = 49.82 k^2 \left[ \ln \left( \frac{z_r - d_0}{z_o} \right) \right]^{-2} \left( \frac{z_r - d_0}{z_o} \right)^{1/2} \quad (\text{B.4c})$$

Similarly, Kustas et al. (1994) has shown the use of stability correction factor of Morris (1989) as,

$$C_{h,adj} = C_n (1 - 58 R_{iB})^{0.25} \quad (R_{iB} < 0, \text{ Unstable condition}) \quad (\text{B.5a})$$

$$C_{h,adj} = C_n (1 + 10 R_{iB})^{-0.1} \quad (R_{iB} > 0, \text{ Stable condition}) \quad (\text{B.5b})$$

$$C_{e,adj} = 0.5 C_{h,adj} \quad (\text{B.5c})$$

where  $C_{h,adj}$  and  $C_{e,adj}$  are adjusted bulk transfer coefficient for sensible heat and latent heat respectively.

## References

Bathurst, J. C., and Cooley, K.R. (1996), Use of the SHE hydrological modeling system to investigate basin response to snowmelt at Reynolds Creek, Idaho, *J. Hydrol.*, 175:181-211.

- Brutsaert, W. (1982), *Evaporation into the Atmosphere*. D. Reidel Pub. Co., Dordrecht, Holland, 299p.
- Kane, D. L., Gieck, R. E., and Hinzman, L. D. (1997), Snowmelt modeling at small Alaskan arctic watershed. *J. of Hydrologic Engineering*, 2(4):204-210.
- Kondo J., and Yamazaki, T. (1990), A Prediction Model for Snowmelt, Snow Surface Temperature and Freezing Depth Using a Heat Balance Method. *J. of Appl. Meteor.*, 29:375-384.
- Kondo J., and Yamazawa, H. (1986), Bulk transfer coefficient over a snow surface. *Boundary layer Meteor.*, 34:123-135.
- Kustas, W. P., Rango, A., and Uijlenhoet, R. (1994), A simple energy budget algorithm for the snowmelt runoff model. *Water Resour. Res.*, 30(5):1515-1527.
- Liston, G. E. (1995), Local advection of momentum, heat, and moisture during the melt of patchy snow covers. *J. Appl. Meteorol.*, 34:1705-1715.
- Louice, J. F. (1979), A parametric model of vertical eddy fluxes in the atmosphere. *Bound. Layer Meteor.*, 66:281-301.
- Nakawo M., and N. Hayakawa, 1998 (Ed.). Snow and ice science in hydrology: The IHP training course on snow hydrology. *Institute of Hydrospheric-Atmospheric Sciences (IHAS)*, Nagoya University, 133p.
- Morris, E. M. (1989), Turbulent transfer over snow and ice, *J. Hydrol.*, 105:205-223.
- Price, A. G. and T. Dunne, 1976. Energy balance computations of snowmelt in a subarctic area. *Water Resour. Res.*, 12(4):686-694.
- Tarboton D. G., and Luce, C. H. (1996), Utah Energy Balance Snow Accumulation and Melt Model (UEB), Computer model technical description and user's guide prepared by *Utah Water Research Laboratory*. Utah State University and USDA Forest Service, Intermountain Research Station, 64p.
- Yamazaki, T. (1998), A multi-layer heat balance model of snow cover – simulations in Siberia and plans. In: Proc. of second international workshop on energy and water cycle in GAME, Siberia, pp 161-168.

## **Appendix C**

### **Surface Physical Parameters derived from AVHRR Data**

This appendix includes three tables: (1) the surface albedo, (2) the leaf area index or LAI, and (3) the surface temperature, retrieved from AVHRR data of the NOAA-14 spacecraft for different land cover (coniferous forest, mixed forest and open area) of Paddle River Basin during the study periods of 1997-98, 1998-99, and 1999-00 winters.

## C.1 Surface Albedo

Table C.1 AVHRR derived average surface albedo for three different land cover classes used in SDSM for 1997-98, 1998-99, and 1999-00 winters.

Date	Coniferous	Mixed/Deciduous	Open	Date	Coniferous	Mixed/Deciduous	Open
11/1/97	0.2602	0.2555	0.2738	10/24/99	0.6002	0.6008	0.6219
12/25/97	0.5006	0.5012	0.5113	12/03/99	0.7943	0.7920	0.8112
1/2/98	0.6223	0.6110	0.6869	01/15/00	0.8796	0.8546	0.9000
1/5/98	0.6421	0.6342	0.7521	01/22/00	0.8183	0.8074	0.8999
1/12/98	0.5742	0.5326	0.6458	01/24/00	0.6391	0.6089	0.7288
1/21/98	0.4795	0.4663	0.5563	01/30/00	0.6735	0.6621	0.7477
2/3/98	0.3885	0.3564	0.4704	02/04/00	0.4546	0.4290	0.5501
2/17/98	0.3531	0.3404	0.4253	02/06/00	0.6085	0.6050	0.6593
2/27/98	0.4890	0.4602	0.4325	02/16/00	0.5126	0.4987	0.5948
3/7/98	0.4762	0.4485	0.5590	02/18/00	0.5433	0.5098	0.6426
3/10/98	0.4419	0.4157	0.5283	02/25/00	0.4340	0.4176	0.4916
3/17/98	0.3500	0.3356	0.3965	03/04/00	0.3562	0.3561	0.3751
3/29/98	0.1702	0.1767	0.1805	03/15/00	0.4818	0.4825	0.5541
4/6/98	0.1822	0.1824	0.1877	04/02/00	0.1858	0.1837	0.1946
4/18/98	0.1365	0.1328	0.1438	04/08/00	0.2503	0.2488	0.2653
4/30/98	0.1896	0.1916	0.2063	04/18/00	0.1843	0.1829	0.1927
10/22/98	0.2139	0.2071	0.2270	2/10/99	0.5500	0.5368	0.6312
11/26/98	0.6822	0.6272	0.7185	2/15/99	0.4188	0.4130	0.5139
12/7/98	0.5638	0.5704	0.5880	2/25/99	0.4551	0.4225	0.5181
12/14/98	0.6927	0.6714	0.7787	3/2/99	0.4773	0.3811	0.5472
12/23/98	0.7137	0.6890	0.8154	3/9/99	0.5029	0.4722	0.5901
1/1/99	0.6917	0.6594	0.7808	3/11/99	0.4326	0.4291	0.5027
1/6/99	0.6812	0.6299	0.7766	3/22/99	0.4183	0.4193	0.4966
1/17/99	0.6158	0.5757	0.6768	3/28/99	0.4300	0.4251	0.5098
1/23/99	0.6448	0.6002	0.7463	3/31/99	0.3819	0.3683	0.4548
1/29/99	0.4922	0.4714	0.6043	4/15/99	0.3022	0.3023	0.3356
2/3/99	0.5340	0.5221	0.5623	4/24/99	0.1789	0.1765	0.1857

## C.2 Vegetation Index in the form of LAI

Table C.2 AVHRR derived average LAI for three different land cover classes used in SDSM for 1997-98, 1998-99, and 1999-00 winters.

Date	Coniferous	Mixed/Deciduous	Open	Date	Coniferous	Mixed/Deciduous	Open
11/1/97	1.0090	0.5291		10/24/99	0.9181	0.4903	
12/25/97	0.8516	0.4448		12/03/99	0.8269	0.4305	
01/02/98	0.8911	0.4759		01/15/00	0.8291	0.4346	
01/05/98	0.8465	0.4424		01/22/00	0.8015	0.4211	
01/12/98	0.8392	0.4389		01/24/00	0.7904	0.4145	
01/21/98	0.8304	0.4399		01/30/00	0.8356	0.4418	
02/3/98	0.7840	0.4124		02/04/00	0.8425	0.4449	
02/17/98	0.8619	0.4541		02/06/00	0.7550	0.3947	
02/27/98	0.7969	0.4214		02/16/00	0.8780	0.4725	
03/7/98	0.7954	0.4133		02/18/00	0.8115	0.4287	
03/10/98	0.7512	0.3902		02/25/00	0.8907	0.4815	
03/17/98	0.7816	0.4082		03/04/00	0.9507	0.5080	
03/29/98	1.0251	0.5231		03/15/00	0.7102	0.3639	
04/6/98	0.9557	0.5020		04/02/00	1.0774	0.5866	
04/18/98	1.2030	0.6653		04/08/00	0.9898	0.5287	
04/30/98	1.3567	0.7601		04/18/00	1.0873	0.5856	
10/22/98	1.0020	0.5178		2/10/99	0.8808	0.4701	
11/26/98	0.7713	0.4060		2/15/99	0.7826	0.4042	
12/7/98	0.7473	0.3867		2/25/99	0.7024	0.3636	
12/14/98	0.8145	0.4252		03/02/99	0.7837	0.4120	
12/23/98	0.8245	0.4287		03/09/99	0.7562	0.3921	
01/01/99	0.7722	0.3993		03/11/99	0.7720	0.4031	
01/06/99	0.7992	0.4122		03/22/99	0.6776	0.3414	
01/17/99	0.8336	0.4387		03/28/99	0.7524	0.3837	
01/23/99	0.7999	0.4148		03/31/99	0.6585	0.3317	
01/29/99	0.7836	0.4074		04/15/99	0.7664	0.3880	
02/03/99	0.7885	0.4133		04/24/99	1.1437	0.6107	

### C.3 Surface Temperature

Table C.3 AVHRR derived average surface temperature (°K) for different land cover classes used in SDSM for 1997-98, 1998-99, and 1999-00 winters.

Date	Coniferous	Mixed/Deciduous	Open	Date	Coniferous	Mixed/Deciduous	Open
11/1/97	277.70	278.01	278.78	10/24/99	279.06	279.38	281.12
12/25/97	266.48	268.65	271.23	12/03/99	262.36	264.60	266.70
1/2/98	238.33	240.96	241.76	01/15/00	239.76	242.05	243.39
1/5/98	242.65	243.36	244.41	01/22/00	254.28	257.19	258.81
1/12/98	247.94	248.96	247.05	01/24/00	258.19	260.62	261.97
1/21/98	256.26	259.48	258.72	01/30/00	263.78	265.96	266.77
2/3/98	263.90	265.95	265.08	02/04/00	264.37	265.90	266.27
2/17/98	271.28	272.23	272.76	02/06/00	259.05	261.39	261.50
2/27/98	261.59	264.39	267.04	02/16/00	261.15	263.00	264.33
3/7/98	255.70	256.92	257.14	02/18/00	261.10	264.09	264.82
3/10/98	258.42	258.64	258.54	02/25/00	269.03	270.61	272.04
3/17/98	271.58	271.98	271.88	03/04/00	272.69	273.10	274.52
3/29/98	283.04	281.61	281.43	03/15/00	263.83	264.99	264.74
4/6/98	273.96	276.22	277.40	04/02/00	284.50	282.64	283.91
4/18/98	298.47	295.56	295.30	04/08/00	282.61	282.20	283.74
4/30/98	304.90	301.93	300.64	04/18/00	291.42	290.63	291.52
10/22/98	288.02	289.22	289.12	2/10/99	258.45	260.40	258.17
11/26/98	266.96	268.71	269.23	2/15/99	265.72	266.75	267.78
12/7/98	256.28	258.21	258.59	2/25/99	273.56	273.99	273.87
12/14/98	260.90	262.96	265.02	3/2/99	268.67	269.94	269.44
12/23/98	244.22	246.64	248.42	3/9/99	263.49	266.74	264.49
1/1/99	246.97	249.07	250.16	3/11/99	266.67	267.51	266.50
1/6/99	240.12	243.10	242.75	3/22/99	276.95	276.65	274.94
1/17/99	253.04	256.54	257.09	3/28/99	271.63	271.75	272.40
1/23/99	244.53	246.49	246.96	3/31/99	272.77	273.08	272.62
1/29/99	259.60	261.25	261.16	4/15/99	280.90	281.02	281.03
2/3/99	246.18	248.02	250.10	4/24/99	302.89	302.27	300.48

## **Appendix D**

### **Historical Snow Course Data and Climate Trends**

This appendix includes two tables showing the history of snow course data in two of the stations in the study area. Another two tables show the ranking of regional precipitation and temperature departure for the period 1948-2000 according to the Climate Trends and Variations Bulletin for the Northwest forest, the Prairies, and the Mackenzie District of Canada.



Table D.1 Statistics of snow course data for Paddle River Headwaters snow pillow site.

		STATION PADDLE RIVER H.W.				ID CODE 15V08												
		BASIN ATHABASCA				DATA SOURCE ALBERTA ENVIRONMENT												
		LATITUDE 53D 52M 14S		LONGITUDE 115D 32M 36S		ELEVATION 855		METRES										
		REMARKS																
YEAR	JAN 1			FEB 1			MAR 1			MAR 15			APR 1			APR 15		
	DATE	DEPTH CM	SWE MM	DATE	DEPTH CM	SWE MM	DATE	DEPTH CM	SWE MM	DATE	DEPTH CM	SWE MM	DATE	DEPTH CM	SWE MM	DATE	DEPTH CM	SWE MM
1993				Jan-29	26	39	Feb-24	21	42				Mar-29	8	27			
1994	Dec-30	8	15	Feb-01	49	117	Mar-02	60	134				Mar-29	39	123			
1995				Feb-02	26	54	Feb-28	28	70				Mar-28	27	69			
1996							Feb-29	49	134				Mar-27	40	125			
1997				Feb-04	54	134	Feb-26	56	128				Mar-25	59	166			
1998				Jan-29	15	21	Feb-25	11	15				Mar-31	7	15			
1999				Jan-28	54	112	Mar-02	63	137				Mar-30	64	155			
2000				Feb-01	9	13	Feb-28	11	15				Mar-28	4	10			
NO. YRS.			1			7			8									8
AVERAGE		8	15		34	80		38	87				30	88				
MEDIAN			15			54			99									96
MAX.W.E.	1994		15	1997		134	1999		137				1997		166			
MIN.W.E.	1994		15	2000		13	1998 & 2000		15				2000		10			
ST. DEV.																		

NOTE: 1. STANDARD DEVIATION IS COMPUTED ONLY IF TEN YEARS OF DATA ARE AVAILABLE.  
 2. WHERE NO DEPTH IS SHOWN WATER EQUIVALENT IS ESTIMATED FROM THE PILLOW SITE.

(Source: Alberta Environment)

Table D.2 Statistics of snow course data for Mayerthorpe snow pillow site.

YEAR	JAN 1			FEB 1			MAR 1			MAR 15			APR 1			APR 15		
	DATE	DEPTH	SWE	DATE	DEPTH	SWE	DATE	DEPTH	SWE	DATE	DEPTH	SWE	DATE	DEPTH	SWE	DATE	DEPTH	SWE
	CM	MM		CM	MM		CM	MM		CM	MM		CM	MM		CM	MM	
1982				Feb-01	64	114	Feb-26	60	114	Mar-15	71	152	Mar-30	57	150	Apr-08	61	157
1983				Jan-24	15	23	Mar-02	22	36	Mar-15	30	51	Mar-29	21	59			
1984				Feb-03	30	43	Feb-28	31	54	Mar-15	37	71	Mar-29	6	18			
1985				Feb-06	50	80	Feb-27	48	108	Mar-14	41	100	Mar-29	36	95			
1986				Jan-29	19	38	Feb-25	20	38	Mar-18	20	58	Apr-02	3	8			
1987				Jan-27	14	33	Mar-03	21	39				Mar-31	9	30			
1988							Mar-01	14	32	Mar-16	0	0	Mar-30	0	0			
1989				Feb-06	31	52	Mar-01	31	52				Mar-31	25	71			
1990				Jan-31	29	54	Feb-27	27	65				Mar-28	4	10			
1991				Feb-01	39	69	Feb-27	38	89				Mar-27	34	95			
1992				Jan-29	40	81	Mar-04	34	95				Apr-02	0	0			
1993				Jan-29	25	41	Feb-24	29	46				Mar-29	7	25			
1994							Mar-02	56	126				Mar-29	36	140			
1995							Feb-28	27	57				Mar-28	12	41			
1996							Feb-29	54	138				Mar-27	47	144			
1997							Feb-26	52	119				Mar-25	48	130			
1998							Feb-25	12	15				Mar-31	0	0			
1999							Mar-02	55	118				Mar-30	46	112			
2000							Feb-28	13	18				Mar-28	3	8			
NO. YRS.						11			19			6			19			1
AVERAGE					32	57		34	75		33	72		20	63		61	157
MEDIAN						52			57			65			41			157
MAX. SWE				1982		114		1996	138		1982	152		1982	150		1982	157
MIN. SWE				1983		23		1998	15		1988	0		1988	0		1982	157
ST. DEV.					15	27		15	38					19	55			

NOTE: 1. STANDARD DEVIATION IS COMPUTED ONLY IF TEN YEARS OF DATA ARE AVAILABLE.  
 2. WHERE NO DEPTH IS SHOWN WATER EQUIVALENT IS ESTIMATED FROM THE PILLOW SITE.

(Source: Alberta Environment)

Table D.3 Regional precipitation and temperature departure for the period 1948-2000

(a) Winter regional precipitation departures ranked from wettest to driest

Rank	Northwest Forest		Prairies		Mackenzie Dist.	
	Year	Departure	Year	Departure	Year	Departure
1	1956	44.5	1956	40.6	1962	70.1
2	1948	29.3	1948	37.6	1963	68.8
3	1963	26.0	1974	34.5	1964	27.4
4	1954	24.9	1951	32.5	1959	26.0
5	1962	22.1	1969	32.2	1958	21.8
6	1958	19.7	1954	26.4	1987	20.6
7	1974	19.5	1972	22.7	1991	19.0
8	1950	16.4	1965	21.8	1975	17.6
9	1965	14.8	1950	18.1	1961	16.4
10	1972	13.9	1962	16.3	1957	15.8
11	1967	13.8	1957	13.7	1974	14.7
12	1959	13.6	1949	11.5	1985	14.1
13	1971	8.6	1952	9.0	1968	10.9
14	1949	6.7	1976	3.6	1960	10.4
15	1961	5.3	1989	3.4	1983	9.9
16	1955	4.0	1994	1.4	1992	8.5
17	1951	3.0	1953	-0.5	1973	4.6
18	1982	1.3	1960	-1.1	1956	3.4
19	1990	0.2	1996	-1.2	1976	3.3
20	1969	-0.1	1978	-2.9	1971	3.0
21	1976	-0.6	1963	-3.0	1984	-0.1
22	1957	-2.4	1980	-4.9	1977	-3.1
23	1994	-2.7	1971	-5.1	1955	-3.2
24	1973	-3.0	1997	-8.3	1948	-4.1
25	1997	-3.6	1961	-8.9	1990	-4.5
26	1968	-3.9	1967	-9.7	1986	-4.7
27	1953	-4.1	1955	-10.2	1950	-6.2
28	1981	-4.5	1970	-12.0	1967	-7.6
29	1992	-4.6	1966	-13.1	1952	-8.0
30	1977	-8.0	1999	-13.8	1970	-12.2
31	1988	-10.0	1975	-13.9	1988	-12.2
32	1983	-12.2	1991	-15.5	1998	-12.2
33	1996	-12.3	1982	-15.7	1996	-13.4
34	1952	-14.5	1964	-17.0	1995	-14.6
35	1987	-15.7	1968	-17.0	1994	-14.9
36	1979	-16.3	1990	-18.8	1954	-15.3
37	1995	-18.1	1958	-19.1	1993	-15.9
38	1975	-18.3	1959	-23.0	1999	-17.3
39	1991	-19.5	2000	-25.1	1966	-17.4
40	1966	-19.6	1981	-25.6	1972	-18.7
41	1964	-20.0	1985	-25.8	1951	-19.5
42	1986	-20.2	1979	-27.5	1953	-19.8
43	1980	-20.7	1986	-29.5	1981	-21.2
44	1985	-20.9	1998	-32.4	2000	-21.4
45	1999	-24.5	1977	-33.3	1965	-22.8
46	1960	-25.6	1973	-33.7	1997	-23.2
47	2000	-27.5	1992	-36.2	1949	-26.0
48	1970	-28.0	1983	-37.8	1982	-26.0
49	1984	-28.9	1993	-39.8	1980	-26.6
50	1998	-31.5	1995	-42.2	1989	-28.5
51	1989	-32.8	1987	-46.3	1978	-40.8
52	1993	-41.9	1984	-47.9	1969	-42.5
53	1978	-43.1	1988	-48.0		

(source: Climate Trends and Variations Bulletin for Canada)

(b) Winter regional temperature departures ranked from warmest to coolest.

Rank	Northwest Forest		Prairies		Mackenzie Dist.	
	Year	Departure	Year	Departure	Year	Departure
1	1987	7.6	1987	7.0	1987	6.7
2	1998	5.7	1992	5.9	2000	4.8
3	1992	4.5	1998	5.0	1998	4.5
4	2000	4.1	1983	4.6	1999	4.4
5	1964	4.0	1981	3.9	1980	4.2
6	1977	3.9	1958	3.9	1995	4.0
7	1986	3.7	2000	3.8	1981	3.8
8	1960	3.7	1961	3.8	1993	3.7
9	1981	3.3	1964	3.4	1977	3.3
10	1961	3.2	1986	3.2	1986	3.3
11	1955	2.9	1953	3.1	1989	3.0
12	1953	2.8	1988	3.0	1988	3.0
13	1995	2.8	1976	2.8	1970	2.7
14	1988	2.7	1977	2.8	1948	2.7
15	1980	2.7	1955	2.7	1953	2.7
16	1984	2.6	1990	2.6	1960	2.6
17	1983	2.4	1960	2.5	1997	2.3
18	1999	2.4	1999	2.5	1964	2.1
19	1970	2.3	1995	2.4	1978	1.7
20	1975	2.3	1954	2.4	1961	1.7
21	1989	2.0	1984	2.1	1992	1.5
22	1958	2.0	1991	1.8	1968	1.2
23	1948	1.5	1975	1.8	1996	1.0
24	1976	1.4	1963	1.4	1955	0.8
25	1991	1.2	1980	1.4	1991	0.7
26	1993	1.0	1970	1.3	1984	0.7
27	1954	0.9	1968	1.0	1973	0.7
28	1968	0.8	1973	0.9	1963	0.4
29	1990	0.4	1948	0.7	1954	0.2
30	1973	0.4	1989	0.5	1958	0.2
31	1997	0.3	1967	0.1	1959	-0.1
32	1963	0.2	1974	-0.6	1975	-0.2
33	1967	-0.4	1957	-0.9	1967	-0.3
34	1957	-0.8	1994	-1.0	1951	-0.3
35	1978	-0.8	1993	-1.1	1957	-0.3
36	1985	-1.0	1997	-1.1	1983	-0.4
37	1996	-1.1	1959	-1.2	1974	-1.0
38	1951	-1.2	1985	-1.2	1985	-1.0
39	1959	-1.3	1951	-1.2	1976	-1.0
40	1994	-1.3	1952	-1.4	1982	-1.2
41	1974	-1.8	1971	-1.7	1994	-1.5
42	1952	-1.8	1962	-2.1	1956	-1.6
43	1966	-1.8	1996	-2.1	1990	-1.6
44	1971	-2.0	1966	-2.3	1969	-1.8
45	1956	-2.7	1956	-2.9	1971	-1.9
46	1949	-2.7	1982	-2.9	1979	-1.9
47	1962	-3.0	1965	-3.6	1949	-2.0
48	1979	-3.5	1978	-3.8	1962	-2.0
49	1982	-3.6	1949	-3.9	1952	-2.2
50	1969	-3.6	1972	-4.0	1950	-2.2
51	1965	-4.2	1979	-4.9	1966	-2.9
52	1972	-4.5	1969	-5.0	1972	-3.2
53	1950	-5.5	1950	-5.8	1965	-3.8

<http://www.msc-smc.ec.gc.ca/ccrm/bulletin/winter01/>

## Appendix E

### Atmospheric Attenuation Model

The extraction of land surface parameters requires atmospheric correction, particularly when the observations are at microwave frequencies higher than 10 GHz (Myneini and Choudhury, 1993). Water vapor and oxygen are the main absorbers and emitters of atmospheric microwave radiation. While oxygen shows a range of rotation lines around 60 GHz and single absorption lines at 119 GHz, the absorption lines of water vapor are centered at 22.2 GHz and 183 GHz (Solberg et al., 1997). The above ground brightness temperature,  $T_{B_g}$ , undergoes atmospheric attenuation due to atmospheric oxygen, precipitable water vapor and cloud characteristics (height, thickness, and size distribution of water drops) before resulting in the at-satellite, brightness temperatures  $T_{B_s}$ . The atmospheric transmission coefficient,  $t_a$  is related to the optical thickness,  $\tau$  which was computed based on the total precipitable water vapor in the atmospheric column  $V$  (in mm) (Choudhury, 1993). The effective radiating temperature of the atmosphere,  $T_e$  is related to the air temperature  $T_a$  and the total precipitable water (Choudhury, 1993). Lakshmi (1996) has also used this atmospheric attenuation model for the soil moisture estimation using SSM/I data.

$$TB_{g,p} = \frac{TB_{s,p} - T_{sky}}{t_a} \quad (E.1)$$

$$t_a = \exp\left(-\frac{\tau}{\mu}\right) \quad (E.2)$$

$$\tau = 0.011 + 0.0026V \quad (19 \text{ GHz}) \quad (E.3)$$

$$\tau = 0.037 + 0.0021V \quad (37 \text{ GHz}) \quad (E.4)$$

$$T_{sky} = T_e(1 - t_a) \quad (E.5)$$

$$T_e = T_a - (8 + 0.06V) \quad (19 \text{ GHz}) \quad (E.6)$$

$$T_e = T_a - (18 - 0.12V) \quad (37 \text{ GHz}) \quad (E.7)$$

Where, the subscript p represents the polarization (Horizontal or Vertical),  $\mu$  the cosine of the incidence angle  $53^\circ$  (0.6 for SSM/I radiometer),  $T_{sky}$  is the sky temperature atmospheric temperature,  $T_e$  the effective radiating temperature (isothermal air temperature) and  $T_a$  the air temperature.

Wang et al., (1992) studied the effect of atmospheric absorption on the estimation of snow depth from microwave measurements made over Alaska by aircraft near 90 and 183 GHz. They reported that the radiometric correction for the effect of atmospheric absorption was important even at 37 GHz for a reliable estimation of snow depth, which would otherwise be underestimated by 30 percent. However, Chang et al. (1996) reported that  $T_{sky}$  (sky radiation) and  $T_{atm}$  (emission from the intervening atmosphere) are too small to be considered in the microwave region. The inclusion of these parameters to get the ground observed brightness temperature ( $TB_g$ ) could lead to an improved correlation with SWE. This correlation can further be improved if the coarse resolution of the total precipitable water vapor data from TOVS (the grid size being  $1^\circ$  latitude by  $1^\circ$  longitude) can be improved to finer resolutions.

## References

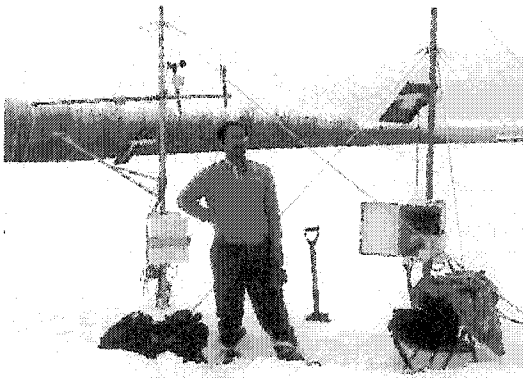
- Chang, A., Foster, J. L. and Hall, D. K. (1996), Effects of forest on the snow parameters derived from microwave measurements during the boreal. *Hydrol. Proc.* 10:1565-1574.
- Choudhury, B. J. (1993), Reflectivities of selected land surfaces types at 19 and 37 GHz from SSM/I observations. *Remote Sens. Environ.* 46:1-17.
- Lakshmi, V. (1996), *Use of special sensor microwave imager data for soil moisture estimation*, Ph.D. thesis, Princeton university, Princeton, New Jersey, 225p.
- Myneni R. B., and Chaudhury, B. J. (1993), Synergistic use of optical and microwave data in agrometeorological applications, *Adv. Space Res.*, 13(5): 239-248.
- Wang, J. R., Chang, A. T. C., and Sharma, A. K. (1992), On the estimation of snow depth from microwave radiometric measurements. *IEEE Trans. Geosc. & Rem. Sens.*, 30(4):785-792.

# **Appendix F**

---

## **Field Observations of Paddle River Basin**

This Appendix includes some of the photographs taken in the Paddle River Basin during the study period, which supports some of our discussions in the Chapters 3 and 4.



(a)



(b)



(c)



Plate F.1 Paddle River Basin's (a) meteorological towers, (b) snow pillow site at Paddle River H.W., and (c) snow course survey in different land cover classes.



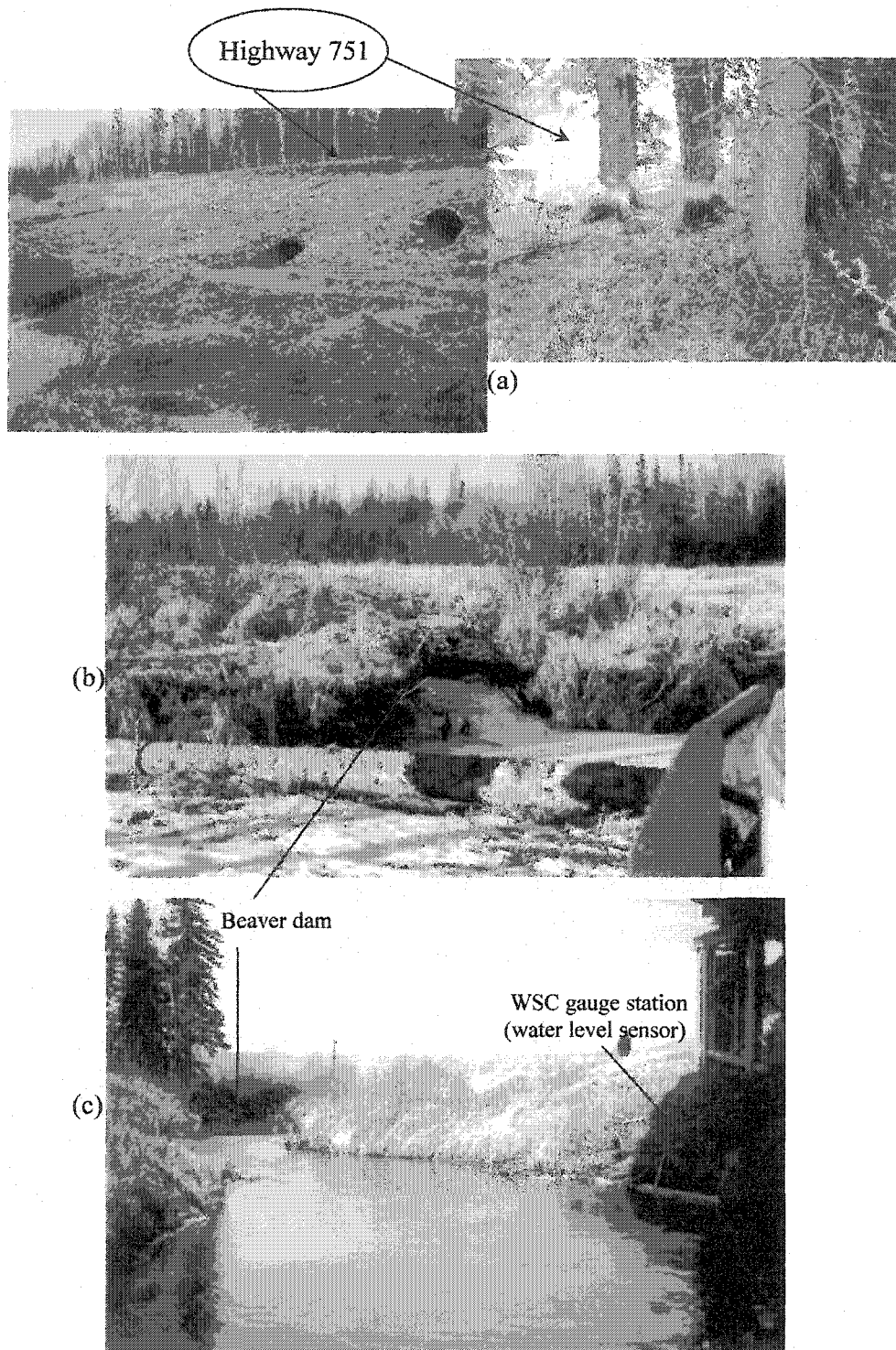


Plate F.2 Strategic locations of beaver dams observed in the Paddle River Basin (a) Highway 751 south of snow pillow site, (b) north of highway 649, (c) just upstream of WSC streamflow gauge station.

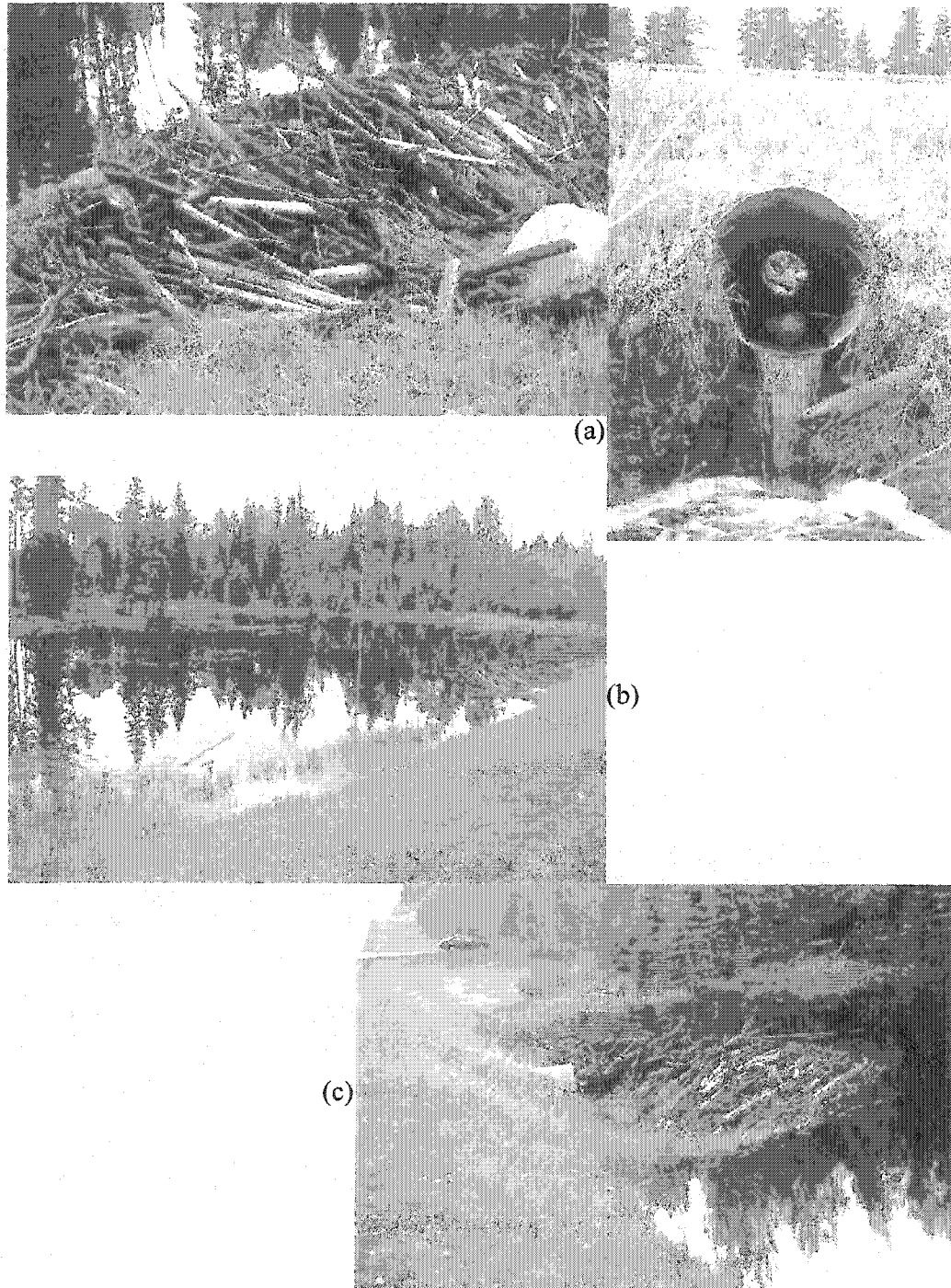


Plate F.3 Details of overflow beaver dam upstream of a twin-culvert in Highway 751, south of snow pillow site, (a) a close view of an upstream and downstream end of culvert, (b) large impounding water body looking towards north-west, (c) impounding water body looking towards south.